

Alma Mater Studiorum – Università di Bologna

DOTTORATO DI RICERCA IN
CHIMICA – CHIMICA FARMACEUTICA

Ciclo XXVIII

Settore Concorsuale di afferenza: 03/D1

Settore Scientifico disciplinare: CHIM/08

NATURALLY INSPIRED PRIVILEGED STRUCTURES IN
DRUG DISCOVERY: MULTIFUNCTIONAL COMPOUNDS
FOR ALZHEIMER'S DISEASE TREATMENT

Presentata da: Rita Maria Concetta Di Martino

Coordinatore Dottorato

Prof. Aldo Roda

Relatore

Prof.ssa Alessandra Bisi

Correlatore

Prof.ssa Federica Belluti

Esame finale anno 2016

Table of Contents

<i>List of abbreviations</i>	1
1. State of the art	7
1.1. ALZHEIMER'S DISEASE: NEURODEGENERATIVE DISORDER	8
1.2. MULTIFACTORIAL NATURE OF AD	13
1.3. THE AMYLOID CASCADE HYPOTHESIS	14
1.3.1. A β -toxicity	15
1.3.2. BACE-1	17
1.3.3. Design of BACE-1 inhibitors: from peptidomimetic to non-peptidic small molecules	20
1.4. TAU HYPOTHESIS	26
1.4.1. GSK-3	28
1.4.2. GSK-3 β inhibitors	32
1.4.3. GSK-3 β : molecular linker between A β and τ	35
1.5. OXIDATIVE STRESS	36
1.6. NEUROINFLAMMATION	38
1.7. NRF2-KEAP1: A NEUROPROTECTIVE SIGNALING PATHWAY	40
1.8. OTHER PROTEIN KINASES INVOLVED IN AD	46
2. Medicinal Chemistry	51
2.1. MULTITARGET APPROACH: IDEAL STRATEGY FOR AN EFFECTIVE AD TREATMENT	52
2.2. PRIVILEGED STRUCTURES	54
2.3. NATURAL PRODUCTS	62

2.3.1. α,β -unsaturated carbonyl compounds	65
2.3.2. Thiol trapping assay	68
2.4. CURCUMIN: A PROMISING THERANOSTIC TOOL FOR AD	70
2.4.1. Curcumin physical-chemical properties	72
2.4.2. Curcuminoids synthesis	73
2.4.3. Strategies aimed at improving curcumin bioavailability and pharmacokinetics	76
2.4.4. Structure-activity relationship studies	77
2.4.5. Curcumin neuroprotective potential in AD therapy	78
2.4.6. Curcumin: a fluorescent probe in AD diagnosis	80
2.5. MOLECULAR IMAGING THERANOSTIC PROBES: A PROMISING FUTURE IN AD TREATMENT	84
2.6. CHITOSAN: A VERY ATTRACTIVE AND USEFUL BIOPOLYMER	86
2.6.1. Physical-chemical properties	88
2.6.2. Applications	89
2.6.3. Chitosan-based bioconjugates	91
3. Aim of the work and Chemistry	97
3.1. DESIGN OF CURCUMIN-BASED COMPOUNDS	98
3.2. DESIGN OF 1,4- AND 1,3-BISCHALCONES [BIS(CINNAMOYL) BENZENE DERIVATIVES]	106
3.3. DESIGN OF CS-BASED BIOCONJUGATES	107
3.4. DESIGN OF INDOLE-BASED ANALOGUES	108
3.5. SYNTHESIS OF SERIES Ia AND Ib	126
3.5.1. Pabon reaction: synthesis of symmetric compounds 4, 5, 8, 11-14, 16 and 17	126
3.5.2. Pabon reaction: synthesis of asymmetric compounds 2, 3, 6, 7, 15 and intermediates 22 and 23	127

3.5.3. Williamson reaction: synthesis of symmetric compound 18 , and of the tautomeric couples 8 and 19 , 9 and 20 , 10 and 21	128
3.5.4. Williamson reaction: synthesis of intermediate benzaldehydes 24-26	129
3.6. SYNTHESIS OF SERIES IIa AND IIb	129
3.6.1. Pabon reaction: synthesis of symmetric analogues 27-31 and asymmetric derivatives 32-38	129
3.6.2. Synthesis of functionalized aldehydes 39-45 , azido derivatives 46-50 and intermediate 51	130
3.6.3. Synthesis of tautomeric couples of curcumin-based derivatives 52a,b-54a,b and intermediates 55a,b , 56 and 57a,b	131
3.7. SYNTHESIS OF SERIES III	133
3.7.1. Synthesis of curcumin analogues 58-60 , 61a,b and 62 and intermediates 64a,b , 65a,b and 63	133
3.8. SYNTHESIS OF SERIES IVa AND IVb	134
3.8.1. Synthesis of curcumin analogues 66-72 and aldehyde 73	134
3.8.2. Synthesis of curcumin-DF hybrids 74-78	136
3.9. SYNTHESIS OF SERIES Va AND Vb	137
3.9.1. Synthesis of curcumin-coumarin hybrids 79-82 and 85a,b-89a,b and intermediates 92-102	137
3.9.2. Synthesis of curcumin-coumarin hybrids 83a,b , 84a,b and 90a,b and azido intermediates 103-105	138
3.9.3. Synthesis of amido curcuminoids 91a,b and amine intermediate 106	139
3.10. SYNTHESIS OF SERIES VIa AND VIb	140
3.10.1. Synthesis of difluoroboron-derivatized curcuminoids 107 and 108	140
3.10.2. Synthesis of pyrazoles 109-113 , 116-120 , 122 , of dihydropyrazole 115 and of isoxazoles 114 and 121	141
3.10.3. Synthesis of curcumin-based pyrazoles 123-125	143

3.11. SYNTHESIS OF SERIES VII	144
3.11.1. Synthesis of 1,4- and 1,3-bis(chalcones 126-129	144
3.12. SYNTHESIS OF SERIES VIII	144
3.12.1. Synthesis of CS bioconjugates 130 and 131 and aldehyde 132	144
3.13. SYNTHESIS OF SERIES IX	146
3.13.1. Synthesis of indole-based derivatives 133-143	146
4. Results and discussion	148
4.1. BACE-1 INHIBITION	149
4.2. GSK-3β INHIBITION	152
4.3. NEUROPROTECTION	158
4.3.1. SH-SY5Y neuroblastoma cell viability	158
4.3.2. Antioxidant activity	158
4.3.3. Total GSH levels enhancement	159
4.4. NEUROINFLAMMATION	160
4.4.1. Neurotoxicity: microglial cell viability	161
4.4.2. Neuroinflammatory potential	162
4.5. THIOL TRAPPING ASSAY AND COVALENT DOCKING SIMULATION ON GSK-3β	169
4.6. CK1 AND LRRK2 INHIBITION	170
4.6.1. CK1δ and CK1ϵ inhibition	170
4.6.2. LRRK2 and G2019S-LRRK2 inhibition	172
4.7. BBB PERMEATION	174
5. Conclusions	177

6. <i>Experimental section</i>	181
7. <i>Appendix</i>	268
7.1. 1D AND 2D-NMR SAMPLE COMPOUNDS	269
8. <i>Bibliographic references</i>	276

List of abbreviations

- A β** amyloid β
- ABAD** A β -binding alcohol dehydrogenase protein
- Ac** acetyl
- ACh** acetylcholine
- AChE** acetylcholinesterase
- AChEIs** acetylcholinesterase inhibitors
- AD** Alzheimer's disease
- ALG** alginate
- ALS** amyotrophic lateral sclerosis
- APP** amyloid β protein precursor
- ARE** antioxidant-response element
- ATP** adenosine 5'-triphosphate
- BACE-1** β -site APP cleaving enzyme (β -secretase)
- BBB** blood-brain barrier
- BChE** butyrylcholinesterase
- Bn** benzyl
- bZip** basic region leucine zipper
- CAA** congophilic amyloid angiopathy
- CADD** computer-assisted drug discovery
- CaMKII** calcium and calmodulin-dependent protein kinase II
- CC** click chemistry (approach)
- CCR** click chemistry reaction
- CDCl₃** deuterated chloroform
- CDI** carbonyldiimidazole
- CDK5** cyclin dependent protein kinase 5

CK1 casein kinase 1

¹³C-NMR carbon nuclear magnetic resonance

CNS central nervous system

COSY correlation spectroscopy (NMR)

CS chitosan

CT computed tomography

Cul Cullin

DA degree of acetylation

Da Dalton

DD degree of deacetylation

DDI drug-drug interactions

DDSs drug delivery systems

DF dimethyl fumarate

DMAP 4-(dimethylamino)pyridin

DMF *N,N*-dimethylformamide

DMSO dimethyl sulfoxide

D₂O deuterium oxide

DOS diversity-oriented synthesis

DS degree of substitution

E entgegen (opposite, trans)

EDC *N*-(3-dimethylaminopropyl)-*N'*-ethylcarbodiimide hydrochloride

EMA European Medicines Agency

EpRE electrophile-responsive element

equiv equivalent

ERK extracellular receptor kinase

ESI-MS electron spray ionization-mass spectrometry

Et ethyl

EtOAc ethyl acetate
FDA Food and Drug Administration
GDP guanosine diphosphate
GPCRs G-protein coupled receptors
GSH glutathione
GSK-3 β glycogen synthase kinase-3 β
GST glutathione-S-transferase
GTP guanosine triphosphate
HB hydrogen-bonding
HCl hydrochloric acid
HE hydroxyethylene
HMKS halomethylketones
HMBC heteronuclear multiple-bond correlation (NMR)
HMTA hexamethylenetetramine
4HNE 4-hydroxynonenal
¹H-NMR proton nuclear magnetic resonance
HO-1 heme oxygenase-1
HPB hydrophobic (interactions)
HPLC high performance liquid chromatography
HSQC heteronuclear single-quantum coherence (NMR)
Hz Hertz
INF- γ interferon gamma
IONs iron oxide nanoparticles
I2PP2A inhibitor-2 of phosphatase protein PP2A
IR infrared (spectroscopy)
JNK Jun-N-terminal kinase
Keap1 Kelch-like ECH-associated protein 1

LPS lipopolysaccharide
LRRK2 leucine-rich repeat kinase 2
M molar mol/L
MAOS microwave assisted organic synthesis
MAP microtubule-associated protein
MAPKs mitogen-activated protein kinases
MCM multiple-compound medication
MD molecular dynamic
MI molecular imaging
MMT multiple-medication therapy
MNPs magnetic nanoparticles
MRI magnetic resonance imaging
MTDD multitarget drug design
MTDLs multi-target-directed ligands
MTDs multitarget drugs
MW molecular weight
nAChR nicotinic receptor
NBS *N*-bromosuccinimide
***n*-BuNH₂** *n*-butylamine
NDs neurodegenerative diseases
NF-κB nuclear factor-κB
NFTs neurofibrillary tangles
NMDA *N*-methyl-*D*-aspartate
NMDAR *N*-methyl-*D*-aspartate receptor
NMP *N*-methyl-2-pyrrolidinone
NPs natural products
NQO1 NAD(P)H: quinone oxidoreductase-1

Nrf2 nuclear factor erythroid 2-related factor 2

Nu nucleophile

OMT O-methyltransferase

PAMPA parallel artificial membrane permeability assay

PCL poly(caprolactone)

PD Parkinson's disease

PE petroleum ether

PEG polyethylene glycol

PERK PKR-like endoplasmic reticulum kinase

PET positron emission tomography

Ph phenyl

PHFs paired helical filaments

PhRMA Pharmaceutical Research and Manufacturers of America

PI3K phosphatidylinositol 3-kinase

PKA protein kinase A

PKC protein kinase C

PKs protein kinases

PLGA poly(lactide-co-glycolide)

ppm parts per million

PPs protein phosphatases

PS1 presenilin-1

RNS reactive nitrogen species

ROC Ras of complex proteins

ROS reactive oxygen species

r.t. room temperature

SAPKs stress-activated protein kinases

SFN sulforaphane

SN2 second-order nucleophilic substitution
SOD superoxide dismutase
SPECT single photon emission computed tomography
SPIONs small superparamagnetic iron oxide particles
SPs senile plaques
TBH *tert*-butyl hydroperoxide
***t*-Bu** *tert*-butyl
TDZDs thiadiazolidinones
TEA triethylamine
TFA trifluoroacetic acid
THF tetrahydrofuran
TMC *N,N,N*-trimethyl CS chloride
TMS tetramethylsilane
TMSA trimethylsilylacetylene
TNF- α tumor necrosis factor- α
TOS target oriented synthesis
UV ultraviolet-visible (spectroscopy)
VDCC voltage-dependent chloride channel
Z zusammen (together, cis)

1. *State of the art*

1.1. ALZHEIMER'S DISEASE: NEURODEGENERATIVE DISORDER

Neurodegenerative disease (ND) is an umbrella term to define a range of conditions characterized by progressive nervous system dysfunction and recognized as overwhelming health and socio-economic problems. They are incurable and debilitating disorders that result in progressive degeneration and/or death of nerve cells with consequent problems with movement (called ataxias), or mental functioning (called dementias). Among them, dementias are responsible for the greatest burden of these pathologies with Alzheimer's disease (AD) representing the most common form of dementia in industrialized nations among the elderly. It is the sixth leading cause of death, affecting more than 44 million people worldwide, and, due to its debilitating nature, causes an enormous financial and emotional stress on patients and caregivers.

Given that age constitutes the main risk factor for dementia and the population worldwide is rapidly aging, the number of AD patients is projected to reach 116 million by 2050.¹ Thus, this devastating disorder has been identified as one of the major public health concerns and a real research priority.

AD, described for the first time by the German psychiatrist Alois Alzheimer in 1906, is a progressive neurological disorder characterized by short-term memory impairment, at the beginning, and a profound cognitive and physical disability at the later stage.

The vast majority of AD cases are the late-onset sporadic forms whose greatest environmental risk factor is represented by aging. However, rare, familial, early-onset autosomal dominant forms, approximately 5 % only of all AD cases, exist and are caused by missense mutations in genes encoding amyloid β ($A\beta$) precursor protein (APP), presenilin-1 (PS1) and presenilin-2 (PS2).²

Diagnosis of AD is based on a careful analysis of the clinical features, although it should be confirmed by a depth histopathological examination of patients' brains. In general, three different clinical stages of the pathology have been identified, in which the progressive cognitive and functional decline stretches over 5-8 years:

- 1) Mild: that usually lasts 2-3 years, characterized by short-term memory impairment often accompanied by anxiety and depression.
- 2) Moderate: in which the symptoms of the previous stage decrease and some neuropsychiatric manifestations such as visual hallucinations, false beliefs and reversal of sleep patterns emerge.
- 3) Severe: characterized by motor signs, such as motor rigidity and prominent cognitive decline.³

Two additional clinical features of the pathology are the deterioration of language skills,⁴ and visuospatial deficits.⁵

The precise onset of clinical AD is very difficult to recognize by both patient and family because the earliest symptoms are often subtle and sporadic deficits in the remembrance of minor events of everyday life, referred to as loss of episodic memory. Although, after many years (a decade or more), a profound dementia develops and is often accompanied by extrapyramidal motor signs, slowed gait, and incontinence; death usually comes for minor respiratory complications, such as aspiration or pneumonia often in the middle of the night.⁶

In the final stage of the malady, the brains of AD patients are pathologically characterized by hippocampal and cerebral cortex atrophy and ventricular enlargement. Moreover, the brain regions involved in learning and memory processes, including the temporal and frontal lobes, are reduced in size as consequence of synaptic degeneration and neuronal death (Fig. 1). Microscopically, the numbers of neuronal cell bodies in the limbic and association cortices and in certain subcortical nuclei that project to them are decreased,⁷ even though this cellular loss can be difficult to appreciate without performing formal stereological quantification.

A distinctive feature of AD is an aberrant protein processing, in which amyloid β ($A\beta$) peptide and abnormally hyperphosphorylated tau (τ) protein, upon misfolding and self-assembly, generate neurotoxic aggregates into the brain, namely amyloid senile plaques (SPs) and neurofibrillary tangles (NFTs), respectively. These assemblies, usually identified in the *hippocampus*, amygdala,

association cortices and certain subcortical nuclei, represent the most relevant histopathological hallmarks of the disease and have been considered to play crucial roles in its pathogenesis triggering a cascade of biological processes, namely amyloid and tau cascades, ultimately culminating in neuronal cell death, brain atrophy, and cognitive decline.^{6,8} Variable numbers of amyloid-bearing meningeal and cortical microvessels [i.e., congophilic amyloid angiopathy (CAA)] constitute additional neuropathological AD changes.

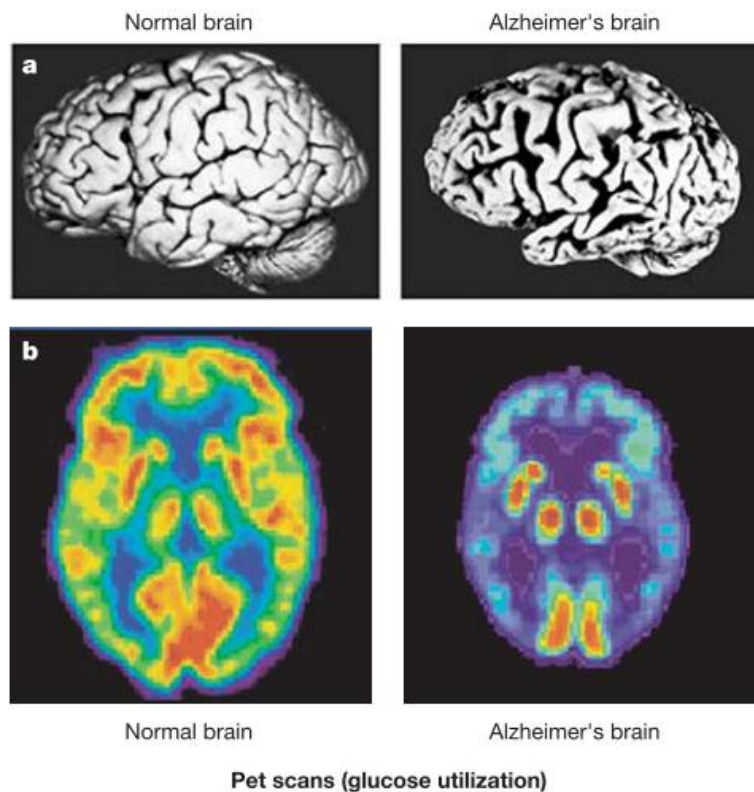


Figure 1. a) Comparison between a healthy brain and an AD brain; b) positron emission tomography (PET) images showing glucose uptake (red and yellow indicate high levels of glucose uptake) in a living healthy person and an AD patient.⁹

Regarding the correlation between the pathological features and the clinical manifestations of AD, surely, the synaptic loss is better correlated to the cognitive decline, and synaptic dysfunction is evident long before synapses and neurons are lost.¹⁰ Furthermore, in AD brains the levels of several neurotransmitters, namely

noradrenaline, dopamine, serotonin, glutamate, substance P and acetylcholine (ACh), are very low. In particular, ACh concentration has been found to be drastically lower compared to that in healthy individuals, and the same has been seen for cholinergic neurons, mainly in the basal forebrain and in the late stage of the malady, and nicotinic receptor (nAChR) subtypes in the *hippocampus* and cortex.¹¹

Taking into account the pivotal role of ACh in areas of the brain involved in memory formation, the loss of ACh activity has been closely associated with the severity of the pathology. In particular, according to the *cholinergic hypothesis*, the first working AD hypothesis, formulated about 30 years ago,¹² the cholinergic dysfunction represents the principal AD abnormality and a dynamic imbalance between ACh and its degrading enzymes, acetylcholinesterase (AChE) and butyrylcholinesterase (BChE), causes cognitive decline.

From a therapeutic point of view, the inhibition of ACh downregulation represents a strategy for the treatment of AD because it might increase ACh levels within synaptic clefts. Furthermore, considering that AChE terminates transmission at cholinergic synapses by rapidly hydrolyzing ACh, the most pursued approach is represented by AChE inhibition.¹³ For this reason, several series of AChE inhibitors (AChEIs), characterized by different molecular scaffolds and mechanisms of action, have been designed and synthesized, although only a small number of these compounds has been approved by the US Food and Drug Administration (FDA) and the European Medicines Agency (EMA), for moderate to severe AD treatment. In particular, four different AChEIs, tacrine (Cognex®, **a**), donepezil (Aricept®, **b**), rivastigmine (Exelon®, **c**), and galanthamine (Razadyne®, **d**) have been marketed for the cure of mild to moderate AD, whereas the AChEI donepezil and the non competitive N-methyl-D-aspartate (NMDA) antagonist, memantine (Namenda®, **e**), have been introduced in therapy for the treatment of moderate to severe AD (Fig. 2).¹⁴

Nowadays, tacrine is no longer used in Europe due to its capability to induce hepatotoxicity. Donepezil and galantamine are selective AChEIs, however

galantamine is endowed with an additional mechanism of action based on an allosteric modulation of the nicotinic receptors responsible of promoting ACh presynaptic release and postsynaptic neurotransmission.¹⁵ Furthermore, rivastigmine inhibits BChE, which is about 10 % of the total cholinesterases in normal human brains and is mainly associated with glial cells. Memantine, approved in Europe in February 2002, is able to protect neurons from glutamate-mediated excitotoxicity, without preventing the physiological activation of the NMDA receptor; its introduction in therapy is justified by the fact that in AD pathogenesis an increment of extracellular glutamate levels is thought to induce an excessive activation of NMDA receptors, which ultimately leads to neuronal death for Ca^{2+} intracellular accumulation.¹⁴

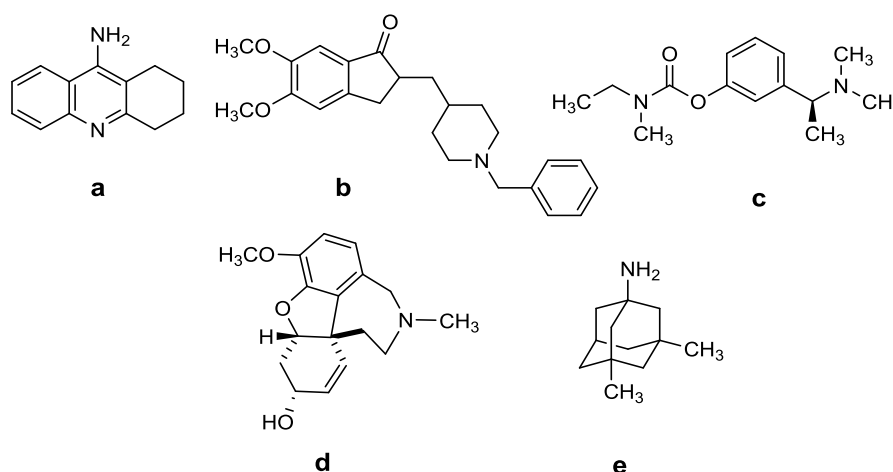


Figure 2. Commercially available drugs for AD treatment.

Unfortunately, all the current approved AD therapies offer only temporary and incomplete symptomatic relief, and represent a palliative tool by which to slow down the clinical course of the disease.^{8,16}

Despite the considerable advances in the understanding of the molecular and cellular changes associated with AD pathology and the enormous progresses in the medicinal chemistry field, no practical treatments have been introduced over the past quarter of a century. In this context, the Pharmaceutical Research and

Manufacturers of America (PhRMA), an industry trade group, reported 123 failures and only four new medicines approved to treat AD symptoms since 1998.

Thus, the discovery of disease-modifying agents able to control both onset and progression of the neurodegenerative process is a goal of increasing urgency.¹⁷

1.2. MULTIFACTORIAL NATURE OF AD

The cause or causes of AD are not yet known, nonetheless available evidence suggests that both A β peptides and hyperphosphorylated τ protein play crucial roles in its development. Accumulating evidence proposes that compared to a linear model of AD pathogenesis, which begins with a single factor, such as β -amyloid (e.g. *amyloid hypothesis*), AD pathogenesis is better explained by the idea that a complex network of events, including neuroinflammation, oxidative stress, reduced energy metabolism, and decreased synaptic function, interact in a feed-forward loop (Fig. 3).

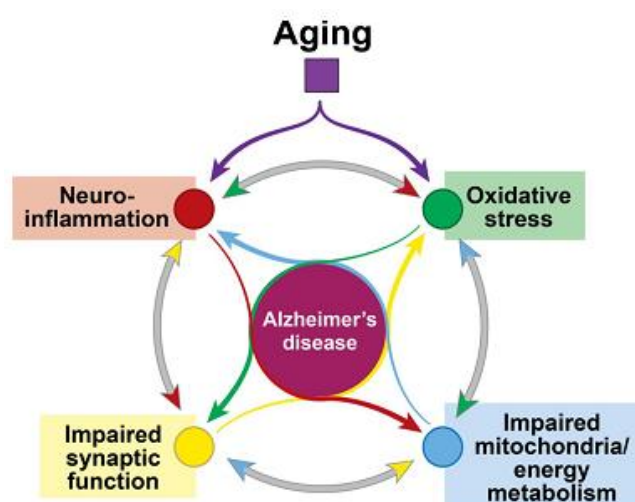


Figure 3. Complex heterogeneous view of AD pathogenesis.¹⁸

Aging is the most significant risk factor for the late onset of AD. Normally, several feedback homeostatic mechanisms automatically block neuroinflammation and oxidative stress. During aging, such mechanisms are less robust, resulting in a

sustained inflammatory environment in the brain that can trigger oxidative stress and inhibit synaptic transmission, causing synaptic dysfunction. In this pathological scenario, neuroinflammation and oxidative stress also result in altered mitochondria and impaired energy metabolism. Each of these pathological events promote other pathological features, resulting in the progressive cognitive decline observed in AD.¹⁸

This new heterogeneous view of the malady, emphasizing the important role of neuroinflammation and oxidative stress, allowed to identify additional pathways and molecular targets, involved in both onset and progression of the disease, interplaying with the well known and accredited *cholinergic*, *amyloid* and *tau hypothesis*.

1.3. THE AMYLOID CASCADE HYPOTHESIS

One of the pathological hallmarks of AD are extracellular deposits of fibrous protein aggregates, called SPs, in brain regions responsible for cognitive functions, such as *hippocampus* and association cortices. In particular, SPs, isolated by Glenner and Wong in 1984, consist of fibrillary β -pleated structures composed by $A\beta$ peptides. Among these peptides of 39-43 aminoacids length, $A\beta_{42}$ is predominant and presents the highest tendency to aggregate. According to the *amyloid cascade hypothesis*, proposed more than 25 years ago,¹⁹ $A\beta_{42}$ itself and its aggregates are able to trigger a neurotoxic cascade, playing thus an early and crucial role in the onset and development of AD.

$A\beta_{42}$ is generated by an anomalous proteolytic processing of the amyloid β precursor protein (APP),²⁰ a type I transmembrane protein, conserved and expressed in many tissues. In the central nervous system (CNS), the APP most abundant isoform consists of 695 aminoacids and is highly concentrated at the synaptic cleft. The precise physiological role of this protein remains uncertain, although it is supposed to be involved in several physiological processes, such as cell growth, neurite outgrowth, cell adhesion, cell signaling, and cell survival.²¹

APP processing can follow two different pathways: the non-amyloidogenic (Fig. 4A) and the amyloidogenic one (Fig. 4B) in which three different enzymes, called α -, β -, and γ -secretases, are involved in catalyzing different steps.

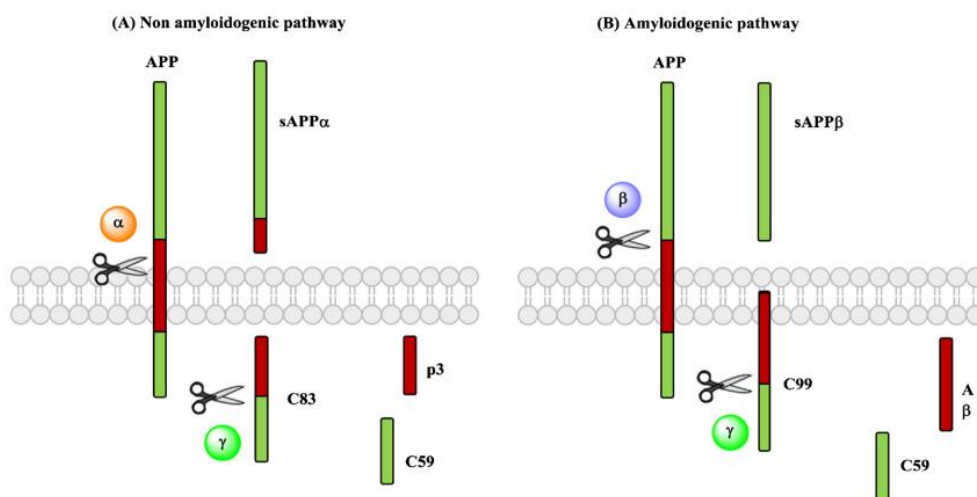


Figure 4. Enzymatic APP processing: non-amyloidogenic (A) and amyloidogenic (B) pathways. α) α -secretase, β) β -secretase, γ) γ -secretase.²²

In the non-amyloidogenic pathway, α -secretase cleaves APP, releasing the soluble APP α peptide (sAPP α) and the shorter membrane-bound C-terminal fragment (C83), that after cleavage by γ -secretase, a large multidomain aspartyl protease complex, leads to no toxic p3 and C59 fragments. Alternatively, in the amyloidogenic pathway, APP is firstly cleaved by β -secretase, also known as β -site APP cleaving enzyme (BACE-1), releasing a large soluble fragment called sAPP β . The remaining 99 aminoacid C-terminal fragment (C99) is then processed by γ -secretase to produce A β fragments of varying sizes, including neurotoxic A β ₄₂ peptide.²³

1.3.1. A β -toxicity

Originally, several neuropathological, biochemical, and genetic studies supported the idea that a gradual cerebral accumulation of soluble and insoluble A β assemblies is responsible for triggering the cascade of cellular events that untimely

result in the clinical AD phenotype. Actually, it is very difficult to define the nature of the neurotoxic A β species, because studies show that both A β monomers, and their aggregation products namely soluble oligomers, protofibrils, and insoluble amyloid fibrils can accumulate in the brain. In this context, ever-increased studies have identified the soluble A β oligomers as the most toxic species, capable of negatively affecting synaptic integrity and inducing memory functional deficits.²⁴

In general, A β oligomers proved to influence functionality and integrity of both pre- and postsynaptic terminals by induction of three different processes (Fig. 5):

- 1) oxidative stress;
- 2) calcium homeostasis disruption;
- 3) mitochondria and endoplasmic reticulum (ER) dysfunctions.

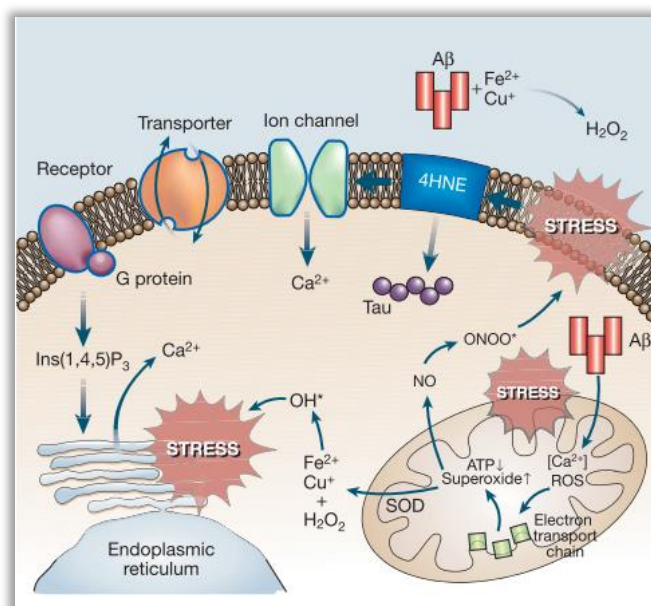


Figure 5. Pathways associated to A β neurotoxicity.⁹

Regarding the first one, A β oligomers interactions with specific metals, namely Fe²⁺ and Cu⁺, as well as A β aggregation at the cell membrane, promoting membrane-associated oxidative stress, lead to lipid peroxidation and consequent generation of 4-hydroxynonenal (4HNE), a neurotoxic aldehyde that covalently

modifies several proteins such as membrane transporters (ion-motive ATPases, a glucose transporter and a glutamate transporter), receptors, GTP-binding proteins (“G proteins”), ion channels (VDCC, voltage-dependent chloride channel, NMDAR, N-methyl-D-aspartate receptor) and also τ protein, promoting its subsequent aggregation in NFTs.

In addition, A β oligomers inducing mitochondrial oxidative stress and dysregulation of Ca²⁺ homeostasis, cause impairment of the electron transport chain, decrease of adenosine 5'-triphosphate (ATP) production and increment of superoxide anion radical (O₂^{•-}) levels. These last reactive oxygen species (ROS) can in turn produce peroxynitrites interacting with nitric oxide (NO) and/or H₂O₂ by superoxide dismutase (SOD) activity. The final interaction of H₂O₂ with Fe²⁺ or Cu⁺ generates the hydroxyl radical (HO[•]), a highly reactive oxyradical and potent inducer of membrane-associated oxidative stress, that contributes to ER dysfunction.

Afterward, neurotoxic forms of A β proved to induce neuronal death triggering the apoptotic cascade through different mechanisms⁹ and may exert their neurotoxic effects in a variety of additional ways including the interaction with the A β -binding alcohol dehydrogenase protein (ABAD, molecular linker between A β and mitochondrial toxicity in AD),²⁵ stimulation of the stress-activated protein kinases (SAPK) pathways,²⁶ and/or activation of the microglial cells with consequent induction of pro-inflammatory genes expression.

1.3.2. BACE-1

The recognition of A β as the main cause of neurodegeneration in AD and the genetic evidence that links AD pathology with the APP proteolytic processing, focused the interest of the scientific community for the three enzymes responsible of APP cleavage: α -, β - and γ -secretases. Among them BACE-1, catalyzing the first and rate-limiting step of the amyloid APP proteolysis, has aroused particular interest and become a valuable target supporting the *amyloid hypothesis*.

Originally, five different research groups simultaneously identified this beta-site APP-cleaving enzyme (BACE-1), also defined as Asp2 and memapsin, as a type I integral membrane protein, composed by 501 aminoacid residues, belonging to the pepsin-like A1 family of aspartic proteases. The enzyme is characterized by a protease domain facing the lumen/extracellular space in the same orientation as its substrate, APP, it is highly glycosylate and synthesized with a prosequence rapidly removed during Golgi transit by a furin-like convertase.

Although, a high degree of identity with its homologue BACE-2 was observed, a number of data concerning substrate specificity, as well as tissue and cellular distribution, lead to recognize BACE-1 as the main β -secretase in the brain.²⁷

BACE-1 presents the classical bilobal structure of the mammalian aspartyl proteases, but characterizes a novel subgroup of this family, being the first reported aspartic protease characterized by a transmembrane domain, a C-terminal cytoplasmic tail²⁸ and a unique disulphide bridge distribution.²⁹ The crystal structure of BACE-1 domain in complex with OM99-2, a highly potent inhibitor ($K_i = 1.6$ nM) (Fig. 6), allowed to establish that this enzyme is a monomer, characterized by two domains that likely evolved from gene duplication. Its active site is an open, elongated (about 20 Å long), and hydrophilic cavity of remarkable size (over 1000 Å), localized at the interface of the two domains, and turns around two catalytic aspartic acid residues, Asp32 and Asp228, facing each other.

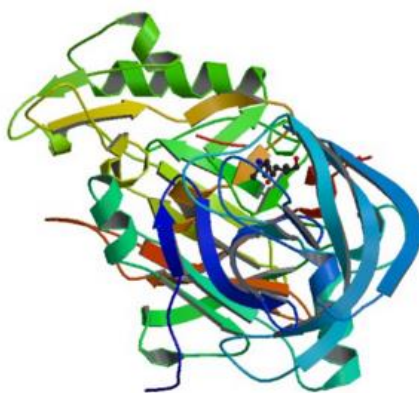


Figure 6. X-ray structure of BACE-1 in complex with OM99-2 at pH 5.0 (PDBid: 2ZHR).

The binding site cleft is partially covered by a highly flexible antiparallel hairpin-loop, known as the “flap”, which controls the substrate access and the correct geometry of it for the catalytic reaction.³⁰ This takes place by a general acid-base mechanism, common to all the aspartyl proteases, in which a base-catalyzed attack of a nucleophilic molecule of water gives a key tetrahedral intermediate, which finally collapses yielding the product of proteolysis (Fig. 7). In the presence of the substrate, the overall charge of the catalytic dyad is -1, because Asp32 is protonated, while Asp228 is deprotonated, as confirmed by several computational studies; furthermore, a complex network of hydrogen bonds at the active site is essential for the catalytic process.

BACE-1 shows maximum activity in an acid environment (pH 4.0-4.5), and an acidic pH is usually employed for the *in vitro* assays.³¹

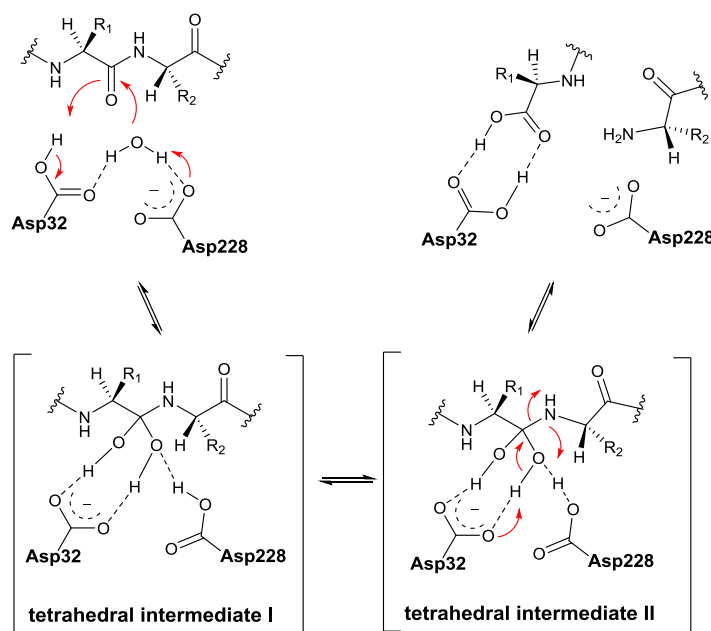


Figure 7. Schematic representation of BACE-1 catalytic mechanism.

Interestingly, several studies have shown a higher BACE-1 expression and activity in AD patients' brain, also as a consequence of the A β -induced oxidative stress.³²

1.3.3. Design of BACE-1 inhibitors: from peptidomimetic to non-peptidic small molecules

The first generation of BACE-1 inhibitors was characterized by a peptidomimetic structure and was developed based upon enzymes specificity studies employing a design strategy focused on the incorporation of non-cleavable transition state mimicking groups. One such inhibitor is OM99-2 bearing a non-cleavable Leu-Ala hydroxyethylene dipeptide isostere, blocking normal proteolytic BACE-1 cleavage (Fig. 8).

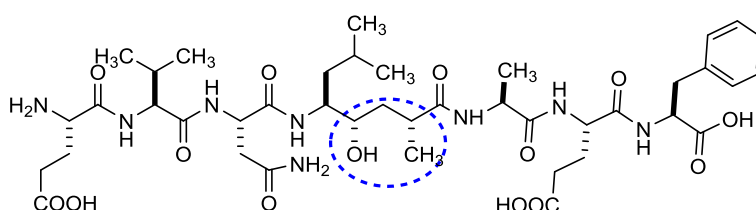


Figure 8. Chemical structure of BACE-1 inhibitor OM99-2.

The X-ray crystal structure of OM99-2 in complex with recombinant BACE-1 provided important molecular insight, that served as basis to design more potent peptidomimetic inhibitors such as cycloamide-urethane derivatives (Fig. 9), among which a 16-membered ring analogue turned out to be more potent than the acyclic counterpart showing a K_i value of 14.2 nM (Fig. 9).³³

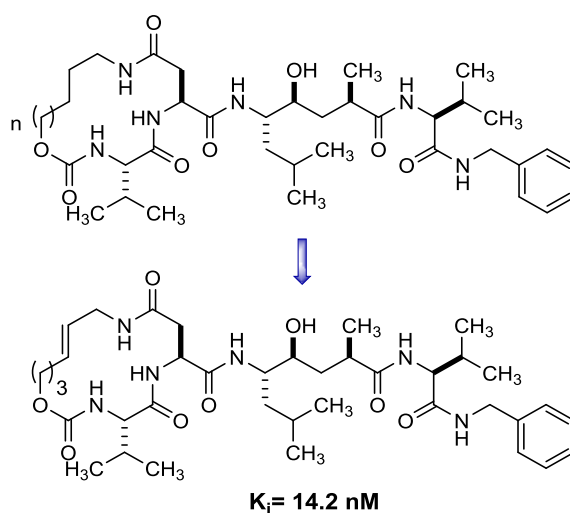


Figure 9. Chemical structure of cycloamide-urethane analogues as BACE-1 inhibitors.

Additional synthetic efforts from both academia and industry led to develop new series of BACE-1 inhibitors, including hydroxymethylcarbonyl and phenylnorstatin transition state analogues, designed with the aim to improve the inhibitory potency *in vivo* and BACE-1/BACE-2 selectivity.

Unfortunately, the majority of the inhibitors based on the peptidomimetic strategy showed well-known drawbacks associated with their polypeptide nature, such as: poor blood-brain barrier (BBB) crossing and oral bioavailability, together with susceptibility to P-glycoprotein transport; therefore, research work was focused on the development of non-peptidic inhibitors with improved pharmacokinetic and biological properties. In this context, in 2001 Takeda Chem. Ind. reported the first non-peptidomimetic BACE-1 inhibitors based on the tetralin scaffold, among which **I** showed the best inhibitory result in a fluorescent assay ($IC_{50} = 0.349 \mu\text{M}$, Fig. 10).

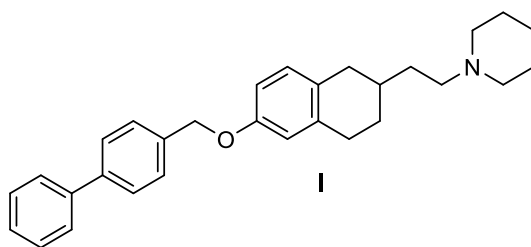


Figure 10. Chemical structure of the most potent tetralin-based BACE-1 inhibitor.

In 2002, Vertex divulged hundreds of different heterocyclic inhibitors characterized by K_i values around micromolar range, and proposed a 3-D pharmacophore map of BACE-1, according to which the inhibitory potency of the synthesized compounds was associated to their capability to adopt at the binding pocket of the enzyme the suitable conformation to give hydrogen-bonding moiety (HB) and hydrophobic (HPB) interactions with the active site and the subsites of BACE-1, respectively (Fig. 11).

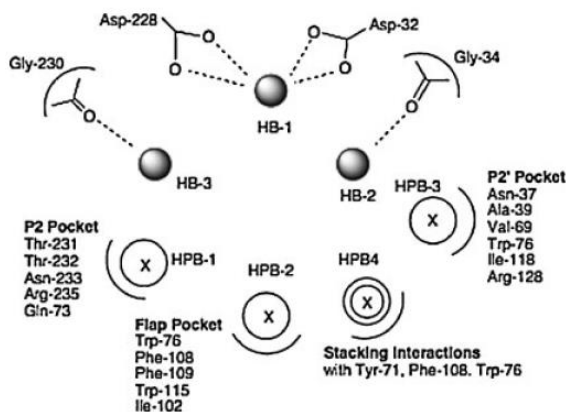


Figure 11. Schematic illustration of seven features binding mode with BACE-1.³⁴

To date, the literature reported a wide range of structurally different classes of small molecules as BACE-1 inhibitors, among which isophthalamide-based compounds displayed a remarkable inhibitory potency. The first series was synthesized by Elan starting from potent and selective peptidic BACE-1 inhibitors, in which the statine fragment was replaced with a hydroxyethylene (HE) isostere moiety bearing an isophthalamide N-terminus and different chemical groups were

inserted to the C-terminus. Within this series, **II** characterized by a *m*-iodo benzylamino moiety was recognized as the most potent inhibitor showing an $IC_{50} = 5$ nM (Fig. 12).

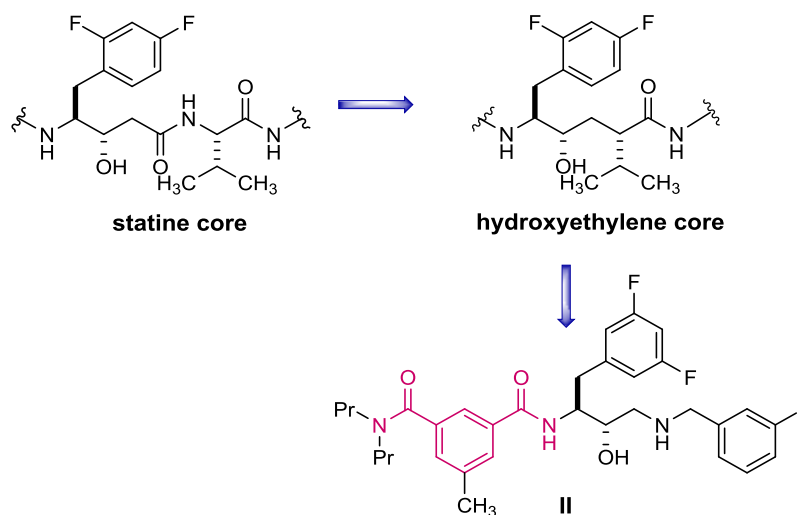


Figure 12. Chemical structure of isophthalamide-based BACE-1 inhibitors.

These exciting preliminary results encouraged several research groups to introduce properly addressed chemical modifications in different position of the isophthalamide scaffold in order to discovery analogues with higher inhibitory potency. In particular, the choice of groups such as sulfonate, macrocycle, isonicotinamide, guanidine and heterocycles (indole, imidazole, piperidine, morpholine, isoquinoline) allowed to obtain potent inhibitors, which showed IC_{50} s < 10 nM.

Interestingly, the simultaneous incorporation of a sulfonamide function and either small alkyl groups or longer hydrophilic substituents led to the development of libraries of derivatives with a strong increase in cellular potency and IC_{50} values in the nanomolar range of concentration (Fig. 13). Among them, particular interest was focused on analogue **III** ($IC_{50} = 8$ nM) due to its capability to give H-bond with only half of the enzyme catalytic dyad, specifically Asp228 by its nitrogen atom (Fig. 13).³⁴

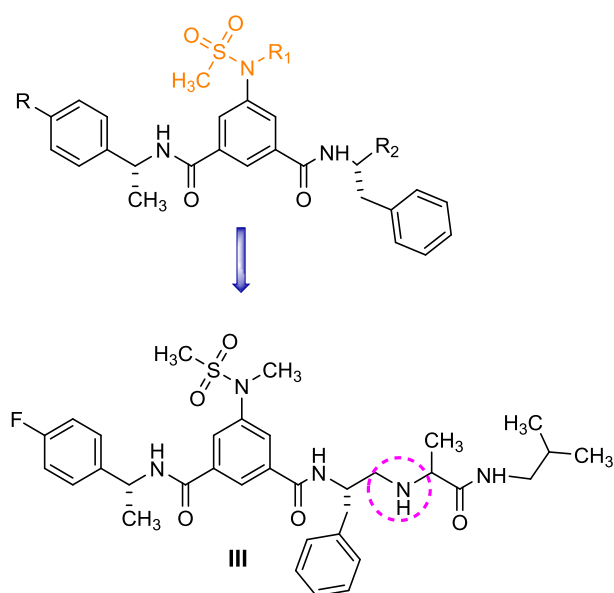


Figure 13. Chemical structure of isophthalamide analogues.

In 2014, as part of a multitarget drug discovery project aimed at identifying new anti-AD modifying agents, the versatility of the benzophenone scaffold was exploited for obtaining novel well-balanced BACE-1 and AChE inhibitors. In this context, since the 3-fluoro-4-hydroxy-benzophenone nucleus emerged as essential chemical feature for the binding with BACE-1 catalytic dyad, it was employed as a starting point to develop a small library of analogues characterized by different tertiary amine functions. Among them, compound **IV** bearing a *N,N'*-benzylmethylamine moiety (Fig. 14), showing $IC_{50} = 3.66 \mu M$ and $IC_{50} = 7.00 \mu M$ against BACE-1 and AChE, respectively, was selected as hit compound and its optimization allowed to identify **V** as the best well-balanced dual inhibitor ($IC_{50} = 2.32 \mu M$ and $IC_{50} = 2.52 \mu M$ against BACE-1 and AChE, respectively) with expanded biological profile (Fig. 14).³⁵

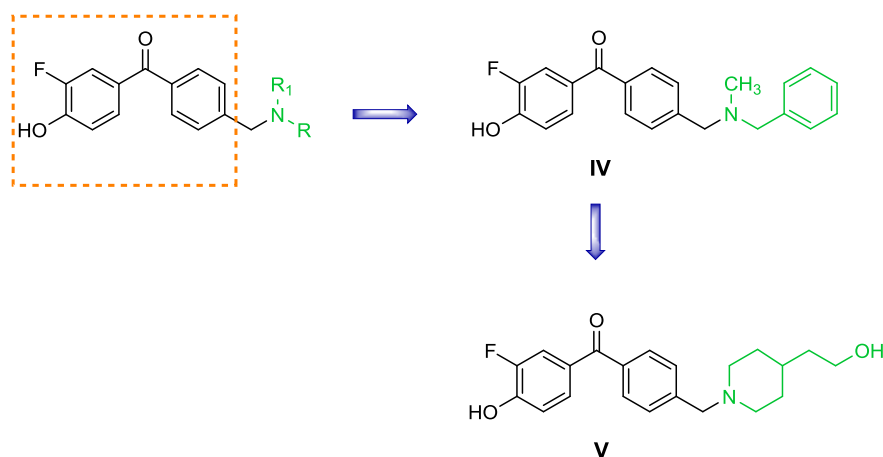


Figure 14. Design of benzophenone-based compounds as BACE-1 and AchE dual inhibitors.

In 2015, the same *N,N'*-benzylmethyl group of compound **IV** was inserted in a novel and potent class of indanone hybrid molecules, structurally derived from donepezil and the well-known AChE inhibitor AP2238 (Fig. 15). In particular, starting from derivative **VI**, emerged as new lead with submicromolar inhibitory potency on human AChE and promising A β antiaggregating activity, in an effort to improve its multitarget profile with particular focus on BACE-1 two new sets of derivatives were developed (Fig. 15).

Taking into account both the presence of fluorine atoms in several BACE-1 inhibitors reported in literature and the possible improvement of pharmacokinetic and physical-chemical properties due to the introduction of this halogen atoms into potential drugs or diagnostics, the terminal piperidine nucleus of **VI** was replaced with different related substituted amines including 4-F-benzyl- and bis(4-F-phenyl)methylpiperazines. Among all synthesized derivatives, compound **VII** was identified as the most potent BACE-1 inhibitor of the series ($IC_{50} = 2.49 \mu M$) due to the ability of its bulky bis(4-fluorophenyl)methylpiperazine fragment to contact different aminoacidic residues located outside the binding pocket of BACE-1.³⁶

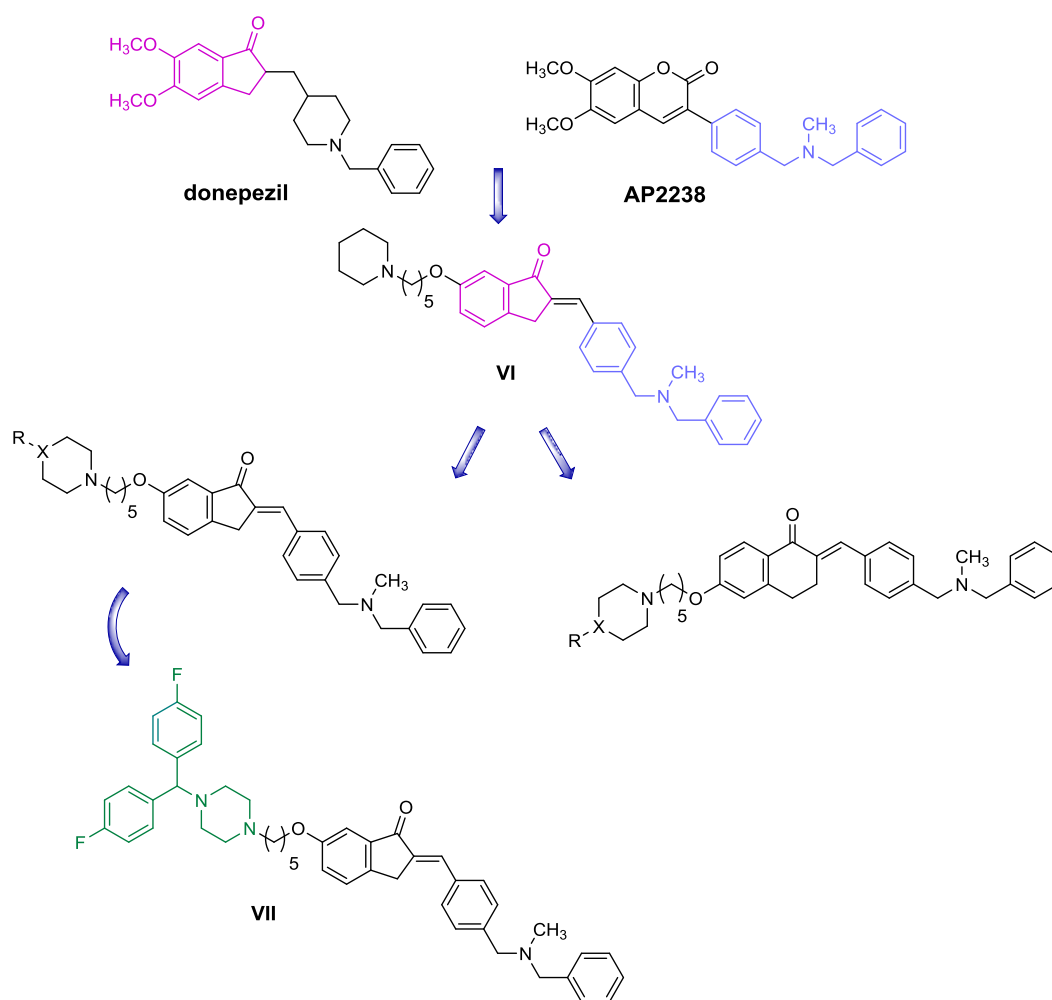


Figure 15. Design strategy of indanone hybrid derivatives.

1.4. TAU HYPOTHESIS

Actually, despite the compelling evidence supporting the *amyloid hypothesis*, in AD the density of NFTs, correlates more closely with cognitive impairment than senile plaques.³⁷

NFTs are intraneuronal aggregates, mainly composed of abnormally hyperphosphorylated τ protein, the principal neuronal microtubule-associated protein (MAP), coded by a single gene on chromosome 17 but expressed in several molecular isoforms, that are generated by alternative splicing of its mRNA. In human brain, six different molecular isoforms of τ are expressed and differ in

containing three or four microtubule binding repeats of 31-32 aminoacids in the C-terminal half and one, two, or zero N-terminal inserts of 29 aminoacids. Among them, the isoform with a total of 441 aminoacids (τ_{441}) in length is the largest size human brain τ protein predominantly expressed in neuronal axons, although recent studies reported that it is also expressed in glia and astrocytes.³⁸

Under physiological conditions, τ stabilizes microtubules, promotes their assembly, and affects their dynamics by interaction with tubulin. These biological activities are finely modulated through τ phosphorylation in correspondence of a specific number of Ser/Thr sites. In the longest isoform of τ protein, 79 potential Ser and Thr phosphate acceptor residues have been identified, although only about 30 of them seem to act as real sites of physiological phosphorylation.

In contrast, an abnormal τ phosphorylation, leading to its dissociation from microtubules and resulting in cellular cytoarchitecture disruption, and further τ accumulation in paired helical filaments (PHFs), is a characteristic AD feature. Moreover, when τ is highly phosphorylated and crosslinked by disulphide bonds, a sequential proteolytic processing was shown to take place and promote the formation of τ oligomers and insoluble NFTs (Fig. 16). This cascade of toxic processes, according to the *tau hypothesis*, is thought to contribute to neuronal dysfunction and eventually cell death in AD.^{39,40}

This hypothesis has recently been modified, since several animal models led to argue that τ -mediated dysfunction/toxicity may not necessarily require large τ aggregates, but may be also caused by soluble hyperphosphorylated τ proteins or by its oligomers.⁴¹

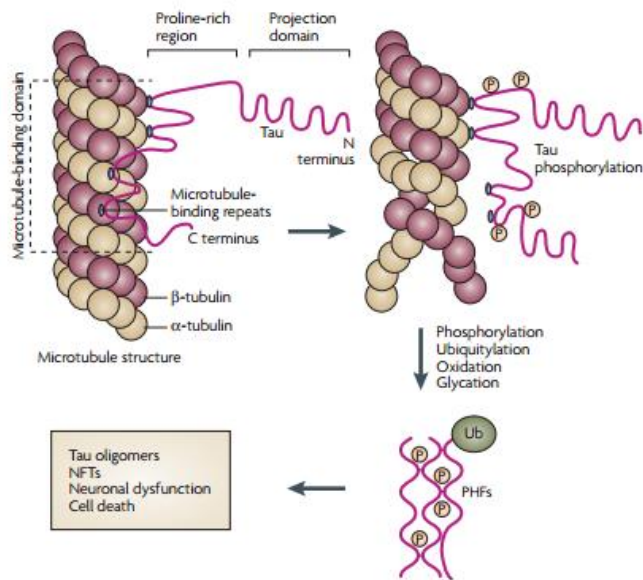


Figure 16. Intracellular neuronal aggregation of hyperphosphorylated τ protein.³⁹

Nowadays, causal factors affecting τ phosphorylation and sequential formation of NFTs are not fully understood, however, a large number of studies revealed the critical role of $A\beta$ and/or chronic oxidative stress in τ hyperphosphorylation and aggregation.⁴⁰ In particular, several evidence supports that different products of oxidative stress, such as 4-HNE, together with a large number of oxidative stress-activated kinases, namely glycogen synthase kinase-3 (GSK-3), mitogen-activated protein kinases (MAPKs), extracellular receptor kinase (ERK), p38 MAPK and Jun-N-terminal kinase (JNK), are involved in intracellular NFTs deposition.⁴²

1.4.1. GSK-3

The state of τ phosphorylation is the result of the balance between protein kinases (PKs) and phosphatases (PPs) activities. Several Ser/Thr protein kinases have been associated to the abnormal hyperphosphorylation of τ protein, among which GSK-3, cyclin dependent protein kinase 5 (CDK5), protein kinase A (PKA),

calcium and calmodulin-dependent protein kinase II (CaMKII), casein kinase 1 (CK1), mitogen activated protein (MAP) kinase ERK1/2, and SAPKs.

There are 518 genes that encode for more than 2000 different protein kinases. These proteins are specific Ser, Thr or Tyr kinases and are responsible for the regulation of several physiological processes, including cellular death and division, transport and secretion of molecules, as well as, modulation of some brain functions, blood pressure, metabolism and protein synthesis.⁴³

Structurally, PKs have a highly conserved catalytic domain, nevertheless they differ in the way in which their catalytic function is regulated. In particular, Ser/Thr kinases can be classified as proline-directed or non-proline-directed proteins. Within the first class, GSK-3 β has been recognized as validated AD target^{38,39} due to the observed link between its overactivity and/or overexpression and the neuropathological hallmarks described for the disorder (A β deposition, τ hyperphosphorylation, gliosis, and neuronal cells death).⁴⁴

GSK-3 is involved in the regulation of several cellular processes, including cellular division, proliferation, differentiation and adhesion. In 1980, it was isolated from skeletal muscle and recognized as one of the five enzymes involved in glycogen synthase phosphorylation.⁴⁵ Two different isoforms of this enzyme exist, namely GSK-3 α and GSK-3 β , which are similarly regulated although encoded by different genes. GSK-3 α (51 kDa) differs from isoform β (47 kDa) for the presence of a glycine-rich extension at the N-terminal end. Both isoforms are ubiquitously expressed in the brain, with high levels of expression in the *hippocampus*, cerebral cortex, and the Purkinje cells of the cerebellum, the expression ratio of these two isoforms favors GSK-3 β (Fig. 17).

In vitro and in cell culture models both GSK-3 isoforms have shown their capacity to phosphorylate τ at various sites, consistent with the epitopes found to be hyperphosphorylated in AD brains. However, in several animal models overexpression of GSK-3 β proved to both induce τ hyperphosphorylation mainly at Ser199, Ser396, and Ser413 and accelerate neurodegeneration, whereas an inhibition of this enzyme led to a decrement of τ toxicity.⁴⁶

Interestingly, τ overexpression promotes GSK-3 β activation and mediates GSK-3 β toxicity; in τ absence, indeed, the neurodegenerative and cognitive phenotypes observed in GSK-3-overexpressing mice is ameliorated.⁴⁷

Structurally, GSK-3 β (Fig. 17) contains a typical two-domain kinase fold composed by a β -strand domain (residues 25-138) and an α -helical domain (residues 139-343) at the N- and C-terminal ends, respectively. The ATP-binding site is located at the interface of the α -helical and β -strand domains and the glycine-rich loop and the hinge border it. The activation loop (residues 200-226) runs along the surface of the substrate binding groove and the β -strand domain includes a short helix (residue 96-102), high conserved in all kinases, in which there are two residues, Arg96 and Glu97, that play key roles in the catalytic activity of the protein.⁴⁸ In addition, at the entrance of the GSK-3 β ATP binding site there is a key Cys199 residue, whose covalent interaction with electrophilic species by sulfur-carbon bond formation plays a crucial role in the irreversible or pseudo-irreversible inactivation of the enzyme.

In general, the phosphorylation of specific aminoacid residues such as Val214 and Tyr216 within the activation loop induces its conformational change and consequent increase of the kinase activity. Nevertheless, several data suggest that, unlike MAP kinase or cAMP-dependent kinases, GSK-3 β can also achieve a catalytically active conformation in absence of this specific phosphorylation.

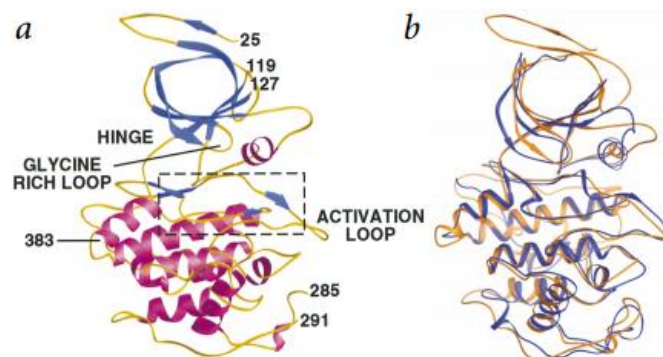


Figure 17. a) The overall structure of GSK-3 β ; b) superposition of GSK-3 β (blue) and activated substrate-bound CDK2 (red).⁴⁸

Generally, GSK-3 is constitutively active, and the activation sites can undergo autophosphorylation; furthermore, different PKs can regulate its activity in different ways, depending on the particular site of phosphorylation. Concerning GSK-3 β , phosphorylation at Ser9 decreases the activity, while at Tyr216 leads to enzyme overactivation. Currently, a large variety of GSK-3 regulatory pathways are known, and their underlying molecular basis have been elucidated. Among these, the most studied is based on Akt (protein kinase B) activation, in which insulin stimulation, activates phosphatidylinositol 3-kinase (PI3K) and leads to Akt (protein kinase B) phosphorylation and consequent GSK-3 β inhibition. However, a brief exposure to insulin can also transiently activate GSK-3 β through phosphorylation of Tyr216 promoted by the non-receptor tyrosine kinase Fyn. Besides PI3K, even other kinases, including protein kinase C (PKC), are able to inhibit GSK-3 by phosphorylation at Ser9 and, within the brain, p38 mitogen-activated protein kinase (MAPK) proved to inactivate this enzyme by direct phosphorylation at its C-terminus end.

An additional mechanism associated to GSK-3 activation consists in its dephosphorylation at specific inhibitory sites by means of different phosphatases, such as protein phosphatase 1 (PP1) for GSK-3 β , protein phosphatase 2A (PP2A) which favors GSK-3 α , and protein phosphatase 2B (PP2B, calcineurin).^{47,49}

Interestingly, in a particular study aimed at identifying potential allosteric binding sites of GSK-3 β , seven well conserved cavities have been identified on the surface of 25 different structures of the kinase by employing the free geometry-based algorithm fpocket and hpocket programs. Three of these pockets correspond to the known binding sites of GSK-3 β : ATP (1), substrate (2) and peptides axin/fratide (3), while the others are situated on the C-terminal lobe of the kinase, in the hinge region between the C- and N-terminal lobes, and finally two on the N-lobe of the enzyme (Fig. 18).⁴⁴

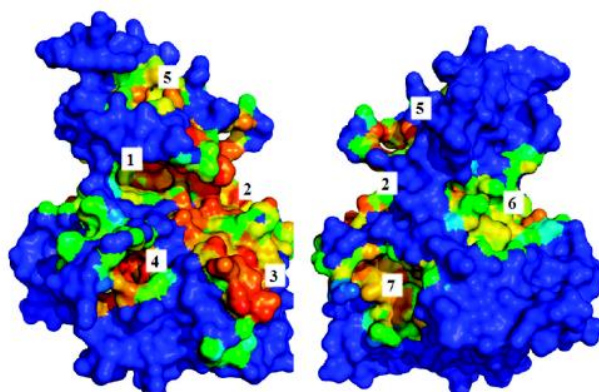


Figure 18. Seven cavities found by hpocket in the 25 PDB structures of GSK-3 β analyzed independently.⁴⁴

1.4.2. GSK-3 β inhibitors

Over the last decade, the increased interest in GSK-3 β led to the discovery of a large number of inhibitors, based on chemically different molecular scaffolds, and acting with diverse mechanisms of action, such as ATP competition, allosteric modulation, and enzyme irreversible inhibition. The majority of inhibitors reported in the literature are ATP competitive agents such as hymenialdisine, paullones, indirubines and maleimides (Fig. 19). Among them, indirubins proved to be powerful inhibitors of GSK-3 β showing a potency in the nanomolar range (IC_{50} = 5-50 nM), as well as the bisindolylmaleimide derivatives of staurosporine, GF 109203x and Ro 31-8220 (Fig. 19). Furthermore, the optimization process of an arylindolemaleimide family of compounds, recognized as equipotent GSK-3 α and GSK-3 β inhibitors, allowed to obtain the best inhibitory results from derivatives **I** (IC_{50} = 20 nM), **II** (IC_{50} = 28 nM), and **III** (IC_{50} = 26 nM) (Fig.19).

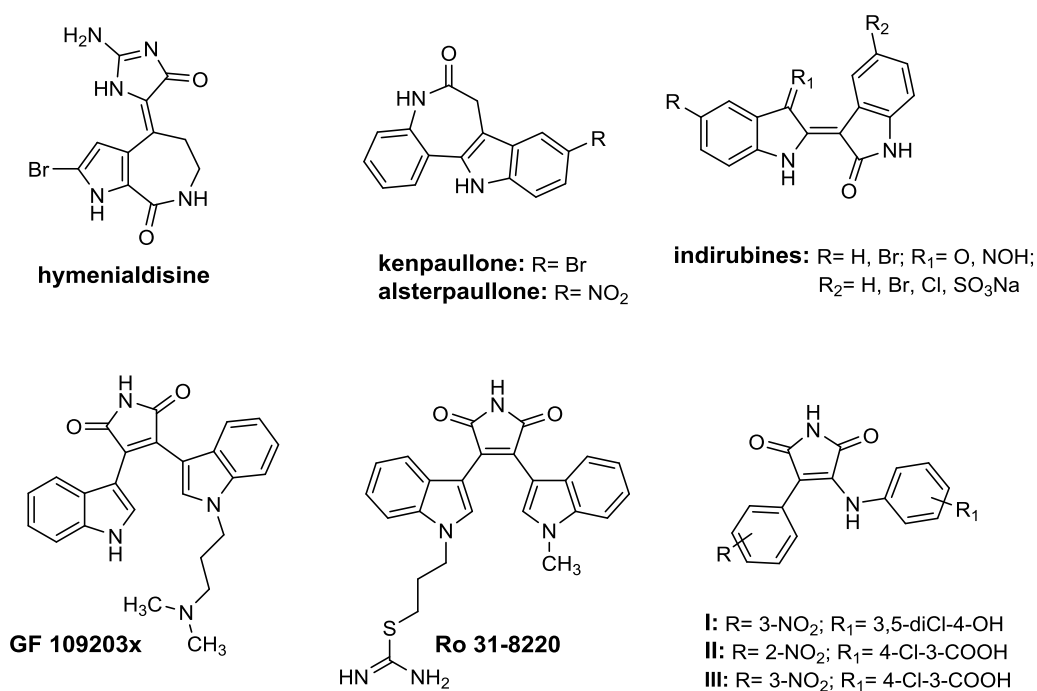


Figure 19. Chemical structure of ATP competitive GSK-3 β inhibitors.

Generally, one of the main limitations for the therapeutic use of ATP competitive inhibitors consists in the lack of kinase selectivity, as consequence of the high degree of PKs identity in the catalytic site. Therefore, in a potential chronic treatment these compounds could offer adverse secondary effects.⁵⁰

In contrast, non-ATP competitive inhibitors, showing better cellular and *in vivo* potency in comparison with competitive inhibitors together with better kinase selectivity, have recently attracted ever-increased attention as promising candidates to achieve an effective treatment of chronic disorders including AD.

To date, small thiadiazolidinones (TDZDs, Fig. 20) represent the first class of non-ATP competitive GSK-3 β inhibitors reported in the literature, and tideglusib (Fig. 20) has recently finished a pivotal phase II clinical trial in 20 mild to moderate AD patients, showing not only safety and tolerability but also a trend in the enhancement of cognition abilities in patients.⁴⁴ Concerning the precise mechanism of action of this class of inhibitors, a hypothetical GSK-3 β binding mode has been proposed, in where the TDZDs may bind to the primed phosphate substrate binding

site of the enzyme. In addition to them, two marine natural compounds, the alkaloid manzamine and the sesquiterpene palinurin (Fig. 20), have been reported as cell permeable non-ATP competitive inhibitors, able to reduce tau phosphorylation in cell cultures. In particular, the binding site of manzamine has been recently postulated as an allosteric site at the back of the ATP site⁵¹ and results derived from both experimental data and molecular dynamic (MD) simulations suggested that the palinurin allosteric site is located at the N-terminal lobe of GSK-3 β (pocket 5, Fig. 18).⁵² These allosteric inhibitors are likely to be more selective and may be useful in overcoming resistance developed to ATP competitive drugs. Furthermore, they provide more subtle modulation of kinase activity than simply blocking ATP entrance.⁴⁴

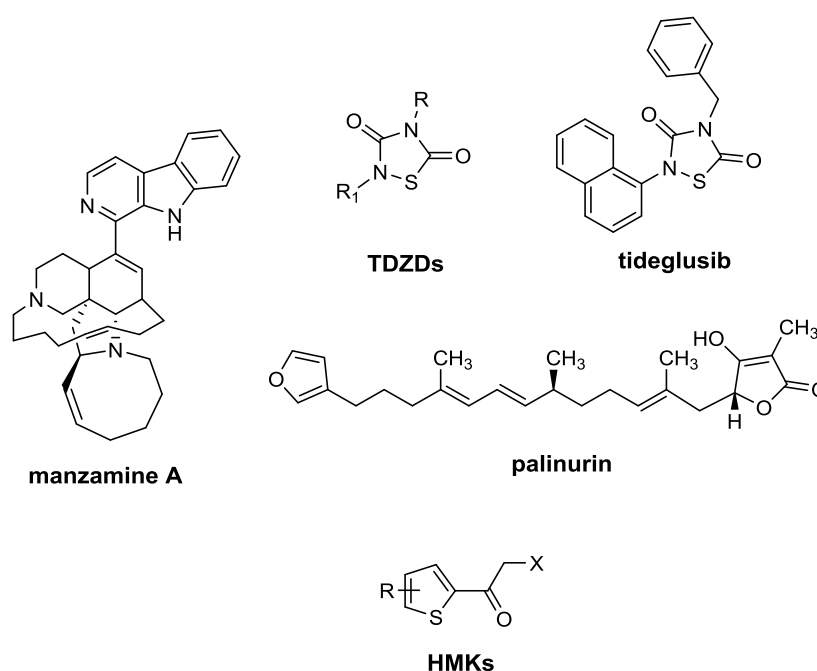


Figure 20. Chemical structure of non-ATP competitive GSK-3 β inhibitors.

The irreversible GSK-3 β inhibition, by selective targeting of Cys199 in the ATP-binding site, has recently been reported as a promising strategy to minimize the undesirable off-target effects associated with enzyme inhibition obtaining useful pharmacological tools.⁸ In this context, halomethylketones (HMKs, Fig. 20),

irreversible inhibitors with IC₅₀ values in the low micromolar range, have just been reported representing valid alternative for the future design of specific and potent inhibitors, due to their ability to decrease tau phosphorylation in cell cultures, to cross the BBB, together with their good kinase selectivity.⁵¹

1.4.3. GSK-3 β : molecular link between A β and τ

Although A β and τ exert toxic effects through separate mechanisms, several lines of evidence, from both *in vitro* and *in vivo* models, confirm the existence of a molecular interplay between these two proteins in causing synergic toxicity and a cross-talk between A β and GSK-3 β has been reported. Indeed, several studies confirmed both the pivotal role of A β in driving τ pathology by a general induction of τ hyperphosphorylation and NFTs formation, and τ aptitude to mediate A β -toxicity. The interaction of these two proteins, together with their ability to amplify each other's toxic effects by synergistically targeting cellular processes or organelles, represent three possible mechanisms of A β and τ link (Fig. 21).⁵³

A good example of A β and τ relationship involves the impairment of mitochondrial respiration; in particular, it has been demonstrated how the synergistic block of the respiratory chain complexes I and IV by τ and A β , respectively, leads to an higher mitochondrial impairment compared to the dysfunction associated to τ and APP overexpression alone.

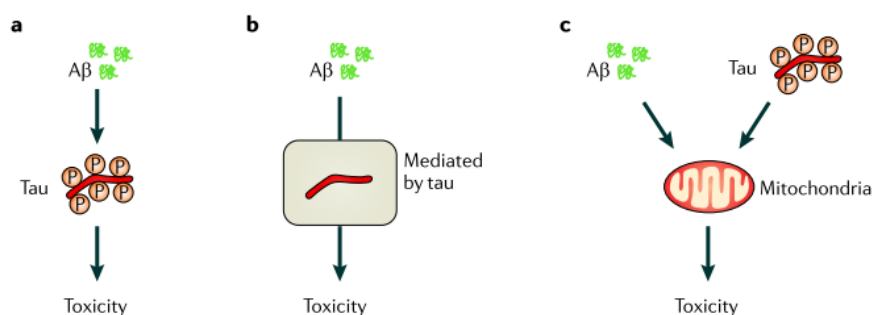


Figure 21. Three possible mechanisms of A β and τ link; a) A β induction of τ pathology, by causing tau hyperphosphorylation; b) τ aptitude to mediate A β -toxicity; c) A β and τ synergic toxicity in AD pathology by synergistically targeting cellular processes or organelles.⁵³

Interestingly, GSK-3 β represents the molecular link between A β and τ neurotoxic cascades. *In vitro* studies and transgenic animal models of AD have been shown as the pathologic activation of GSK-3 β by A β , prevents inhibitory phosphorylation of the enzyme, and leads to an increment of τ phosphorylation. On the contrary, GSK-3 β inhibition decreases A β production and A β -induced neurotoxicity by reducing BACE-1 cleavage of APP.⁸ Additional investigations also confirmed GSK-3 β capability to promote the amyloidogenic APP processing by inhibition of the α -secretase complex and interfering with APP cleavage at the γ -secretase complex step.⁴⁹

1.5. OXIDATIVE STRESS

According to the multifactorial view of AD, oxidative stress has been recognized as a common pathological feature of the disorder. Recently, experimental evidence indicates that a dysregulation of the redox state contributes to the onset of the neurodegenerative process.

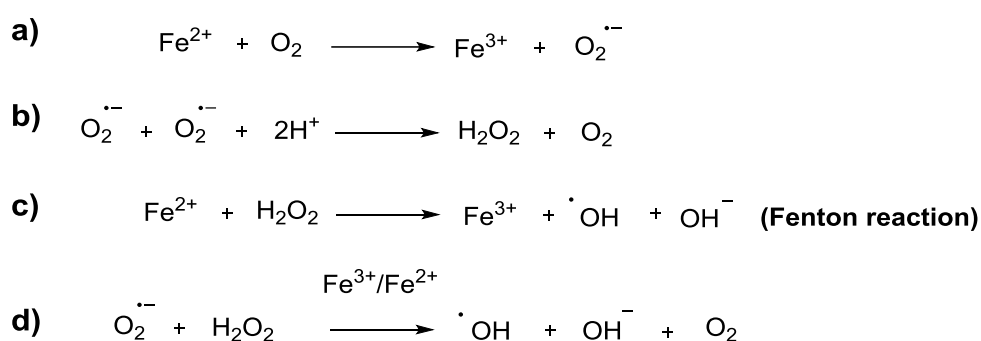
Commonly, oxidative stress is caused by an imbalance between reactive radical species, among others ROS, and a loss of function of many antioxidant defense enzymes, resulting in a disequilibrium between the formation of cellular oxidants and the antioxidative processes.⁵⁴ This impairment of the cellular redox balance leads to oxidative alterations of biological macromolecules, such as proteins, lipids, and nucleic acids, identified as biochemical markers in AD brains. In addition, modifications in the activities or expression of antioxidant enzymes such as SOD and catalase have been observed in both CNS and peripheral tissues of AD patients.⁵⁵

ROS, namely O₂^{•-}, H₂O₂ and [•]OH, are small biological molecules, which are continuously produced in aerobic organisms such as a natural by-product of oxygen metabolism. Although they play an important physiological role in cell signaling, the long-term exposure of cells to higher levels of ROS leads to toxic effects. ROS production occurs largely in mitochondria, starting from O₂^{•-}, the product of one-electron reduction of oxygen that is converted, spontaneously or enzymatically by

SOD, into H₂O₂ and oxygen (Scheme 1b). H₂O₂ can easily diffuse across the biological membranes and damage essential macromolecules.⁵⁶ Alternatively, O₂^{•-} can react with nitric oxide producing highly toxic peroxynitrite.

Several evidence supports the important pathophysiologic role of some trace elements, namely aluminum (Al), mercury (Hg), iron (Fe) and copper (Cu) in promoting oxidative stress by direct and indirect mechanisms. In particular, they act as catalysts for free radical generation and lipid peroxidation due to their ability to exist in more than one valence. For example, the stable redox state of iron is Fe³⁺, but only the bivalent form, Fe²⁺, transferring one electron to O₂, produces O₂^{•-}, ultimately leading to the formation of H₂O₂ (Scheme 1a). Moreover, Fe³⁺ reacts with H₂O₂ by Fenton reaction (Scheme 1c) to give the highly reactive [•]OH that can be also formed through the Haber-Weiss reaction upon interaction between O₂^{•-} and H₂O₂, in presence of Fe²⁺ or Fe³⁺ (Scheme 1d).

The involvement of these trace metals in AD pathogenesis by means of oxidative modifications of Aβ and τ proteins has also been demonstrated thus promoting Aβ deposition, τ hyperphosphorylation, and triggering the subsequent cascade of neurotoxic processes including the autophagic dysfunction as a result of a defensive mechanism aimed to maintain cellular homeostasis during stress conditions (Fig. 22).⁵⁷



Scheme 1. a) O₂^{•-} production by oxidation of Fe²⁺ to Fe³⁺; b) production of H₂O₂ starting from O₂^{•-}; c) [•]OH generation by Fe²⁺ oxidation; d) Haber-Weiss reaction.

Concerning A β oxidative changes, the Butterfield group demonstrated in 1994 the crucial role of the metal-induced oxidation of the sulphur atom of Met35 residue in A β ₄₂, in imparting pro-oxidant and neurotoxic properties *in vitro*, while Greenough *et al.* alternatively proposed a direct binding of metal ions (Cu and Fe) to A β peptide as possible mechanism of A β pro-oxidant activity.⁵⁸

Oxidative stress can also stimulate abnormal τ hyperphosphorylation and aggregation through a direct interaction with GSK-3, over-activated under oxidative stress, and with the inhibitor-2 of phosphatase protein PP2A (I2PPA) (Fig. 22). This effect provides a link between GSK-3 β and oxidative stress, although the relationship of this protein kinase with oxidative stress remains to be further investigated.⁵⁴

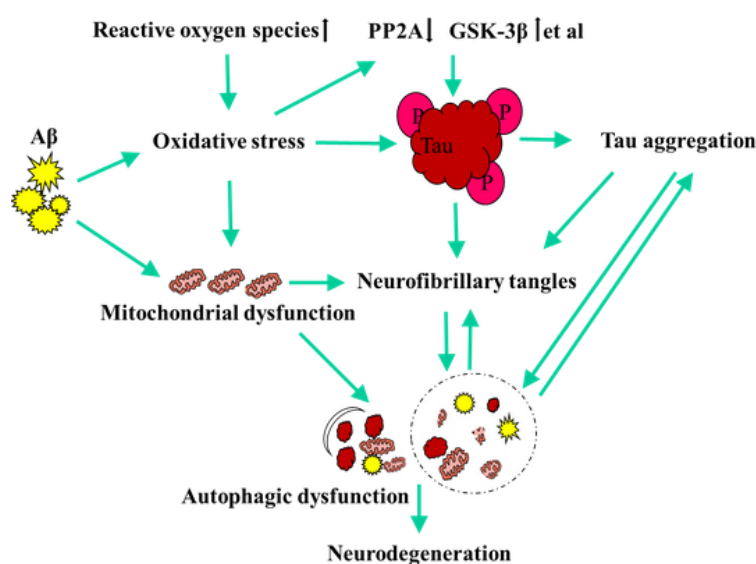


Figure 22. Oxidative stress and mitochondria dysfunction, caused by A β oligomers and ROS, promote τ protein hyperphosphorylation and aggregation in NFTs that together with autophagic dysfunction, lead to neurodegeneration and cell death.⁵⁴

1.6. NEUROINFLAMMATION

The concept that neuroinflammation is crucially associated with AD pathogenesis has been proposed almost two decades ago. Early studies revealed an activation of both the complement and the innate immune systems in brains of AD patients. Indeed, the term “neuroinflammation” is used to describe the inflammatory

response originated in the injured CNS, characterized by an accumulation of glial cells, i.e., microglia and astrocytes, aimed at repairing damaged area. Nevertheless, in presence of a persistent stimulus, a chronic inflammatory condition develops causing cumulative damages. All these events generate complex interactions and feedback loops between glial and neuronal cells, and lead to neurodegeneration.⁵⁹

Microglia can be readily activated producing beneficial functions, essential to neuron survival, through the release of trophic and antiinflammatory factors. However, under particular circumstances, including chronic inflammation, it turn out to be overactivated and it can induce neurotoxicity through the production of pro-inflammatory cytokines, namely IL-1 β , IL-6, IL-12, interferon gamma (INF- γ) and tumor necrosis factor- α (TNF- α), and the synthesis and the release of several cytotoxic factors such as O₂⁻, nitric oxide (NO) and ROS.¹⁸

In AD, microglial cells are able to respond to various stimuli, including A β peptides, APP and NFTs. In the early stages of AD, microglial activation can promote A β clearance, but its persistent activation, increasing the production of A β and reducing its degradation, creates a vicious circle between microglia activation, neuroinflammation, and A β accumulation (Fig. 23).⁶⁰

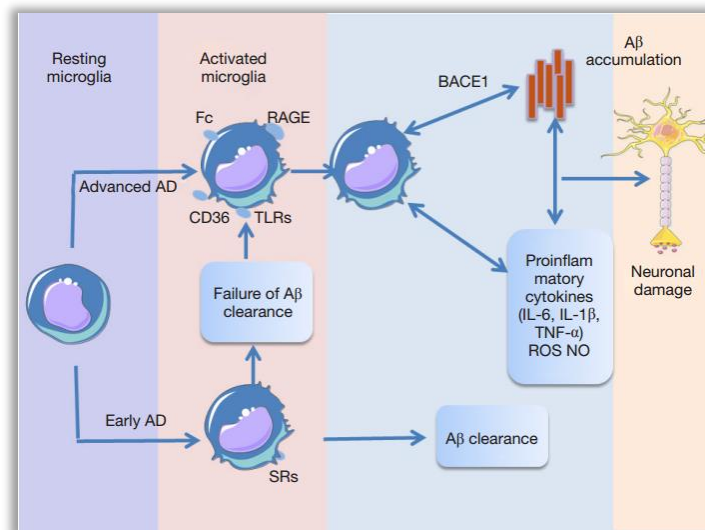


Figure 23. Essential mechanisms associated to microglial activation in AD; the persistent microglial activation by A β produces a vicious circle between microglia activation, neuroinflammation, and A β deposit.⁶⁰

Interestingly, small diffusible A β oligomers activate microglia, leading to a more potent induction of inflammation, whereas fibrillary A β or SPs maintain the chronic inflammation characteristic of the terminal stage of AD pathogenesis. In fact, both pro-inflammatory cytokines and oxidative damage are observed early in AD progression and can be identified prior to fibrillary A β deposition in AD brain. Furthermore, A β oligomers proved to be able to damage microglial phagocytic function, in particular the terminal A β fibrils clearance, providing a probable explanation for the inability of “activated” microglia surrounding plaques to phagocytize A β deposits during the terminal stage of AD.

Taking into account these intriguingly findings, it has been proposed that, in AD, A β oligomers first trigger an acute inflammation, and subsequently A β fibrils sustain a chronic inflammatory environment, which inhibits the activation of the phagocytic machinery, inducing a secondary immune response and worsening brain inflammation. In this context, cytokines, as mediators of the so-called secondary damage, may in turn promote A β production through β - and γ -secretases stimulation and/or reduce A β clearance.⁶¹

Pathological tau aggregates are also able to induce microglial activation triggering the events of the neuroinflammatory cascade. In particular, after neuronal death, these aggregates are released into the extracellular medium causing activation of microglia and generation of a cascade of toxic signals. Moreover, several evidence suggests that a peripheral sustained inflammation can cause breakdown of the BBB, exposure of brain parenchyma to serum proteins, microglia activation and consequent release of inflammatory mediators that can contribute to cognitive decline in AD patients.¹⁸

1.7. NRF2-KEAP1: A NEUROPROTECTIVE SIGNALING PATHWAY

In the early stage of AD pathology, as a result of a defensive mechanism, a battery of genes with detoxificant, antioxidant and antiinflammatory capacities have been found to be remarkably increased, while they decrease at a later stage.

In particular, several postmortem studies of AD patients' temporal cortex and *hippocampus* showed that the percentage of astrocytes expressing heme oxygenase-1 (HO-1), a cytoprotective microsomal enzyme that catalyses the degradation of the heme group to yield biliverdin, iron and carbon monoxide,⁶² was significantly higher than in non-demented individuals. In additional studies, the activity and expression of NAD(P)H: quinone oxidoreductase 1 (NQO1), a detoxifying phase II enzyme that catalyzes the reduction of quinones to hydroquinones and scavenges superoxide molecules, were increased in neurons and astrocytes to reduce the highly oxidant environment typical of AD brains.⁶³ These intriguing findings lead to propose the NQO1 upregulation as a first indicator of the pathology.⁶⁴ Furthermore, most of the postmortem analyses of AD brains report depleted levels of glutathione (GSH: 1 glutamyl-cysteinyl-glycine), the main endogenous antioxidant enzyme responsible for ROS detoxification and regulation of the intracellular redox environment, suggesting a correlation between AD pathology and reduced GSH levels.⁶⁵

Although the mechanisms underlying the fluctuations in these enzymes contents in AD have not been yet clarified, impairment of some pathways involved in their expression might be associated with the progression of the disease. In this context, particular attention was focused on the Nrf2-Keap1-ARE pathway (Fig. 24) recognized as the major regulator of cytoprotective responses to endogenous and exogenous stresses caused by ROS, electrophiles, and inflammation and the main determinant of phase II gene induction, including NQO1, HO-1 and glutathione-S-transferase (GST), a key enzyme that catalyzes the reaction between GSH and nucleophilic compounds.

Nuclear factor erythroid 2-related factor 2 (Nrf2) is a redox-sensitive transcription factor belonging to a protein family characterized by a conserved basic region leucine zipper (bZip) dimerization domain, and ubiquitously expressed in the body, including the CNS. It regulates the basal expression of some cytoprotective genes through interaction with a cis-acting enhancer sequence, namely antioxidant-

response element (ARE) or electrophile-responsive element (EpRE), located in their promoters.⁶⁶

Under basal conditions, Nrf2 remains in the cytoplasm, associated with the actin cytoskeleton through the repressor Kelch-like ECH-associated protein 1 (Keap1), an adaptor protein that, connecting Nrf2 to Cullin (Cul) 3, promotes Nrf2 degradation by the proteasome (Fig. 24). Nrf2 contains two Keap1 binding sites, DLG and ETGE, within the Neh2 regulatory N-terminus domain, suitable for the formation of a complex with two molecules of Keap1 (Fig. 24). This, in turn, is characterized by two known protein-interacting domains: the BTB (bric-a-brac, tramtrack, broad-complex) domain in the N-terminal region and the Kelch repeats in the C-terminal region [Kelch repeat, double glycine repeat (DGR) domain]. The BTB domain mediates Keap1 homodimerization and binding to Cul3, while DGR favors the binding of the repressor with Nrf2 Neh2 domain. Between BTB and DGR is the intervening region (IVR) or linker region (LR) rich in cysteine residues (27 in human Keap1), some of which reactive and critical for Nrf2 modulation. Originally, a study by Dinkova-Kostova *et al.* identified Cys257, Cys273, Cys288, and Cys297 as the cysteine residues of Keap1 mediating Nrf2 activation. Subsequent independent studies confirmed the central role of Cys273, Cys288, and Cys151 in Nrf2 modulation and defined Keap1 as a sensor protein responding to oxidative and environmental stresses through dynamic changes in the reducing status of these cysteine residues.⁶⁷

Under stress conditions and in the presence of different chemicals, including phytochemicals and derivatives (sulforaphane, SFN), therapeutics (oltipraz, auranofin), environmental agents (paraquat, arsenic), endogenous chemicals (NO, nitro-fatty acids, and 4-HNE) and electrophilic compounds, the Nrf2-Keap1 pathway is activated with consequent Keap1 detachment from Nrf2, translocation of the latter in the nucleus and induction of cytoprotective gene expression through Nrf2 binding to DNA assisted by small Maf proteins (Fig. 24).⁶⁸

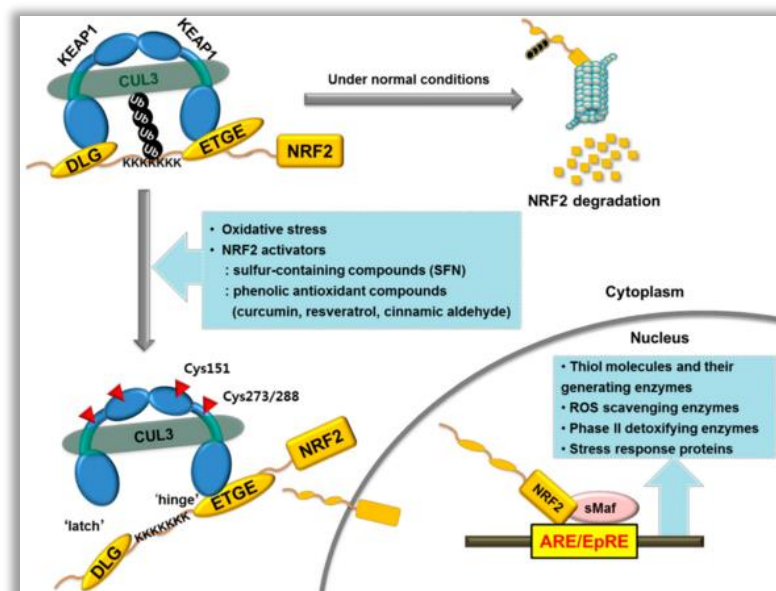


Figure 24. Schematic illustration of the Nrf2-Keap1-ARE/EpRE pathway under basal and stress conditions.⁶⁹

The mechanisms underlying Nrf2 activation are different but can be divided into two principal types:

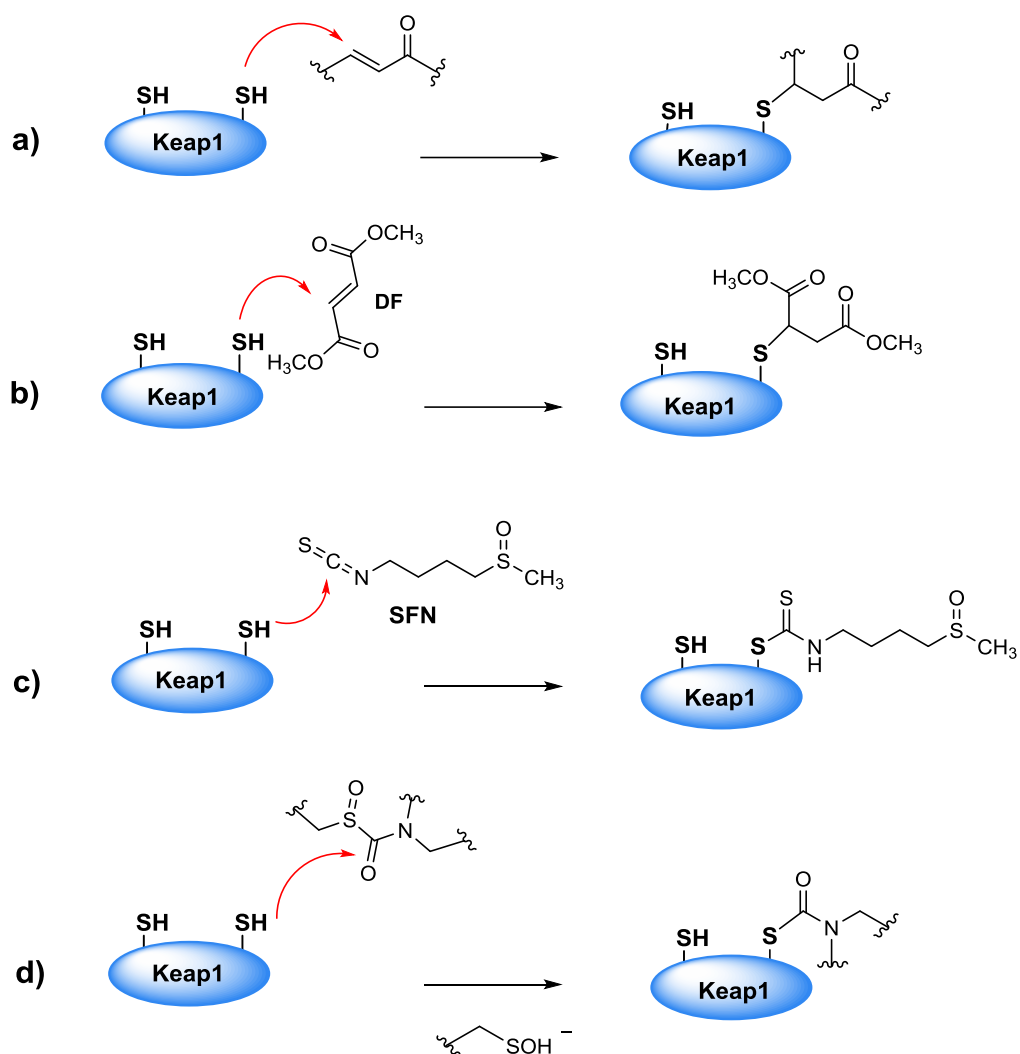
- 1) inducer-cysteine thiol interaction;
- 2) independent thiol cysteine interaction.

The first one is based on a covalent modification of some reactive Keap1 thiol (SH) cysteine functions by electrophilic/oxidant molecules that, inducing a conformational change of Keap1, lead to Nrf2-Keap1-Cul3 complex destruction and to Nrf2 ubiquitination inhibition. These inducers are structurally diverse small molecules of both endogenous (e.g., 15-deoxy- $\Delta^{12,14}$ -prostaglandin J₂, nitro oleic acid, NO, H₂O₂, hydrogen sulphide), and exogenous origin,⁷⁰ and have been grouped into different classes on the basis of the specific type of chemical reaction involved in the process:

1. simple second-order nucleophilic substitution (SN2) alkylating agents;
2. Michael acceptors;
3. bifunctional molecules containing an SN2 alkylator and a Michael acceptor site;
4. thiocarbamoylating agents;

5. oxidant agents.⁷¹

Among them, the second class, including many synthetic, semisynthetic and naturally-inspired electrophilic compounds, mainly bearing an essential α,β -unsaturated carbonyl system, have been investigated. In particular, the discovery that their inducer potency correlates with the capability to react with the reactive cysteine sulphhydryl (SH) functions of Keap1 via Michael reaction (Scheme 2a) was a critical milestone in the understanding of the mechanism of Nrf2 activation.⁷² The Michael addition is properly the reaction by which dimethyl fumarate (DF), a well known Nrf2 inducer, activates several cytoprotective phase II enzymes (Scheme 2b).⁷³ Furthermore, additional studies allowed to elucidate the mechanism underlying the cytoprotective action of some thiocarbamoylating agents, namely isothiocyanates [e.g. SFN, (Scheme 2c)] and sulfoxythiocarbamates, based on reversible and irreversible interactions between their electrophilic moieties and Keap1 cysteine thiol functions, respectively (Scheme 2c and 2d).⁷⁰



Scheme 2. Examples of covalent interactions between Keap1 and different classes of Nrf2 inducers: a) and b) Michael acceptors; c) isothiocyanates; d) thiocarbamoylating agents.

The independent thiol cysteine mechanisms of Nrf2-ARE pathway modulation are various and include modifications of Nrf2 by phosphorylation/dephosphorylation, acetylation/deacetylation, and a directly Keap1-Nrf2 binding destruction through a competitive interaction with the repressor Keap1. Several evidence proposes the implication of numerous intracellular protein kinases, such as PI3K, PKR-like endoplasmic reticulum kinase (PERK), PKC, Fyn kinase, and GSK-3 β , in ARE-dependent gene regulation.

Interestingly, Jain *et al.* reported that activated GSK-3 β phosphorylates Fyn, leading to Nrf2 phosphorylation at Tyr568 and consequent nuclear export (Fig. 25).⁷⁴ Furthermore, *in vitro* studies showed that GSK-3 β is upstream to Fyn in regulation of nuclear export of Nrf2 and that phosphorylation at Tyr216 residue and/or dephosphorylation of Ser9 result in GSK-3 β activation. Thus, GSK-3 β inhibition could offer additional promises for a therapeutic benefit against oxidative stress in AD by affecting the Nrf2-ARE pathway.⁷⁵ Nevertheless, upstream events that control signal transduction from oxidative and electrophilic stress to Fyn remain unknown, and there is no evidence regarding a direct Nrf2 phosphorylation by GSK-3 β .⁷⁶

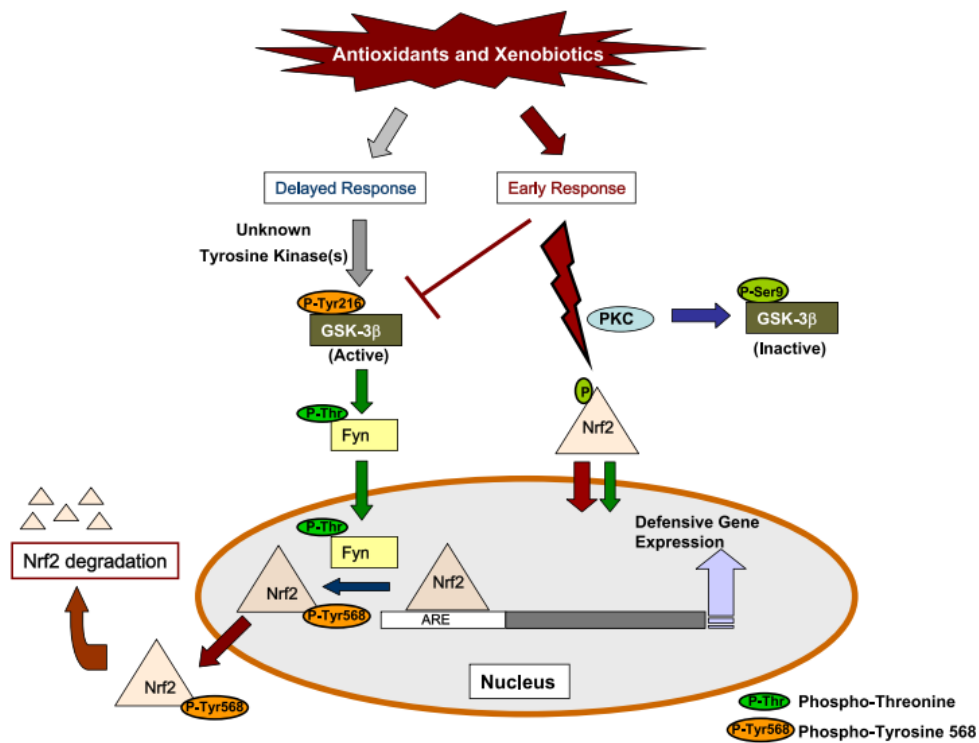


Figure 25. Regulation mechanism of Nrf2 nuclear export via Fyn phosphorylation by GSK-3 β .⁷⁶

1.8. OTHER PROTEIN KINASES INVOLVED IN AD

In recent years, several studies have highlighted the existence of a close association between the aggregation of pathological phosphorylated proteins and

the dysregulation of specific PKs in AD and in other neurodegenerative disorders, including tauopathies, Parkinson's disease (PD) and amyotrophic lateral sclerosis (ALS). In this context, next to GSK-3 β , a validated AD target, CK1 and leucine-rich repeat kinase 2 (LRRK2) are gaining ever-increased attention as intriguing kinases also involved in A β and τ cascades.

CK1 is a Ser/Thr protein kinase, found in plants and animals, whose activity has been detected in various subcellular compartments including cell membranes, cytosol, and nuclei. It has been associated to various biological functions, such as DNA repair, cell morphology, modulation of the metabolic Wnt/ β -catenin pathway, Hedgehog pathway, circadian rhythms and sleep disorders, cancer, inflammation as well as different neurodegenerative diseases including AD, PD, ALS. With the first cloning of CK1 cDNAs, it became evident that CK1 constituted a subfamily of PKs composed of seven isoforms (α , β , γ 1-3, δ and ϵ) characterized by a catalytic domain of about 300 aminoacids which shares more than 50 % sequence identity in the different isoforms. In contrast, CK1 enzymes have highly variable C-terminal domains, that have been implicated in both subcellular targeting and activity regulation.⁷⁷ All the different isoforms act as monomeric and constitutive enzymes, although autophosphorylation of C-terminal residues inhibits the activity of CK1 α , CK1 δ , and CK1 ϵ and helps regulating their catalytic activity. Furthermore, they exclusively use ATP as a phosphate donor, and are cofactor independent proteins.⁷⁸

Several evidence confirms that all isoforms are overexpressed in AD *hippocampus*, nevertheless only CK1 δ and CK1 ϵ proved to be implicated in AD pathogenesis. In particular, CK1 δ (Fig. 26a), whose levels have been found to be more than 30-fold higher in AD brain compared with equivalent controls, demonstrated to play a central role in τ aggregation, phosphorylating τ protein at level of specific residues (Ser202/Thr205 and Ser396/Ser404) responsible of its binding to tubulin. Moreover, CK1 ϵ overexpression (Fig. 26b) proved to favor A β production, as confirmed by the identification of multiple CK1 consensus phosphorylation sites, many of them highly conserved among human, rat, and mouse species, in the intracellular regions of APP, BACE-1 and γ -secretase.⁷⁹

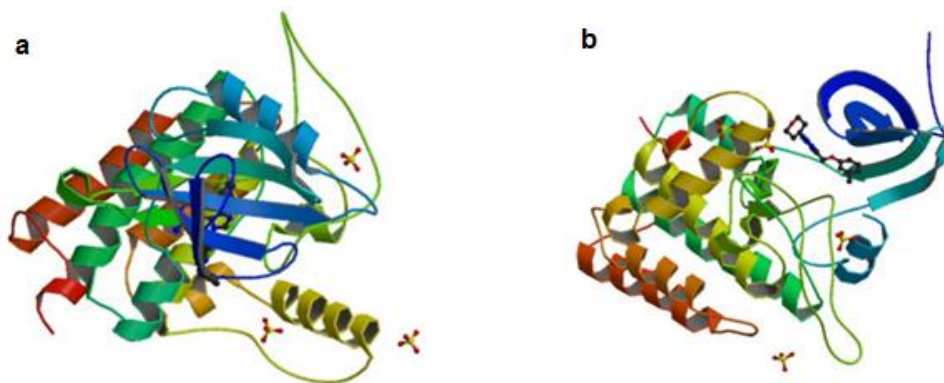


Figure 26. X-ray structure of a) CK1 δ (PDBid: 4TN6) and b) CK1 ϵ (PDBid: 4HNI), each of them in complex with a specific inhibitor.

Taking into account all these exciting findings, CK1, in particular CK1 δ and CK1 ϵ isoforms, appear new promising AD targets, whose simultaneous inhibition could represent an additional therapeutic strategy to affect both A β and τ proteins misfolding and consequent aggregation.

LRRK2 is a 280 KDa multidomain protein that belongs to the ROCO proteins family characterized by the presence of a ROC (Ras complex proteins)/GTPase domain followed by a COR (C-terminal of ROC) domain of unknown function (Fig. 27). In addition to ROC and COR, LRRK2 consists of four more independent domains including akyrin domain (ANK), leucine-rich repeat domain (LRR), kinase domain (kinase) and a C-terminal WD40 domain (Fig. 27). The domains that surrounded the central catalytic tridomain with GTPase and kinase activities are involved in a series of protein-protein interactions.⁸⁰



Figure 27. Domains structure of LRRK2.⁸⁰

To date, LRRK2 is not completely crystallized even though the X-ray structure of some LRRK2 domains, such as ROC domain, characterized by a unique dimeric structure, in complex with GDP-Mg²⁺ has been reported. (Fig. 28).

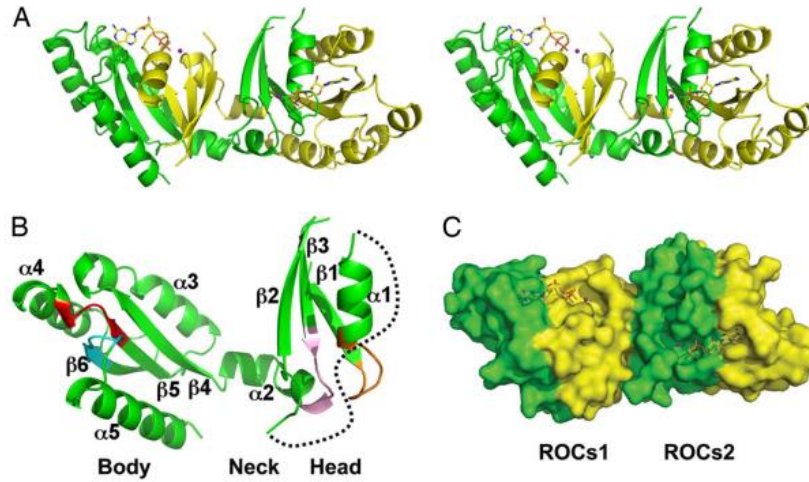


Figure 28. Unique dimeric structure of ROC domain. A) Stereoview of the domain-swapped dimer in which the two single monomers are shown in yellow and in green; B) ribbon representation of a single monomer; C) GDP-Mg²⁺ binding pocket on the surface of the dimer that is contributed from both monomers. The pair of functional units are shown as ROCs1 and ROCs2, respectively.⁸¹

In particular, the structure of the LRRK2 ROC domain shows a unique homodimer with extensive domain-swapping (Fig. 28A). Each monomer contains five α -helices and six β -strands connected by loops, presenting three subdomains: head, neck, and body (Fig. 28B). The head domain and the first half of the neck domain from one monomer couple with the body domain from the other, making two compact units (ROCs1 and ROCs2; Fig. 28C).

LRRK2 is an unusual PK, actually the guanosine triphosphate (GTP) binding to ROC stimulates the kinase activity, with an unclear mechanism. In this context, it is reasonable to postulate that ROC regulates the kinase activity by alternating its conformations through a GTP-bound (active) and GDP-bound (inactive) cycle, suggesting that loss of GTP binding or increasing GTP turnover to guanosine diphosphate (GDP) should result in lowered kinase activity.⁸¹

LRRK2 has been identified as the causal molecule for autosomal-dominant PD and some of its mutations, such as R1441, I1371 and principally G2019S, have been recognized as the most common genetic cause of the malady. Recently, several evidence suggests the important role of LRRK2 in the pathologies induced by abnormal τ phosphorylation, including AD. In particular, in SH-SY5Y cells, a direct interaction between LRRK2 kinase domain and GSK-3 β , enhancing the kinase activity of this latter, proved to induce τ phosphorylation at Ser396.⁸² Interestingly, additional studies showed the higher binding affinity of G2019S-LRRK2 mutant for GSK-3 β and suggest LRRK2 as a positive modulator of neuroinflammation in murine microglial cells, due to its capability to increase the expression of pro-inflammatory mediators, namely TNF- α , IL-1 β , IL-6 and NO, as well as the ability of its mutations to alter the brain microenvironment inducing oxidative stress.⁸³

Taking into account these stimulating results, LRRK2 emerges as a novel GSK-3 β enhancer and a PK able to stimulate microglial inflammatory responses; its inhibition could therefore offer promises to decrease τ phosphorylation and neuroinflammation.

2. *Medicinal Chemistry*

2.1. MULTITARGET APPROACH: IDEAL STRATEGY FOR AN EFFECTIVE AD TREATMENT

Neurodegenerative diseases, including AD, have long been viewed as among the most enigmatic and problematic issues in biomedicine due to the complex and heterogeneous nature of the several networked factors involved in their pathogenesis. In this scenario, the classic “one target, one drug” concept has partially or fully failed, and polypharmacology (Fig. 29) offers a model by which the drug discovery process can evolve to achieve efficacious treatments.^{84,85} In other words, in contrast to the “single-target drug” approach, networked medicines represent an ideal strategy to concurrently modulate different key molecular targets of these multifactorial disorders.⁸⁶

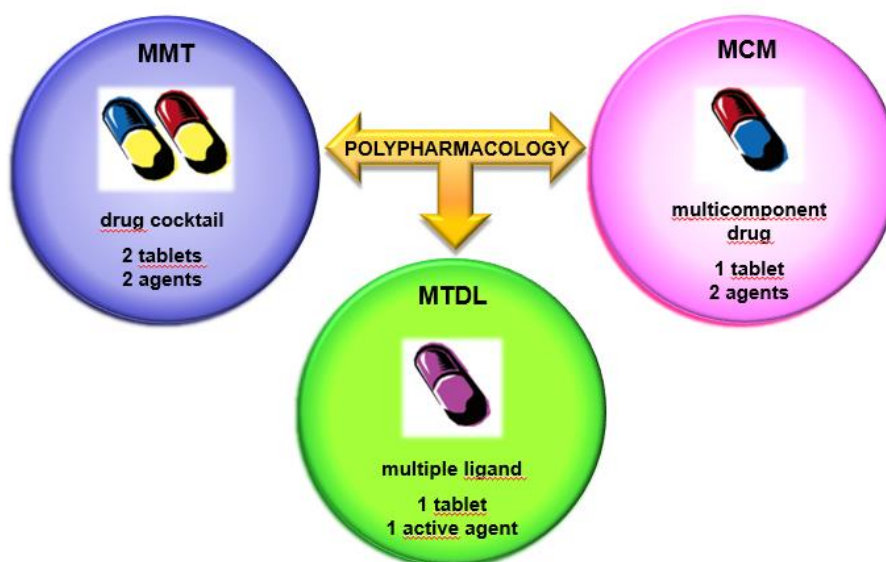


Figure 29. Clinical scenarios for multitarget AD therapy. MMT: multiple-medication therapy; MCM: multiple-compound medication; MTDL: multi-target-directed ligands.

Currently, the definition of “polypharmacology” includes three possible clinical approaches (Fig. 29):

- 1) multiple-medication therapy (MMT);
- 2) multiple-compound medication (MCM);
- 3) multi-target-directed ligands (MTDLs).⁸⁷

The first one, also referred to as a “cocktail” or “combination of drugs”, is based on the administration of two or three different drugs, in the form of two or more individual tablets, which combine different therapeutic mechanisms. However, the benefits of this approach are often compromised by poor patient compliance and possibility of drug-drug interactions (DDI).

A second approach involves the use of MCM, also known as a “single-pill drug combination” or “multicomponent drugs”, in which two or more agents are coformulated in a single tablet with the aim to simplify dosing regimens and improve patient compliance. Although several multicomponent drugs have recently been launched from pharmaceutical industry, there are significant risks involved in their development because clinicians might still prefer prescribing combinations of existing monotherapies that may offer greater dose flexibility and lower cost treatment. Furthermore, DDI are possible and the fixed-dose combination is not practicable in cases in which the routes of administration of two or more starting drugs are different.

An alternative strategy consists in the administration of MTDL, a single chemical entity able to simultaneously modulate several targets involved in the disease.⁸⁷ In general, this approach consists in the combination of various pharmacophores, of different known drugs, in order to obtain a new hybrid molecule able to interact with the selected targets.

In 2005, Morphy and Rankovic introduced the definition “designed multiple ligands” to highlight how the multitarget profile of these compounds was rationally designed and not discovered in retrospect. Afterwards, additional terms to illustrate the same concept were introduced including “multimodal” or “multi-functional” by Moussa Youdim, “dual- and triple-acting agents” by Mark Millan, “hybrid drugs” and “multi-target-direct ligands”. Nowadays, “multitarget drugs” (MTDs) appears a standardized terminology that could also improve the accuracy of future bibliographic searches.⁸⁴

Compared to multicomponent drugs, the multiple ligand approach has a profoundly different risk-benefit profile. Although it is significantly more difficult

to regulate the ratio of activities at the different targets, the clinical development of multiple drugs, in terms of the risks and costs involved, is no different from that of any other single chemical entity. Furthermore, the possible DDI associated to multiple agents administration are lower than cocktails or multicomponent drugs.⁸⁷

Currently, the multitarget drug discovery represents a hot topic within the medicinal chemistry community, as confirmed by the variety of design strategies that has been proposed and successfully employed. In this context, fragment-based and computational strategies are showing promising potential in accelerating and optimizing the MTDs development. In particular, the fragment-based approach, that consists in the step-wise addition of functional groups to simpler low-molecular-weight chemical entities, has gained ever-increased interest both in academia and industry. On the contrary, the application of computer-assisted drug discovery (CADD) to the multitarget drug design (MTDD) is very recent and episodic, although it has been an attractive idea for some time.⁸⁸

In addition to these strategies, the ligand-based approach is still the method of choice in which two starting structures and/or their pharmacophore elements are combined for obtaining a new single molecule with both activities. Alternatively, single fragments, even though interacting with modest affinity with the corresponding targets, can be used as core scaffolds to be properly functionalized in order to generate higher affinity derivatives.⁸⁴

In conclusion, despite resistance of some research groups within the pharmaceutical community, polypharmacology-based strategies are gaining ever-increasing consideration as innovative approach to obtain potentially effective disease-modifying drug candidates for the treatment of multifactorial diseases.⁸⁸

2.2. PRIVILEGED STRUCTURES

Over the past 15 years, the “privileged structure” concept gained particular attention in the discovery and optimization of novel biologically active molecules. In particular, it emerged as a possible way to accelerate the drug discovery process, especially for targets with unknown 3D structure, including G-protein coupled

receptors (GPCRs). Similarly, in the MTDD, the use of “privileged structures” has been identified as a fruitful approach to develop multipotent drug candidates and chemical probes for the treatment of several neurodegenerative disorders, including AD.

Nowadays, a “privileged structure” is defined as a molecular fragment able to interact with more than one biological macromolecule and to exhibit a number of properties associated with drug-like molecules. However, this definition has undergone some refinements since its introduction by Evans and coworkers in 1988, as a single molecular framework able to provide ligands for diverse receptors, with refer to the 1,4-benzodiazepine-2-one heterocycle.⁸⁹

The term “structure” is technically incorrect because it is only a substructure, the essential core of the molecule, to be considered as “privileged”. Although there are no rigorous rules to classify a subunit as “privileged”, it must constitute a significant part of the molecular size to give a big contribution to the molecular interactions. For instance, in a large number of bioactive molecules there are some small groups, such as halogens or amides, that can hardly be considered as “privileged structures” due to their ubiquitous nature and small overall contribution to the binding activities. On the contrary, molecular scaffolds characterized by relatively rigid frameworks, that present optimal functionalities for molecular recognition of the target, could be defined as “privileged structures”. In some cases, these molecular arrangements, probably as a result of the ubiquitous nature of their aromatic ring systems (connected by single bonds or ring fusion) showed versatile binding properties. Thus, the selectivity could represent a potential issue; nevertheless, the functionalization of these rigid frameworks, can allow to confer selectivity to them.

Several “privileged structures” have been identified simply by empirical observations, although, computational techniques helped to recognize them in existing compounds sets.

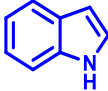
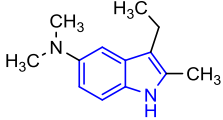
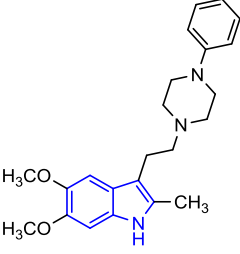
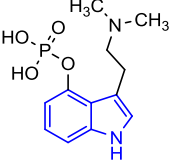
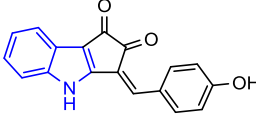
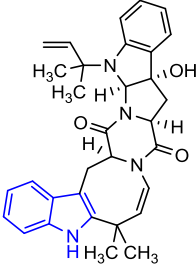
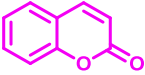
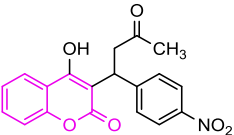
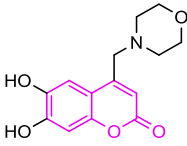
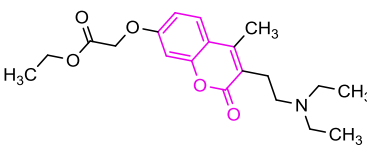
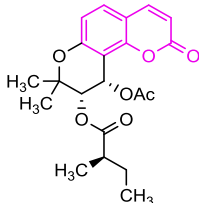
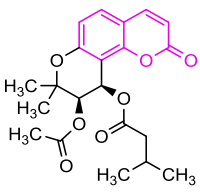
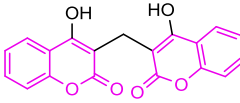
These “privileged structures” can serve as useful starting points for the rational design of focused libraries of bioactive compounds. To this aim, the selection of the

appropriate molecular scaffold for a biological target is of paramount importance because it can increase the hit rates. In this context, a scaffold with a molecular weight within the 100-300 range would be preferred, as it is well known that only a substantial portion of the final molecule represents a “privileged structure”. Furthermore, to obtain analogues with improved pharmacokinetic properties and the desired diversity, i.e. different functionalities hanging from the same central core, the selected scaffold should have a well-balanced polarity profile and 1-3 molecular points suitable for a rapid functionalization. Indeed, the synthetic accessibility of the employed scaffolds is of pivotal importance.⁹⁰

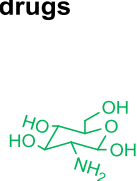
Literature reports several sets of privileged scaffolds that have been identified from molecules synthesized *de novo*, from marketed drugs, as well as from natural products (NPs) that served as inspiration for medicinal chemistry programs (Tables 1 and 2).

Among them, indoles, coumarins, chalcones and carbohydrates (Tables 1 and 2) have attracted particular attention, from both academia and pharmaceutical industry, and have been appropriately used as starting points to develop collections of biologically active analogues.

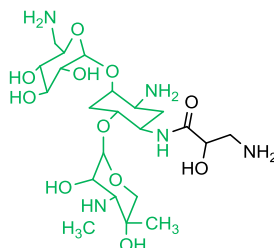
Table 1. Example of significant privileged scaffolds identified in drugs and NPs.

privileged scaffold	chemical structure			
 <p data-bbox="323 819 392 848">indole</p>	drugs	 <p data-bbox="564 680 671 710">Medmain (serotonin inhibitor)</p>	 <p data-bbox="852 680 975 710">Oxypertine (antidepressant)</p>	 <p data-bbox="1171 680 1294 710">Psilocybin (psychomimetic)</p>
	NPs	 <p data-bbox="596 1039 751 1068">Nostodione A source: the terrestrial blue-green algae Nostocommune (mitotic spindle poison)</p>	 <p data-bbox="970 1039 1118 1068">Okaramine N source: Penicillium simplicissium (insecticide)</p>	
 <p data-bbox="292 1576 392 1606">coumarin</p>	drugs	 <p data-bbox="517 1391 687 1420">Acenocoumarol (anticoagulant)</p>	 <p data-bbox="810 1391 927 1420">Folescutol (capillary protectant)</p>	 <p data-bbox="1059 1391 1182 1420">Chromonar (coronary vasodilator)</p>
	NPs	 <p data-bbox="592 1738 687 1767">Visnadin source: fruits of Ammi visnaga and Phlodonocarpus (calcium channels blocker)</p>	 <p data-bbox="847 1738 975 1767">Suksdorfin source: Lomatium suksdorfii (anti-HIV agent)</p>	 <p data-bbox="1091 1738 1214 1767">Dicoumarol source: spoiled hay (anticoagulant)</p>

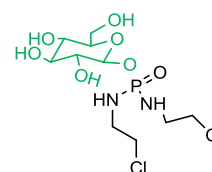
drugs



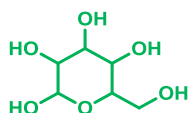
Glucosamine
(antiarthritic)



Isepamicin
(antibacterial)

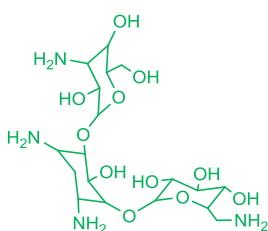


Glufosfamide
(antineoplastic)

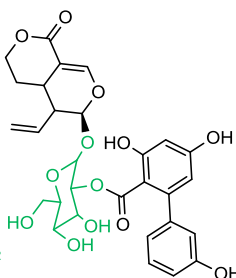


carbohydrate

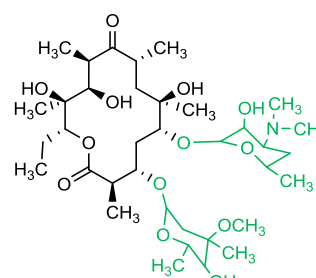
NPs



Kanamycin A
source: Streptomyces
Griseus
(antibiotic)



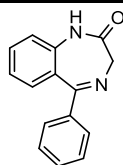
Amarogentin
source: upper parts
of Swertia chirata
(Loganiaceae)
(Leishmanicidal agent)



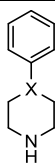
Erythromycin
source: Saccharopolyspora
erythraea
(antibiotic)

Table 2. Examples of other important privileged scaffolds.

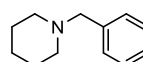
privileged scaffolds found primarily in drugs



benzodiazepine



arylpiperidine: X= CH
arylpiperazine: X= N

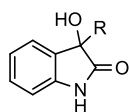


benzylpiperidine

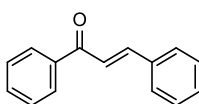


dihydropyridine

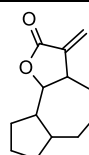
privileged scaffolds in NPs



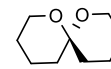
**3-substituted-
3-hydroxy-2-oxindole**



chalcone

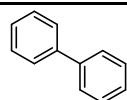


**5-7-5 lactone ring
system**

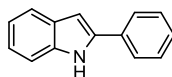


6,6-spiroacetal

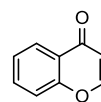
other privileged scaffolds



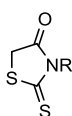
biphenyl



2-arylindole



chromone



rhodanine



benzofuran: X= O; Y= CH

benzothiophene: X= S; Y= CH

benzoxazole: X= O; Y= N

benzimidazole: X= NH; Y= N

The indole scaffold probably represents one of the most important subunits for the development of new drug candidates; indeed, several indole-based derivatives represent useful chemical templates in different therapeutic areas, including the treatment of neurodegeneration, psychiatric disorders and inflammation. The indole core characterizes the neurotransmitter 5-hydroxytryptamine (serotonin) and the naturally-occurring aminoacid tryptophan (Fig. 30) and has been found in a vast number of drugs and biologically active NPs (Table 1) acting as antiinflammatory agents, phosphodiesterase inhibitors, 5-hydroxytryptamine receptor agonists and antagonists, cannabinoid receptors agonists and 3-hydroxy-3-methylglutaryl-CoA reductase inhibitors. Interestingly, many of the indole targeted-receptors belong to the class of GPCRs in which, a conserved binding pocket proved to be able to recognize this structural element.⁹¹ While the indole ring is a ubiquitous heterocyclic structure, literature data indicated that 2-arylindole (Table 2) is scarcely reported among pharmaceutical compounds.⁸⁹

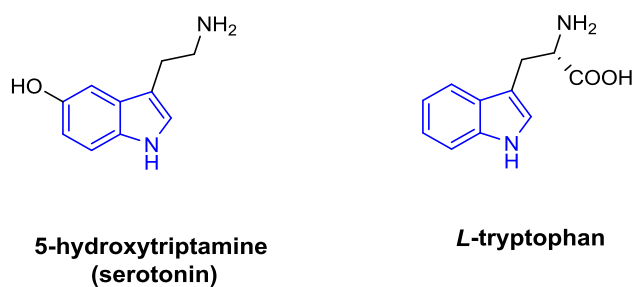


Figure 30. Serotonin and *L*-tryptophan chemical structures.

Coumarins represent an assorted and useful class of bioactive NPs identified in several plant families, as well as in different microorganisms and animal sources (Table 1). Chemically, they are lactones (5,6-benzo- α -pyrone analogues) derived from *ortho*-hydroxy-cinnamic acid, (Fig. 31), characterized by a conjugated electron-rich system with good charge-transport properties. The structural diversity of this family of compounds led to their division into different categories including simple coumarins, furano-coumarins, pyrano-coumarins, phenyl-coumarins, bi-coumarins.⁹² Among them, the simple coumarin and its analogues have attracted particular interest due to their wide range of biological activities namely antiinflammatory, antioxidant, antiadipogenic, anticancer, antiviral, anticoagulant, neuroprotective, and chemopreventive. The simplicity and versatility of this scaffold make it an attractive starting point for a wide range of applications including the design and development of antineurodegenerative agents.⁹³

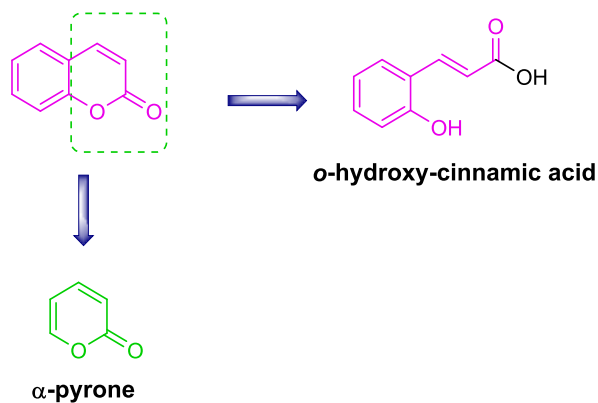


Figure 31. Simple coumarin scaffold.

Furthermore, carbohydrates (Table 1), particularly monosaccharides, represent a very attractive scaffold in drug discovery, due to their favorable properties such as the easy accessibility, optical activity and conformational rigidity, together with stability in gastric acid environment and to glycosidases hydrolysis. Their numerous hydroxy groups can act as vectors for the introduction of properly addressed substituents. Several evidence showed that the appropriate functionalization of the D-glucose (by using diastereomeric and enantiomeric monosaccharide scaffolds) allowed obtaining derivatives able to bind diverse GPCRs and to modulate receptor and receptor subtype affinities.⁸⁹

Chalcones (1,3-diaryl-2-propen-1-ones), identified in a wide range of NPs (Table 2), may also represent very intriguing “privileged structures”. These compounds, also defined as opened chain precursors of flavonoids, are characterized by two aromatic rings (A and B, Fig. 32) connected by an enone linker (Fig. 32), and have been found in a large range of biologically active molecules. Naturally occurring chalcones, and their synthetic analogues, exhibit various activities including antiinflammatory, anticancer, antimicrobial, antiprotozoal, antiulcer, antihistaminic and antimalarial.⁹⁴ Extensive scientific efforts have been directed to the study of the mechanisms of action and the structure-activity relationships of chalcones, in order to prepare libraries of pharmacologically active analogues.

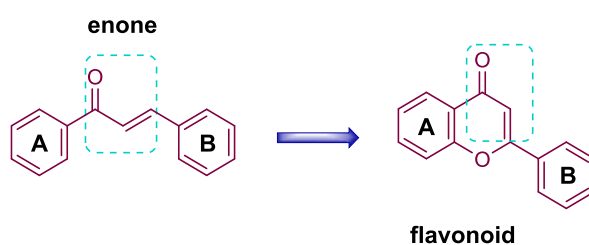


Figure 32. Chalcone and flavone scaffolds.

Analyzing the large amount of privileged subunits recognized between drugs and NPs (Tables 1 and 2), a remarkable overlap among structures of both

classes can be detected, since that the vast majority of the reported scaffolds have members in both groups. This result should not be so surprising because nature frequently repeats itself after the identification of an appropriate solution to a particular biochemical problem, and, obviously, the macromolecular structures in living systems have a high level of non-random patterning. However, there are few examples of molecules synthesized by chemists whose essential cores are not typically obtained from a natural source (Table 2).⁹⁵

2.3. NATURAL PRODUCTS

Despite competition from other “privileged structures”, we have recently seen a real explosion of interest in NPs as excellent source of lead scaffolds for new clinical candidates and drugs. Review of NPs over 30 years, from 1981 to 2010, revealed that approximately 40 % of the developed therapeutic agents approved by FDA were NPs, their derivatives, or synthetic mimetics related to NPs.⁹⁶ Between 2005 and 2010, 19 NPs-based drugs were approved worldwide for the treatment of infectious, immunological, cardiovascular, neurological, inflammatory and related diseases, as well as cancer.⁹⁷

NPs have produced a profound impact on both chemical biology and drug development, as the consequence of the large diversity in their chemical space. In particular, through the natural selection process, they have developed a unique and vast chemical diversity and have been evolved for an optimal interaction with biological macromolecules (targets). In general, these compounds proved to have an enormous potential as:

- 1) essential source for drug discovery;
- 2) inspiration for combinatorial chemistry libraries;
- 3) source of chemical probes for biomolecular functions.

Over the last decades, collections of NPs-inspired small molecules have been designed applying innovative combinatorial techniques, among which the diversity-oriented synthesis (DOS) emerged as valuable strategy to explore the chemical space. In contrast to the traditional target oriented synthesis (TOS), based

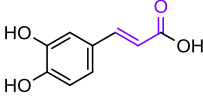
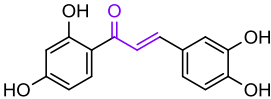
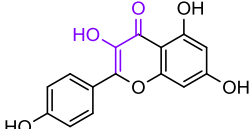
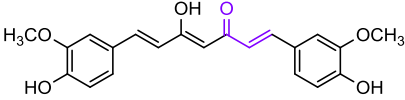
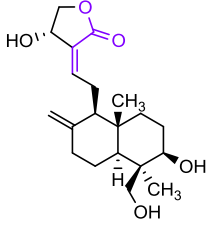
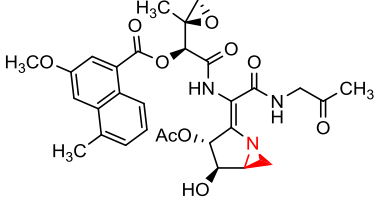
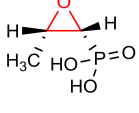
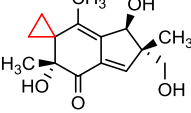
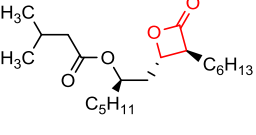
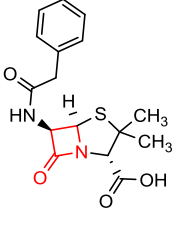
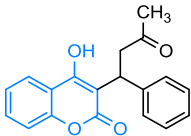
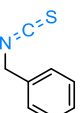
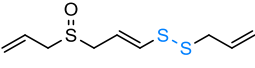
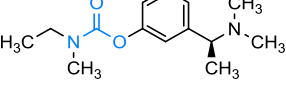
on a retrosynthetic analysis to plan a synthetic route from a complex product to structurally simple building blocks, DOS requires the development of a forward synthetic analysis to support the conversion of simple and alike starting materials into complex and diverse products.⁹⁸

Furthermore, most NPs have been recognized as highly attractive starting points to develop molecular probes for protein activity profiling experiments, by employing their capability to covalently react with several target enzymes. In this context, several evidence led to identify in NPs a large number of structural features such as electrophilic functions suitable for covalent interaction with specific target active sites including different nucleophilic protein residues (Ser, Thr, Cys, Lys and His).⁹⁹

Literature reported lists of electrophilic NPs, whose particular aptitude to covalently interact with nucleophilic species has largely facilitated the identification of the biological targets. In one of these classifications, NPs are grouped depending on the nature of the electrophilic moieties involved in the interaction with the nucleophilic counterparts present in proteins, DNA and other compounds including GSH. Three different categories have been generated (Table 3):

- 1) Michael acceptor systems;
- 2) ring-strained scaffolds;
- 3) other compounds.¹⁰⁰

Table 3. Three different classes of electrophilic NPs.

1. Michael acceptor systems			
			
caffeic acid	butein (chalcone)	kaempferol (flavonol)	
			
curcumin (β -keto-enol form) 1a	andrographolide (α,β -unsaturated γ -lactone)		
2. Ring-strained scaffolds			
			
azinomycin A (aziridine)	fosfomicin (epoxide)	illudin S (cyclopropyl derivative)	
			
valilactone (β -lactone)	penicillin G (β -lactame)		
3. Other electrophilic NPs			
			
warfarin (4-hydroxycoumarin)	benzyl isothiocyanate (isothiocyanate)	ajoene (disulfide)	rivastigmine (carbamate)

The first category comprises carbonyl α,β -unsaturated-based compounds, among which caffeic acid, chalcones, curcumin, etc., whose beneficial biological activities proved to be strictly related to their electrophilic nature as Michael-acceptor systems.¹⁰¹

The second one encompasses all ring-strained electrophiles, from three to five membered rings, namely: epoxides/spiroepoxides, monocyclic and bicyclic aziridines, cyclopropyl derivatives, monocyclic and bicyclic β -lactones and β -lactams. They undergo a ring-opening and, in some cases, a subsequent molecular arrangement after the nucleophilic target attack.¹⁰⁰

The last class includes electrophilic compounds such as: 4-hydroxycoumarins, isothiocyanates, disulfides, carbamates etc., able to form covalent target-adducts by means of different chemical reactions.¹⁰²

In this classification, the interest was focused on well-studied electrophilic compounds, for which, the covalent attachment to target proteins or to binding site residues are known and proceed *via* nucleophilic attack (either via substitution or addition); nevertheless, the literature reports several additional examples of NPs able to form covalent adducts *via* alternative mechanisms including radical-based or redox-based processes.

2.3.1. α,β -unsaturated carbonyl compounds

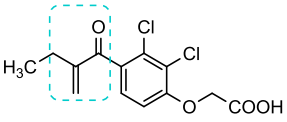
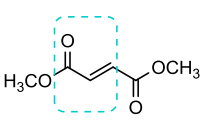
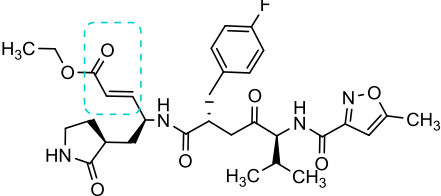
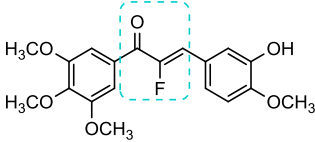
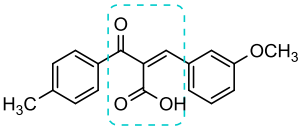
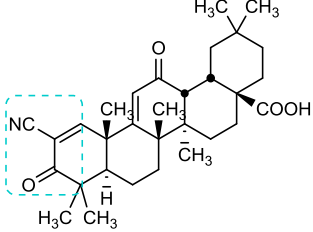
The α,β -unsaturated carbonyl function of certain electrophilic NPs proved to be essential for their biological activity.

For instance, several phytochemicals, especially polyphenols abundant in food plants such as tea leaves, parsley, dill, peppers, onions, kale, cocoa, and cranberries, act as cancer chemopreventive and chemoprotective agents due to their capability to add to the electrophilic β -position of their unsaturated carbonyl system nucleophiles (activity a, Scheme 3). These last consist in a large variety of species characterized by heteroatomic groups containing critical Lewis basic sulfur, oxygen and nitrogen atoms. Among these reactive moieties, the sulfhydryl function of

cysteine residues plays the major role in the Michael-addition-based activation processes.

The α,β -unsaturated carbonyl-based compounds include not only biologically active NPs, but also several chemical entities such as drugs, drug candidates and α -modenones (Table 4). These last are molecules also called α -modified enones, characterized by addressed modifications of the α -position of the unsaturated carbonyl system, aimed at affecting its electrophilicity, thus allowing a fine-tuning of its reactivity.

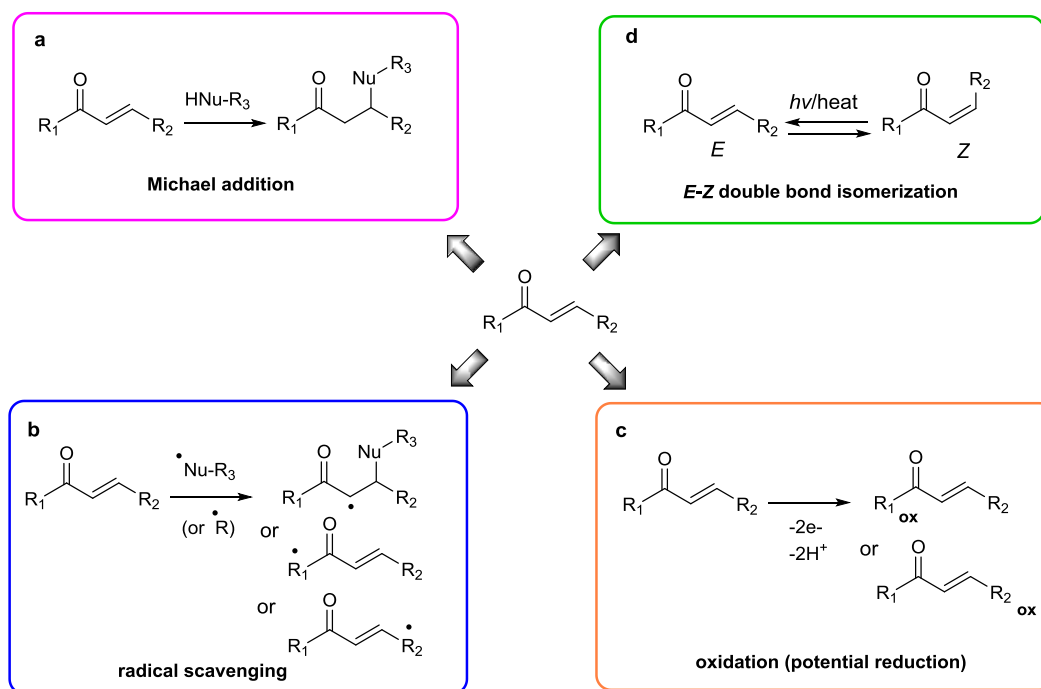
Table 4. Example of synthetic α,β -unsaturated carbonyl compounds.

drug	drug candidates	
 <p data-bbox="331 1106 512 1167">Ethacrynic acid (Edecrin™)</p>	 <p data-bbox="660 1106 852 1167">DF (Panaclar, BG-12)</p>	 <p data-bbox="1027 1106 1145 1167">Rupintrivir (AG7088)</p>
α-modenones		
 <p data-bbox="304 1570 571 1626">Tubulin polymerization inhibitor</p>	 <p data-bbox="667 1570 959 1626">Glutathione S-transferase inhibitor</p>	 <p data-bbox="1082 1570 1235 1626">HO-1 inducer (CDDO)</p>

Interestingly, the α,β -unsaturated carbonyl-based molecules, in addition to the previously described Michael acceptor activity are characterized by three important chemical behaviors namely:

- radical scavenging activity (b, Scheme 3);

- oxidation (reduction potential, activity c, Scheme 3);
- *E-Z* double bond isomerization (activity d, Scheme 3).¹⁰¹



Scheme 3. α,β -unsaturated carbonyl compounds reactions.

In particular, the radical scavenging activity (b, Scheme 3) was envisaged in α,β -unsaturated carbonyl-based compounds containing conjugated π -electron systems, and consists in the capacity to trap free radicals and to stabilize the radical species leading to a decrement of ROS and reactive nitrogen species (RNS) levels. Furthermore, many natural polyphenols bearing the α,β -unsaturated structural motif, including chalcones (e.g., butein, Table 3) and flavonoids (e.g. the flavonol kaempferol, Table 3), can be considered as bifunctional powerful antioxidants. Precisely, their phenolic hydroxy groups, being oxidized to quinones, are essential for the antioxidant behavior (c, Scheme 3), since they prevent or retard the effects triggered by ROS and RNS. In this context, the nature of the R groups is more important than the α,β -unsaturated carbonyl system. In the literature, this

antioxidant action is often referred to as “radical scavenging activity” since the radicals are being reduced to, or “trapped”, as non radical species.

The last reactivity, maybe less frequently addressed, is the unsaturated carbonyl compounds’ potential to show thermal and photoisomerization of their double bond (activity d, Scheme 3). There are different examples of this kind of reactivity in biology, such as the photoisomerization of 11-*cis*-retinal to all-*trans*-retinal when one photon is absorbed in the initial phase of the signal cascade occurring in vision.

From a medicinal chemistry standpoint, the exploitation of α,β -unsaturated carbonyl compounds as potential drug candidates is a controversial topic considering that these electrophiles, as highly reactive and low selective species, can lead to cell damage and cytotoxicity as a result of concomitant covalent modifications of essential biological macromolecules. To avoid this drawback, several efforts have been directed to a fine-tuning of the α,β -unsaturated carbonyl system reactivity, aimed at the improvement of the specificity of action. In this context, different approaches have been applied to predict the reactivity of the α,β -unsaturated carbonyl compounds. Among them, ^{13}C -NMR studies gained particular attention and allowed to correlate Michael acceptor reactivity, reduction potential, and double bond photoisomerization with decreasing values of the α,β -unsaturated carbonyl system electrophilicity. Interestingly, these studies demonstrated that Michael acceptor reactivity correlates to lower E_{LUMO} and E_{HOMO} values, and that the presence of a substituent in the α -position of the α,β -unsaturated carbonyl unit has a strong influence on its reactivity.

In the light of these intriguing results, a recent drug design approach was focused on an appropriate choice of the α -substituent, allowing to manipulate the reactivity of the electrophilic centre, obtaining α -modenones (Table 4) endowed with several promising activities often obtained by modifying inactive NPs.¹⁰¹

2.3.2. Thiol trapping assay

Although Michael acceptors have been avoided in modern drug discovery as thought to exert toxic effects due to their tendency to irreversibly inhibit enzymes

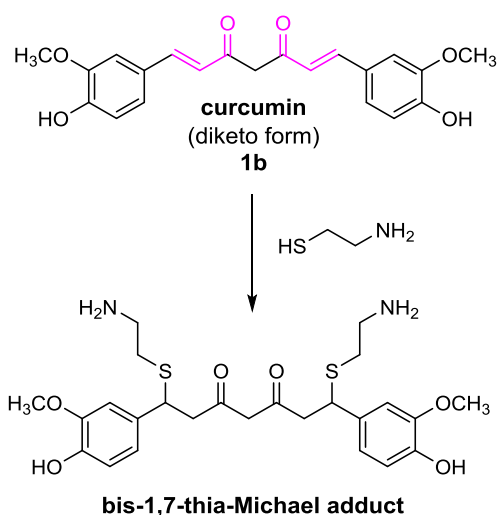
through covalent modification (i.e. trapping of peripheral reactive cysteine thiol functions), the α,β -unsaturated carbonyl group has proven to be essential for disease-fighting activity. Indeed, for this class of compounds the capability to affect many biologically relevant pathways such as Nrf2-Keap1-ARE and the pro-inflammatory nuclear factor- κ B (NF- κ B) has been largely reported (or documented).¹⁰¹

Taking into account the strong correlation between α,β -unsaturated carbonyl compound's bioactivity and reactivity as Michael acceptors, the assessment of their tendency to react with thiols at the β -position of the α,β -unsaturated carbonyl framework, is a very helpful tool to predict their biological activity.

In this context, different methods aimed to identify Michael acceptors and to sort them into reversible and irreversible thiol sinks have been developed, among which the spectroscopic ¹H-NMR-based thiol trapping assay, certainly, plays a major role.

The concept involves the reaction, in a NMR test tube, between the studied electrophile and a reactive thiol-based compound such as cysteamine, β -mercaptoethanol or thiophenol, using DMSO-*d*₆, as solvent. Experimentally, cysteamine (2-aminoethanethiol), 2.0 molar equivalent per each potential electrophilic site, is added to a solution of the α,β -unsaturated carbonyl compound, in DMSO-*d*₆, and the Michael reaction is assessed by ¹H-NMR spectroscopic analysis. The positivity of the assay is evidenced by the disappearance, in the spectra, of the olefin system signals, and the irreversible nature of the addition is also demonstrated by the failure of the reappearance of the characteristic olefin signals upon appropriate dilution with CDCl₃.¹⁰³

This procedure has been described for several electrophilic compounds, such as dienones, α,β -unsaturated esters, amides, lactones, and enones. Among the members of this last class, the symmetric diketo tautomer of curcumin **1b** (see Table 3 for the β -keto-enol counterpart **1a**), one of the most thoroughly investigated and promising dietary NPs, was reported to irreversibly and rapidly react with cysteamine in DMSO-*d*₆ affording the corresponding bis-1,7-thia-Michael adduct (Scheme 4).¹⁰⁴



Scheme 4. Reaction between the symmetric diketo tautomer of curcumin **1b** and cysteamine in DMSO-*d*₆.

2.4. CURCUMIN: A PROMISING THERANOSTIC TOOL FOR AD

The polyphenol curcumin, (1*E*,6*E*)-1,7-bis(4-hydroxy-3-methoxyphenyl)-1,6-heptadien-3,5-dione (diketo tautomer **1b**, Fig. 33), is the primary bioactive compound found in the rhizome of *Curcuma longa* L., an Asian tropical plant belonging to the ginger family (Zingiberaceae), frequently claimed in the ancient medicinal texts of Ayurveda and in traditional Chinese medicine for its therapeutic properties regarding both prevention and cure of a variety of human disorders.¹⁰⁵ Curiously, the rhizome as a dried powder, also called turmeric, is commonly used in sub-continental cooking and represents the main ingredient in all forms of “curry” preparations.¹⁰⁶

Curcuma longa also includes additional curcuminoids, namely demethoxycurcumin [4-hydroxycinnamoyl-(feruloyl)methane, 17 %] and bisdemethoxycurcumin [bis(4-hydroxycinnamoyl)methane, 3 %] (Fig. 33).

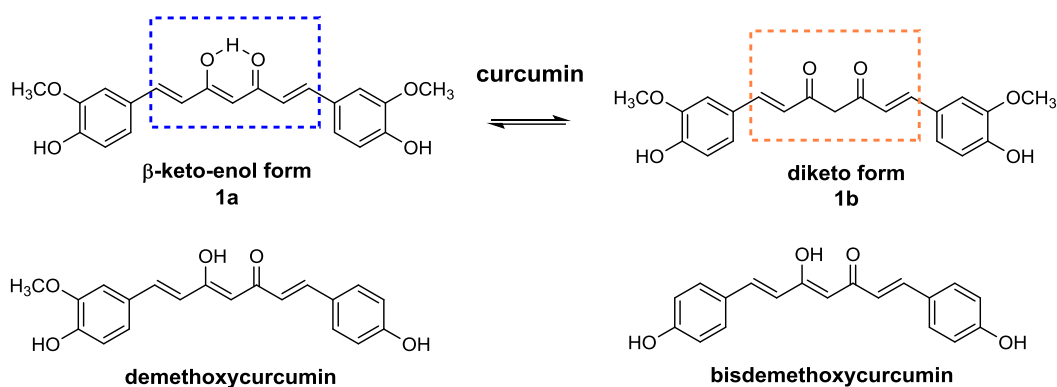
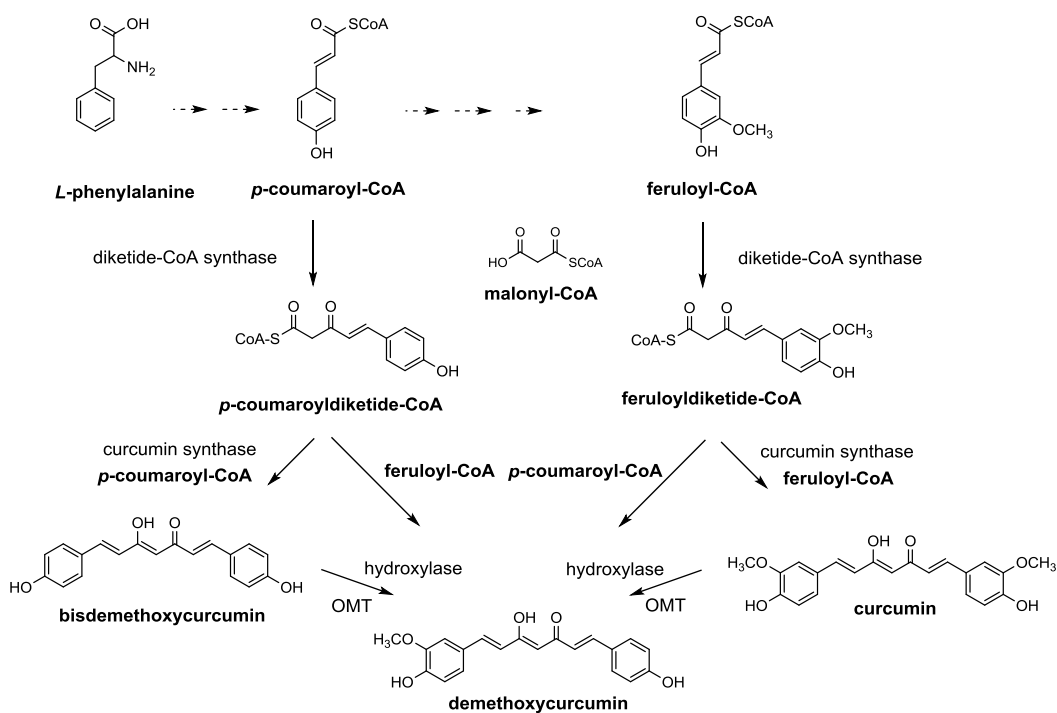


Figure 33. Chemical structure of main curcuminoids found in *Curcuma longa*.

In solution, the chemical structure of curcumin has been represented as an interconverting mixture of the symmetric diketo tautomer (**1b**) and the asymmetric β -keto-enol form (**1a**, 1*E*,4*Z*,6*E*-5-hydroxy-1,7-bis-4-hydroxy-3-methoxyphenylhepta-1,4,6-trien-3-one, Fig. 33). This tautomeric equilibrium proved to partly depend on the polarity and the pH of the solvent. Indeed, nonpolar solvents and pH values above 8 favor the enol form, whereas in polar solvents and acidic or neutral media the diketo tautomer is the principal form.¹⁰⁷ Recently, several theoretical and spectroscopic evidence shows that the β -keto-enol tautomer is the predominant form in a wide range of organic solvents and buffered solutions, due to the stabilizing effect of the intramolecular H-bond on the α,γ -unsaturated-keto-enol moiety (Fig. 33). In particular, this is believed to play a pivotal role in determining the affinity for a wide range of biological targets.⁸

The biosynthesis of curcuminoids is a complex and fascinating pathway, described as a multistep process. It starts from *p*-coumaroyl-CoA, that is in turn produced from the amino acid *L*-phenylalanine, and proceeds with cinnamic acid and *p*-coumaric acid as intermediates (Scheme 5). In this context, alternative biosynthetic routes have been proposed such as that starting from cinnamoyl-CoA according to Kita *et al.*¹⁰⁷



Scheme 5. Curcuminoids biosynthesis pathways starting from *p*-coumaroyl-CoA; OMT: O-methyltransferase.

2.4.1. Curcumin physical-chemical properties

Curcumin, first isolated in 1815 by Vogel and Pelletier and successfully produced in its crystallized form in 1870, is an orange-yellow powder. The molecular formula is $C_{21}H_{20}O_6$, as confirmed by Milobedzka *et al.*, the molecular weight (MW) consists in 368.39 gmol^{-1} , and the melting point (mp) is about 170–175 °C. Chemically, it is composed by two ferulic acid units (bis- α,β -unsaturated β -diketone) connected through a methylene linker, that confers to the molecule electrophilic properties to react with thiol functions.

Curcumin has a good solubility in a large variety of solvents including ethanol, in which it shows a weak green fluorescence, acetic acid, dichloromethane, chloroform, methanol, ethyl acetate, dimethyl sulfoxide, and acetone. In aqueous solution, curcumin stability is pH-dependent: the highest stability is in the 1–6 pH range (e.g. pH found in the stomach or small intestine), although the solubility in this pH range is poor; while at pH values equal or superior to 7 the stability is very

low, as confirmed by *in vitro* studies in which, under physiological conditions (0.1 M phosphate buffer solution, 37 °C, pH 7.2), 90 % of curcumin was degraded within 30 min.^{107,108}

Additional investigations reported that curcumin **1a** degradation has a first-order kinetic, with a fast degradation in the 8.2-8.5 pH range; the main degradation products correspond to four different chemical fragments: *trans*-6-(4'-hydroxy-3'-methoxyphenyl)-2,4-dioxo-5-hexenal, feruloylmethane, ferulic acid and vanillin (Fig. 34). Surprisingly, a lower aptitude for bisdemethoxycurcumin to undergo degradation, with respect to curcumin and demethoxycurcumin, has been noticed, maybe due to the absence of the 3-methoxy groups on the side aryl rings.¹⁰⁷

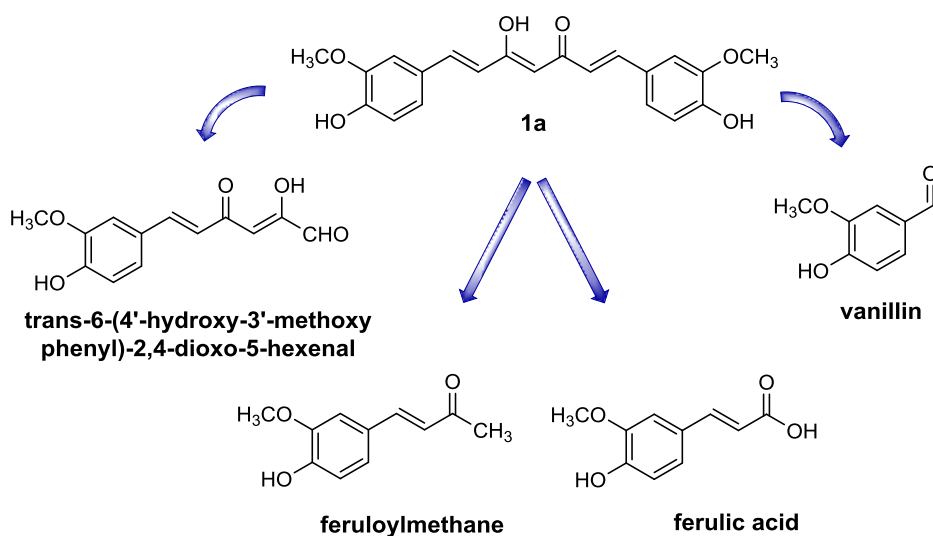


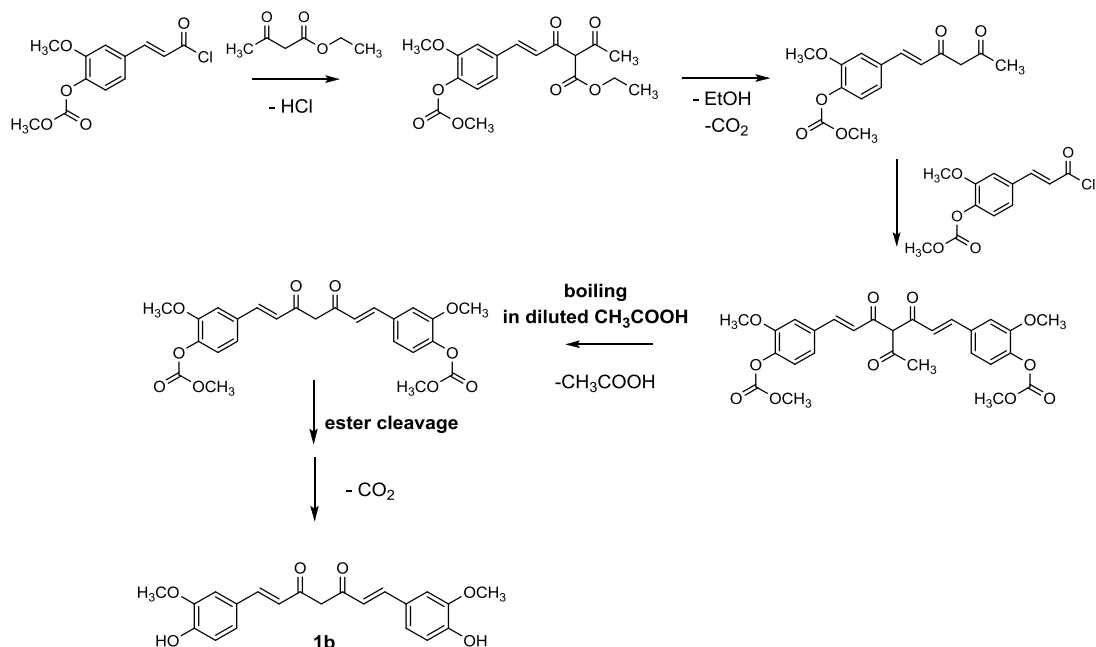
Figure 34. Main degradation products of curcumin **1a** under physiological conditions (0.1 M phosphate buffer, pH 7.2, 37 °C).

2.4.2. Curcuminoids synthesis

The isolation of curcuminoids as standard compounds requires extremely long and expensive extraction procedures. To avoid this drawback, since 1918 several synthetic routes have been developed.

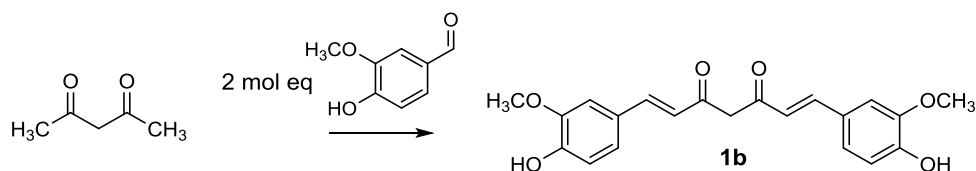
Lampe proposed the first curcumin synthetic procedure (Scheme 6), characterized by five steps, in which a preliminary condensation between ethyl

acetoacetate and carbomethoxy feruloyl chloride, followed by saponification and decarboxylation reactions, gives a first key intermediate. A further condensation with an additional unit of carbomethoxy feruloyl chloride allows to obtain the carbomethoxy diferuloylacetone derivative that, finally, by hot acidic cleavage and subsequent saponification and decarboxylation, affords curcumin **1b** (Scheme 6).



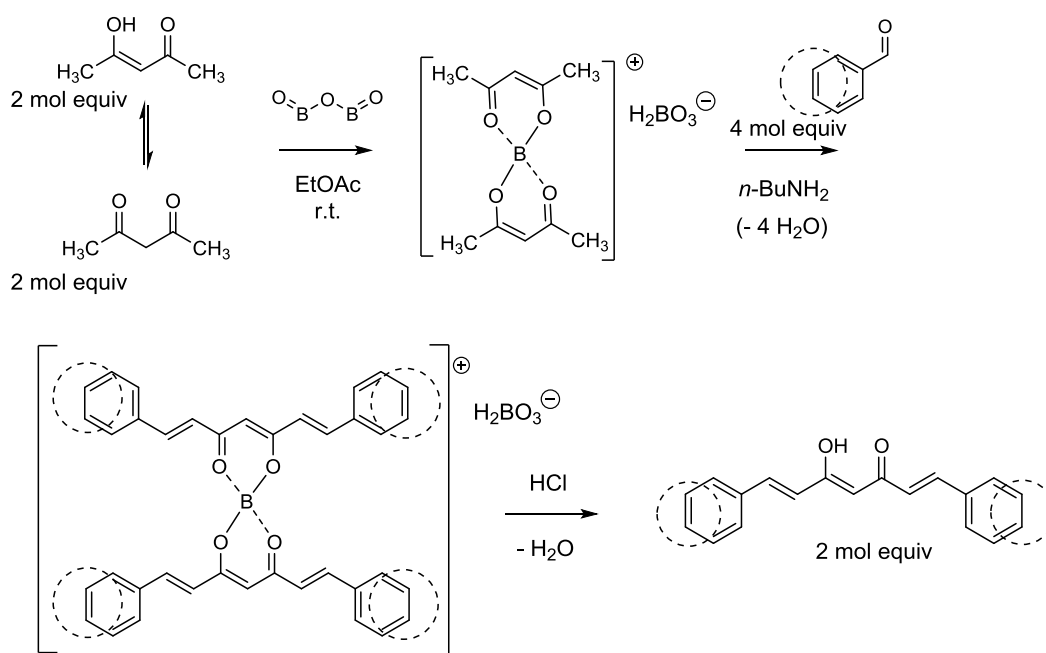
Scheme 6. First synthesis of curcumin **1b** according to Lampe's strategy.

In 1950, Pavolini also synthesized curcumin in a one-step procedure (Scheme 7) by heating vanillin and acetylacetone (pentane-2,4-dione), in 2:1 stoichiometric ratio and in the presence of boron trioxide (B₂O₃), in only 30 min. Unfortunately, with this synthetic route yield is only about 10 %.



Scheme 7. One-step curcumin **1b** synthesis in line with Pavolini.

Finally, in 1964, Pabon developed a new general method for curcuminoids synthesis in which, through introduction of trialkyl borates and *n*-butylamine (*n*-BuNH₂) as reagents, the yield of curcumin was increased up to 80 % (Scheme 8). According to this procedure, acetylacetone is firstly complexed with B₂O₃ in ethyl acetate (EtOAc) to avoid the methylene-centered reactivity toward the Knoevenagel reaction, and to favor the nucleophilic attack at the side methyl groups. The boric complex is then condensed with the suitable benzaldehyde and finally a step-wise addition of trialkyl borate and *n*-BuNH₂ is carried out. Treatment with hydrochloric acid (HCl) allowed complex dissociation, obtaining the desired curcuminoid.



Scheme 8. Curcuminoids synthesis according to Pabon.

Following the described route, Pabon established a synthetic procedure suitable for both symmetric and asymmetric curcuminoid analogues. However, regarding the asymmetric compounds, such as demethoxycurcumin, synthesized almost 20 years later from acetylacetone and equimolar amounts of vanillin and 4-hydroxybenzaldehyde, the use of two different aldehydes gives a complex mixture of curcuminoids, which requires subsequent purification.¹⁰⁷

Currently, the Pabon reaction represents the most followed procedure for the synthesis of curcuminoids and the corresponding derivatives.⁸

2.4.3. Strategies aimed at improving curcumin bioavailability and pharmacokinetics

Curcumin is now recognized as multifunctional compound and “privileged structure”, due to its capability to simultaneously modulate several molecular targets or pathways involved in complex diseases including cancer, inflammation, arthritis, diabetes, nephropathy, acquired immunodeficiency syndrome, chronic bacterial prostatitis, disorders of cardiovascular, gastric, pulmonary and renal systems and those affecting CNS such as AD and PD.^{109,110}

Nowadays, curcumin is used in several countries as a dietary supplement, due to its proven efficacy and safety; nevertheless, its therapeutic use is limited by different drawbacks including the color, the lack of water solubility and the fast degradation, together with a relatively poor bioavailability. Among them, the latter represents the major concern and several strategies, including curcumin conjugation and structural modifications, have been developed in an effort to improve its pharmacokinetic and pharmacological profiles.¹⁰⁹ In this context, apart from the synthesis of curcumin analogues, different adjuvants (e.g. piperine, quercetin, genistein, etc.) have been selected to prevent the rapid metabolism of curcumin by interfering with the enzymes that catalyze its degradation. Furthermore, a large variety of pharmaceutical formulations such as nanoparticles, liposomes, micelles, and phospholipid complexes have been developed to overcome challenges and to ease the translation of curcumin from bench to clinical application.^{110,111}

In particular, several drug carrier-curcumin systems, namely nanocurcumin, poly(lactic-co-glycolic acid) (PLGA) encapsulated curcumin, liposome-encapsulated curcumin (LEC), silica-coated and uncoated flexible liposomes loaded curcumin (CUR-SLs), *N*-trimethyl chitosan chloride (TMC)-coated curcumin liposomes and cyclodextrin encapsulated curcumin (CDC), proved to effectively increase the curcumin bioavailability in animals and in humans.¹⁰⁹ Interestingly, some of these

nanoformulations or nanomedicines have been developed as advanced drug delivery systems in cancer therapy with the aim to increase curcumin's anticancer therapeutic benefits by improving its binding, internalization and targeting of cancer cells and minimizing systemic toxicity. In this scenario, particular attention has been focused on PLGA or poly(caprolactone) (PCL) nanoparticles, liposomal and self-assembly formulations due to their attractive biocompatibility and the intrinsic curcumin fluorescence property has been exploited to study the effective internalization process of curcumin nanoformulations by fluorescence or confocal microscope.¹¹¹

Moreover, in additional investigations aimed at improving the curcumin low water solubility, it has been demonstrated its increase of 12-fold by heat treatment.¹¹²

2.4.4. Structure-activity relationship studies

Nowadays, in addition to the different health benefits that have already been attributed to curcumin, further effects including anticarcinogenic and neuroprotective properties are also being investigated.¹¹³

To date, the exact role of curcumin's functionalities in affecting its physico-chemical properties and pharmacological pleiotropic behavior is far from elucidated. Nevertheless, several structure-activity relationship (SAR) studies revealed some pharmacophore elements strictly associated to its ability to simultaneously interact with different biological macromolecules. In particular, the relatively flexible chain connecting the two hydrophobic phenyl rings has been proposed to be an essential fragment by which the molecule can adopt the suitable conformations for optimal π - π and van der Waals interactions with both the aromatic and the hydrophobic amino acid residues of the protein targets. Furthermore, the hydroxy and the methoxy groups on the side aryl rings, as well as the β -keto-enol central framework, have been identified as the key structural elements involved in strong hydrogen-bonding interactions. Additionally, the α,β -unsaturated ketone moiety acts as high reactive Michael acceptor for the nucleophilic attack by thiol moieties of cysteine residues (Fig. 35).¹¹⁴

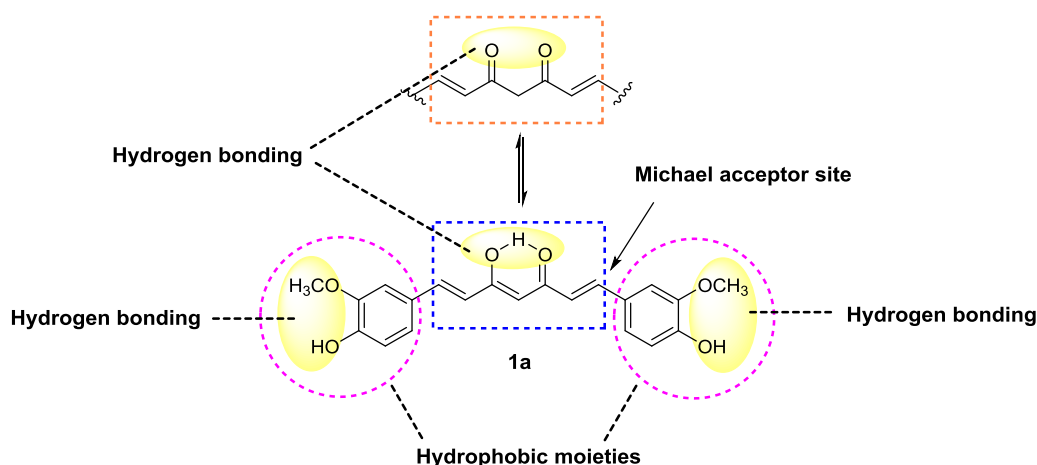


Figure 35. Curcumin's structural elements involved in the interaction with different biological targets.

Interestingly, supplementary investigations aimed at understanding which group is responsible for the different biological effects of curcumin, demethoxycurcumin and bisdemethoxycurcumin confirmed the central role of the methoxy substituent.¹¹⁰

2.4.5. Curcumin neuroprotective potential in AD therapy

Recently, a large number of studies confirmed curcumin ability to modulate a wide range of AD-pathways such as A β and τ aggregation, oxidative stress, and neuroinflammation that may account for its potential neuroprotective properties. Concerning the anti-amyloidogenic effects, evidence suggests that curcumin is able to reduce soluble A β levels, alleviate SPs burden and attenuate A β neurotoxic effects. In particular, it proves to dose-dependently inhibit the A β fibril formation from A β monomers, and to destabilize preformed β -amyloid fibrils with EC₅₀ values ranging from 0.1 to 1.0 μ M. In addition, it inhibits A β fibril aggregation in a dose-dependent manner (0.5-8.0 μ M). The potential mechanism of action through which curcumin hampers A β aggregation and SPs formation could be related to:

- 1) interaction between curcumin's phenolic groups and the aromatic residues of A β fibrils;

2) creation of competitive hydrogen bonds between the hydroxy groups present in the curcumin's β -diketone unit and the β -sheet of A β .

Furthermore, curcumin proves to reduce A β levels via two possible mechanisms, i.e. by delaying the APP maturation and through the suppression of A β ₄₂-induced BACE-1 expression.^{107,115}

On the other hand, the potential effects of this NP on the τ protein pathways have not been so extensively studied: curcumin treatment proves to reduce both mRNA and protein levels of GSK-3 β , and to inhibit the PK activity inducing the enzyme phosphorylation at Ser9 with consequent prevention of NFTs formation and neuroprotection against A β -induced mitochondrial dysfunction.^{115,116}

A large amount of studies also confirmed the antiinflammatory and antioxidant effects of curcumin both *in vitro* and *in vivo*. Regarding the protection against inflammation, several evidence proposed curcumin ability to inhibit (nuclear factor- κ B) NF- κ B, a ubiquitously expressed transcription factor involved in the regulation of numerous pro-inflammatory genes including TNF- α , IL-1 β , iNOS and COX2. Under normal conditions, NF- κ B cannot translocate from cytosol to the nucleus and activate genes transcription, being bound to the inhibitory protein I κ B; the repressor phosphorylation promotes NF- κ B release and its nuclear translocation. In this context, it has been demonstrated that curcumin prevents NF- κ B activation through inhibition of I κ B phosphorylation.¹⁰⁷

Several investigations were also focused on elucidation of the molecular mechanisms associated to curcumin antioxidant effects. Remarkably, it has been shown how curcumin protection includes not only a free radical scavenging activity but also an endogenous induction of the antioxidant defenses.¹¹⁷ Indeed, as a result of its polyphenolic nature, curcumin proved to be endowed with antioxidative properties; for instance, its free radical scavenging activity has been attributed to the phenolic groups, even if recent evidence also supported involvement of the methoxy groups, as well as of the β -diketone framework and its β -keto-enol form.¹¹⁸

Furthermore, several investigations demonstrated indirect antioxidative properties for curcumin, due to its capability to modulate the cytoprotective gene

expression by activation of the Nrf2-Keap1-ARE pathway. The exact mechanism through which curcumin activates Nrf2 is still unclear, but a possible involvement of a Michael addition with some critical cysteine residues of the repressor Keap1 could account for the induction of additional phase II detoxifying enzymes, among which HO-1 and GSH.¹⁰⁷ Moreover, curcumin prevents Nrf2 nuclear export through GSK-3 β inhibition in order to avoid phosphorylation of Fyn protein.¹¹⁹

Interestingly, the cytoprotective effects of curcumin have also been related to its metal ions chelating capacity, in particular Fe²⁺, Cu²⁺, Zn²⁺, largely found in A β plaques and responsible for ROS generation, oxidative stress, and neuronal cell death. ¹H-NMR study showed a directly participation of the curcumin β -keto-enol fragment in metal ion chelation, and the high stability of the formed complexes at physiological pH.^{115,120}

Taking into account the large variety of curcumin neuroprotective effects, its versatile scaffold clearly emerged as promising pharmacological tool for a multitarget AD-modifying treatment. Moreover, from a medicinal chemistry standpoint, the curcumin pharmacophore proved to be an excellent lead for the design of analogues with expanded biological profile.⁸

2.4.6. Curcumin: a fluorescent probe in AD diagnosis

Curcumin absorbs in the visible region and gives fluorescence with low quantum yield¹²¹ due to its unique structural features such as the two symmetric chromophores of the structural motif C=O-C=C and the conjugated double bond that are involved in its characteristic yellow pigmentation.

Recently curcumin, due to its fluorescent properties, emerged as an attractive molecular tool for the diagnosis of AD, and thus it has been employed for molecular imaging (MI).

MI is a fascinating modality that has largely been applied in biomedical research, not only with the aim of characterizing and quantifying biological processes at the cellular and subcellular level in intact living subjects, but also for the early detection of diseases including cancer, inflammation and

neurodegeneration. To achieve these ambitious goals, chemical probes, small molecules able to specifically interact with cellular and sub-cellular endogenous components and to generate a detectable signal, have been exploited.

Generally, imaging modalities can be divided into two categories:

1. primarily morphological/anatomical imaging technologies: such as computed tomography (CT) and magnetic resonance imaging (MRI) characterized by high spatial resolution but with low ability to detect diseases.
2. Primarily molecular imaging modalities: including optical imaging, positron emission tomography (PET) and single photon emission computed tomography (SPECT), which offer the potential to detect molecular and cellular changes associated to pathological conditions, but suffer from a poor spatial resolution.

Combining the strengths of the two classes allows the detection of pathophysiological changes in early disease phases at high structural resolution (for example, PET-MRI technology). Furthermore, each MI modality is based on the use of a particular kind of chemical probe.¹²²

Within the first group, MRI represents one of the most reliable diagnostic imaging modalities, coupling high spatial resolution with exquisite dynamic information and anatomical contrast. Therefore, it is now extensively used to map human brain activity. Similarly to nuclear magnetic resonance (NMR), MRI depend on the relaxation efficiency of protons placed in a fixed magnetic field. In this case, the magnetically active protons are those of the water present in different tissues and the contrast obtained in images is commonly due to their different relaxation rates. So-called contrast agents are need to achieve a contrast enhancement and they include complexes of paramagnetic ions such as gadolinium (Gd^{3+}) and other lanthanide ions, as well as ferromagnetic iron oxide particles and nanoparticles.¹²³

Regarding the MI modalities of the second class, with the advent of laser technology and sophisticated optical devices characterized by high sensitivity, selectivity and simplicity, optical imaging methods have gained ever-increased

attention. In particular, they can be broadly divided into fluorescence and bioluminescence imaging modalities, both of them characterized by easy accessibility, high sensitivity, together with quick and easy performance *in vivo*. In bioluminescence imaging, a chemiluminescent reaction between an enzyme (for example, luciferase) and its substrate (for example, D-Luciferin) generates light. Hence, the externally detected light is an indicator of a biological/molecular process. The bioluminescent reactions are exergonic, with molecular oxygen reacting with luciferase and the substrate to form a luciferase-bound peroxy-intermediate, which, in turn, releases photons over an emission spectrum of 400-620 nm.

Fluorescence imaging exploits the ability of a fluorochrome to absorb energy from an external excitation light of one wavelength and re-emit photons at a longer wavelength of lower energy.

In detail, the absorption of light by a fluorescent molecule yields a singlet excited-state and the key parameters used to describe this process are the absorption maxima (λ_{\max}) and the extinction coefficient at λ_{\max} (ϵ). Fluorescence occurs when this excited state relaxes to the ground state (S_0) through emission of photons. Typically, the emission wavelength is longer than the absorption maximum due to the energy loss stemming from relaxation to S_1 and solvent reorganization around the excited molecule. Interestingly, each fluorophore has a characteristic emission maximum (λ_{em}) and “Stokes shift” consisting in the difference between λ_{\max} and λ_{em} . Fluorophores characterized by small “Stokes shifts” being susceptible to self-quenching via energy transfer are hardly used as labels for biomolecules. Another important fluorophore feature is the quantum yield or quantum efficiency (Φ) that represents the ratio of emitted photons to those absorbed.¹²⁴

Each fluorophore presents specific chemical (e.g., reactivity, lipophilicity, pKa, stability) and photophysical properties (e.g., λ_{\max} , λ_{em} , Φ , etc) based on which it is possible to identify the most suitable probes for fluorescence imaging.

Curcumin, thanks to its intrinsic fluorescence and high binding affinity to SPs and NFTs, has been employed as an *in vivo* dye for MI studies both in animal species and AD patients (Figs. 36 and 37).¹²⁵

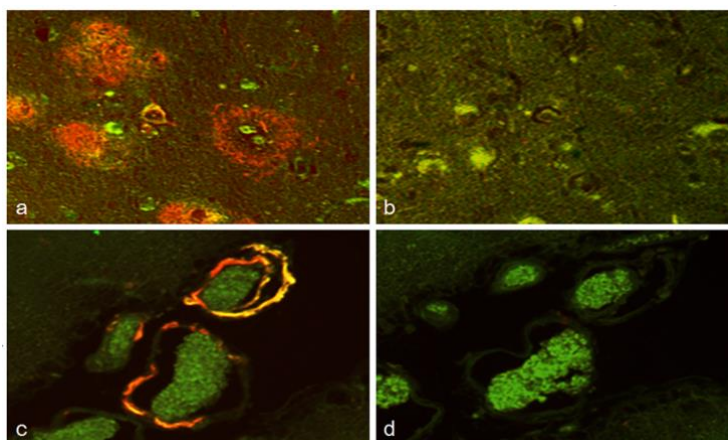


Figure 36. Curcumin stain without formic acid treatment (a and c) and with formic acid pretreatment (b and d). SPs of an AD patient (a and b) and CAA of a Japanese macaque (c and d). By formic acid pretreatment, curcumin-positive SPs and CAA became negative.¹²⁵

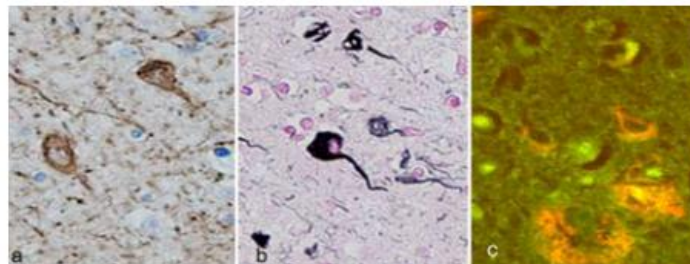


Figure 37. NFTs in the cerebral cortex of an AD patient. a) Immunostain for PHF-tau; b) Gallyas silver stain; c) curcumin stain. Gallyas silver stain was more sensitive than curcumin stain.¹²⁵

Furthermore, as A β plaques have been found in the retina of AD patients, probably at the presymptomatic stage, a study has been conducted in which a systemic administration of curcumin to live AD transgenic mice allowed to improve the early detection of the malady and to monitor the retinal A β plaques (Fig. 38). This evidence validated curcumin as a promising fluorescent probe for the early, non-invasive, and accurate AD diagnosis and therapy assessment.¹²⁶

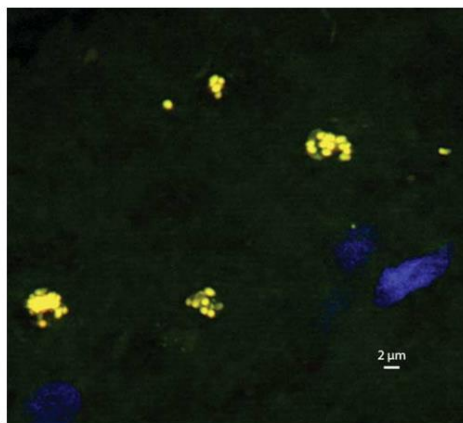


Figure 38. A β plaques (yellow) found in a postmortem retina from an AD patient and identified with curcumin and anti-A β_{42} monoclonal antibody (12F4).¹²⁶

2.5. MOLECULAR IMAGING THERANOSTIC PROBES: A PROMISING FUTURE IN AD TREATMENT

Taking into account the distinct advantages offered by molecular imaging (MI) in living subjects, when compared to conventional *in vitro* and cell culture research techniques in biology, together with the great potential of imaging probes as promising approach to detect neurodegenerative disorders such as AD, the design and development of high quality probes is becoming one of the major subjects of imaging.

Structurally, MI probes are characterized by a signal agent, suitable for producing signals for imaging purpose, a targeting moiety and a linker/delivery vehicle between the targeting moiety and the signal agent.

They represent important tools for scientists and clinicians to better diagnose and understand the diseases allowing a non-invasive diseases' identification as well as the reproduction in the format of images of the pathological information.

Generally, a MI probe with clinical translation potential should have the following features:

1. high binding affinity and specificity to target;
2. high sensitivity;

3. high contrast ratio;
4. high stability *in vivo*;
5. low immunogenicity and toxicity;
6. production and economical feasibility.

The fulfillment of all these requirements in a single chemical entity is very problematic; therefore, several efforts are needed to develop high quality probes for *in vivo* imaging and to understand the molecular biology behind the identified disease.

Unfortunately, several *in vitro* molecular probes are clinically unemployable due to their incapability to cross biological or pharmacological barriers and to reach the specific target with a sufficient concentration. In this context, a possible strategy to improve their pharmacokinetic profile consists in the incorporation of a delivery vehicle into an imaging probe. For example, many nanoparticles, both inorganic and organic, can serve as targeting moieties as well as delivery vehicles.¹²⁷

In traditional approaches, imaging probes and drugs are pursued separately, which can be time-consuming and costly. Recently, to overcome this disadvantage, new approaches, called “theranostic” and based on the development of agents that have potentials for both therapy and imaging, are widely applied with the aim of optimizing the efficacy and safety of the therapy, as well as to rationalize the drug development process.¹²⁸

Nowadays, several examples of theranostic systems have been reported in the literature for the treatment of cancer, atherosclerosis, and gene delivery, while few examples have been described for the neuropathological field. Among them, magnetic nanoparticles (MNPs) as MRI agents and very small superparamagnetic iron oxide particles (SPIONs), able to detect the AD lesions in CNS in animal models, have been recognized as promising theragnostic agents to inhibit A β fibril formation, due to their multitask capabilities (e.g., drug delivery, hyperthermia, and imaging within the same nanosystem).¹²⁹

MNPs consist in a magnetic core (e.g. maghemite) and a biocompatible coating [e.g. polyethylene glycol (PEG)] and can be used as target-specific agents if functionalized, for instance by antibodies incorporation. For example, in a study by Padoslo *et al.*, A β plaques were targeted using a Gadolinium-loaded molecular probe, that after intravenous injection in animals, due to its small size, was able to cross the BBB and specifically bind to the SPs, resulting in their selective enhancement in MRI. Furthermore, an additional investigation of Mahmoudi *et al.* showed “dual” SPIONs’ effects on the fibrillation kinetics, depending on the size, surface area and charge of these small particles. Specifically, lower concentrations of SPIONs proved to inhibit A β fibrillation rate, while higher concentrations enhanced it and positively charged SPIONs promoting the fibrillation process at significantly lower particle concentrations than both negatively charged and essentially uncharged (plain) SPIONs.¹³⁰

Taking into account the great potential of purposely-designed theranostics as promising future to combat neurodegenerative disorders including AD, further investigations and efforts are still urgently needed to access *in vivo* studies.

2.6. CHITOSAN: A VERY ATTRACTIVE AND USEFUL BIOPOLYMER

Chitosan (CS) is a natural non toxic biopolymer, widely recognized as one of the most popular and applied materials for drug delivery and biomedical applications, due to its interesting structural and biological properties, including the cationic character and the solubility in aqueous acidic medium on one side and, most important, the biodegradability and mucoadhesivity on the other. These properties are the result of its peculiar structure, which is composed of repeating alternated units of N-acetylglucosamine and D-glucosamine, linked by β -(1-4) glycosidic bonds (Fig. 39).¹³¹ Similarly to cellulose (Fig. 39), CS is composed by linear β -(1-4)-linked monosaccharides, but is characterized by 2-amino-2-deoxy- β -D-glucan units, whose primary amino groups confer special features, such as the chemical reactivity, that make it a very attractive polysaccharide.

CS is not present as such in nature and thus it cannot be directly extracted from natural resources; it is obtained from deacetylation of chitin (Fig. 39), a naturally occurring and abundantly available biocompatible polysaccharide found in marine crustaceans and characterized by high water insolubility and chemical inertness. Chitin treatment with an alkaline solution converts about 50 % of its acetamide groups ($\text{CH}_3\text{CONH}-$) into $-\text{NH}_2$ functions, allowing to obtain CS.¹³²

From a medicinal chemistry standpoint, both chitin and chitosan have attracted considerable interest due to their wide range of biological properties including antimicrobial, hypocholesterolemic, immunostimulating, antitumor and anticancer effects, antiinflammatory, antioxidant, and Angiotensin-I-converting enzyme inhibitory activities,¹³³ and CS proved to be one of the most promising polysaccharide for applications in pharmaceutical and biomedical fields, in new drug delivery systems (DDSs), or as versatile scaffold for tissue engineering.

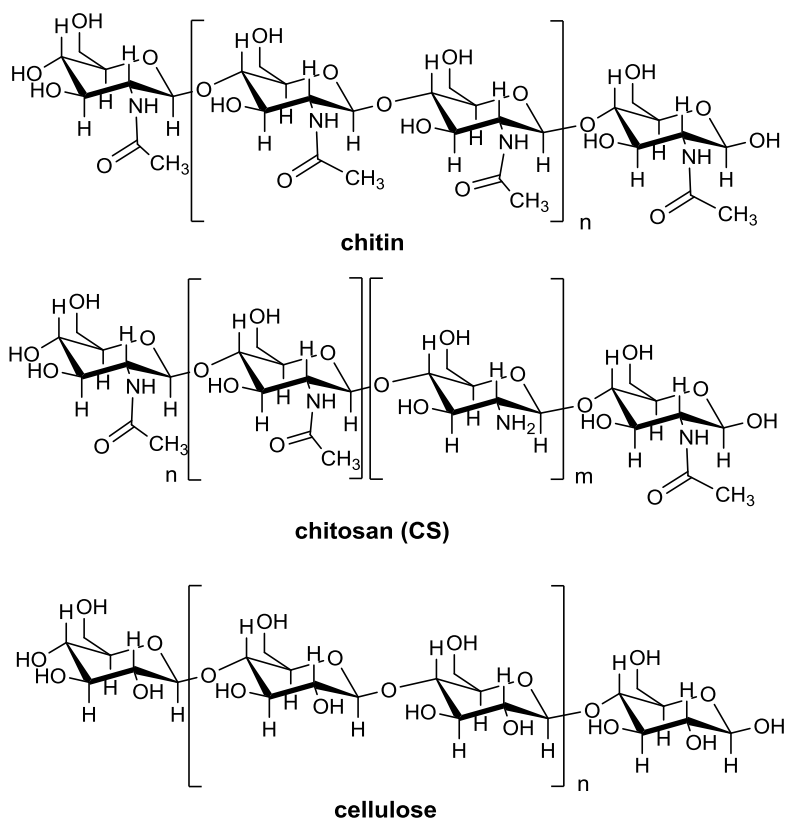


Figure 39. Chemical structure of chitin, CS and cellulose.

2.6.1. Physical-chemical properties

CS is commercially available in various forms including powder, paste, film, fiber, etc.; it is characterized by a MW ranging between 3800 and 20000 Daltons and a degree of deacetylation (% DD) from 66 % to 95 %.¹³⁴

Within these large varieties of species, strong differences in water solubility and mucoadhesivity have been detected, mainly associated to changes in MW and degree of acetylation (% DA) values.

CS is soluble in acidic aqueous media, such as diluted CH₃COOH and HCOOH, due to the protonation of its -NH₂ functions at C-2 positions; on the contrary, it is slightly soluble in organic solvents such as DMSO and *p*-toluene sulfonic acid. Accordingly, aqueous 1% CH₃COOH solution has been selected to test the solubility of different CS samples. In this context, the concentration of acidic solution needed for obtaining CS dissolution depends on the amount of -NH₂ units involved in the ionization process.¹³² Therefore, water solubility is closely dependent on chitosan % DA: highly deacetylated samples (85 %) show a good solubility in media with pH up to 6.5, a more difficult solubilization is observed with the progressive decrement of the % DD, until getting a complete insolubility for degree of acetylation greater than 60 %.¹³¹

CS solubility is a very difficult parameter to regulate, being influenced by additional properties including pH and pKa of the acid selected for protonation, distribution of acetyl groups along the polymeric chain, the intra-chain H-bonds between the hydroxyl functions of the N-acetylglucosamine and D-glucosamine units and, finally, the ionic concentration of the solution. Regarding this last issue, an interesting salting-out effect in excess of HCl (1 M HCl) has been observed, and was exploited to prepare the hydrochloride form of the polymer.¹³²

Regarding mucoadhesivity, several studies confirmed its increment with the increase of the % DD, as this characteristic provides a large number of positively charged -NH₂ groups thus available for the interaction with the negatively charged residues of the mucus, such as the sialic acid units.¹³¹

Currently, various techniques such as IR and UV spectroscopies, elemental analysis, ^{13}C -NMR and ^1H -NMR are employed to characterize the different CS samples, mainly based on the determination of their % DA. In particular, ^1H -NMR in D_2O is largely used for calculating the acetyl content and viscometry and HPLC are employed for the determination of the MW and the molecular weight distributions, respectively.

2.6.2. Applications

During the past 20 years, a substantial amount of works has been published on CS and its uses in the fields of agriculture, industry, and medicine. In particular, it has been described as plant antiviral, additive in liquid multicomponent fertilizers, metal trap in wastewater due to its capability to adsorb several toxic metals including Cu^{2+} , Hg^{2+} , Ni^{2+} and Zn^{2+} .¹³⁵

In the biomedical field, CS has largely been used as biomaterial to prepare hydrogels, films, fibers or sponges owing to its biocompatibility, antibacterial, antifungal and anticoagulant activities, together with its hydrophilicity, introduced by addition of polar groups able to form secondary interactions (-OH and -NH₂ groups involved in H bonds with other polymers). Furthermore, CS proved to be an ideal polymer for developing substratum for skin replacement and for making contact lenses, by exploiting its optical clarity, mechanical stability, oxygen permeability, wettability and immunological compatibility.^{132,136}

At present, the most promising developments are in the pharmaceutical area, particularly in the drug delivery field. Interesting applications may also be seen in cosmetics, where organic acids are usually selected as good solvents and CS is used in the formulation of creams, lotions, and permanent waving lotions, due to its fungicidal and fungistatic properties and to its ability to modulate viscosity.¹³⁶

In the field of drug delivery, CS is extensively used to form matrixes or membranes able to control drug release, thus avoiding repetitive dosing, to produce carriers for the delivery of poorly soluble and/or instable drugs and for biotechnology-based active molecules.

Within this large variety of DDSs, nano and microparticles represent the most usual form of carriers with a chitosan-based composition, mainly aimed at improving the encapsulated molecules performance and effectiveness.^{131,137} Importantly, many works also report the use of chitosan as a coating material of several different core structures, including solid lipid nanoparticles, polymeric nano and microparticles and liposomes.

CS proved to be an ideal polysaccharide for drug delivery due to its high biocompatibility, defined as capability to perform the desired function without eliciting any undesirable local or systemic effects, and biodegradability, as consequence of the fact that, under physiological conditions, its molecular chains can be digested by lysozyme and chitinase. In addition, when oral delivery is under consideration, the hydrolytic activity of the acidic gastric medium can be considered as an extra mean of polymer degradation.¹³¹

In the literature, several chitosan nanoparticles are reported as delivery system for drugs or drug candidates characterized by different biological activities and administration modalities. Among them, chitosan nanoparticle for tacrine and rivastigmine delivery to CNS and for curcumin encapsulation in cancer therapy represent three very attractive examples.

In particular, tacrine-loaded chitosan nanoparticles coated by Polysorbate 80 were prepared and investigated in a pre-clinical study with the aim of improving the bioavailability of the drug in the brain, by promoting its release in a sustained manner, considering the tacrine ability to freely crosses the BBB, as well as prolonging its residence time in blood after intravenous injection.¹³⁸

Similarly, in an additional study rivastigmine-loaded chitosan (CS-RHT) nanoparticles were exploited to improve the bioavailability of the drug and enhance its uptake to the brain via intranasal (i.n.) delivery.¹³⁹

Furthermore, composite nanoparticles prepared by three biocompatible polymers: alginate (ALG), CS, and pluronic F127 were investigated as hydrophobic DDS to cancer cells. Interestingly, in this study curcumin was used as model drug

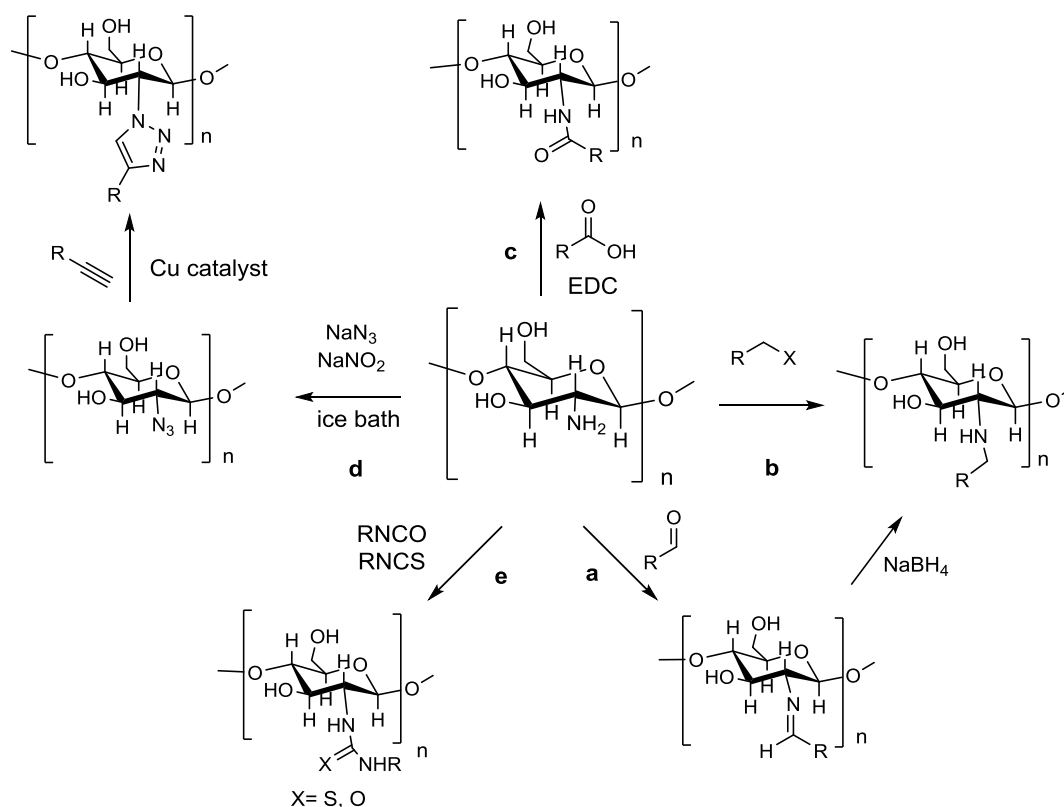
and the curcumin-loaded composite nanoparticles cellular internalization was confirmed from green fluorescence inside the cancer cells.¹⁴⁰

There are several additional examples of CS-based nanoparticles formulated with the aim of improving curcumin bioavailability by its encapsulation and delivery to cancer cells. Among them, cationic curcumin-CS poly (butyl cyanoacrylate) nanoparticles proved to suppress hepatocellular carcinoma growth and to inhibit tumor angiogenesis efficiently *in vitro* and *in vivo*. Furthermore, biodegradable thermoresponsive CS-g-poly (*N*-vinylcaprolactam) (TRC) nanoparticles containing curcumin have also been recognized as promising candidates for cancer drug delivery.¹⁴¹

2.6.3. Chitosan-based bioconjugates

CS, due to its -NH₂ and -OH functions, is an excellent starting point for the design of polysaccharide-based conjugates very useful for drug, gene, macromolecule delivery and tissue engineering, together with additional uses in the biomedical field. In particular, different CS-based bioconjugates have been developed by functionalization of the primary -NH₂ groups through the classical amine reactions such as (Scheme 9):

- a) reductive amination;
- b) *N*-alkylation;
- c) *N*-acylation;
- d) azide formation;
- e) synthesis of urea or thiourea derivatives using isocyanates or thiocyanates.



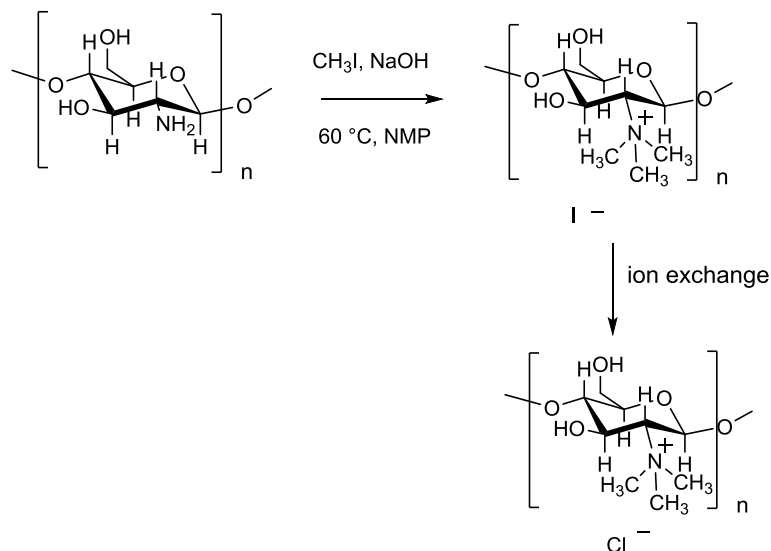
Scheme 9. Possible chemical modifications of the $-\text{NH}_2$ groups of CS.

Several functionalities (e.g. benzaldehyde) have been selectively grafted onto CS $-\text{NH}_2$ groups, by condensation with suitable aldehydes and ketones, under very mild conditions and in aqueous solution, obtaining the corresponding Schiff bases, followed by reduction (Scheme 9, a), to obtain methylenamino derivatives.

Furthermore, with the purpose of obtaining CS-based amphiphilic copolymer with only natural and renewable compounds, different fatty acids were covalently linked to CS through an amide bond in the presence of EDC [1-Ethyl-3-(3-dimethylaminopropyl)carbodiimide] as selective amine coupling agent (Scheme 9, c).

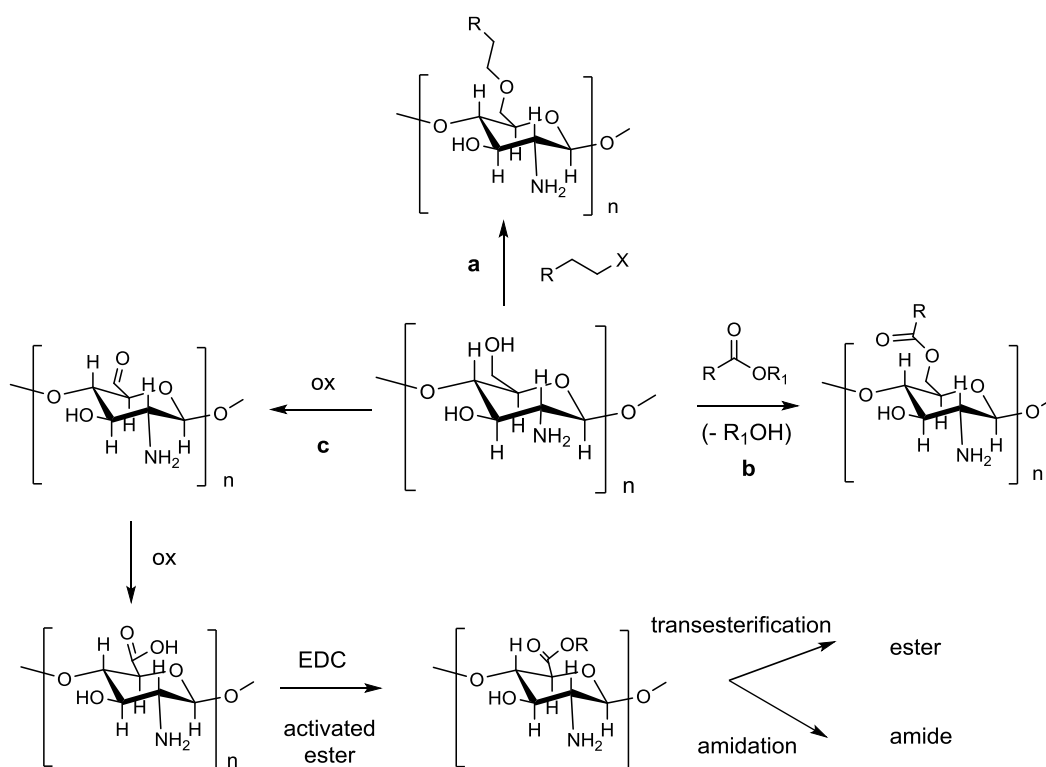
Additionally, the high versatile conjugation reactions represented by the copper-mediated “click-chemistry” (CC) approach, involving an initial conversion of the $-\text{NH}_2$ groups into azide (N_3) followed by reaction with a selected alkyne, allowed to functionalize CS with different moieties, by using a triazole linker (Scheme 9, d).¹⁴²

Curiously, $-\text{NH}_2$ quaternarization, typically using methyl iodide (Scheme 10), represents a common strategy carried out to improve CS water solubility over a wide pH range. Among the quaternarized CS derivatives reported in the literature, *N,N,N*-trimethyl CS chloride (TMC) has been employed for gene therapy applications.¹³⁷



Scheme 10. General synthesis of TMC.

The chemical modifications at the primary and secondary $-\text{OH}$ groups, mainly at the C-3 and C-6 positions, consist in reactions of etherification and esterification (Scheme 11, a and b, respectively). Although these reactions were earlier carried out using strong bases to activate the alcohol groups, recently the use of activated esterification/etherification reagents such as carbonyldiimidazole (CDI) has been reported. Alternatively, the $-\text{OH}$ at C-6 position has been oxidized, in order to obtain an aldehyde- or carboxyl-CS derivative, suitable for further functionalization by condensation or esterification and amidation (Scheme 11, c), respectively.



Scheme 11. Possible chemical modifications when CS is used as an alcohol polysaccharide.

In all described procedures, a fine-tuning of the experimental conditions allows to obtain bioconjugates with a specific degree of substitutions (% DS), and therefore characterized by properties suitable for a wide range of pharmaceutical applications including the preparation of nanoparticles for controlled release and targeted delivery of drug, dyes, proteins, and nuclear materials.

For example, in aqueous solution oleic acid-conjugated CS (oleyl-CS) was used to produce nanomicelles characterized by a hydrophobic core and a hydrophilic shell. Interestingly, the subsequent oleyl-CS conjugation with a dye, called Cy5.5, allowed the encapsulation of oleic acid-decorated iron oxide nanoparticles (IONs) (Fig. 40) as a highly effective dual optical/MR imaging probes for the *in vivo* tumor detection.¹⁴³

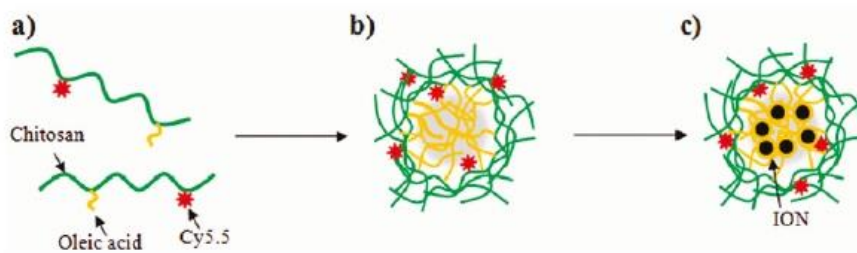


Figure 40. Diagram of ION-Cy5.5-oleyl-chitosan nanoparticles formation: a) Cy5.5 and oleic acid-conjugated chitosan; b) self-assembled nanoparticles for the conjugate; c) ION-Cy5.5-oleyl-chitosan nanoparticles.¹⁴³

Furthermore, in a very attractive study, poly(vinyl alcohol) microcapsules, used as carrier to deliver camptothecin, a poorly soluble anticancer agent, have been reacted with a CS-folate complex, in order to selectively target cancer cells overexpressing the folic acid receptor.¹⁴⁴

The literature also reported a large variety of CS conjugates such as: CS-VitE-acetylcysteine, CS-globotriose and CS-destrano conjugates. Curiously, the first conjugate was used to formulate particles with a hydrophobic core to load drugs like paclitaxel for overcoming the problem of drug absorption from gastric mucosa (Fig. 41). In particular, the choice of acetylcysteine moiety was addressed at improving the mucosal bioadhesion, and Vitamin E was selected to make the inner core hydrophobic.

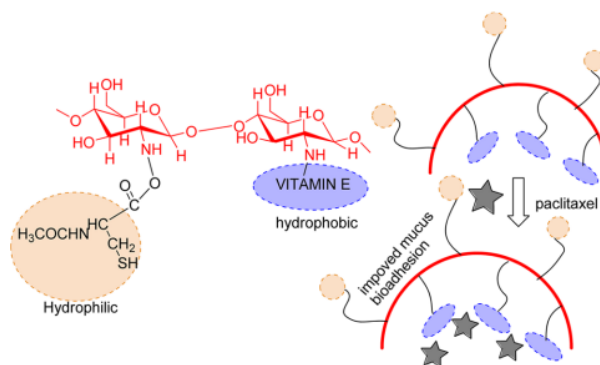


Figure 41. CS-VitE-acetylcysteine conjugate used to improve the bioadhesion to gastric mucosa.¹⁴²

Additionally, CS conjugate bearing the Shiga toxin (Stx) ligand (globotriose) proved to inhibit the Stx-producing *Escherichia coli* (Fig. 42), and dextran and CS conjugates have been employed for making, through thia-Michael addition reaction, hydrogels for the topical loading of vancomycin on the wound surface (Fig. 43).¹⁴²

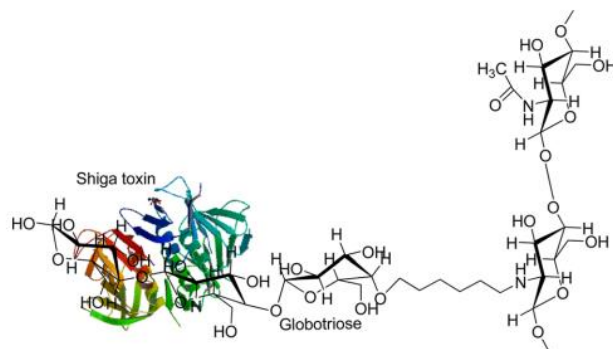


Figure 42. CS glycol-conjugate used as protein carrier, Shiga toxin (*E. coli*).¹⁴²

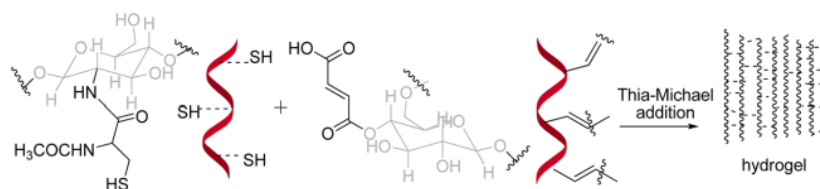


Figure 43. Dextran-CS conjugate used to make hydrogel through thia-Michael addition.¹⁴²

Nowadays, although further investigations will be needed to overcome some CS drawbacks as low solubility above pH 6.5 and pH-dependence of the ionic interactions, the wide range of pharmaceutical and therapeutic application of CS-based conjugates confirmed CS as versatile and functional biopolymer.

3. *Aim of the work and Chemistry*

3.1. DESIGN OF CURCUMIN-BASED COMPOUNDS

The heterogeneous nature of AD directed attention to polypharmacological strategies and multitarget drugs that, acting on several targets involved in the pathology, could offer promises to achieve a successful treatment. In this scenario, the central roles of A β aggregation and τ hyperphosphorylation in AD pathogenesis, together with the molecular interplay between A β and τ proteins in causing synergic toxicity, led to recognize BACE-1 and GSK-3 β as two validated targets. The simultaneous inhibition of these enzymes represents a promising therapeutic modifying strategy, able to halt the disease progression.

Although BACE-1 and GSK-3 β are structurally unrelated enzymes and greatly differ in both three-dimensional structures and binding site topologies, we rationally envisaged the 5-hydroxy-1,7-diarylhepta-1,4,6-trien-3-one framework of curcumin **1a** (Fig. 33), as essential structural element for their concurrent modulation. In particular, the curcumin β -keto-enol central core looked suitable for the contact with BACE-1 catalytic dyad (Asp32 and Asp228), whereas the highly electrophilic α,β -unsaturated carbonyl system, a well-known Michael acceptor system, seemed appropriate to react with the crucial Cys199 residue of GSK-3 β hinge region.

To validate our hypothesis, the interactions of curcumin **1a** with the binding pocket of both targets (Figs. 44a and 44b) were investigated by docking simulations from which clearly emerged how:

- 1) in the BACE-1 catalytic pocket (Fig. 44a), the central curcumin core was hydrogen bonded to the crucial Asp32 and Asp228 residues, while the side aryl rings established contacts with Tyr198, Lys224, and Tyr71.
- 2) In the GSK-3 β binding site (Fig. 44b), the central β -keto-enol function participated in a H-bond with Tyr134 and Val135, and the two aryl functions contacted Lys85, Glu97, and Arg141, Glu173, respectively.

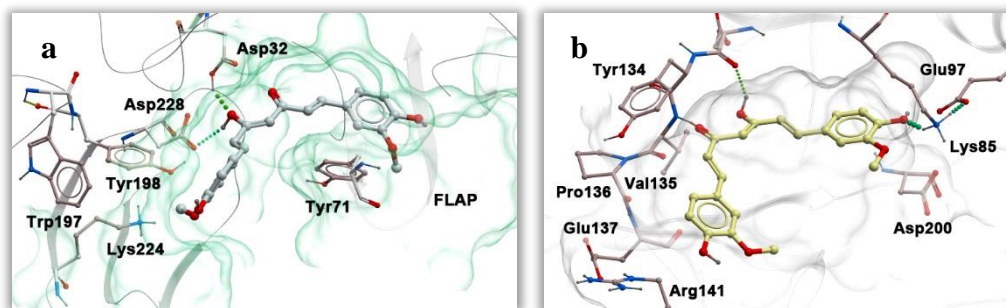


Figure 44. a) Curcumin **1a** docked into the catalytic region of BACE-1; b) curcumin **1a** docked into the binding site of GSK-3 β .

Furthermore, curcumin **1a** capability to inhibit both enzymes was established by *in vitro* assays, in which a moderate potency against BACE-1 (in our *in vitro* assay no inhibition up to 3 μ M) and a micromolar inhibitory activity (IC_{50} = 17.95 μ M) on GSK-3 β were observed.

Taken together, these exiting preliminary results confirmed the suitability of the curcumin scaffold for the development of effective dual BACE-1 and GSK-3 β inhibitors, and encouraged us to design and synthesize a small library of novel curcumin-based analogues (**2-17**, series Ia, and **18-21**, series Ib, Fig. 45, Tables 5 and 6, respectively). In particular, following a drug design approach aimed at exploring the chemical space of the two selected targets and performing preliminary SAR studies, the versatility of the curcumin pharmacophore was exploited by introducing different chemical moieties on the side aryl rings of the main scaffold, while the central 5-hydroxyhepta-1,4,6-trien-3-one fragment was retained. The choice of the substituents was mainly addressed to favor the crossing of the blood-brain barrier (BBB), as this pharmacokinetic property represents an essential requirement for drugs targeting CNS.⁸

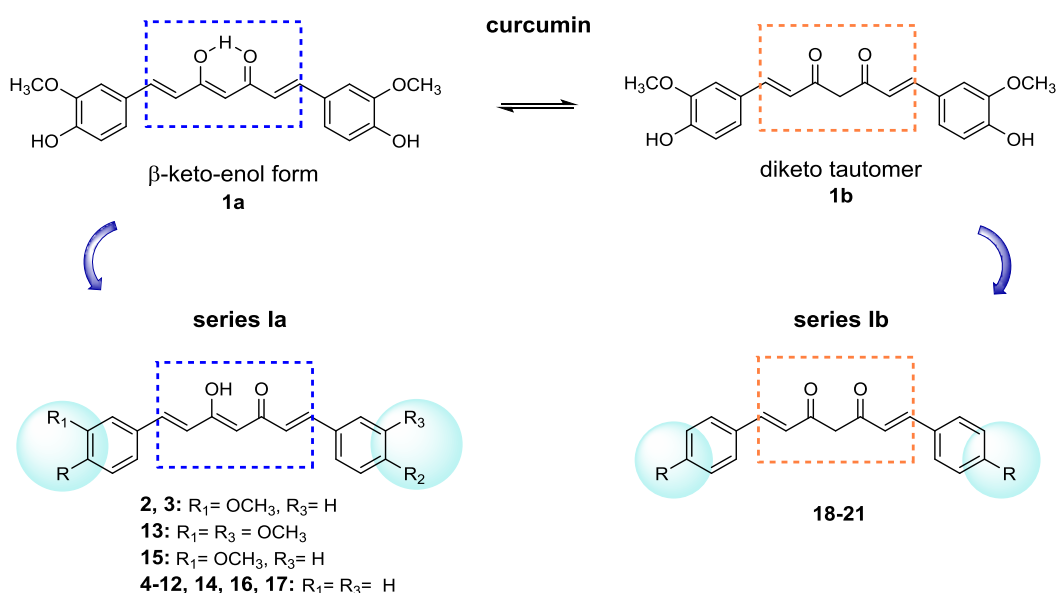


Figure 45. Design strategy for series Ia and Ib.

Furthermore, aiming to improve the BBB crossing of several lead compounds of series I, that demonstrated a border-line behavior, and to explore the chemical space of both targets, two new series (IIa and IIb, Fig. 46, Tables 7 and 8, respectively) were developed, and a number of curcumin-based analogues were obtained performing a CC approach (1,3-dipolar cycloaddition). In particular, in series IIa some selected substituents (among them the aryl functions that in series Ia allowed to effectively inhibit the two targets) were introduced on the curcumin side aryl ring(s) by using a triazole linker. Thus, series IIa consists of symmetric compounds **27-31** and of asymmetric analogues **32-38** (Fig. 46). Analogously, the application of the same CC strategy at the 4-position of the curcumin scaffold, afforded series IIb (derivatives **52a,b-54a,b**) as couples of β -keto-enol tautomer and the corresponding diketo counterpart in a different stoichiometric ratio (Fig. 46).

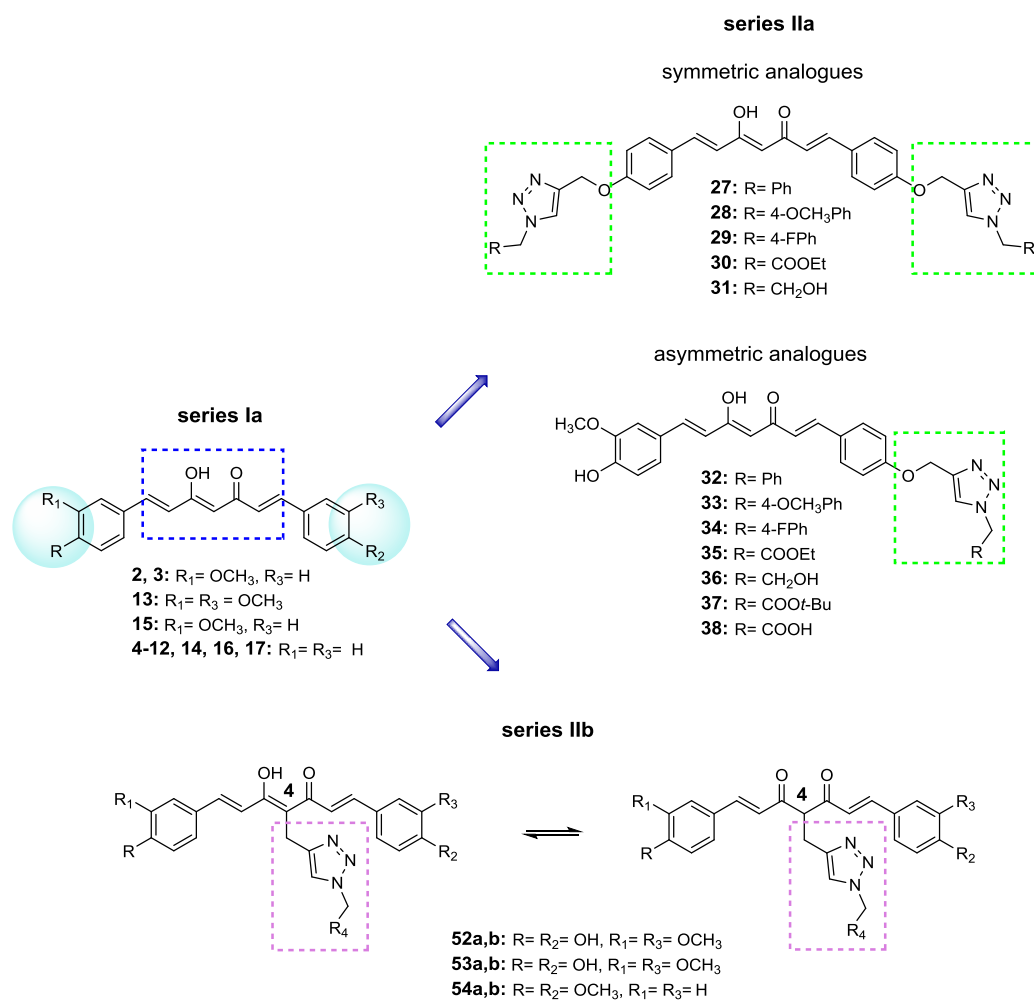


Figure 46. Design strategy for series IIa and IIb.

Curcumin's poor bioavailability represents one of the most important restrictions for its therapeutic use. In the medicinal chemistry field, a promising strategy to overcome this drawback consists in the development of analogues bearing different moieties able to well-balance the hydrophilic/hydrophobic properties of the whole molecule. Therefore, in an effort to improve the pharmacokinetic profile of the lead compounds **5** and **8** of series Ia (Fig. 45), series III (Fig. 47, Table 9) was designed and synthesized by introducing in the 4-position of the curcuminoid scaffold, through a methylene spacer, a carboxylic moiety

(**61a,b**), ethyl (Et) and *tert*-butyl (*t*-Bu) esters (**58-60**), and a 2-aminoethanol-based amide function (**62**). (Fig. 47).

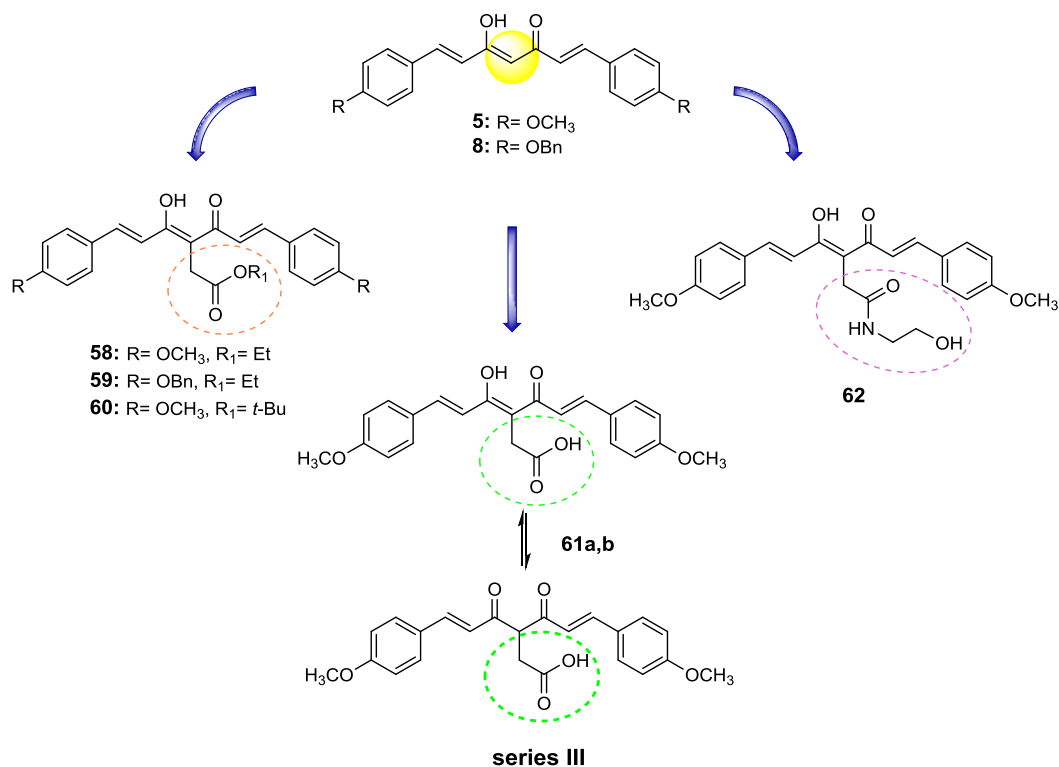


Figure 47. Design strategy for series III.

At this point of my PhD work, starting from the previously emerged lead compounds, a new series of curcumin-based derivatives was developed aimed at expanding the neuroprotective profile, by engaging different targets. In this context, the ability of curcumin to exert neuroprotection through the activation of the Nrf2-Keap1-ARE signaling pathway, thanks to its electrophilic character, was considered an attractive effect. Thus, two series (IVa and IVb, Fig. 48, Tables 10 and 11) of derivatives were designed and synthesized, in which chemical modifications were addressed to affect the electrophilicity of the α,β -unsaturated carbonyl fragment, as the fine-tuning of this reactivity could allow obtaining an improvement of the specificity of action. In particular, in series IVa curcumin was bis- or mono-functionalized by introducing some electrophilic functions such as bromo,

boronate, or acrylate on the side aryl ring(s). Symmetrical **66** and **67** and asymmetric derivatives **68-72** were thus obtained (Fig. 48). In series IVb, the insertion of the acrylate function, molecular fragment found in the potent Nrf2 modulator DF, was performed in the 4-position of the curcumin core, allowing to obtain the hybrid compounds **74-78**. (Fig. 48).

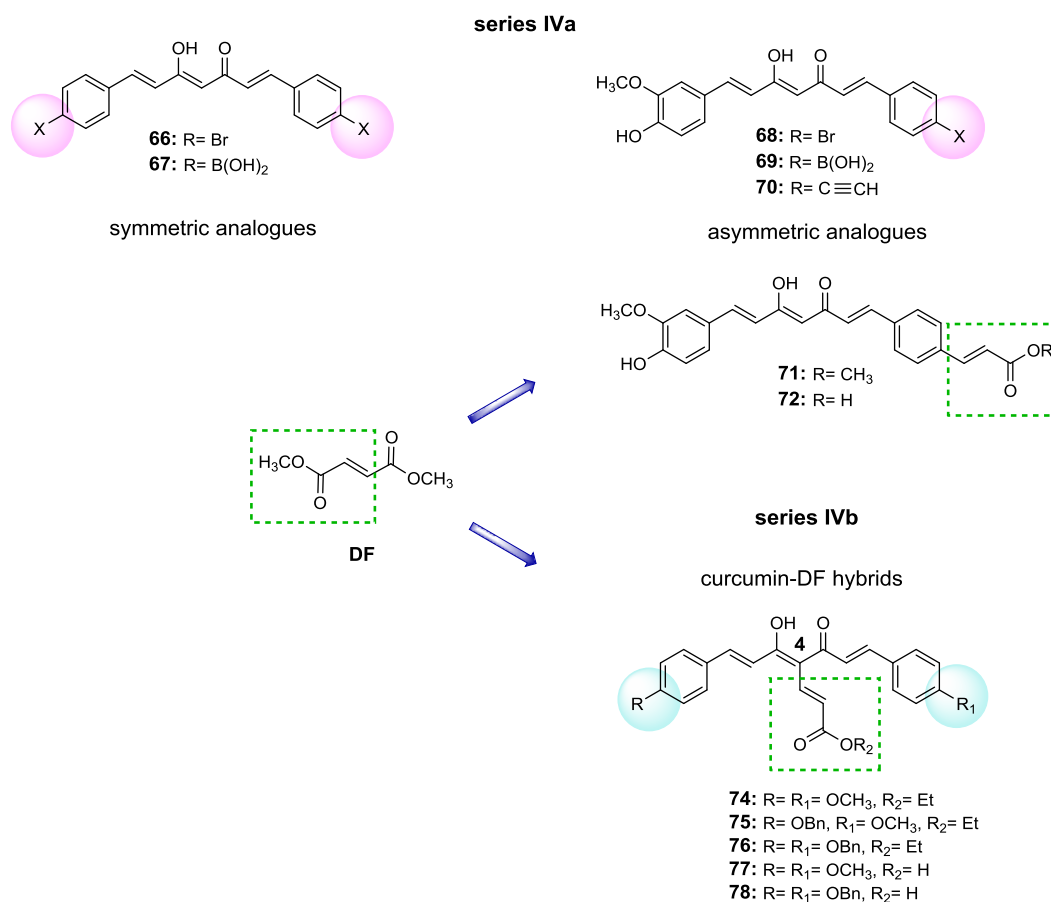


Figure 48. Design strategy for series IVa and IVb.

The molecular hybridization strategy was further exploited and curcumin-coumarin hybrids were designed as promising multifunctional neuroprotective agents for AD treatment. In this context, the neuroprotective and antioxidant potential of coumarins, also recognized as “privileged structures”, was considered to be an added value. Thus, two different sets of hybrids were designed and synthesized by introducing a simple coumarin into the 4-position of curcumin **1a** or

GSK-3 β lead **5** (series Va and Vb, Fig. 49, Tables 12 and 13, respectively). In order to perform a SAR study, explore the chemical space of the targets, and improve the pharmacokinetic profile of the new compounds, different insertion positions of coumarin were explored, by employing linkers of different nature. Analogues **79-81a,b** (series Va) and **85a,b-88** (series Vb) were characterized by a methylene spacer (Fig. 49). This tether was replaced with phenyl (Ph) (**82**, series Va and **89a,b**, series Vb), triazole (**83a,b** and **84a,b**, series Va and **90a,b**, series Vb), and acetamido moieties (**91a,b**, series Vb) (Fig. 49).

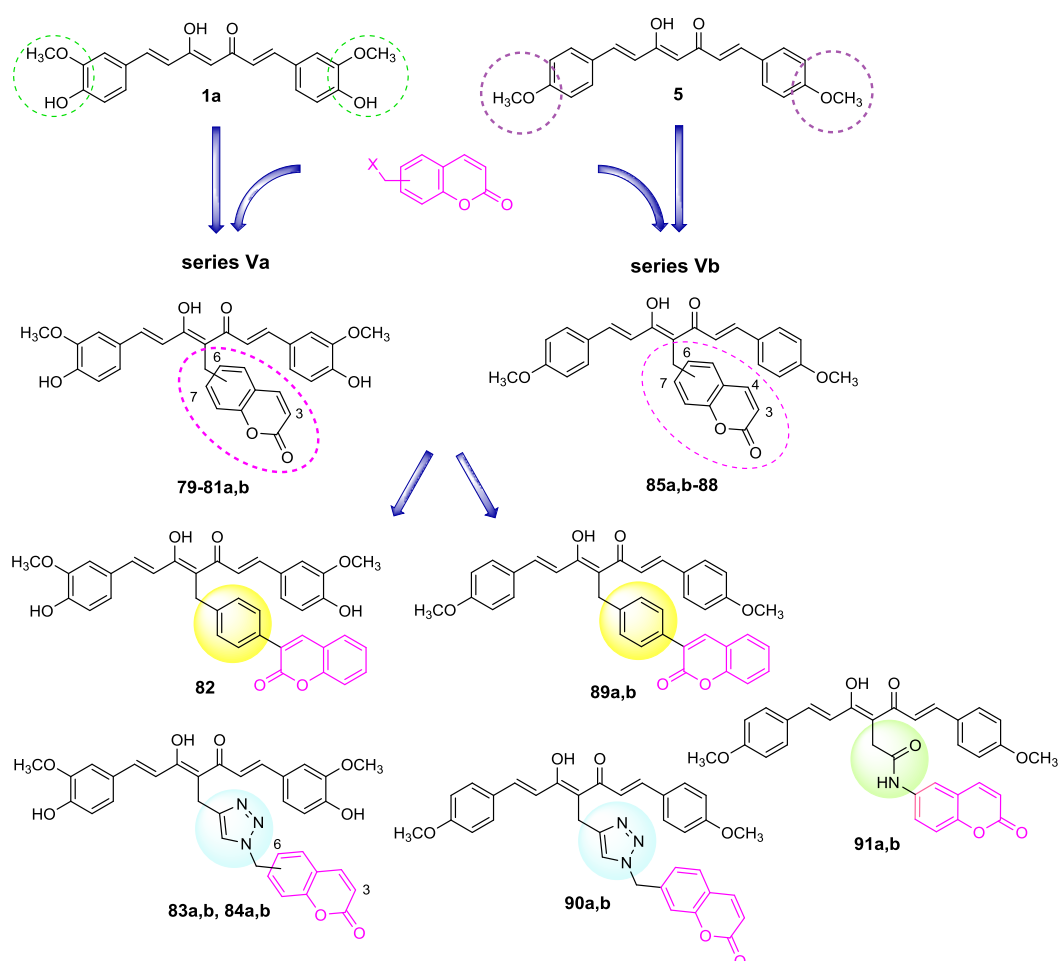


Figure 49. Design strategy for series Va and Vb.

Considering the important role of the intramolecular H-bond network of the curcumin's central fragment as β -keto-enol tautomer for establishing appropriate

interactions with BACE-1 and GSK-3 β binding sites, two design approaches were performed aimed at maintaining this pattern:

- 1) a complexation strategy might maintain this active interaction pattern, thus, difluoroboron-complexes (**107** and **108**) of the corresponding derivatives of series Ia **4** and **8** were prepared (Fig. 50, route a, Table 14).
- 2) The cyclization of the central 3,5-dione structural motif of **4**, **6** and **8** in a bioisosteric heterocycle, such as pyrazole and isoxazole, allowed obtaining analogues **109-113**, **117-120**, **122** and **114**, **121**, respectively (Fig. 50, route b, Table 15).

Furthermore, due to the versatility and good affordability of this cyclization reaction, the functionalization of the curcumin-based pyrazole (**125**) seemed to be an ideal strategy to improve structural diversity of the analogues. Thus, the simple coumarin core was introduced in this new scaffold obtaining compounds **123** and **124** (Fig. 50, route c, Table 15).

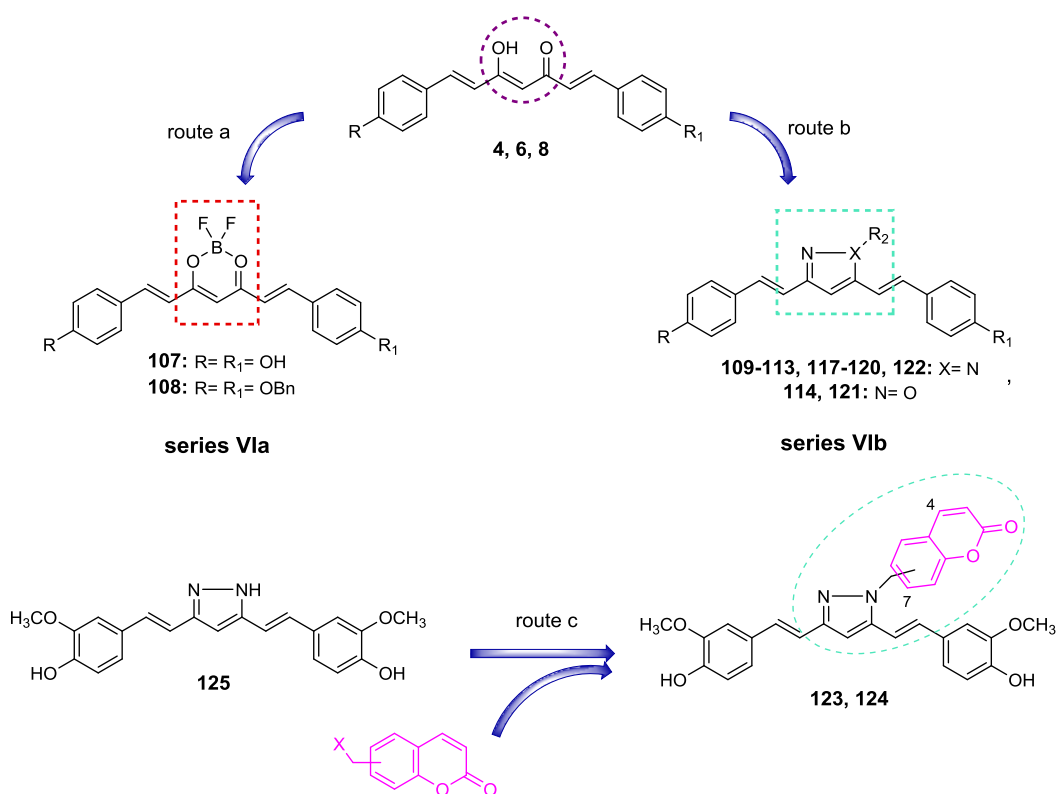


Figure 50. Design strategy for series VIa and VIb.

3.2. DESIGN OF 1,4- AND 1,3-BISCHALCONES [BIS(CINNAMOYL)BENZENE DERIVATIVES]

In drug discovery, the ring homologation approach represents a strategy for the optimization of a lead compound, as it allows to discover analogues with improved biological properties and to perform SAR investigations. It is based on the incorporation of suitable chemical rings into specific positions of the lead scaffold, maintaining the pharmacophore elements responsible for the direct interaction with the selected targets. Taking into account the pivotal role of the α,β -unsaturated carbonyl system for the interaction with Cys residues of some biologically relevant targets (GSK-3 β and Nrf2-Keap1 complex) by means of a Michael addition, the curcumin central core of some selected lead compounds of series Ia was replaced with the bis(cinnamoyl)benzene framework found in chalcones.

Thus, **4**, **5** and **8**, as potent BACE-1 and GSK-3 β inhibitors, were selected for the homologation process and a small library of 1,4- and 1,3-bischalcones (series VII, Fig. 51, Table 16) was obtained by introducing two α,β -unsaturated carbonyl systems into positions 1,3- or 1,4- of a central phenyl ring.

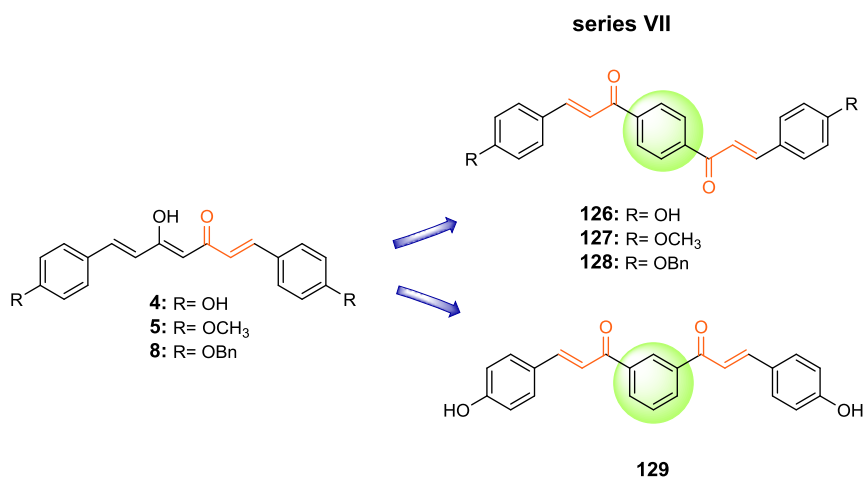


Figure 51. Design strategy for series VII.

3.3. DESIGN OF CS-BASED BIOCONJUGATES

Nowadays, the covalent linkage of bioactive agents to polymer carriers is gaining ever-increased attention as promising strategy aimed at improving their pharmacokinetic and/or pharmacodynamic properties. Among the large variety of polymers, CS, a natural, nontoxic, biocompatible and biodegradable polysaccharide, plays a central role due to its extensive range of biological activities including antitumor, antioxidant, and antimicrobial. In particular, the high chemical reactivity of the CS D-glucosamine-NH₂ repeating functions makes it a very attractive and useful starting point for the development of bioconjugates devoted to different applications in both pharmaceutical and biomedical fields.

Therefore, in an effort to obtain valuable CS-based conjugates for nanoparticles' preparation as innovative drug delivery and drug targeting systems, CS was reacted at the amino functions with a curcumin and a coumarin fragment, as fluorescent probes, to obtain the conjugates **130** and **131**, respectively (series VIII, Fig. 52, Table 17). Following two different chemical approaches (1 and 2), these fragments were covalently linked to CS through different connectors (Fig. 52):

- 1) direct amidation of the carboxylic acid function of **72** and CS-NH₂ under the classical coupling reaction conditions;
- 2) Schiff base reaction by condensation of the aldehyde group of **132** with CS-NH₂.

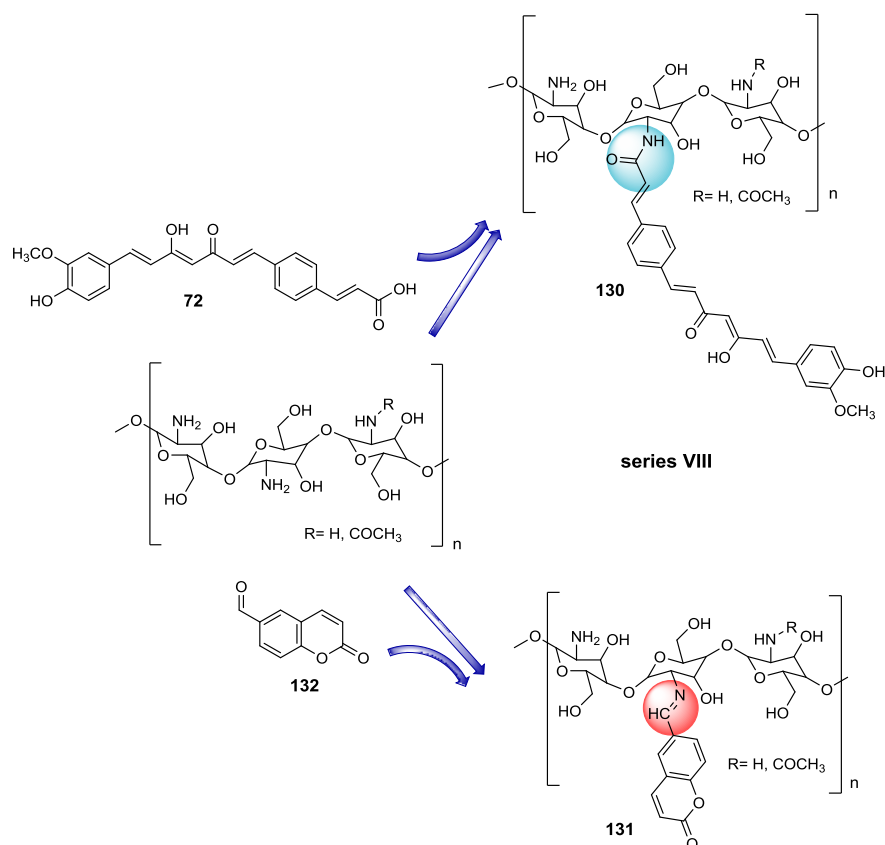


Figure 52. Design strategy for series VIII.

3.4. DESIGN OF INDOLE-BASED ANALOGUES

Nowadays, as a consequence of PKs' key roles in several neurological disorders, including AD, PKs inhibition emerges as new promising therapeutic approach to develop drug candidates for neurodegeneration treatment. In this context, besides GSK-3 β , other kinases such as CK1 and LRRK2 are recently gaining ever-increased attention, due to their involvement in different AD pathways, namely A β and τ cascades, oxidative stress and neuroinflammation.

Regarding CK1, a validated ALS target, several evidence suggests the close correlation between overexpression of CK1 isoforms (δ and ϵ) and the aggregation of τ and A β proteins. Furthermore, even if LRRK2 and one of its prevalent mutant forms G2019-LRRK2 have been mainly associated with PD pathogenesis, the recent intriguing discovery of their capability to enhance GSK-3 β kinase activity

and to promote the expression of pro-inflammatory mediators, by activation of the microglial cells, proved that their inhibition could be a promising strategy to decrease τ phosphorylation and neuroinflammation.

During the second year of my PhD course, I spent a 6 months of training period in the research group of Professor Ana Martinez in Madrid (Spain), at the IQM-CSIC and CIB-CSIC. In particular, I was involved in a project of NDs drug discovery focused on the design and synthesis of a library of new PKs inhibitors, characterized by a heterocyclic structure, as potential source of lead compounds to be further developed. Generally, the search for novel inhibitors was carried out by classical medicinal chemistry approaches starting from compounds reported in the literature in order to maintain or increase their inhibitory PK potency and ensure the permeability into the BBB. Having identified the indole scaffold as “privileged structure”, a new series of amide derivatives was designed and synthesized by employing a coupling reaction between 1*H*-indole-3-carboxylic acid and different heterocyclic amines (series IX, Fig. 53, Table 18).

At the beginning, following a hit discovery approach, a small library of derivatives (**133-139**, Fig. 53) was developed, in which the maximum structural diversity was introduced. Then, the application of a hit-to-lead design strategy with the aim to optimize the PK inhibitory profile of interesting indole-based analogues allowed to obtain **140-143** (Fig. 53).

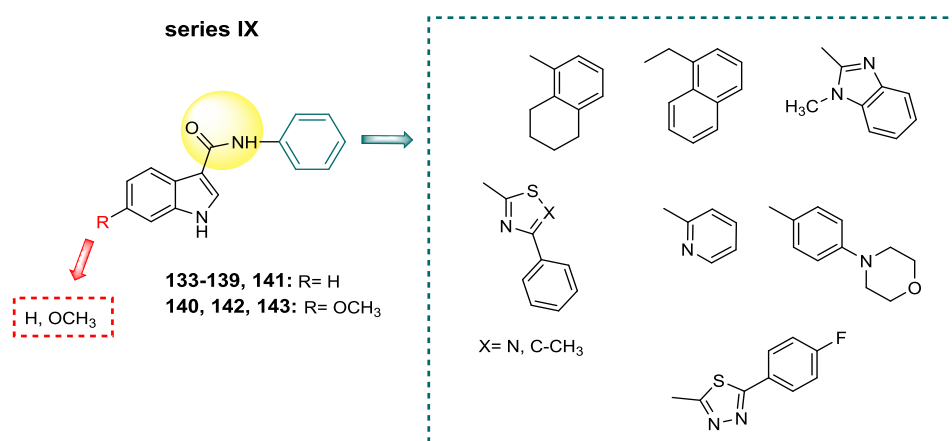
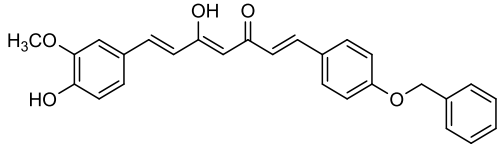
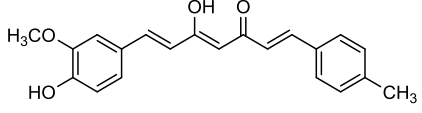
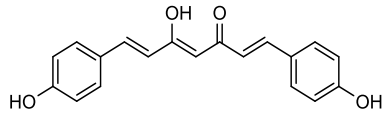
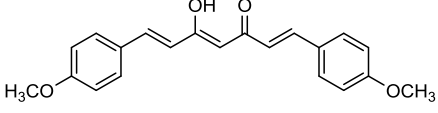
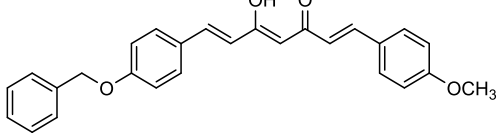
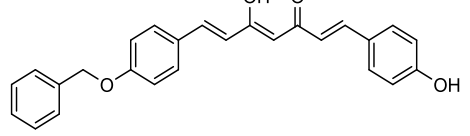
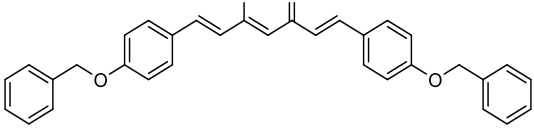
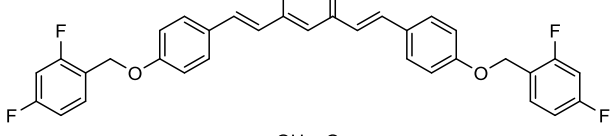
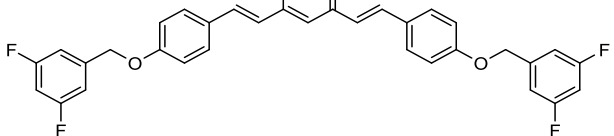
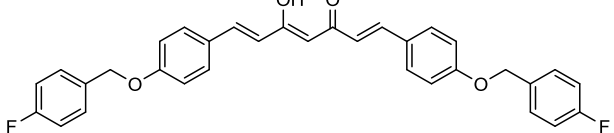
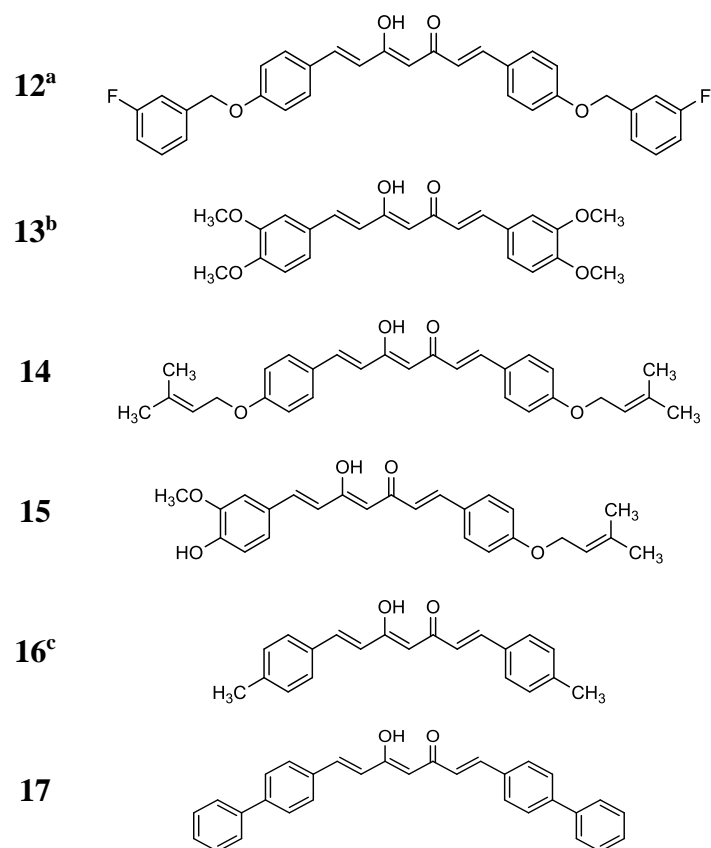


Figure 53. Design strategy for series IX.

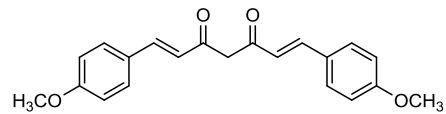
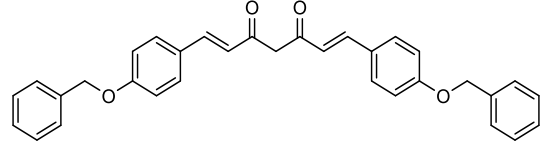
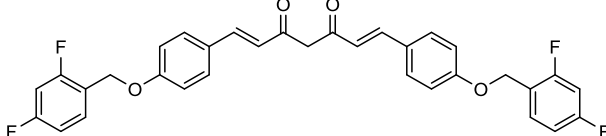
Table 5. Curcumin analogues of series Ia.

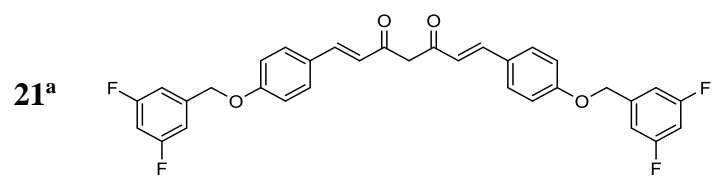
comp	chemical structure
2^a	
3^a	
4^a	
5^a	
6^a	
7^a	
8^a	
9^a	
10^a	
11^a	



^aref 8; ^bref 145; ^cref 146,147.

Table 6. Curcumin analogues of series Ib.

comp	chemical structure
18^{a,b}	
19^a	
20^a	

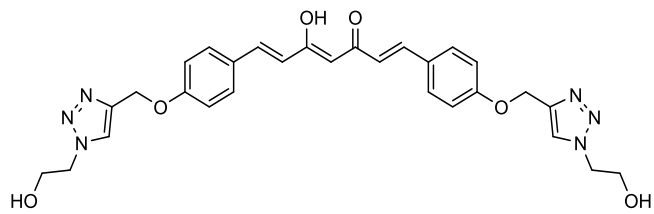


^aref 8; ^bref 147.

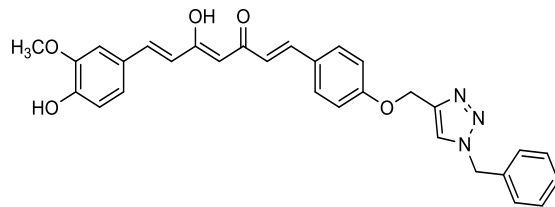
Table 7. Curcumin analogues of series IIa.

comp	chemical structure
27	
28a	
28a,b	
29	
30	

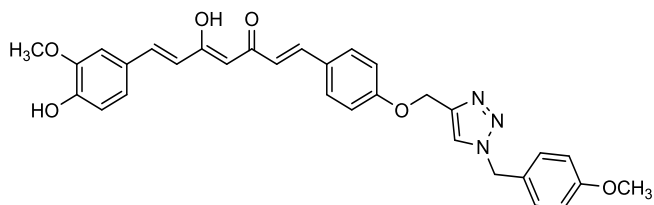
31



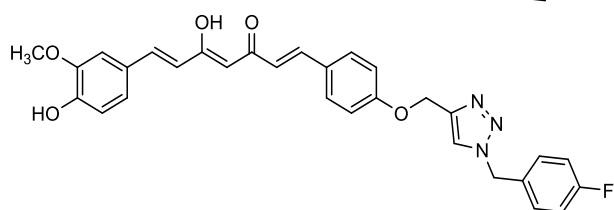
32



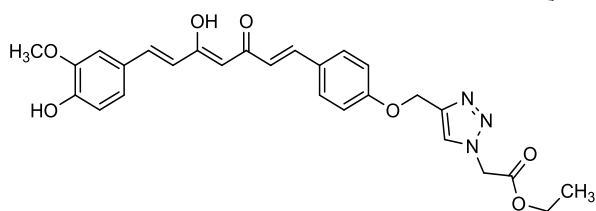
33



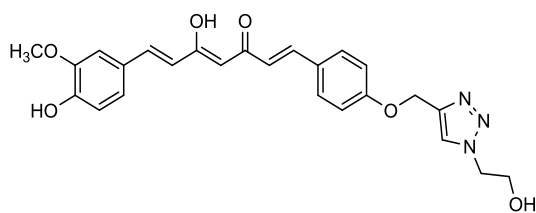
34



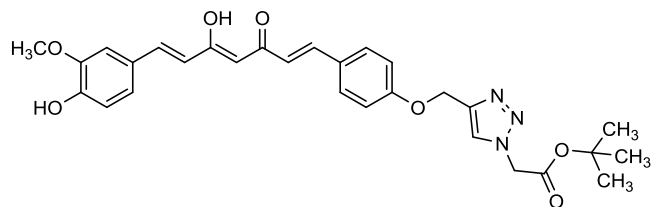
35



36



37



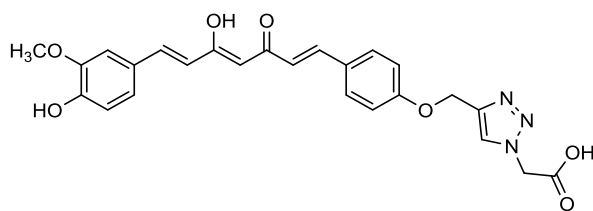


Table 8. Curcumin analogues of serie IIb.

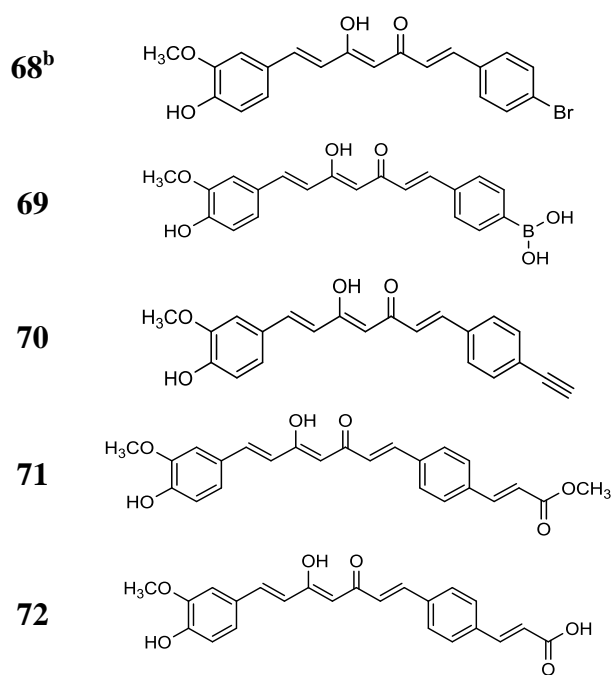
comp	chemical structure
52a,b	
53a,b	
54a,b	

Table 9. Curcumin analogues of series III.

comp	chemical structure
58	<p>Chemical structure of compound 58: A curcumin analogue with two 4-methoxyphenyl groups and a methyl ester group.</p>
59	<p>Chemical structure of compound 59: A curcumin analogue with two benzyl ether groups and a methyl ester group.</p>
60	<p>Chemical structure of compound 60: A curcumin analogue with two 4-methoxyphenyl groups and a tert-butyl ester group.</p>
61a,b	<p>Chemical structure of compound 61a,b: A curcumin analogue with two 4-methoxyphenyl groups and a hydroxyl group.</p>
62	<p>Chemical structure of compound 62: A curcumin analogue with two 4-methoxyphenyl groups and a hydroxyethylamino group.</p>

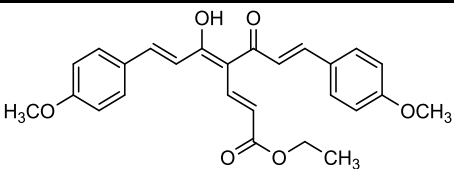
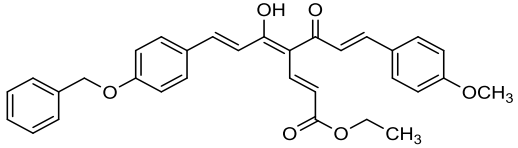
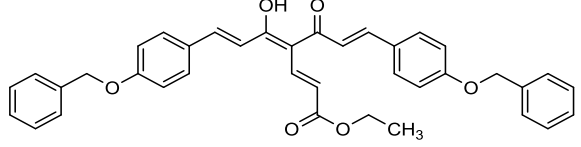
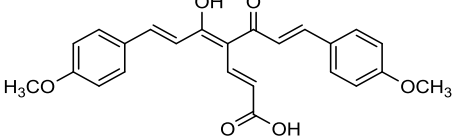
Table 10. Curcumin analogues of series IVa.

comp	chemical structure
66 ^a	<p>Chemical structure of compound 66^a: A curcumin analogue with two 4-bromophenyl groups.</p>
67	<p>Chemical structure of compound 67: A curcumin analogue with two 4-boronic acid groups.</p>



^aref¹⁴⁸; ^bref¹⁴⁹.

Table 11. Curcumin-DF hybrids of series IVb.

comp	chemical structure
74	
75	
76	
77	

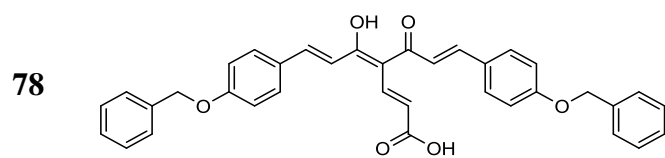
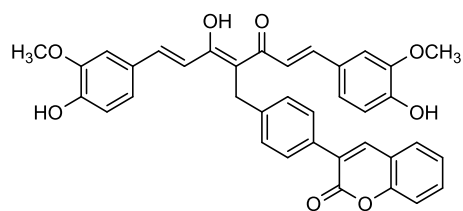


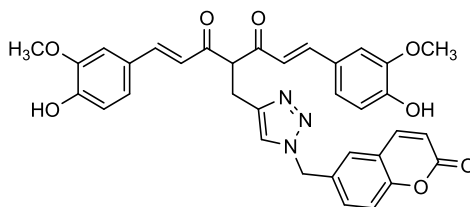
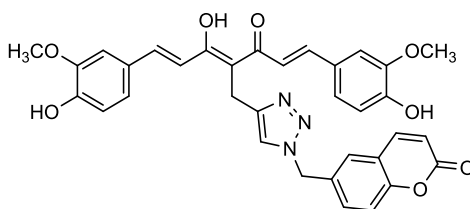
Table 12. Curcumin-coumarin hybrids of series Va.

comp	chemical structure
79	
80a,b	
81a	
81a,b	

82



83a,b



84a,b

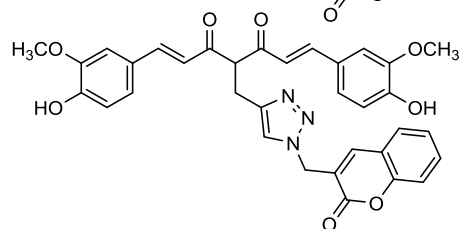
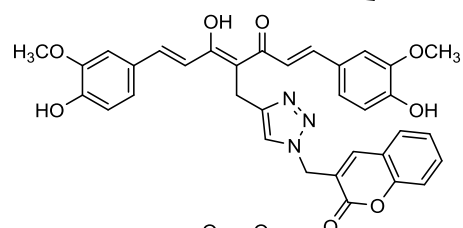


Table 13. Curcumin-coumarin hybrids of series Vb.

comp	chemical structure
85a,b	
86	
87	
88	
89a,b	

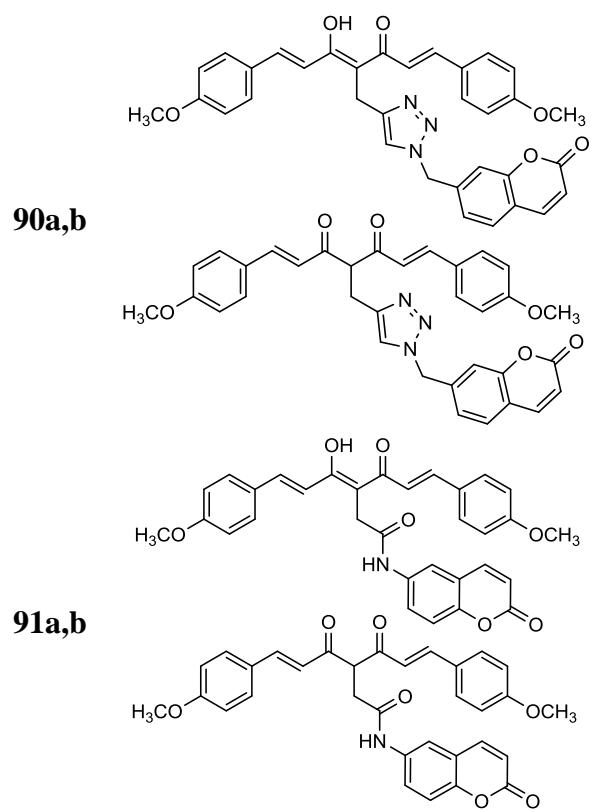
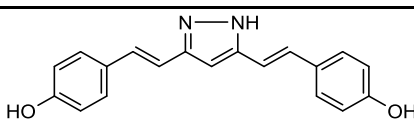
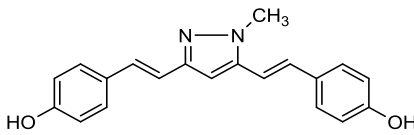
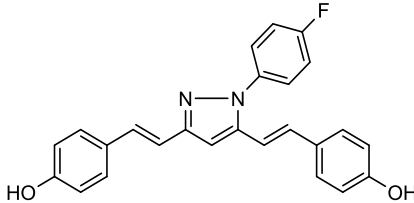
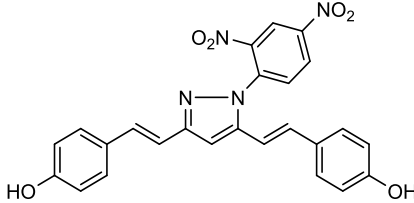
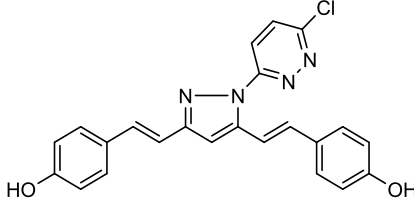
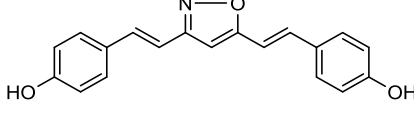
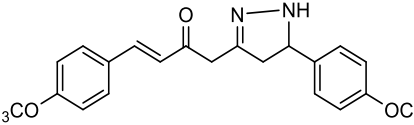
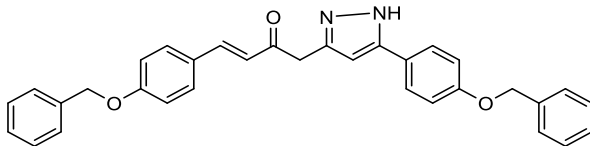
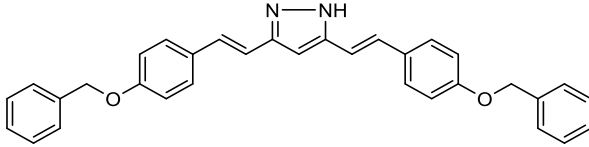


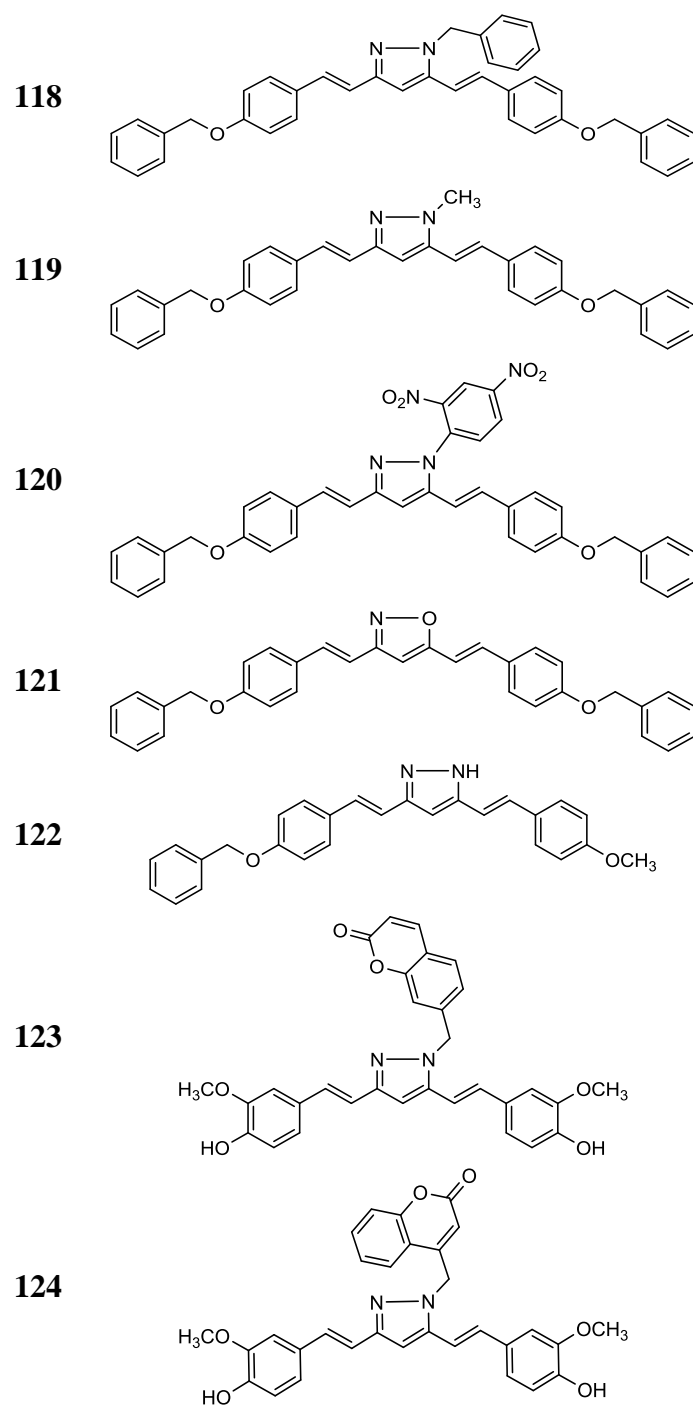
Table 14. Difluoroboron-derivatized curcuminoids of series VIa.

comp	chemical structure
107^a	
108	

^aref 150.

Table 15. Curcumin-based pyrazoles and isoxazoles of series VIb.

comp	chemical structure
109 ^a	
110 ^a	
111 ^a	
112 ^a	
113	
114 ^b	
115	
116	
117	



^aref ¹⁵¹; ^bref ¹⁵².

Table 16. 1,4- and 1,3-bis(chalcones) of series VII.

comp	chemical structure
126 ^a	
127 ^a	
128	
129 ^b	

^aref¹⁵³; ^bref¹⁵⁴.

Table 17. CS-based bioconjugates of series VIII.

comp	chemical structure
130	

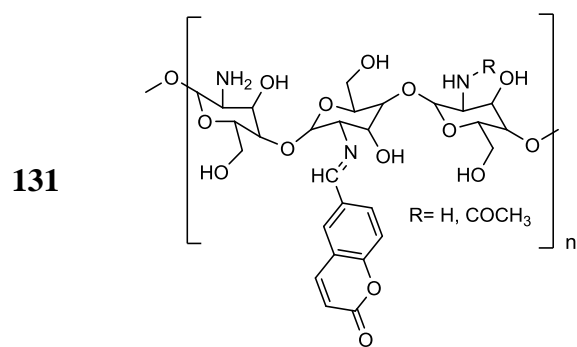
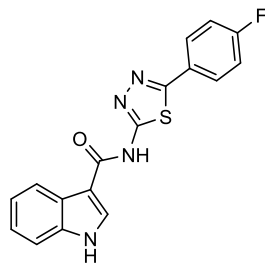


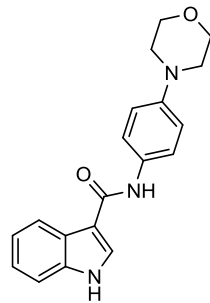
Table 18. Indole-based derivatives of series IX.

comp	chemical structure
133	
134	
135	
136	
137	

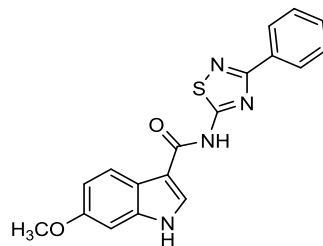
138



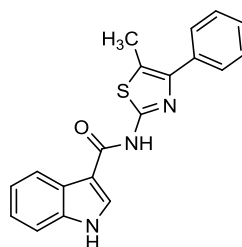
139



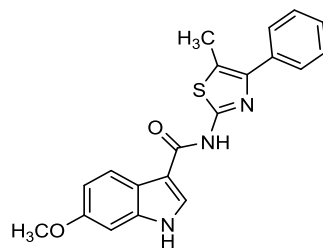
140



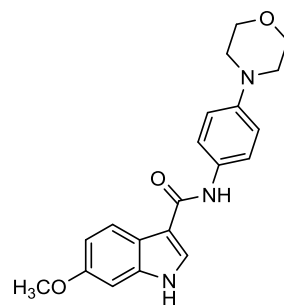
141



142



143

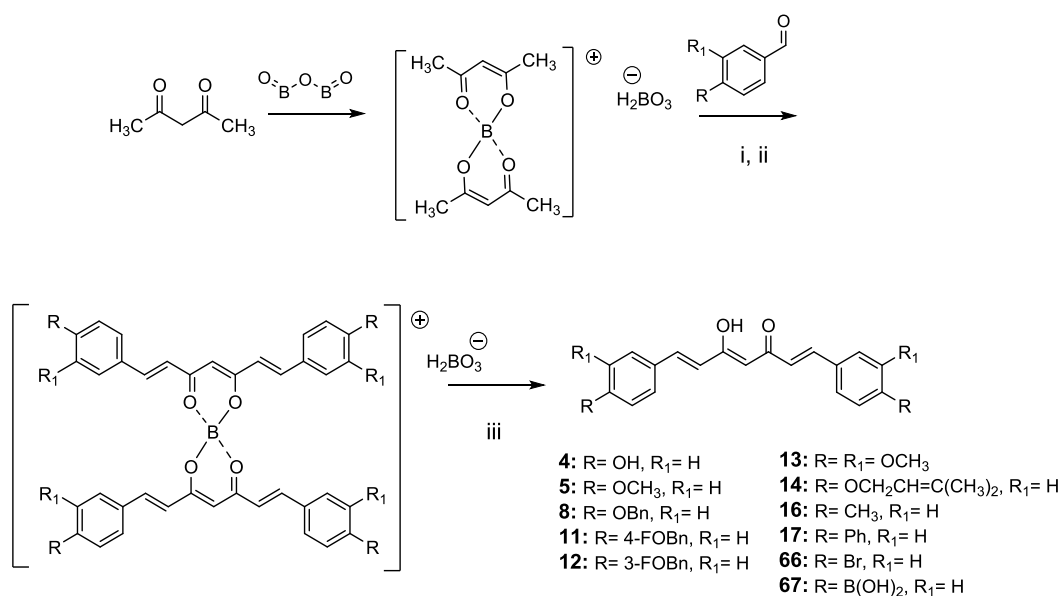


3.5. SYNTHESIS OF SERIES Ia AND Ib

3.5.1. Pabon reaction:^{8,155} synthesis of symmetric compounds **4**, **5**, **8**, **11-14**, **16** and **17**

The target curcumin-based compounds **4**, **5**, **8**, **11-14**, **16** and **17** were prepared as shown in Scheme 12 applying the classical Pabon reaction. In summary, pentane-2,4-dione was complexed with B₂O₃ in EtOAc to avoid the methylene-centred reactivity toward the Knoevenagel reaction and to favour the nucleophilic attack at the side methyl groups. The resulting boric complex was then condensed with the suitable aldehyde and finally a step-wise addition of *n*-tributylborate [B(*n*-BuO)₃] and *n*-BuNH₂ was carried out. Acidic treatment (HCl, 0.5 N) allowed the complex dissociation and the obtaining of the desired compounds as β-keto-enol tautomers (Scheme 12).

Scheme 12^a

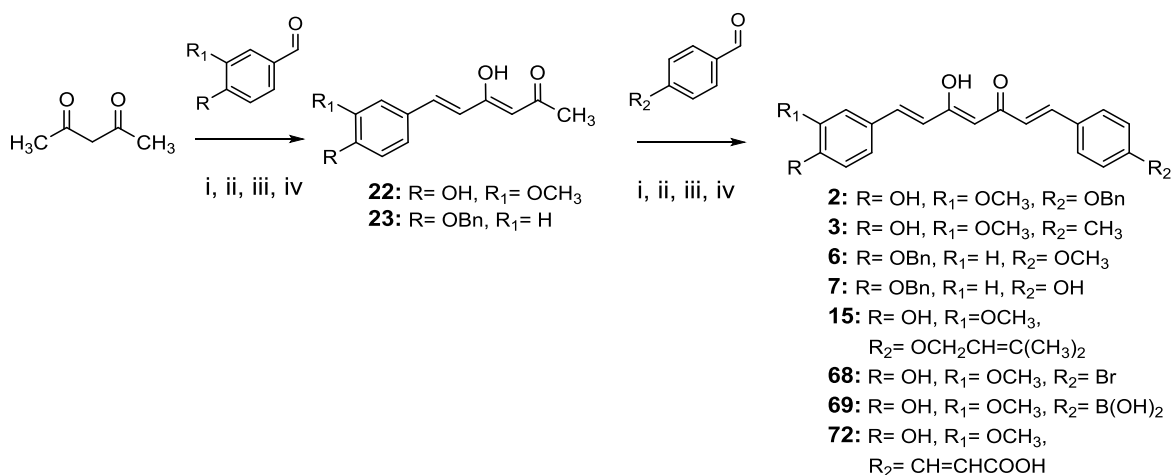


^a**Reagents and conditions:** i) B(*n*-BuO)₃, EtOAc or DMF; ii) *n*-BuNH₂, 80 °C; iii) HCl, 80 °C.

3.5.2. Pabon reaction:⁸ synthesis of asymmetric compounds **2**, **3**, **6**, **7**, **15** and intermediates **22** and **23**

The synthesis of the asymmetric curcumin analogues **2**, **3**, **6**, **7** and **15** were performed via a two-steps strategy, in which the mono-aryl curcumin synthetic intermediates **22** and **23** were first prepared under the classical reaction conditions, employing vanillin or 4-benzyloxybenzaldehyde, respectively. Subsequently, a second Pabon reaction, with the additional appropriate aldehyde, gave the final compounds in β -keto-enol tautomeric form (Scheme 13). In this case, the one-pot procedure was avoided because the employment of two different aldehydes would give a complex mixture of compounds, among which the asymmetrical and the two symmetrical curcuminoids, including the semi-reaction products (mono-aryl curcumin). Therefore, obtaining the desired compounds in a good yield and purity grade would require several purification processes (column chromatography and/or crystallization).

Scheme 13^a

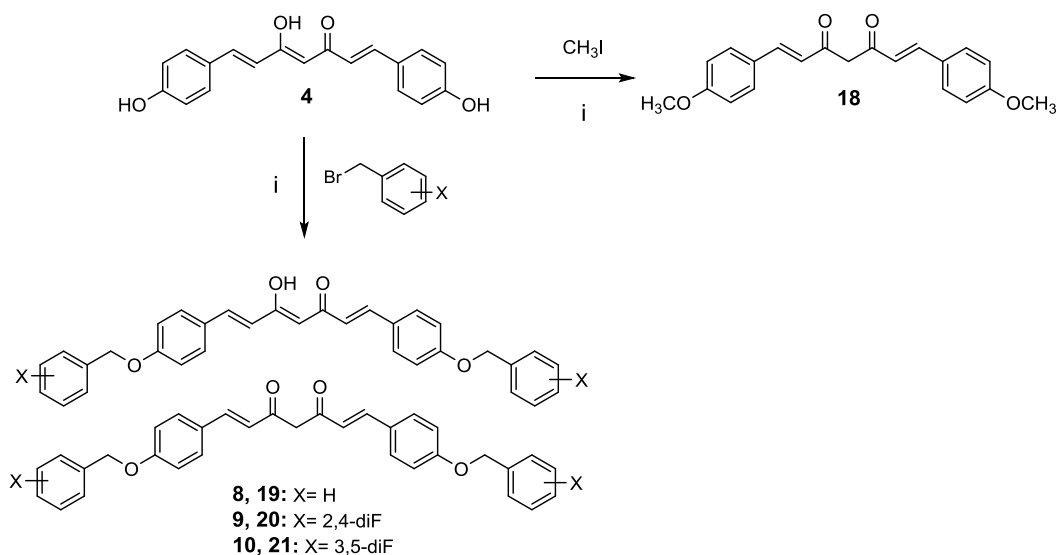


^a**Reagents and conditions:** i) B₂O₃, EtOAc or DMF; ii) B(*n*-BuO)₃; iii) *n*-BuNH₂, 80 °C; iv) HCl, 80 °C.

3.5.3. Williamson reaction:⁸ synthesis of symmetric compound 18, and of the tautomeric couples 8 and 19, 9 and 20, 10 and 21

The Williamson ether synthesis (Scheme 14) between the phenol-key compound **4** and a selected benzyl halide, in the presence of K_2CO_3 as base, gave the desired products in a mixture of β -keto-enol (**8-10**) and symmetric diketo tautomers (**19-21**). In particular, the employment of a sterically demanding alkylating reagent was essential for obtaining both the tautomeric ethers into the reaction mixture. Each single tautomer, due to its fairly different chromatographic behaviour, was then successfully and carefully isolated from the crude reaction by flash column chromatography, and further purified by crystallization from a suitable solvent or system of solvents. Interestingly, when methyl iodide was used as alkylating reagent (Scheme 14), it was not possible to obtain the corresponding tautomers **5** and **18** as chromatographically different compounds and, to avoid separation difficulties, reaction time was lengthened in order to convert **5** into **18**.

Scheme 14^a

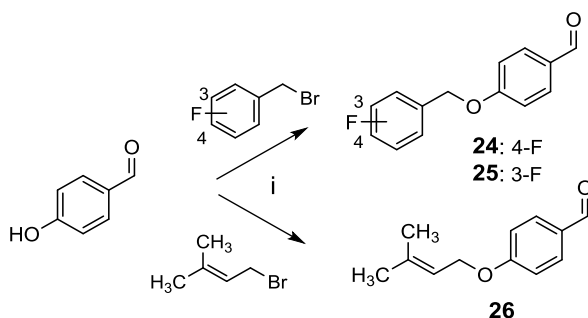


^aReagents and conditions: i) K_2CO_3 , acetone, 80 °C.

3.5.4. Williamson reaction:⁸ synthesis of intermediate benzaldehydes 24-26

The intermediate benzaldehydes **24**, **25** and **26** were prepared in the same experimental conditions of Williamson ether synthesis starting from 4-hydroxybenzaldehyde and using the suitable benzyl or alkyl bromide as alkylating agent (Scheme 15).

Scheme 15^a



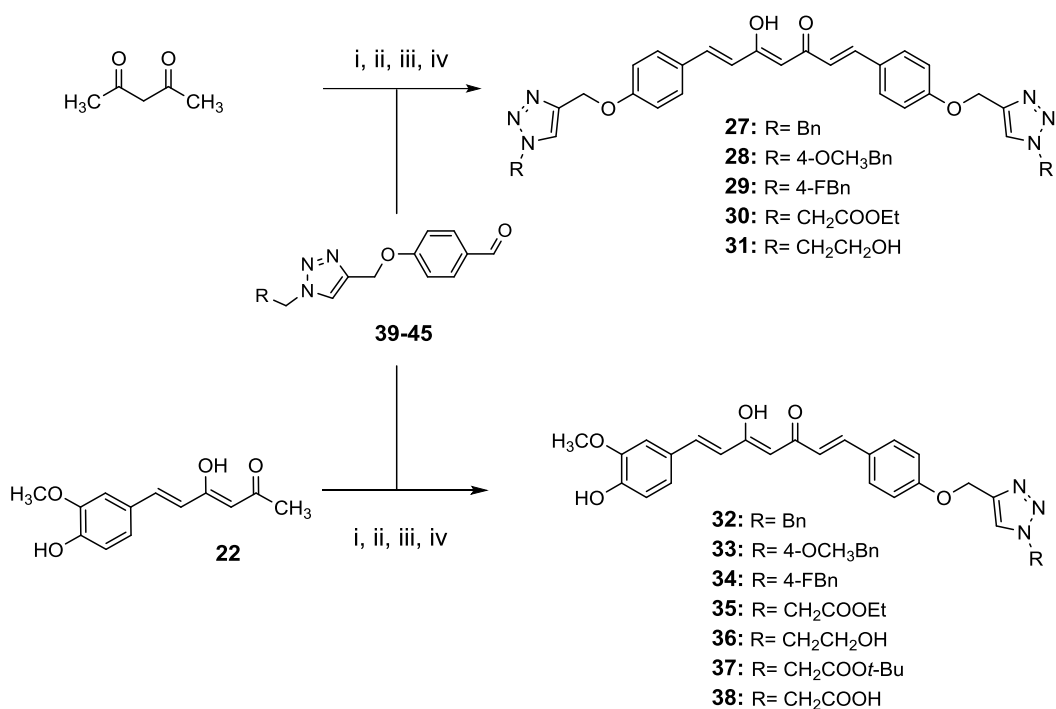
^aReagents and conditions: i) K₂CO₃, acetone, 80 °C.

3.6. SYNTHESIS OF SERIES IIa AND IIb

3.6.1. Pabon reaction: synthesis of symmetric analogues 27-31 and asymmetric derivatives 32-38

The classical Pabon reaction between pentane-2,4-dione and the appropriate functionalized aldehyde (**39-45**) using (*N,N*-dimethylformamide) DMF instead of EtOAc allowed to obtain the symmetric curcumin-based derivatives **27-31** (Scheme 16). The preparation of the asymmetric analogues **32-38** was performed in the same reaction conditions employing the condensation of the boric complex of intermediate **22** with the suitable aldehyde (**39-45**, Scheme 16). Interestingly, the substitution of EtOAc with DMF allowed to increase the reaction yield, maintaining the β -keto-enol tautomeric form.

Scheme 16^a

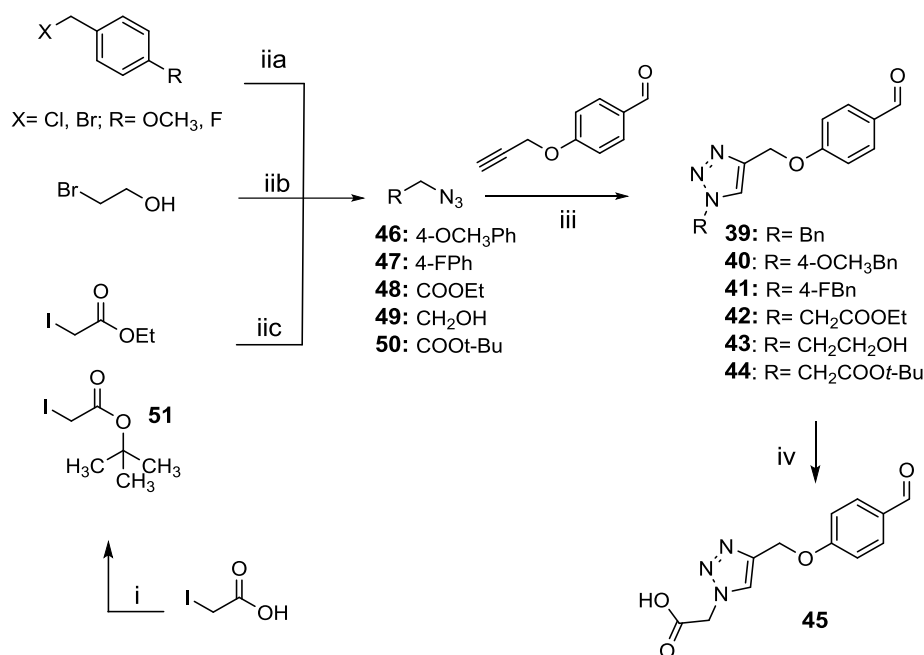


^a**Reagents and conditions:** i) B₂O₃, DMF; ii) B(*n*-BuO)₃; iii) *n*-BuNH₂, 80 °C; iv) HCl, 80 °C.

3.6.2. Synthesis of functionalized aldehydes 39-45, azido derivatives 46-50 and intermediate 51

A 1,3-dipolar cycloaddition (“click chemistry reaction”, CCR) between 4-(prop-2-yn-1-yloxy)benzaldehyde and the appropriate azido derivative (**46-50** including the commercially available benzyl azide) in DMSO or DMF at room temperature, using triethylamine (TEA) as base and a water solution of copper sulphate (CuSO₄) and (+)-sodium *L*-ascorbate as catalysts, allowed to obtain the desired aldehydes **39-44** (Scheme 17). A further hydrolysis of **44** with trifluoroacetic acid (TFA) in dichloromethane (CH₂Cl₂) at room temperature gave the corresponding acid **45** (Scheme 17). The azido derivatives **46-50** were prepared by nucleophilic substitutions of the appropriate alkyl or benzyl halides with sodium azide (NaN₃) (Scheme 17).

Scheme 17^a



^a**Reagents and conditions:** i) *t*-BuOH, MgSO₄, H₂SO₄ (cat), r.t.; iia) NaN₃, DMF, 60 °C; iib) NaN₃, H₂O, 50 °C; iic) NaN₃, acetone/H₂O₂ (4:1), r.t.; iii) TEA, CuSO₄, (+)-sodium *L*-ascorbate, DMF or DMSO, r.t.; iv) TFA, CH₂Cl₂, r.t.

In particular, depending on the nature of the starting halide, three different experimental conditions were applied:

- 1) DMF at 60 °C (**46** and **47**);
- 2) water at 50 °C (**49**);
- 3) a mixture of acetone/H₂O (4:1) at room temperature (**48** and **50**).

To obtain intermediate **51**, iodoacetic acid was treated with *tert*-butanol (*t*-BuOH) in the presence of magnesium sulphate (MgSO₄) and a catalytic amount of concentrated sulfuric acid (H₂SO₄) at room temperature (Scheme 17).

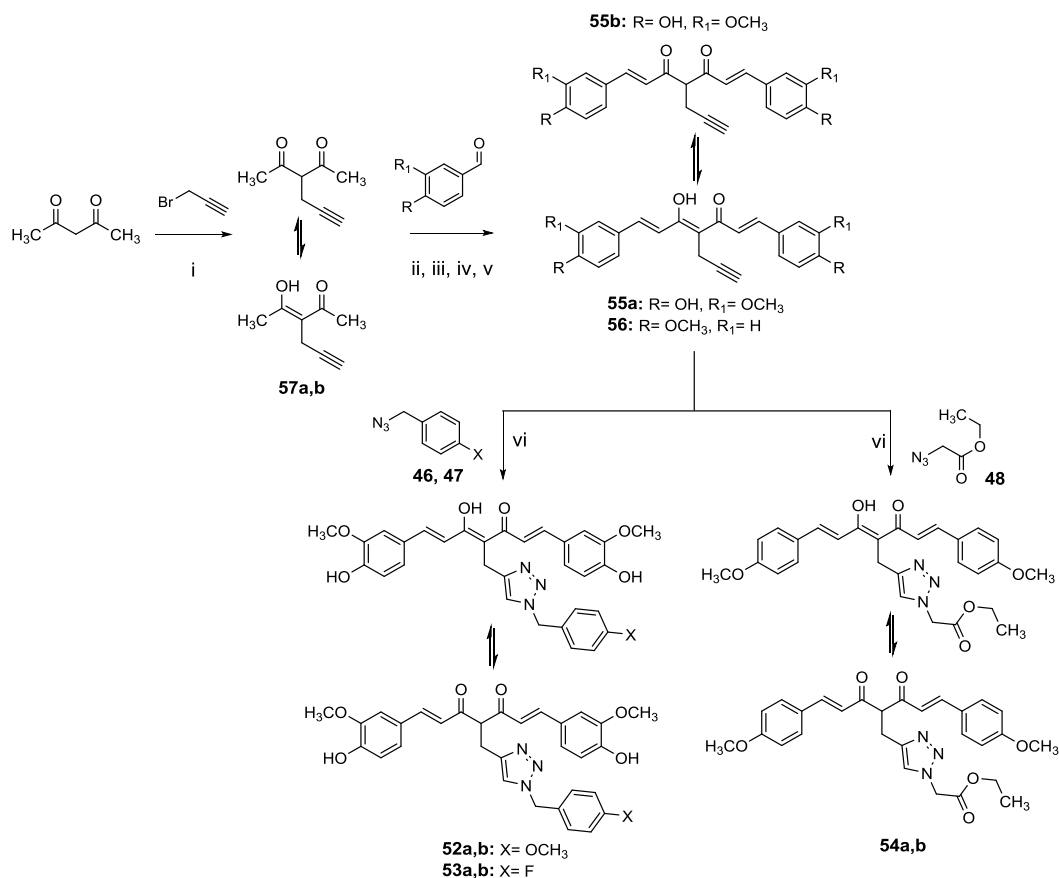
3.6.3. Synthesis of tautomeric couples of curcumin-based derivatives **52a,b-54a,b** and intermediates **55a,b, 56** and **57a,b**

The synthesis of curcumin analogues **52a,b-54a,b** was performed following a multi-step strategy as shown in Scheme 18. At the beginning, the alkylation reaction of pentane-2,4-dione in acetone under reflux, using propargyl bromide

solution 80 wt. % in toluene as alkylating reagent and K_2CO_3 as base, gave **57a,b** as couple of β -keto-enol and diketo tautomers. Then, a classical Pabon reaction in DMF between these intermediates and vanillin or 4-methoxybenzaldehyde allowed to obtain **55a,b** and **56**, respectively (Scheme 18).

Finally, a CCR at the propargyl function in the 4-position of the curcumin scaffold of **55a,b** with the azido derivatives **46** and **47**, according to the previously described experimental conditions in DMF, afforded the tautomeric couples **52a,b** and **53a,b**, respectively. Likewise, CCR between **56** and **48** in DMSO gave the mixture **54a,b** (Scheme 18).

Scheme 18^a



^a**Reagents and conditions:** i) K_2CO_3 , acetone, 80 °C; ii) B_2O_3 , DMF; iii) $B(n-BuO)_3$; iv) $n-BuNH_2$, 80 °C; v) HCl, 80 °C; vi) TEA, $CuSO_4$, (+)-sodium *L*-ascorbate, DMF or DMSO, r.t.

Interestingly, in the synthetic route for series IIb, the addressed modification of the central curcumin framework promoted the partial conversion of its β -keto-enol form into the corresponding diketo counterpart and it was not possible to isolate each single tautomer as chromatographically different compound.

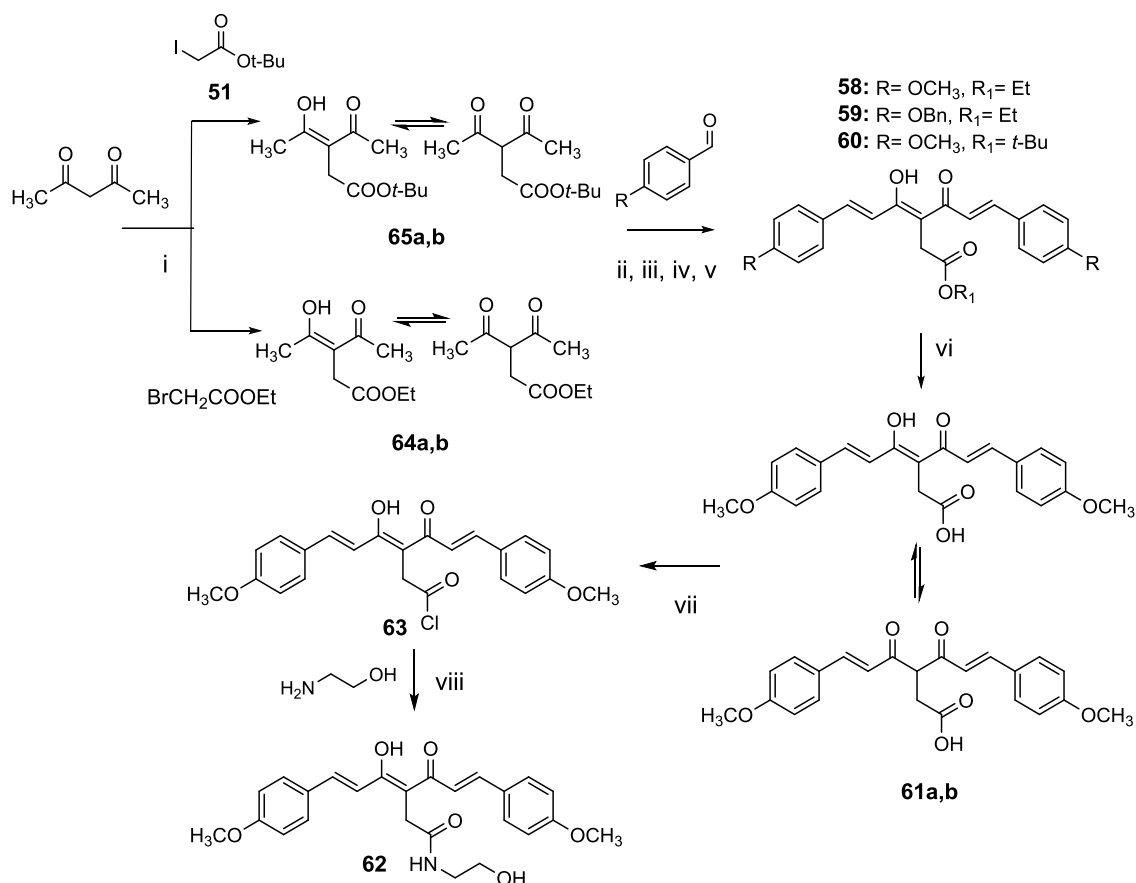
3.7. SYNTHESIS OF SERIES III

3.7.1. Synthesis of curcumin analogues **58-60**, **61a,b** and **62** and intermediates **64a,b**, **65a,b** and **63**

The curcumin-based compounds **58-60** were synthesized by the two-step strategy depicted in Scheme 19. In particular, treatment of pentane-2,4-dione with the suitable alkyl halides, in presence of sodium hydride (NaH) as base, in tetrahydrofuran (THF) and under nitrogen (N₂) atmosphere, gave the key intermediates **64a,b** and **65a,b**, whose condensation with 4-methoxybenzaldehyde and 4-benzyloxybenzaldehyde under classical Pabon reaction conditions in DMF allowed to obtain **58-60** (Scheme 19).

Additionally, the acid **61a,b** was prepared by saponification of the corresponding ethyl ester derivative **58** using a solution of sodium hydroxide (NaOH, 0.2 N) in methanol (CH₃OH, Scheme 19). The synthesis of the amide analogue **62** was carried out by a preliminary conversion of **61a,b** into the acyl chloride **63**, using thionyl chloride (SOCl₂) under reflux, and a further *N*-acylation with ethanolamine in acetonitrile (CH₃CN) at 60 °C (Scheme 19).

Scheme 19^a



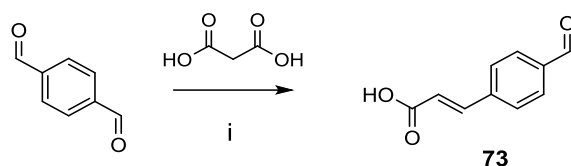
^a**Reagents and conditions:** i) NaH, THF, N₂, 0 °C to r.t.; ii) B₂O₃, DMF; iii) B(*n*-BuO)₃; iv) *n*-BuNH₂, 80 °C; v) HCl, 80 °C; vi) NaOH (CH₃OH, 0.2 N), CH₂Cl₂/CH₃OH (9:1), r.t.; vii) SOCl₂, reflux; viii) CH₃CN, 60 °C.

3.8. SYNTHESIS OF SERIES IV_a AND IV_b

3.8.1. Synthesis of curcumin analogues 66-72 and aldehyde 73

Similarly to curcumin-based derivatives of series I, the symmetric analogues **66** and **67** were synthesized performing the classical Pabon reaction in DMF (Scheme 12), and the asymmetric derivatives **68**, **69** and **72** were obtained starting from **22** (Scheme 13). The selected aldehydes are commercially available except for **73**, that was prepared by Verley-Doebner modification of Knoevenagel condensation using terephthalaldehyde and malonic acid in pyridine in the presence of piperidine at 80-90 °C (Scheme 20).¹⁵⁶

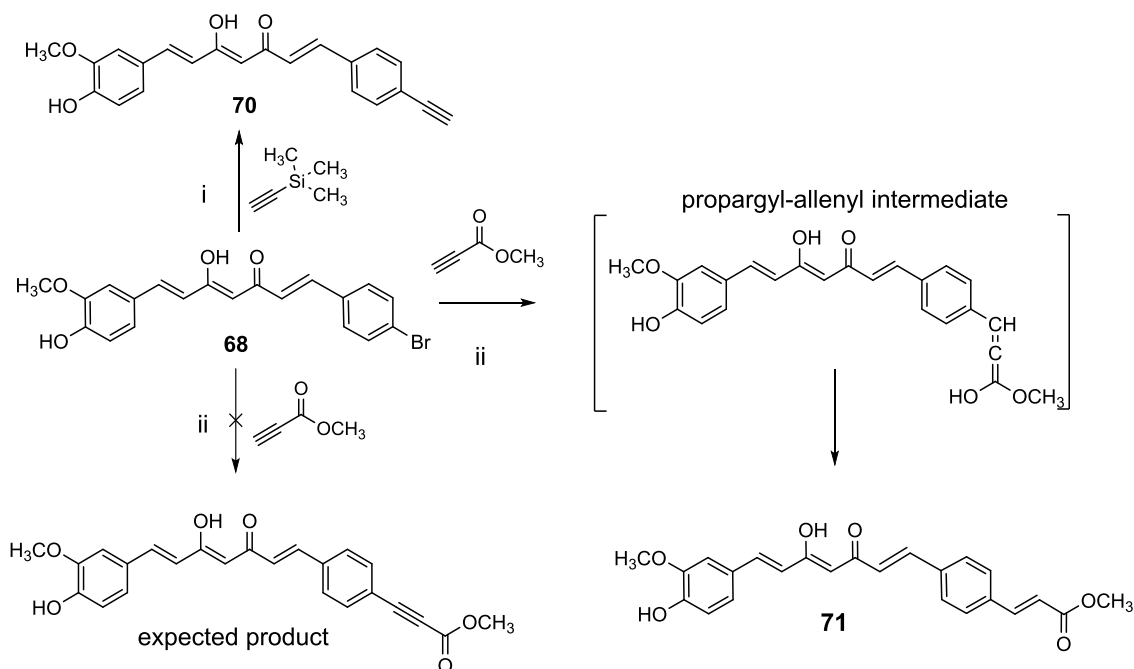
Scheme 20^a



^a**Reagents and conditions:** i) piperidine, pyridine, 80-90 °C.

Moreover, a Sonogashira coupling reaction (Scheme 21) between derivative **68** and ethynyltrimethylsilane in THF under N₂ atmosphere at room temperature in the presence of TEA as base and copper iodide (CuI) and bis(triphenylphosphine)palladium(II) dichloride [PdCl₂(PPh₃)₂] as catalysts, surprisingly gave, after purification of the crude product, the desired compound **70** without cleavage of the protecting group.

Scheme 21^a



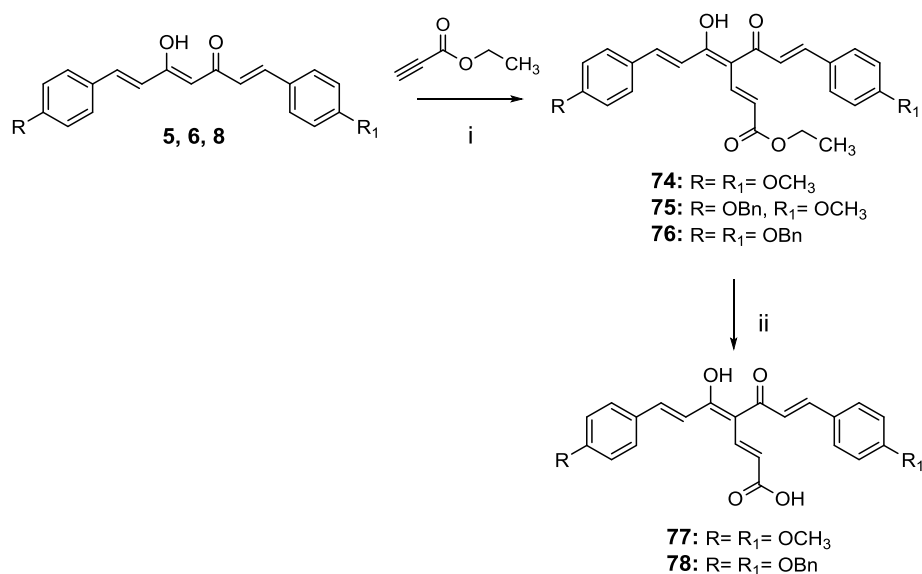
^a**Reagents and conditions:** i) TEA, CuI, PdCl₂(PPh₃)₂, THF, N₂, r.t; ii) TEA, CuI, Pd(PPh₃)₄, DMF, N₂, 70 °C.

Interestingly, when the same reaction (Scheme 21) was performed between **68** and methylpropiolate in DMF, at 70 °C, using TEA as base and CuI and tetrakis(triphenylphosphine)palladium(0) [Pd(PPh₃)₄] as catalysts, instead of isolating the predictable terminal alkyne derivative, compound **71** was obtained. This outcome encouraged us to hypothesize a different synthetic route consisting in a Sonogashira coupling-isomerization reaction in which the classical Sonogashira reaction conditions promoted the formation of a propargyl-allenyl intermediate, whose ending conversion into the more stable alkene by isomerization afforded **71** (Scheme 21).¹⁵⁷

3.8.2. Synthesis of curcumin-DF hybrids **74-78**

The synthetic route for curcumin-DF hybrids preparation is outlined in Scheme 22. In particular, reaction of lead compounds **5**, **6** and **8** with ethylpropiolate in THF under inert atmosphere (N₂ gas), using NaH as base, gave the corresponding analogues **74-76**.

Scheme 22^a



^a**Reagents and conditions:** i) NaH, THF, N₂, 0 °C to r.t.; ii) KOH (CH₃OH, 2.0 N), CH₃OH, 60 °C.

Additionally, the further saponification of compounds **74** and **76** in CH₃OH at 60 °C by employing a solution of potassium hydroxide (KOH) in 2.0 N methanol allowed to obtain the acid derivatives **77** and **78**, respectively (Scheme 22).

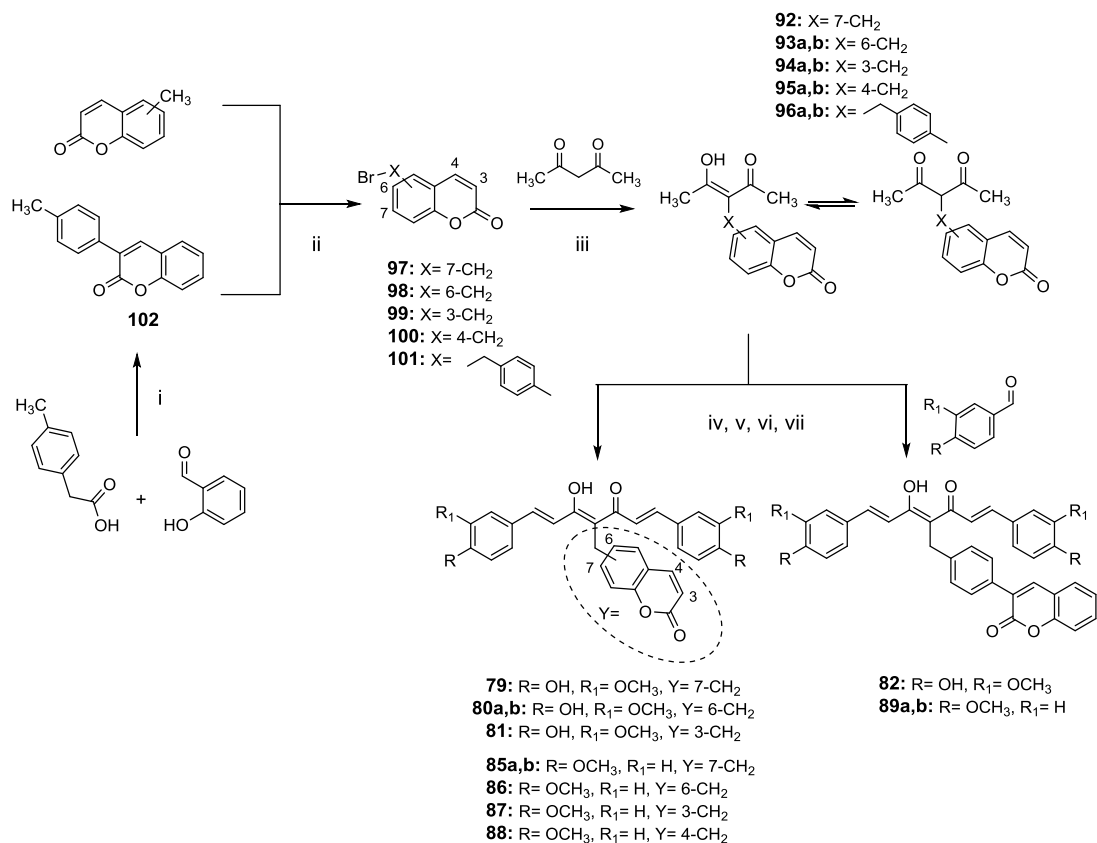
3.9. SYNTHESIS OF SERIES Va AND Vb

3.9.1. Synthesis of curcumin-coumarin hybrids **79-82** and **85a,b-89a,b** and intermediates **92-102**

The target compounds **79-82** and **85a,b-89a,b** were prepared performing a multi-step synthetic procedure as displayed in Scheme 23. Bromination of the appropriate commercial methyl-coumarins and **102** with *N*-bromosuccinimide (NBS), in carbon tetrachloride (CCl₄) using a catalytic amount of benzoyl peroxide [(PhCO)₂O₂] and the light of a lamp to trigger the reaction *via* radical mechanism, gave the corresponding bromo-derivatives **97-101**. Then, pentane-2,4-dione underwent alkylation with these intermediates in THF, in alkaline conditions for NaH and under N₂ atmosphere, or in acetone, under reflux and in presence of K₂CO₃ as base, allowed to obtain **92-96a,b** as key intermediates, whose condensation with vanillin or 4-methoxybenzaldehyde in the classical Pabon reaction conditions in DMF afforded the desired curcumin-coumarin hybrids (Scheme 23). Curiously, in this subset of 4-modified curcumin-based compounds the β-keto-enol form was isolated with a high purity grade with the exception for the tautomeric couples **80a,b**, **85a,b** and **89a,b** (Scheme 23).

Finally, a intramolecular Perkin reaction carried out between 2-hydroxybenzaldehyde and 2-(*p*-tolyl)acetic acid in acetic anhydride at 150 °C with TEA as basic catalyst allowed to obtain the 3-substituted coumarin **102** (Scheme 23).

Scheme 23^a

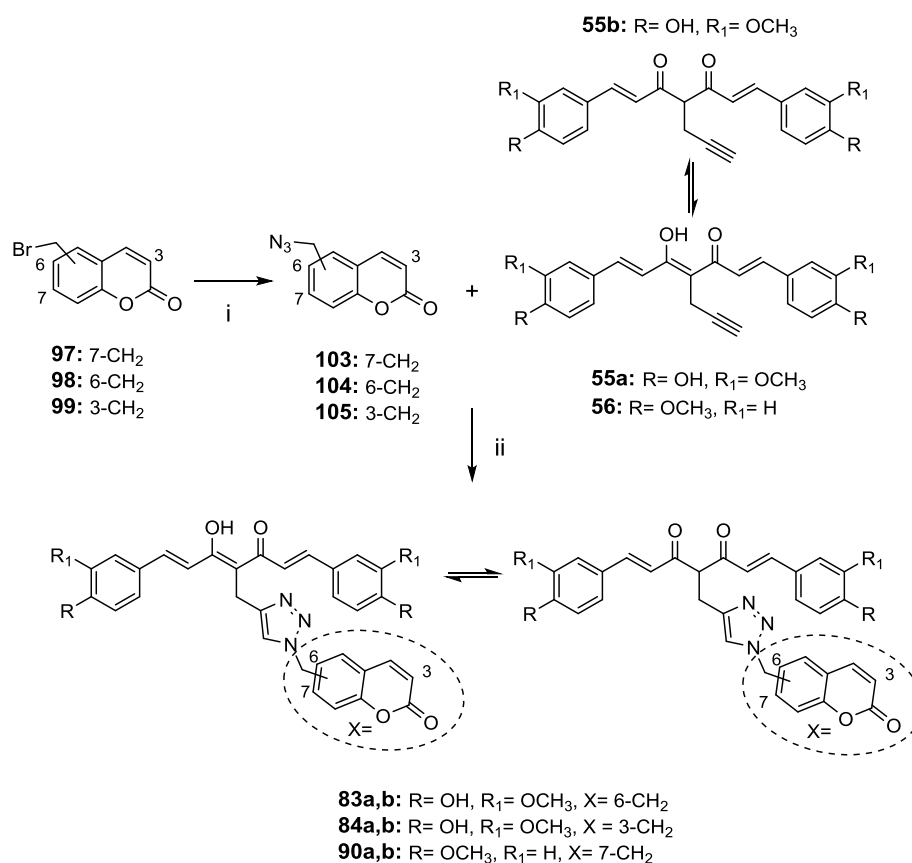


^a**Reagents and conditions:** i) TEA, (CH₃CO)₂O, 150 °C; ii) NBS, (PhCO)₂O₂, CCl₄, *hν*, 50 °C; iii) NaH, THF, N₂, 0 °C to r.t. or K₂CO₃, acetone, 80 °C; iv) B₂O₃, DMF; v) B(*n*-BuO)₃; vi) *n*-BuNH₂, 80 °C; vii) HCl, 80 °C.

3.9.2. Synthesis of curcumin-coumarin hybrids **83a,b**, **84a,b** and **90a,b** and azido intermediates **103-105**

The reaction of curcumin-based intermediates **55a,b** and **56** with the azidomethyl-coumarin **103-105** following a CC approach, in the previously described experimental conditions (DMF or DMSO), afforded hybrid compounds **83a,b**, **84a,b** and **90a,b** as couples of β-keto-enol tautomer and its diketo counterpart (Scheme 24). **103-105** were, in turn, synthesized by nucleophilic substitutions of the corresponding bromomethyl-coumarin analogues **97-99** with NaN₃ in acetone (Scheme 24).

Scheme 24^a

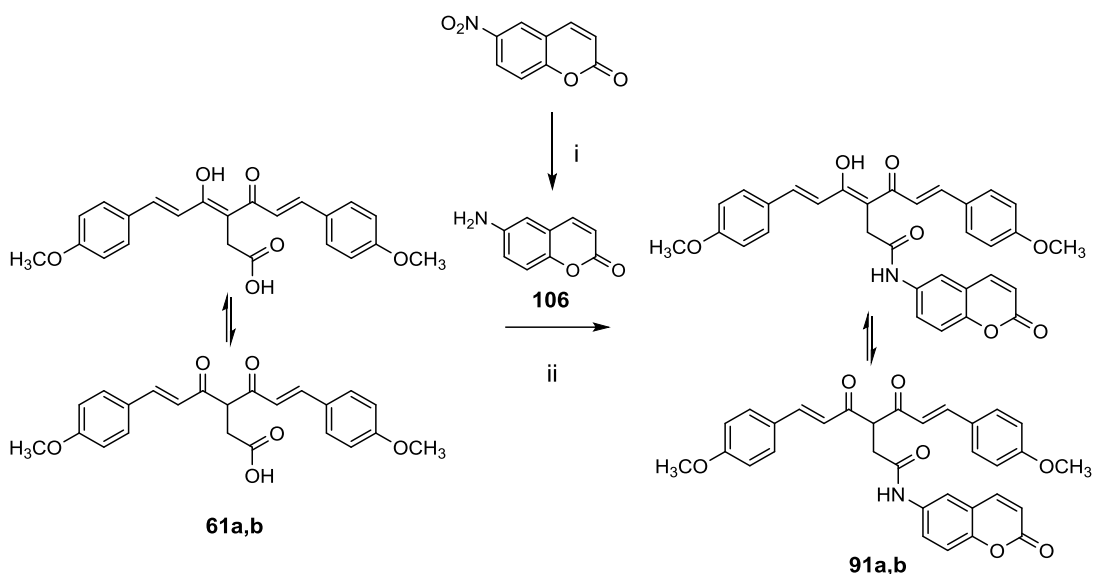


^a**Reagents and conditions:** i) NaN₃, acetone, 40 °C to r.t.; ii) TEA, CuSO₄, (+)-sodium *L*-ascorbate, DMF or DMSO, r.t.

3.9.3. Synthesis of amido curcuminoids **91a,b** and amine intermediate **106**

The synthesis of the β -keto-enol and diketo couple of amido derivatives **91a,b** was carried out by a classical coupling reaction between the corresponding tautomeric mixture of acids **61a,b** and amine **106** in CH₂Cl₂, under inert atmosphere (N₂ gas), using EDC and 4-(dimethylamino)pyridine (DMAP) as coupling agents (Scheme 25). **106** was obtained via a catalytic hydrogenation of the commercially available 6-nitro-2*H*-chromen-2-one in THF over palladium calcium-carbonate (Pd/CaCO₃) as catalyst (Scheme 25).

Scheme 25^a



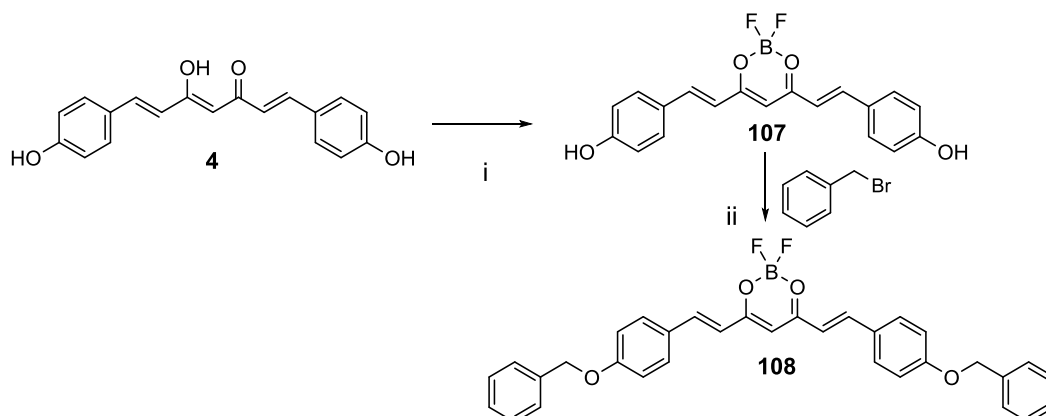
^aReagents and conditions: i) H₂, Pd/CaCO₃, THF; ii) EDC, DMAP, CH₂Cl₂, N₂, 0 °C to r.t.

3.10. SYNTHESIS OF SERIES VIa and VIb

3.10.1. Synthesis of difluoroboron-derivatized curcuminoids 107 and 108

The preparation of the difluoroboron-derivatized curcuminoids **107** and **108** started from the phenol intermediate **4** as shown in Scheme 26. In particular, a first complexation reaction with borontrifluoride etherate (BF₃·Et₂O) in CHCl₃ allowed the isolation of the complex **107**, then a Williamson reaction with benzyl bromide as alkylating reagent gave **108** (Scheme 26).

Scheme 26^a

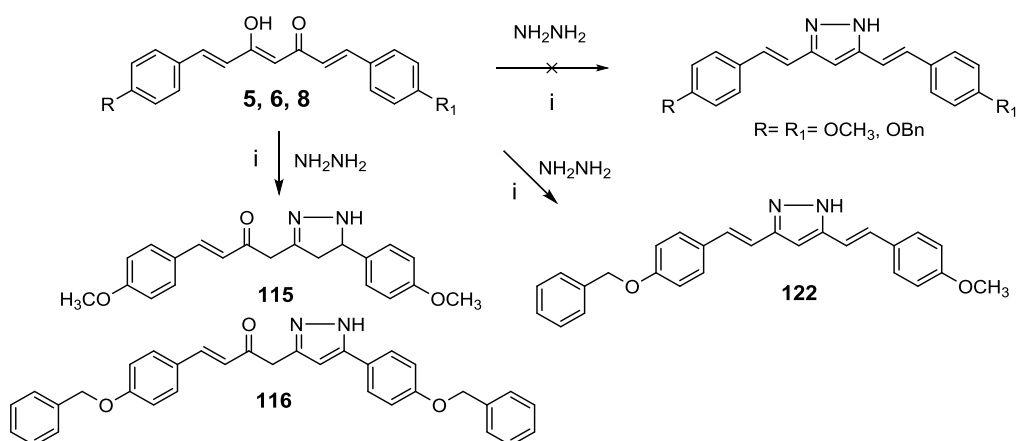


^aReagents and conditions: i) $\text{BF}_3 \cdot \text{Et}_2\text{O}$, CHCl_3 , r.t.; ii) K_2CO_3 , acetone, 80°C .

3.10.2. Synthesis of pyrazoles 109-113, 116-120, 122, dihydropyrazole 115 and isoxazoles 114 and 121

When the central 3,5-dione structural motif of analogues **5**, **6** and **8** was cyclized for treatment with hydrazine monohydrate ($\text{NH}_2\text{NH}_2 \cdot \text{H}_2\text{O}$) in acetic acid (CH_3COOH) under reflux, only the asymmetrical derivative **6** gave the expected pyrazole **122** (Scheme 27). In the other cases, treatment with NH_2NH_2 gave a side Michael reaction, followed by an intramolecular cyclization, affording compounds **115** and **116** (Scheme 27).

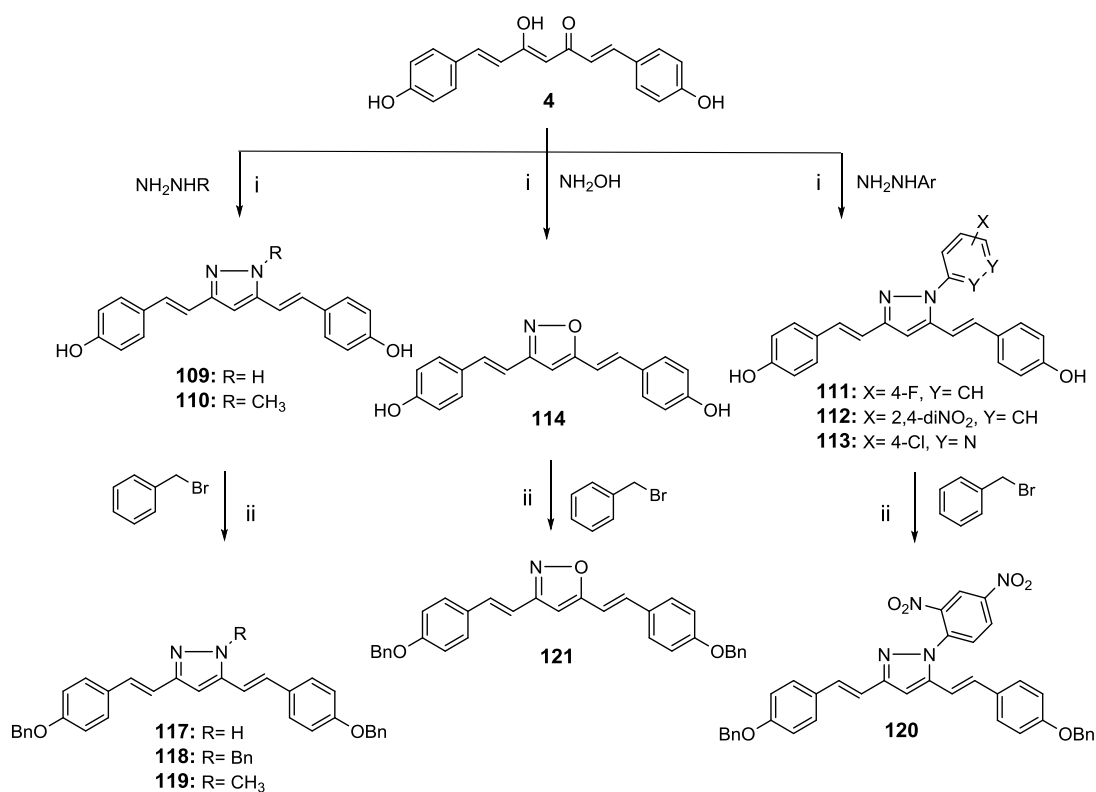
Scheme 27^a



^aReagents and conditions: i) CH_3COOH , reflux to r.t.

Therefore, aimed at obtaining the desired substituted pyrazoles, an alternative synthetic route was applied as shown in Scheme 28. In particular, the reaction of the phenol-key intermediate **4** with hydrazine monohydrate, methylhydrazine and differently substituted arylhydrazines, in the same reaction conditions, afforded the corresponding pyrazoles **109-113**, while treatment with hydroxylamine hydrochloride ($\text{NH}_2\text{OH}\cdot\text{HCl}$) gave the isoxazole **114** (Scheme 28). The alkylation of **109-114** with benzyl bromide in acetone and in alkaline conditions (K_2CO_3) allowed to insert the benzyloxy moiety on the side aryl rings (**117-121**). Interestingly, reaction of **109** gave also **118** with an additional benzyl group on the central pyrazole fragment (Scheme 28).

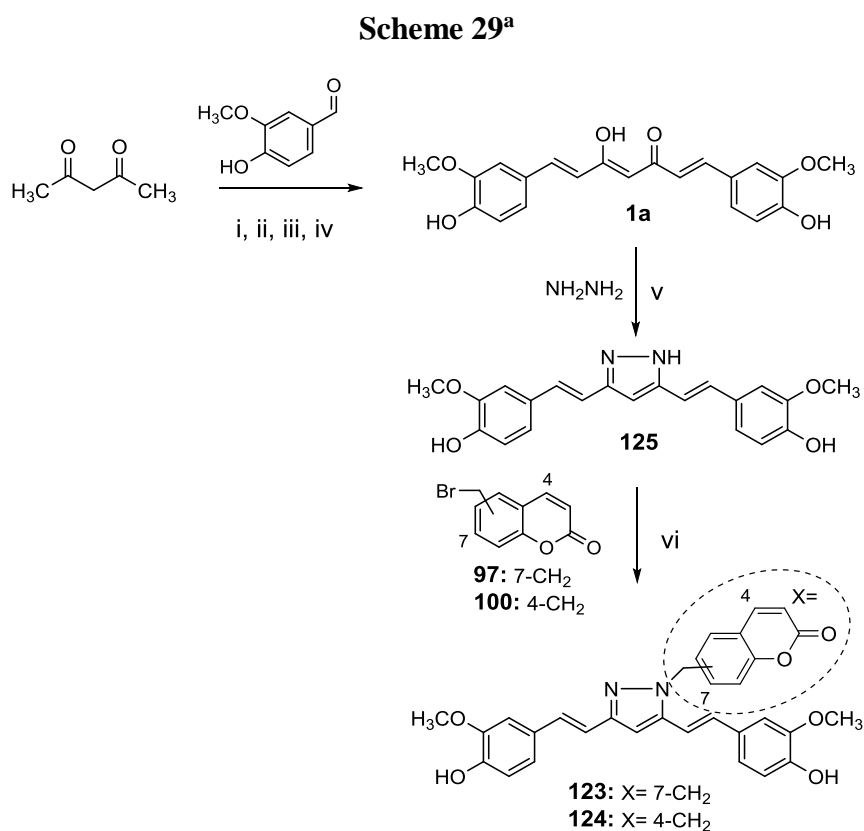
Scheme 28^a



^a**Reagents and conditions:** i) CH_3COOH , reflux to r.t.; ii) K_2CO_3 , acetone, 80 °C.

3.10.3. Synthesis of curcumin-based pyrazoles 123-125

The curcumin-based pyrazoles **123** and **124** were prepared starting from curcumin **1a**, (synthesized by a Pabon reaction in DMF employing vanillin as aldehyde, Scheme 29) that was reacted with $\text{NH}_2\text{NH}_2 \cdot \text{H}_2\text{O}$ in CH_3COOH to give the corresponding pyrazole **125**.¹⁵⁸ The further selective alkylation of the latter at the nitrogen atom with bromomethyl-coumarins **97** and **100** in THF, using TEA as discriminating base, allowed to obtain the desired *N*-substituted pyrazoles **123** and **124** (Scheme 29).



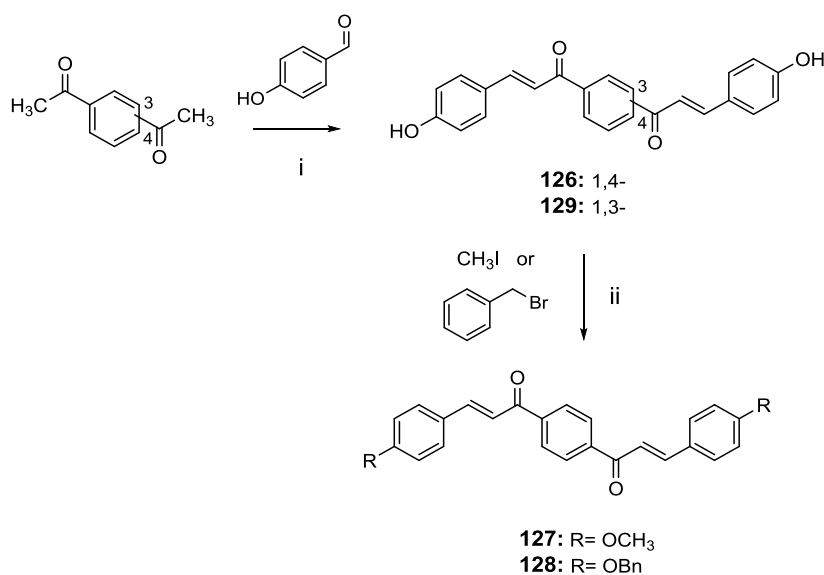
^a**Reagents and conditions:** i) B_2O_3 , DMF; ii) $\text{B}(n\text{-BuO})_3$; iii) $n\text{-BuNH}_2$, 80 °C; iv) HCl, 80 °C; v) CH_3COOH , reflux to r.t.; vi) TEA, THF, reflux.

3.11. SYNTHESIS OF SERIES VII

3.11.1. Synthesis of 1,4- and 1,3-bis(chalcones) 126-129

The synthesis of derivatives **126-129** was carried out as shown in Scheme 30. The condensation of 1,4- and 1,3-diacetylbenzene with 4-hydroxybenzaldehyde in ethanol (EtOH) at 0 °C, under acidic catalysis for treatment with gaseous hydrochloric acid (HCl_g), gave the phenol derivatives **126** and **129**, respectively (Scheme 30). Then, the Williamson reaction of **126** with methyl iodide and benzyl bromide gave the alkylated **127** and **128**, respectively (Scheme 30).

Scheme 30^a



^aReagents and conditions: i) HCl_g, EtOH, 0 °C; ii) K₂CO₃, acetone, 80 °C.

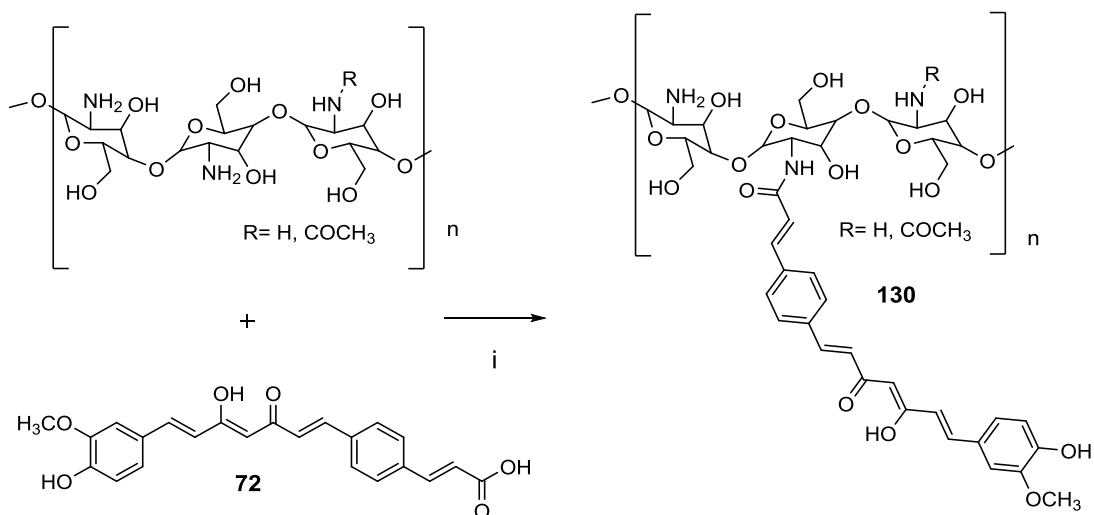
3.12. SYNTHESIS OF SERIES VIII

3.12.1. Synthesis of CS bioconjugates 130 and 131 and aldehyde 132

The bioconjugate **130** (% DS = 14 %) was prepared by functionalization of the primary -NH₂ groups of CS (% DD = 78 %) through a classical coupling

reaction with the acid functional group of **72**, in aqueous 1 % CH₃COOH (v/v), and using EDC and DMAP as coupling agents (Scheme 31).

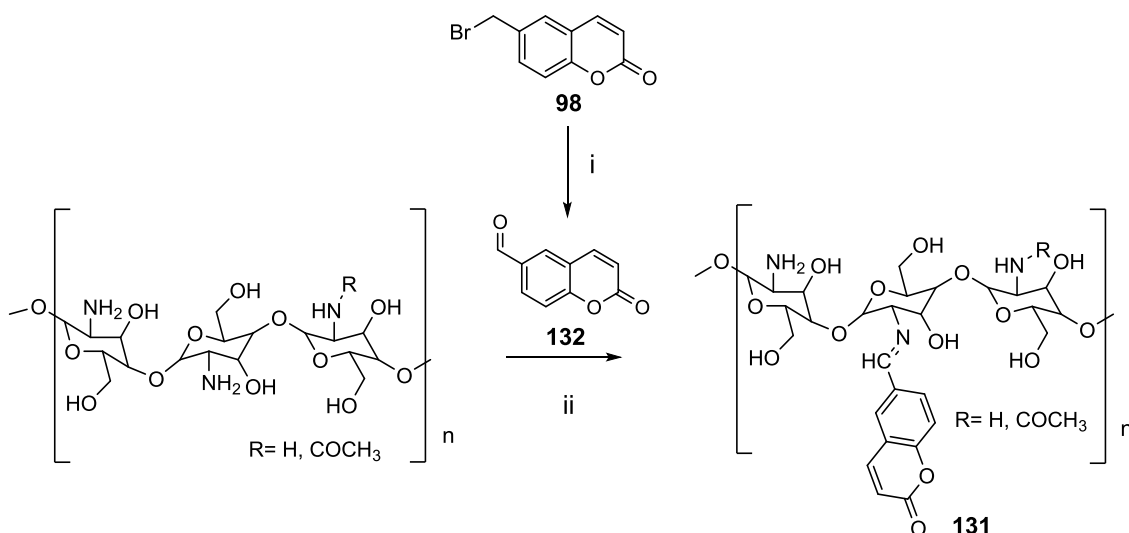
Scheme 31^a



^a**Reagents and conditions:** i) EDC, DMAP, H₂O (1 % CH₃COOH), 0 °C to r.t.

Furthermore, the bioconjugate **131** (% DS = 14 %) was obtained by nucleophilic addition (Schiff base reaction) of the primary -NH₂ groups of CS (% DD = 99 %) to the carbonyl function of aldehyde **132** (Scheme 32) in 1.6:1 mixture of 1 % CH₃COOH:[CH₃OH:acetone (5:1)]. Additionally, **132** was synthesized starting from the corresponding bromomethyl derivative **98**, that was refluxed in EtOH in the presence of hexamethylenetetramine (HMTA) and formic acid (40 %) (Scheme 32).

Scheme 32^a



^a**Reagents and conditions:** i) HMTA, HCOOH (40 %), EtOH, reflux; ii) 1 % $\text{CH}_3\text{COOH}:[\text{CH}_3\text{OH}/\text{acetone} (5:1)] (1.6:1)$, r.t.;

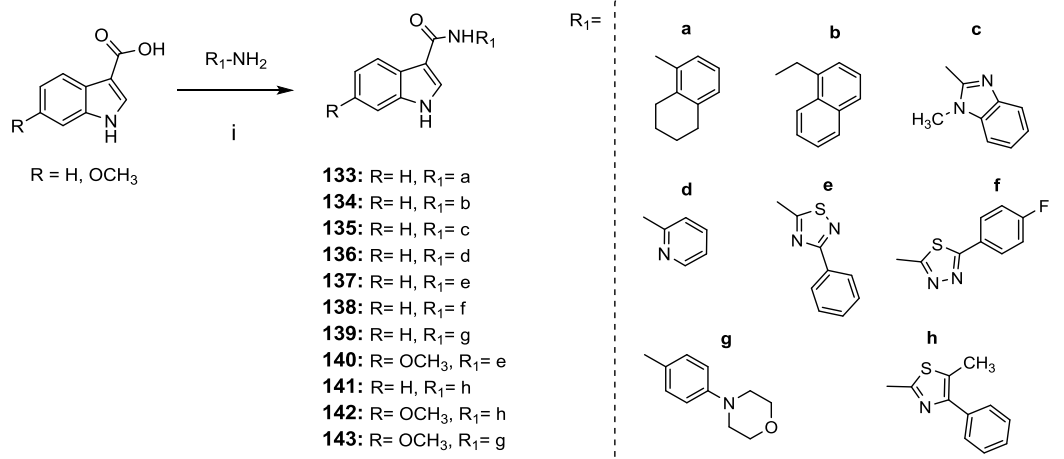
3.13. SYNTHESIS OF SERIES IX

3.13.1. Synthesis of indole-based derivatives 133-143

In general, the synthesis of indole derivatives **133-143** was performed by a classical coupling reaction between *1H*-indole-3-carboxylic acid or 6-methoxy-*1H*-indole-3-carboxylic acid and a large variety of heterocyclic and aromatic amines in DMF, under reflux and inert atmosphere (N_2 gas), using a mixture of EDC, DMAP and TEA in DMF as coupling agents (Scheme 33).

Although, at the beginning, the coupling reaction was carried out under conventional heating for the synthesis of some indole analogues as **133** and **135**, subsequently an approach of microwave assisted organic synthesis (MAOS) was preferred, as under microwave irradiation at 200 °C the experimental conditions are optimized, by reducing the reaction times from 6-15 h to 1-2 h.

Scheme 33^a



^a**Reagents and conditions:** i) EDC, DMAP and TEA, DMF, reflux (conventional heating) or 200 °C (MW).

4. *Results and discussion*

4.1. BACE-1 INHIBITION

Subset of curcumin-based analogues 2-17 (β -keto-enol forms) and 18-21 (diketo tautomers) and reference compound 1a.

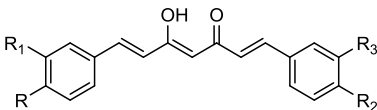
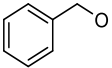
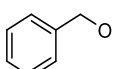
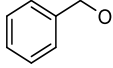
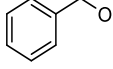
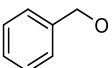
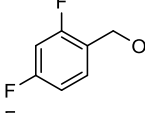
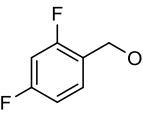
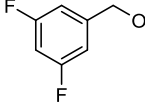
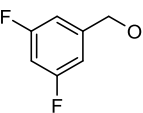
The fluorescence resonance energy transfer (FRET) methodology³¹ was employed to evaluate the BACE-1 *in vitro* inhibitory potency of a set of curcumin-based derivatives (**2-21**), using curcumin **1a** as reference compound (Tables 19 and 20). The compounds, except for **14**, were able to inhibit BACE-1, with IC₅₀ values ranging from low micromolar to nanomolar, being more potent than curcumin **1a**, that in our test did not inhibit the enzyme up to 3 μ M. Moreover, referring to the tautomeric couples **8, 19**; **5, 18**; **9, 20**; and **10, 21** the β -keto-enol forms showed a more favorable trend of inhibition than the corresponding diketo counterparts. The data confirmed the suitability of the β -keto-enol curcumin main scaffold for inhibition of this target, and underlined the potential intense effect on activity exerted by the substituents on the side aryl rings.⁸

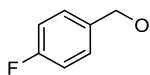
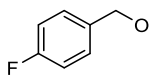
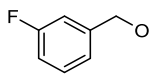
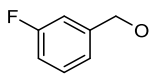
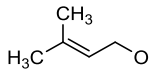
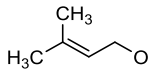
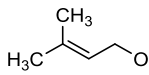
Indeed, for the bis-*p*-prenyloxyphenyl symmetrical analogue **14** no enzyme inhibition was observed up to 3 μ M. On the contrary, the bis-*p*-benzyloxyphenyl analogue **8** showed an IC₅₀ value of 40 nM, and was thus identified as the most active of the series, whereas the corresponding diketo tautomer **19** displayed a notable drop in potency. A decrease in activity was observed when the benzyloxy functions were replaced with the less hindering methoxy groups (**5**, IC₅₀ = 1.65 μ M); again, the corresponding diketo analogue (**18**) was less active than **5**. Low-micromolar potencies were noticed for the other symmetrical derivatives bearing hydroxy, methyl, phenyl groups in position 4 (**4, 16**, and **17**, respectively), and for the bis-3,4-dimethoxy-substituted **13**.

The symmetrical fluorinated analogues of **8** showed a decrease in potency, that was one order of magnitude lower for the 2,4- and 3,5-di-fluorinated **9** and **10**, respectively (IC₅₀ = 0.40 and 0.39 μ M), while their corresponding diketo counterparts **20** and **21**, respectively, showed low-micromolar IC₅₀ values. This level of potency was similarly observed for the 4- and 3- mono-fluorinated analogues of **8** (**11** and **12**, respectively).

An improvement in potency with respect to **1a** was observed for the asymmetrical derivatives **2** and **3**, and **15**, characterized by the curcumin's 4-hydroxy-3-methoxyphenyl ring at one side, and *para*-substituted phenyl ring on the other side; in this context, the methyl moiety gave the best results (**3**, IC₅₀ = 0.14 μM); whereas less active compounds were obtained by inserting the benzyloxy (**2**) and prenyloxy (**15**) substitution pattern. The curcuminoids **6** and **7** (mixed analogues of **8** with **5** and **4**, respectively) inhibited the enzyme with low micromolar potencies, demonstrating that the presence of one benzyl group only was not enough to obtain high potency.

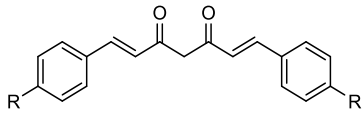
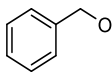
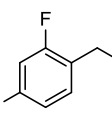
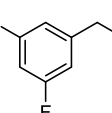
Table 19. BACE-1 inhibition by curcumin-based analogues as β-keto-enol tautomers (**2-17**) and curcumin (**1a**).

					
comp	R	R ₁	R ₂	R ₃	BACE-1 IC ₅₀ (μM) ^a ± SEM
2	OH	OCH ₃		H	0.97 ± 0.43
3	OH	OCH ₃	CH ₃	H	0.14 ± 0.03
4	OH	H	OH	H	2.54 ± 0.02
5	OCH ₃	H	OCH ₃	H	1.65 ± 0.01
6		H	OCH ₃	H	2.28 ± 0.64
7		H	OH	H	2.69 ± 1.01
8		H		H	0.04 ± 0.01
9		H		H	0.40 ± 0.06
10		H		H	0.39 ± 0.34

11		H		H	1.04 ± 0.34
12		H		H	1.08 ± 0.66
13	OCH ₃	OCH ₃	OCH ₃	OCH ₃	3.62 ± 0.28
14		H		H	n.i. ^b
15	OH	OCH ₃		H	3.94 ± 0.22
16	CH ₃	H	CH ₃	H	6.68 ± 0.01
17	Ph	H	Ph	H	7.25 ± 0.86
1a	OH	OCH ₃	OH	OCH ₃	n.i. ^b (343 ± 45) ^c

^aValues are the mean ± SD of two independent measurements, each performed in triplicate. SEM = standard error of the mean. ^bn.i.: not inhibiting up to 3 μM. ^cSee ref¹⁵⁹.

Table 20. Inhibition of BACE-1 by the curcumin-based analogues as diketo tautomers (**18-21**).

		
comp	R	BACE-1 IC ₅₀ (μM) ^a ± SEM
18	OCH ₃	> 5
19		6.04 ± 0.57
20		1.00 ± 0.35
21		0.73 ± 0.24

^aValues are the mean ± SD of two independent measurements, each performed in triplicate. SEM = standard error of the mean.

Taken together, these data allowed to identify **8** as the most active compound within the series, and pointed out that the structural modifications performed on it had, in general, detrimental effects.

Docking studies performed on compounds (**2**, **5-8**) at the binding site of BACE-1 were in line with the experimental results and confirmed **8** as the most potent inhibitor, due to its capability to establish a direct interaction with the enzyme catalytic dyad and to concurrently engage both the S and the S' sub-sites of the enzyme (Fig. 54).⁸

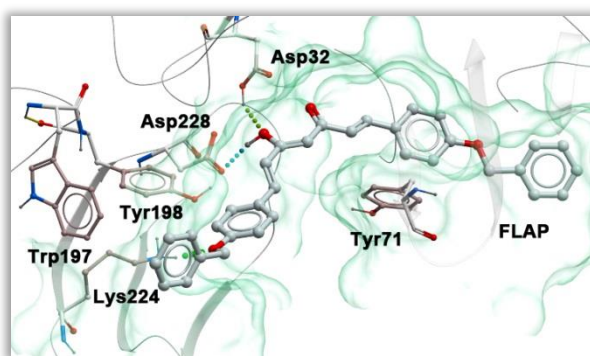


Figure 54. The predicted bound conformation of **8** at the binding site of BACE-1.⁸

4.2. GSK-3 β INHIBITION

Subset of compounds 2-21, 66-69 and reference compound 1a.

A high throughput luminescent assay based on the Kinase-GloTM system, consisting in the quantification of the ATP remaining in solution following a kinase reaction, was employed for the evaluation of the GSK-3 β inhibitory potency.¹⁶⁰ All the curcumin-based analogues (**2-21**) previously tested on BACE-1 were also evaluated on GSK-3 β , together with compounds **66-69**. Data are reported in Tables 21-23.

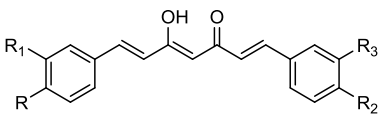
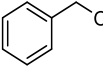
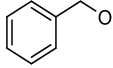
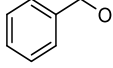
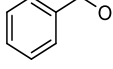
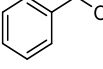
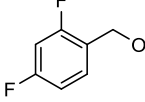
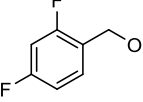
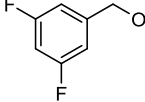
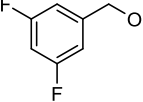
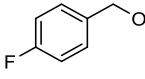
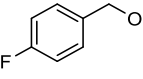
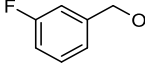
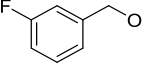
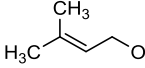
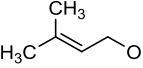
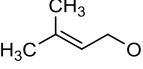
Considering the set of *para*-symmetric analogues **8**, **14**, **16**, **66** and **67**, only **8** displayed a IC₅₀ value of 2.49 μ M, while the other compounds resulted to be less effective GSK-3 β inhibitors: when tested at 10 μ M concentration, **16** and **67** (with methyl and boronic functions) turned out to inhibit GSK-3 β up to 47 % and 28 %; while for **14** and **66** (prenyloxy and Br substituted) no inhibition was detected. On

the contrary, all asymmetric curcuminoids of the corresponding series of vanillin-based (**2**, **3**, **15**, **68** and **69**) showed a good inhibition of the enzyme. In particular, **2**, bearing a 4-benzyloxy function on the other aryl ring displayed an interesting IC_{50} value of 0.90 μ M. Similarly, the introduction of a 4-methyl and 4-Br moiety (**3** and **68**, respectively) allowed to maintain low-micromolar potencies, while the presence of 4-prenyloxy and 4-boronic acid groups (**15** and **69**) resulted in a reduction of potency (40 % of inhibition at 10 μ M).

The 4-benzyloxy-based derivatives (**6-8**), analogues of **2**, displayed IC_{50} values around 2 μ M and, interestingly, only a slight decrease in potency was observed for the diketo analog of **8** (**19**). Considering the bis-fluorinated benzyloxy subset (**9**, **10** and **20**, **21** β -keto-enol and diketo counterpart, respectively), all the compounds showed GSK-3 β modulatory properties in a very narrow range (around 8-9 μ M). Moreover, for the mono-fluorinated analogues **11** and **12** a double-digit potency was noticed (IC_{50} = 12.81 and 16.99 μ M, respectively).

The bis-4-methoxy analogue **5**, with an IC_{50} value of 0.53 μ M, proved to be the most potent inhibitor of the whole series; remarkably, its diketo tautomer **18** showed a significant drop in potency.⁸ Among the analogues of **5**, the removal of the side methyl groups, to obtain bis-demethoxy curcumin **4**, proved to be detrimental for anti-GSK-3 β potency (IC_{50} = 8.39 μ M), as well as the insertion of an additional methoxy function into the 3-position to give **13** (21 % inhibition at 10 μ M); however these compounds were more potent than **1a** (IC_{50} = 17.95 μ M).

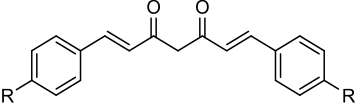
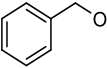
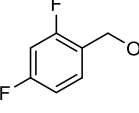
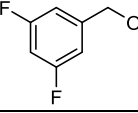
Table 21. GSK-3 β inhibitory potencies of **2-17** and curcumin (**1a**) as keto-enol tautomers.

					
comp	R	R ₁	R ₂	R ₃	GSK-3 β IC ₅₀ (μ M) ^a \pm SEM or % inh @ 10 μ M
2	OH	OCH ₃		H	0.90 \pm 0.38
3	OH	OCH ₃	CH ₃	H	2.09 \pm 0.51
4	OH	H	OH	H	8.39 \pm 1.59
5	OCH ₃	H	OCH ₃	H	0.53 \pm 0.27
6		H	OCH ₃	H	2.78 \pm 0.44
7		H	OH	H	2.01 \pm 0.71
8		H		H	2.49 \pm 0.82
9		H		H	9.63 \pm 0.21
10		H		H	8.30 \pm 0.54
11		H		H	12.81 \pm 0.14
12		H		H	16.99 \pm 2.68
13	OCH ₃	OCH ₃	OCH ₃	OCH ₃	21 %
14		H		H	n.i. ^b
15	OH	OCH ₃		H	40 %
16	CH ₃	H	CH ₃	H	47 %
17	Ph	H	Ph	H	7.74 \pm 0.59

1a	OH	OCH ₃	OH	OCH ₃	17.95 ± 1.03
-----------	----	------------------	----	------------------	--------------

^aValues are the mean ± SD of two independent measurements, each performed in triplicate. SEM = standard error of the mean. ^bn.i.: not inhibiting at 10 μM.

Table 22. GSK-3β inhibitory potencies of **18-21** as diketo tautomers.

		
comp	R	GSK-3β IC ₅₀ (μM) ^a ± SEM
18	OCH ₃	15.30 ± 3.64
19		5.56 ± 0.01
20		9.06 ± 2.07
21		9.66 ± 1.02

^aValues are the mean ± SD of two independent measurements, each performed in triplicate. SEM = standard error of the mean.

In light of these results, among all the tested analogues, **5** proved to be the most potent GSK-3β inhibitor, as confirmed by docking studies at the binding site of the enzyme in which the compound, due to its smaller size, adopted a suitable conformation for the best interaction with the enzyme hinge region (Fig. 55).⁸

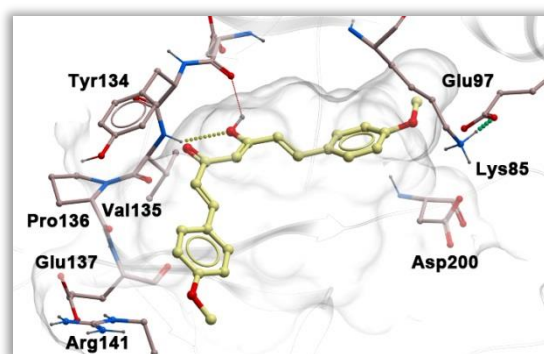


Figure 55. The predicted bound conformation of **5** at the binding site of GSK-3 β .⁸

Table 23. Inhibition of GSK-3 β enzymatic activities by the curcumin-based analogues **66-69**.

comp	R	R ₁	R ₂	GSK-3 β IC ₅₀ (μ M) ^a \pm SEM or % inh @ 10 μ M
66	Br	H	Br	n.i. ^b
67	B(OH) ₂	H	B(OH) ₂	28 %
68	OH	OCH ₃	Br	7.67 \pm 0.18
69	OH	OCH ₃	B(OH) ₂	41 %

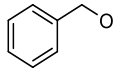
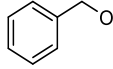
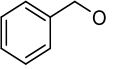
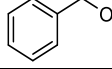
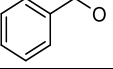
^aValues are the mean \pm SD of two independent measurements, each performed in triplicate. SEM = standard error of the mean. n.i.^b not inhibiting at 10 μ M.

Subset of curcuminoid-DF hybrids (74-76 and 78).

In an effort to obtain derivatives with an expanded biological profile, some of the most effective BACE-1 and GSK-3 β inhibitors (**5**, **6**, and **8**), were selected to be subjected to hybridization strategy, by introducing into the 4-position of the main scaffold a molecular fragment of the potent Nrf2 inducer dimethyl fumarate (DF), to give the curcumin-DF series of compounds **74**, **75** and **76**, respectively (Table

24). When **6** and **8** (IC₅₀s values around 2 μM) were employed as starting backbones to obtain **75** and **76**, a low-micromolar GSK-3β inhibitory activity was maintained (IC₅₀ = 8.39 and 7.26 μM, respectively). A slight decrease in potency was displayed by **78**, as acidic analogue of **76** (46 % of inhibition at 10 μM). On the contrary, for the 5-DF hybrid **74** a remarkable drop of potency was observed, as it showed 20 % inhibition when tested at 10 μM.

Table 24. Inhibition of GSK-3β enzymatic activities by the curcumin-DF hybrids **74-76** and **78**.

comp	R	R ₁	R ₂	GSK-3β IC ₅₀ (μM) ^a ± SEM or % inh @ 10 μM
74	OCH ₃	Et	OCH ₃	20 %
75		Et	OCH ₃	8.39 ± 0.34
76		Et		7.26 ± 0.28
78		H		46 %

^aValues are the mean ± SD of two independent measurements, each performed in triplicate. SEM = standard error of the mean.

These derivatives were also tested to assess their neuroprotective potential, i.e. to offer protection against oxidative stress and to enhance GSH levels (see section 4.3).

4.3. NEUROPROTECTION

The neuroprotective potential of derivatives **5**, **8**, and the corresponding DF-hybrids **74-76** and **78** was investigated through *in vitro* evaluation of their neuronal effects on:

1. cell viability;
2. protection against oxidative stress;
3. enhancement of GSH levels.

In each investigation, DF was used as reference compound.

4.3.1. SH-SY5Y neuroblastoma cell viability

The cellular toxicity of the selected curcumin-based derivatives was examined on SH-SY5Y neuroblastoma cells, which were exposed for 24 h to the tested compounds at 0-10 μM range of concentrations. Cell viability was measured by MTT assay. Similarly to DF, no remarkable decrease in cell viability was observed at the tested concentrations.

4.3.2. Antioxidant activity

Oxidative stress has been recognized as a common pathological AD feature, and it is substantially produced by reactive radical species, among others ROS. Thus, **74-76** and **78** and the parent compounds **5** and **8** were assayed for their scavenging potential, in the absence or presence of pre-treatment, on SH-SY5Y cells exposed to high levels of *tert*-butyl hydroperoxide (TBH, 100 μM).

In particular, SH-SY5Y cells were first incubated for 24 h with 5 μM of the tested compounds and then exposed to TBH for 30 min. At the end of the incubation, ROS formation was detected (using the fluorescent probe DCFH-DA). None of the tested compounds could significantly affect ROS scavenging activity (Fig. 56); interestingly, this effect was increased in cells pre-treated with **74-76**, suggesting an indirect antioxidant mechanism of action. In particular, at 5 μM ,

compound **74** showed a substantial inhibition of TBH-induced total ROS levels, comparable to that of DF.

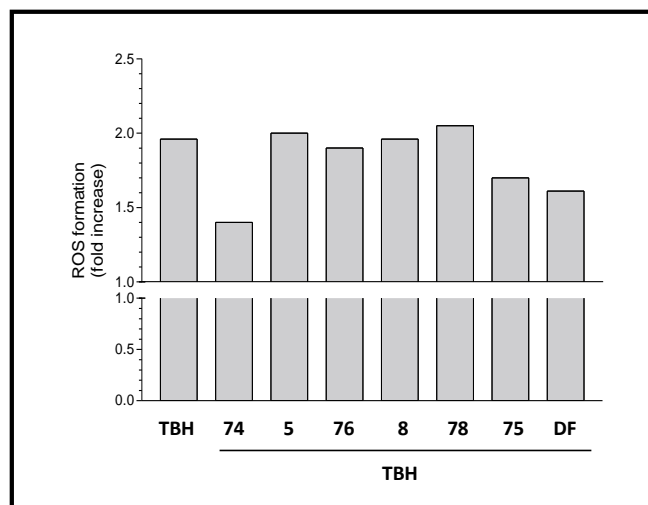


Figure 56. Effects of **5**, **8**, **74-76**, **78** and DF on ROS formation in SH-SY5Y cells. The cells, after treatment with the compounds at the fixed concentration of 5 μ M, were exposed to 100 μ M TBH for 30 min. The increase in DCFH-DA fluorescence was related to the intracellular ROS formation.

4.3.3. Total GSH levels enhancement

In AD brain, the levels of GSH, the main antioxidant enzyme involved in ROS detoxification and regulation of the intracellular redox environment, were found to be remarkably reduced, suggesting a direct correlation between AD pathology and low GSH levels. Therefore, the induction of this antioxidant enzyme may be associated with a protective role, allowing to delay the progression of the malady.

For this reason, the ability of compounds **5**, **8**, **74-76** and **78** to increase the total GSH levels in SH-SY5Y cells was investigated. In particular, SH-SY5Y cells were incubated for 24 h with 5 μ M of each compound and a fluorescent probe (monochlorobimane) was employed to measure GSH levels. Among the tested compounds, **74** and **75** showed a significant increase (~80 % and ~44 %, respectively) in cellular GSH content (Fig. 57). Not surprisingly, and in agreement with the design strategy, **5** did not affect GSH levels, suggesting a direct

involvement of the additional acrylate fragment in the enhancement of the total GSH levels.

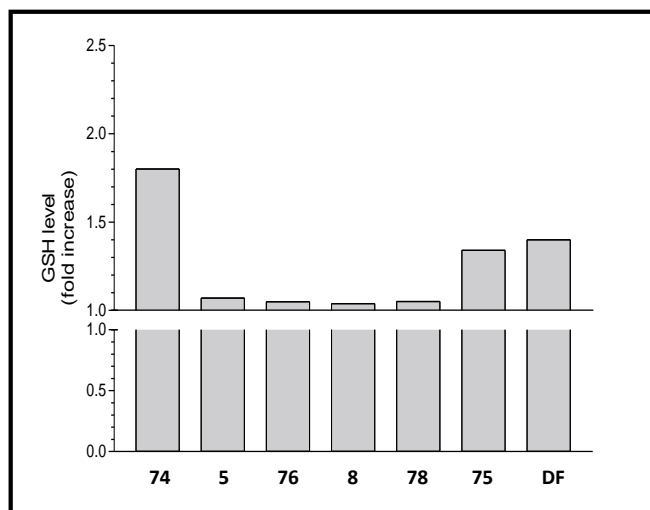


Figure 57. Effects of **5**, **8**, **74-76**, **78** and **DF** on total GSH levels of SH-SY5Y cells after incubation for 24 h with 5 μ M of compound.

Taken together, from these preliminary results compounds **74** and **75**, endowed with an indirect mechanism of antioxydative action and a good capability to enhance total GSH levels, emerged as the most interesting derivatives of the series. Furthermore, considering that the transcription factor Nrf2 tightly regulates enzymes involved in GSH synthesis, for both these hybrid compounds the Nrf2 modulation potential will be studied.

4.4. NEUROINFLAMMATION

A critical issue for curcumin-based analogues is the assessment of their neuronal toxicity. Thus, the *in vitro* biological evaluation of the curcumin-based analogues (**4**, **13-15**, **68**, **79**, **109** and **110**) began with a preliminary assessment of the toxicity profile, by evaluating their effects on cortical microglia cell viability. Then, for compounds showing no toxicity, the determination of antiinflammatory effects was carried out.

1. Subset of compounds 1a, 4, 79, 109 and 110.

4.4.1. Neurotoxicity: microglial cell viability

Generally, the compounds were tested in both primary and lipopolysaccharide (LPS)-activated microglial cells in a 1-40 μM range of concentrations, and cell viability was determined by MTT assay. Results were expressed as percentage of viability relative to the control or LPS treated culture. Morphological examination of the culture were also performed to corroborate the data.

Treatment of **1a, 4, 79, 109** and **110** for 16 h at the fixed concentrations of 1, 5, and 10 μM , in both cellular conditions, did not significantly affect neither cell viability nor cell morphology compared to untreated control (Fig. 58A).

Conversely, in the 20-40 μM range of concentrations, **1a, 4, 79,** and **109** demonstrated toxic effects, particularly evident for **1a**, and the high amount of cell debris observed in the cell cultures also confirmed these data. On the contrary, **110** did not show any toxic behaviour (Fig. 58A).

When LPS-stimulated microglia (100 ng/mL) was treated for 16 h with the selected set of derivatives (1-10 μM , Fig. 58B), an activated phenotype was observed, in which cells presented a macrophage-like morphology, that was not substantially different from that of control (LPS-activated cells). At 10 μM , **79** proved to significantly reduce cell viability. In the same conditions, an increase in cell death was observed upon treatment with higher concentrations (20-40 μM) of derivatives (Fig. 58B).

These preliminary studies allowed identifying the range of concentrations to be employed in the next cytokine release evaluation assay: 1-5 μM for **79**, 1-10 μM for **1a, 4,** and **109**.

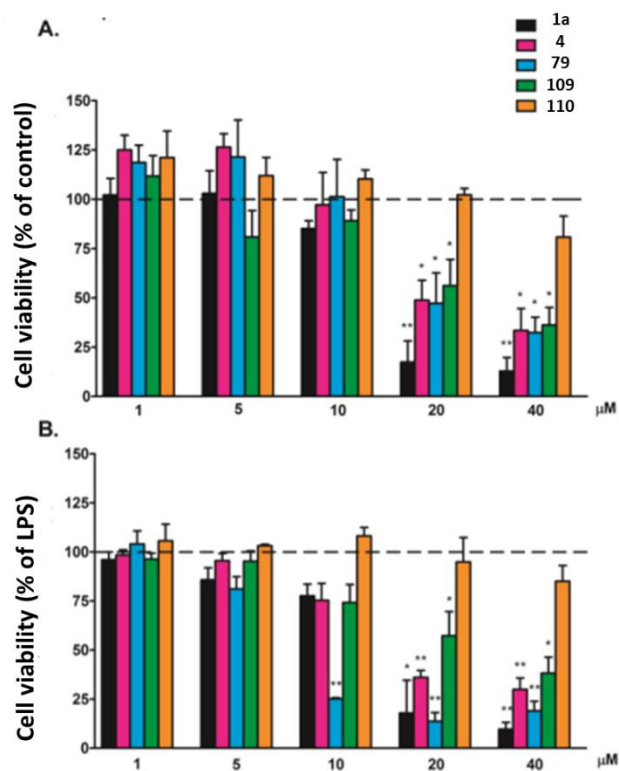


Figure 58. Microglial cell viability for compounds **1a**, **4**, **79**, **109** and **110** tested in the 1-40 μM range of concentrations in unstimulated (**A**) and (100 ng/mL) LPS-stimulated (**B**) microglia. Results are expressed as percentage of cell viability.

4.4.2. Neuroinflammatory potential

Genetic and epidemiological studies proposed the remarkable influence of neuroinflammation in AD pathogenesis. An increase in expression of pro-inflammatory cytokines, namely $\text{TNF-}\alpha$, $\text{IL-1}\beta$, IL-6 , IL-15 by activated microglial cells is a characteristic feature of AD-associated inflammation. These inflammatory mediators are neurotoxic factors and exert detrimental effects mainly by induction of neuronal apoptosis and synaptic dysfunctions, or by astrocytes activation.

Release of pro-inflammatory cytokines by microglia

Microglia cell activation was evaluated by determination of the levels of pro-inflammatory cytokines. A first set of compounds, **1a**, **4**, **79**, and the pyrazole-

based analogues **109** and **110**, was tested for the release of the pro-inflammatory cytokines (IL-1 β , IL-6 and TNF- α) by LPS-stimulated microglia.

Microglial cells were first exposed (1 h) to increasing and not-toxic concentrations (1-10 μ M) of the tested compounds, and then to LPS (100 ng/mL for 6 h). The levels of the released IL-1 β , IL-6, and TNF- α were then determined into the culture medium by means of an enzyme-linked immunosorbent assay (ELISA). Unstimulated cells, characterized by a low or undetectable release of cytokines, were employed as reference; these basal levels were unchanged upon treatment with the tested compounds (data not shown). LPS proved to promote the release of IL-1 β , IL-6, and TNF- α (404 pg/mL, 307 pg/mL, and 1035 pg/mL, respectively).¹⁶¹

In general, treatment with **1a**, **4** and **79** significantly suppressed the release of IL-1 β , IL-6 and TNF- α in a concentration-dependent manner. Conversely, and not surprisingly, this behavior was not shown for **109** and **110** that, in agreement with the design rationale, were ineffective. These data confirmed the pivotal role of the α,β -unsaturated carbonyl moiety in influencing the extent of the inflammatory response elicited by LPS.

IL-1 β release

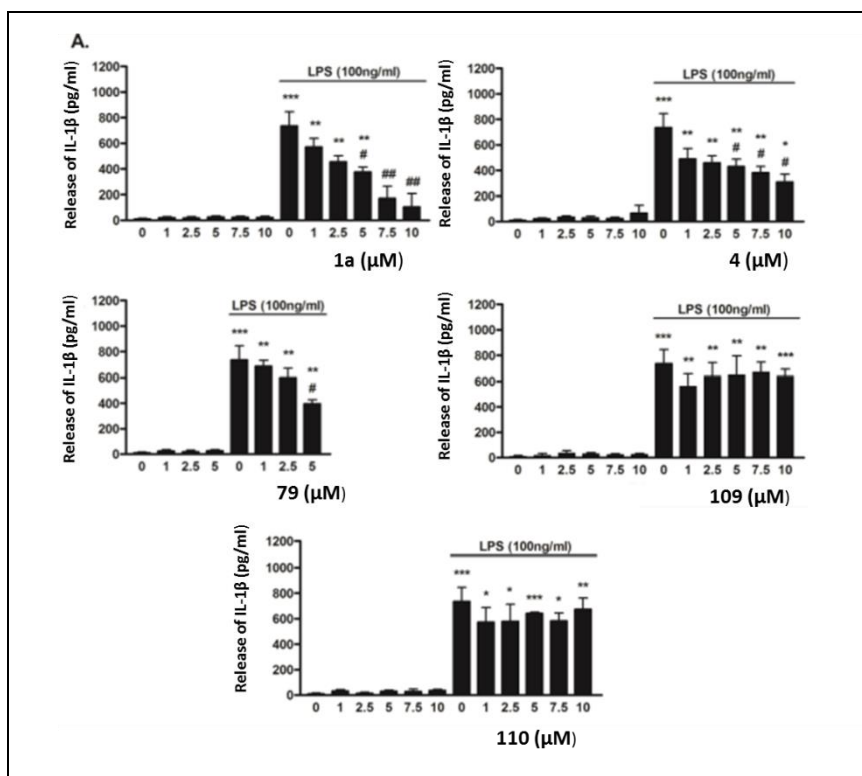
At the concentration of 5 μ M, a 50 % reduction in IL-1 β release was observed. Among the tested compounds, at the higher concentrations of 7.5 and 10 μ M only **1a** achieved a maximum inhibitory effect, in which the IL-1 β levels did not differ from the basal levels (Fig. 59A).

IL-6 release

Interestingly, a very strong inhibitory effect was observed for IL-6 release, that was maximally inhibited (reaching the basal levels) by **1a** and **4** at 5 μ M and by **79** at 2.5 μ M (Fig. 59B).

TNF- α release

TNF- α release was significantly (50 %) reduced by **4** and **79** at the concentration of 5 μ M, while a higher concentration (7.5 μ M) was required to achieve this effect with **1a** (Fig. 59C). Nevertheless, at the non-toxic tested concentrations, all the compounds proved to be unable to decrease TNF- α to the basal level.



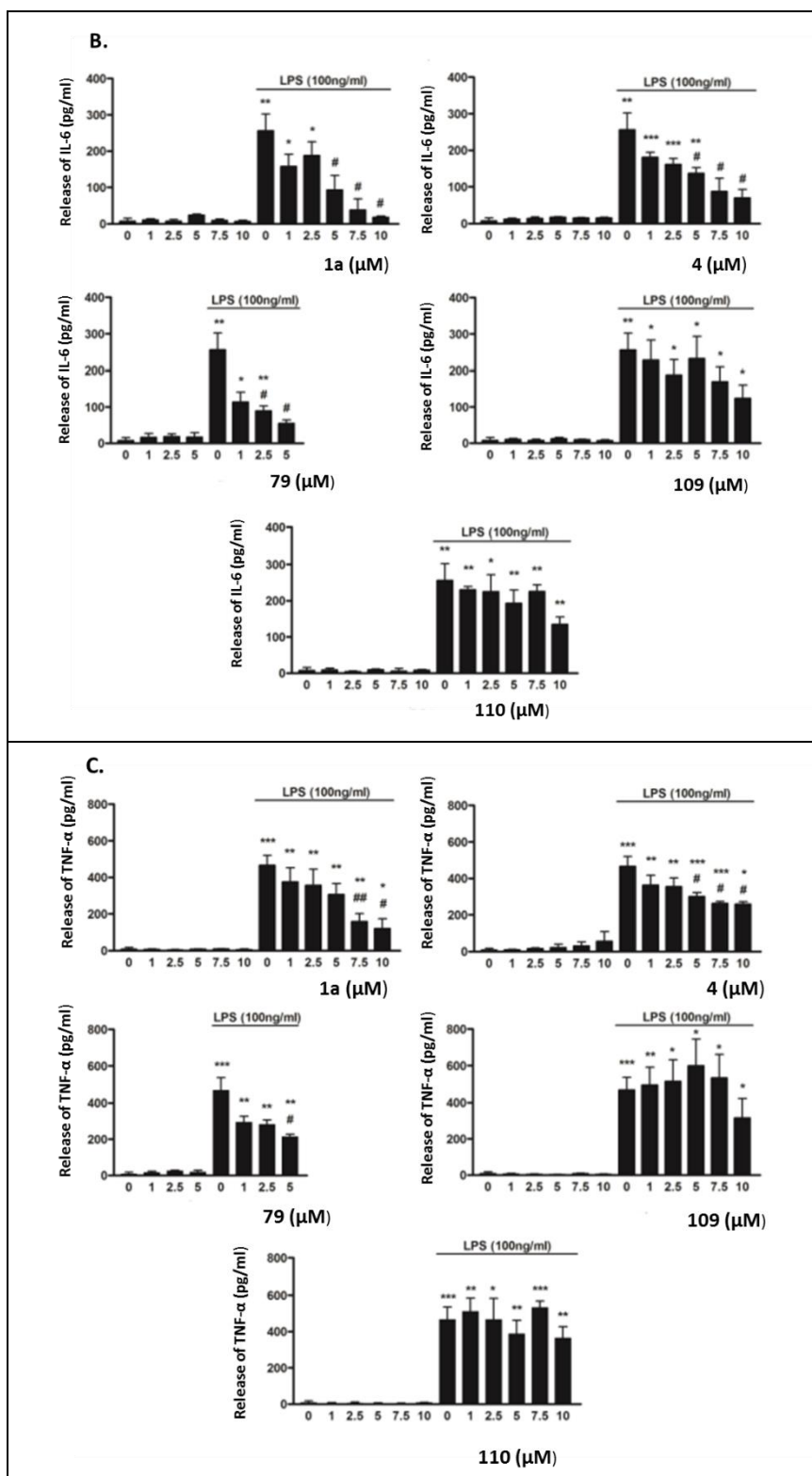


Figure 59. Effect of **1a**, **4**, **79**, **109** and **110** on cytokine release from LPS stimulated cortical microglia. Microglial cells were subcultured for 24 h in 10 % FBS-

containing medium, which was then replaced with serum-free medium treatment for 24 h with increasing concentrations of compounds in the presence of 100 ng/mL LPS. Supernatants were then collected, and analysed for release of IL-1 β (A), IL-6 (B), and TNF- α (C). Data are means \pm SEM (n = 3 in triplicate). * $p < 0.05$, ** $p < 0.01$ vs corresponding control (PLS-stimulated cells); t test.

From the results gathered in this study, it clearly emerged that all the tested compounds showed an intrinsic antiinflammatory activity, since they induced a decrease in pro-inflammatory cytokines release at non-toxic concentrations.

In conclusion, **4** emerged as a promising drug candidate, due to its capability to reduce microglial inflammatory responses without eliciting toxic effects, thus offering promises to slow down the progression of neuroinflammatory disorders.

2. Subset of compounds 13-15 and 68.

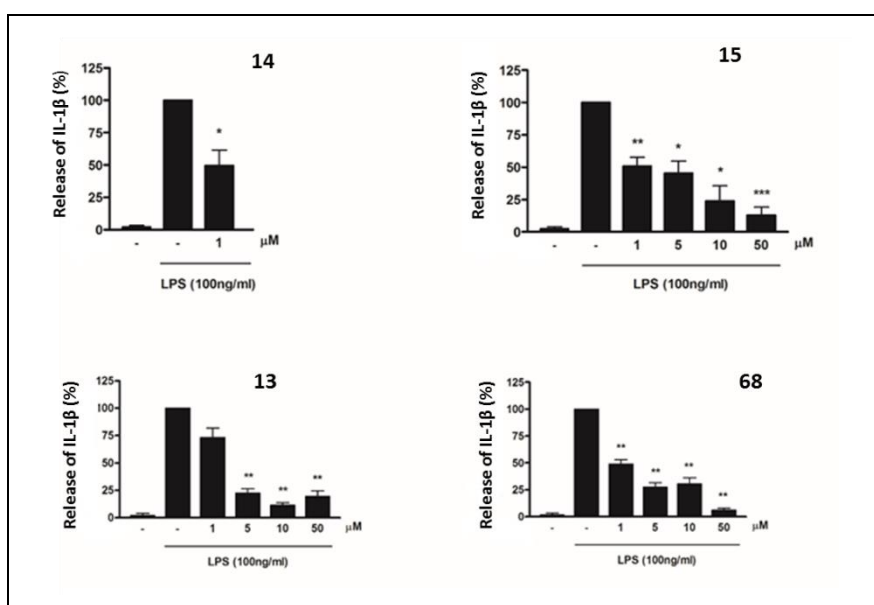
These results represent a starting point for the design of novel effective and not toxic antiinflammatory agents based on the curcumin scaffold. Thus, aimed at exploring the chemical features responsible for the antiinflammatory effect, a new set of molecules (**13-15** and **68**) was designed and evaluated for the inhibitory effects on microglia activation and the resultant inflammatory response.

The preliminary assay aimed at determining the possible cytotoxic effect of the compounds on microglia allowed to assess the lack of toxic effects for **13**, **15**, and **68**, since at the tested concentrations of 1, 5, 10, and 50 μ M, and in absence of LPS stimulation, they did not affect cell viability and morphology. In the same conditions, a toxic behaviour was observed for **14** at the highest concentrations of 10 and 50 μ M.

These experiments were repeated on LPS-stimulated microglia: viability of cell cultures exposed to **13**, **15**, and **68** up to 50 μ M and **14** at 1 μ M was not significantly different with respect to the control.

Cytokine release

The effects of these analogues on microglia activation were studied by examination of their effect on pro-inflammatory cytokine release. All the tested curcumin-based analogues inhibited the release of IL-1 β , IL-6, and TNF- α in a concentration-dependent manner. In particular, **14**, **15** and **68** at 1 μ M significantly affected IL-1 β , IL-6, and TNF- α releases, that were reduced to about 50 % of control level (Fig. 60). A concentration of 5 μ M was necessary to achieve the same results with **13**.



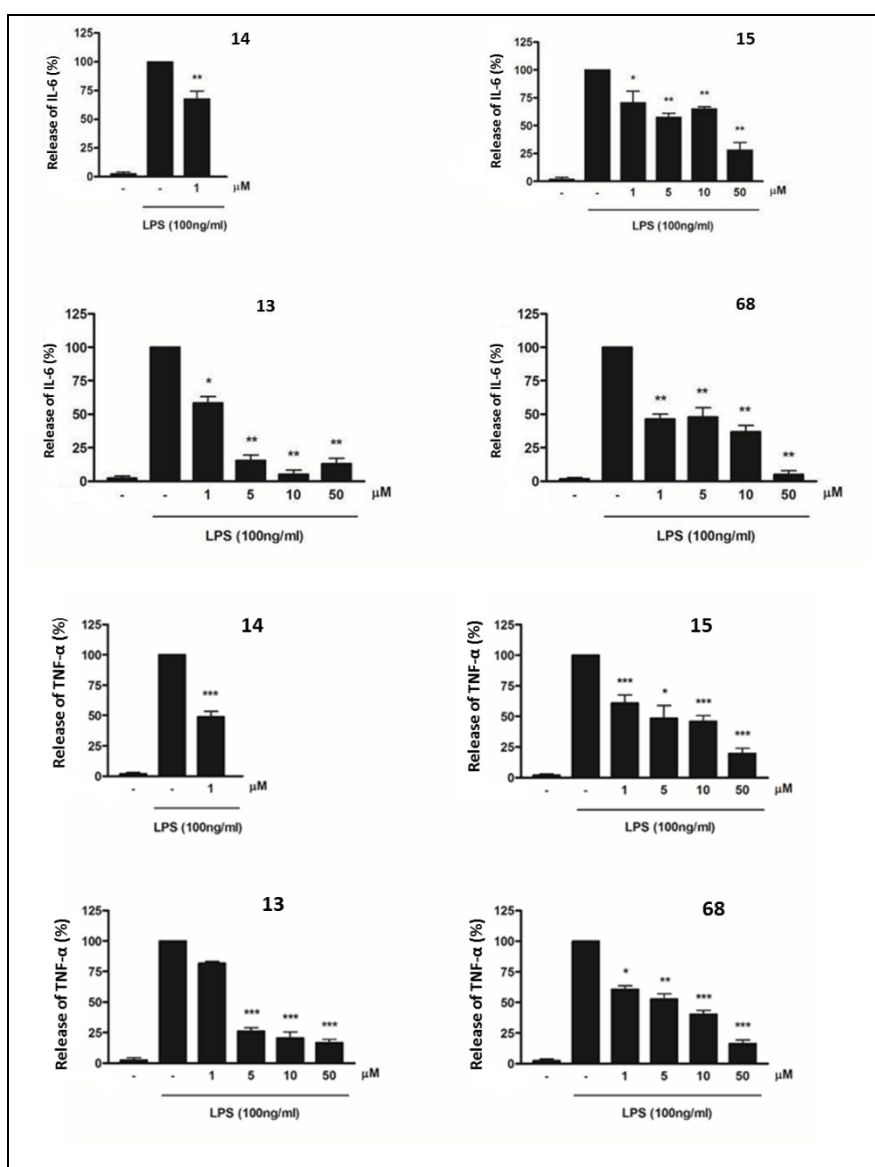


Figure 60. Effect of **13**, **14**, **15** and **68** on cytokine release from LPS stimulated cortical microglia. Microglial cells were subcultured for 24 h in 10 % FBS-containing medium, which was then replaced with serum-free medium treatment for 24 h with increasing concentrations of compounds in the presence of 100 ng/mL LPS. Supernatants were then collected, and analysed for release of IL-1 β , IL-6, and TNF- α . Data are means \pm SEM (n = 3 in triplicate). * p <0.05, ** p <0.01 vs corresponding control (PLS-stimulated cells); t test.

Thus, further studies are needed, aimed to develop new drug candidates or pharmacological agents that may allow slowing down the progression of neuroinflammatory disorders characterized by microglial activation such as AD.

4.5. THIOL TRAPPING ASSAY AND COVALENT DOCKING SIMULATION ON GSK-3 β

Subset of compounds 2, 5-8, 67 and 69.

Taking into account curcumin capability to irreversibly and rapidly react with cysteamine in DMSO- d_6 affording the corresponding bis-1,7-thia-Michael adduct, a spectroscopic $^1\text{H-NMR}$ -based thiol trapping assay was carried out on some interesting curcumin-based analogues, in order to study the aptitude of their electrophilic central framework to undergo a Michael addition.

All tested compounds underwent a thiol-trapping reaction by employing a mixture of compounds/cysteamine in a 1:2 stoichiometric ratio in DMSO- d_6 , affording the corresponding thia-Michael adduct in very short times, as confirmed by the disappearance of the characteristic olefin signals in the $^1\text{H-NMR}$ spectra. In each case, the reaction mixture was monitored at different intervals of time up to several days and the failure of the reappearance of the characteristic olefin signals in the spectra corroborated the irreversible nature of the Michael addition reaction.⁸

The $^1\text{H-NMR}$ spectra of compounds **5**, **67** and **69** and of their corresponding bis-1,7-thia-Michael adducts are reported in appendix (Figs. A1a and A1b, A2a and A2b, A3a and A3b, respectively).

These exciting results supported a covalent docking simulation on GSK-3 β , in which a nucleophilic attack of Cys199 residue of the enzyme on the reactive α,β -unsaturated carbonyl function of **5** was accomplished (Fig. 61).⁸

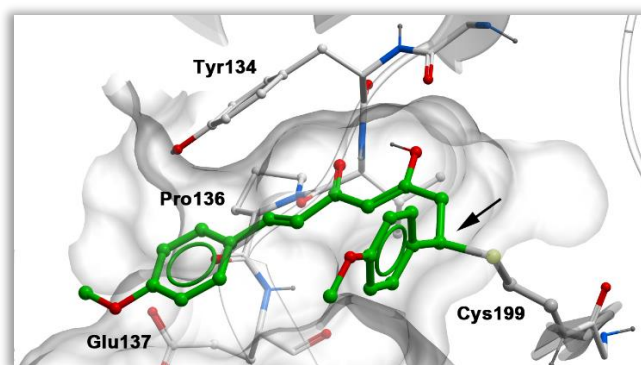


Figure 61. Predicted covalently bound conformation of **5** at the binding site of GSK-3 β .

4.6. CK1 AND LRRK2 INHIBITION

The indole-based derivatives **133-142** were investigated to assess their inhibitory activity on CK1 and LRRK2, two additional PKs involved in AD pathogenesis. The compounds were tested at a fixed concentration of 10 μM to determine the percentage of inhibition (% inh) and, when this was higher than 50 %, IC_{50} was calculated.

4.6.1. CK1 δ and CK1 ϵ inhibition

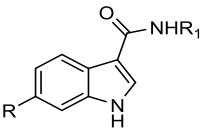
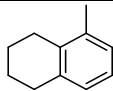
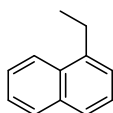
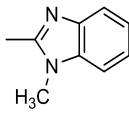
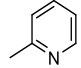
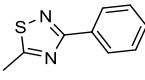
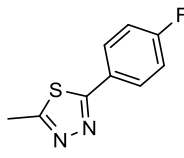
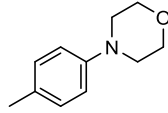
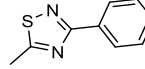
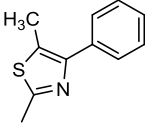
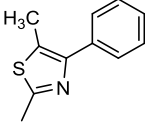
Subset of compounds 133-142.

The Kinase-GloTM methodology,¹⁶⁰ was employed to evaluate the CK1 δ and CK1 ϵ inhibitory potency. At the beginning, the biological evaluation was carried out on the CK1 δ isoform, then for analogues that showed an interesting biological profile, the inhibitory activity on CK1 ϵ was also investigated (Table 25).

The preliminary results on CK1 δ allowed to identify **137** and **140**, bearing a 3-phenyl-1,2,4-thiadiazolyl heterocycle, as active compounds with micromolar values of potency. In particular, derivative **140**, characterized by a methoxy group into the 6-position of the indole scaffold, showing an IC_{50} value of 1.03 μM , proved to be more potent than **137** ($\text{IC}_{50} = 19.49 \mu\text{M}$) and was recognized as the most interesting compound of the series to be subjected to further investigation.

Therefore, **140** was tested on CK1 ϵ , confirming a low micromolar inhibitory profile ($\text{IC}_{50} = 7.31 \mu\text{M}$), although lower than that on CK1 δ .

Table 25. Inhibition of CK1 δ and CK1 ϵ by indole-based derivatives **133-142**.

				
comp	R	R ₁	CK1 δ % inh @ 10 μ M or IC ₅₀ (μ M)	CK1 ϵ % inh @ 10 μ M or IC ₅₀ (μ M)
133	H		< 20 %	-
134	H		< 20 %	-
135	H		< 20 %	-
136	H		< 20 %	-
137	H		19.49 \pm 1.79	-
138	H		< 20 %	-
139	H		< 20 %	-
140	OCH ₃		1.03 \pm 0.18	7.31 \pm 0.20
141	H		< 20 %	< 20 %
142	OCH ₃		<20 %	< 20 %

Furthermore, to elucidate the mechanism of action of **140** on CK1 δ , a kinetic experiment was performed varying both ATP and compound concentrations. In

particular, the kinase activity was investigated at two different concentrations of the inhibitor (1 and 2 μM) and the ATP concentration in the reaction mixture was increased up to 50 μM , while the control concentration was kept constant. Double-reciprocal plotting of the data (Fig. 62) suggested that **140** acted as an ATP competitive inhibitor of the enzyme.

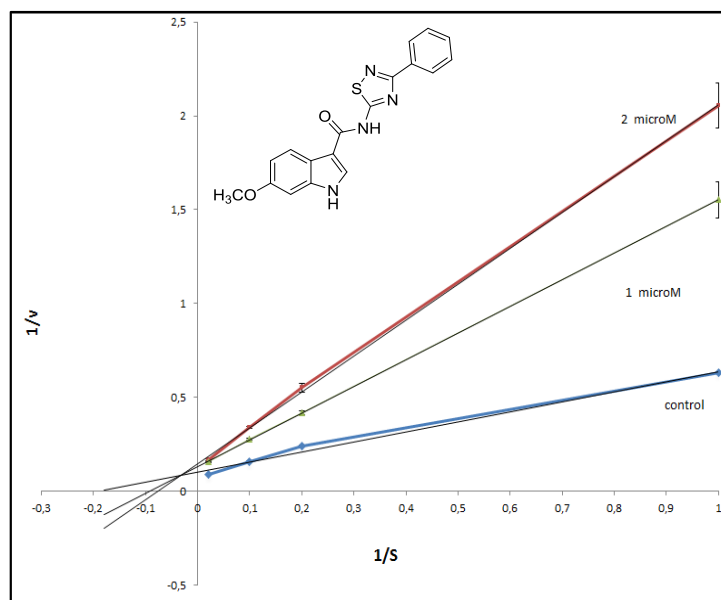


Figure 62. Double-reciprocal plot of kinetic data from assay of CK1 δ protein kinase activity at two different concentrations of **140** (1 and 2 μM). ATP concentrations (S) in the reaction mixture was varied from 1 to 50 μM .

4.6.2. LRRK2 and G2019S-LRRK2 inhibition

Subset of compounds 135, 139 and 143.

The ability to inhibit LRRK2 and its predominant mutant form G2019S-LRRK2 was investigated by means of the Adapta® methodology, based on a homogeneous fluorescent method of ADP detection (Fig. 63).¹⁶²

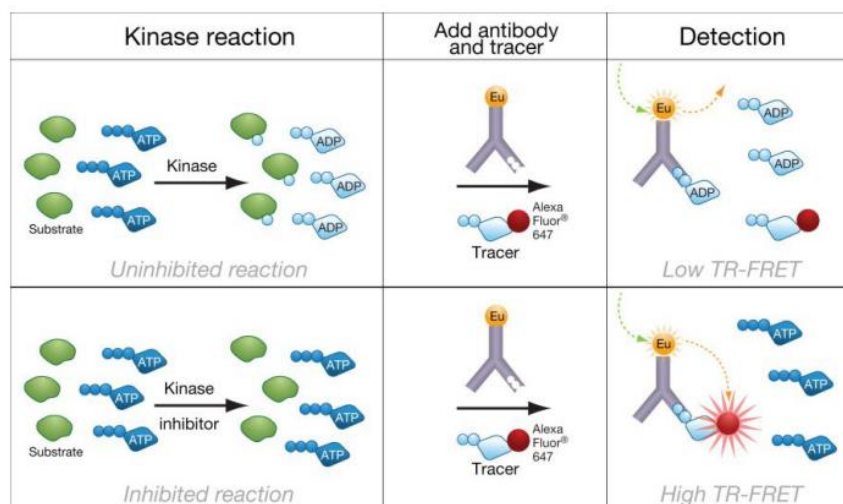


Figure 63. Schematically illustration of Adapta® methodology.

The *in vitro* inhibition results revealed interesting low micromolar inhibitory potencies on both enzymes for derivatives **135** and **139** and a lack of activity for the 6-methoxy substituted **143**. In particular **135**, characterized by a *N*-methyl-benzimidazole moiety, proved to inhibit LRRK2 with an IC_{50} value of 8.30 μ M and showed a slightly higher potency on the mutant form G2019S-LRRK2 (IC_{50} = 7.31 μ M) as reported in Table 26. Furthermore, the *para*-phenylmorpholine derivative **139** displayed a similar trend of inhibition, with IC_{50} values of 5.63 μ M and 4.52 μ M on LRRK2 and G2019S-LRRK2, respectively (Table 26).

Table 26. Inhibition of LRRK2 and G2019S-LRRK2 by indole-based derivatives **135** and **139**.

comp	LRRK2	G2019S-LRRK2
	IC_{50} (μ M)	IC_{50} (μ M)
135	8.30	7.31
139	5.63	4.52

Taken together, these preliminary results suggests **135** and **139** as promising lead compounds to be optimized for the development of more potent LRRK2 and G2019S-LKRR2inhibitors.

4.7. BBB PERMEATION

Subset of compounds 2-6, 8, 135, 137, 139, and 140.

An essential requirement for a CNS targeting drug is its capability to penetrate into the BBB at therapeutic concentrations. For this reason, and taking into account that more than 95 % of compounds cross the BBB by passive transport, an *in vitro* methodology developed by Prof. Martinez research group and based on the high throughput technique PAMPA (Parallel Artificial Membrane Permeability Assay)¹⁶³ was employed to predict the CNS passive permeation of some interesting curcumin- and indole-based derivatives. In this assay, the human BBB was emulated by using a porcine lipid membrane and UV spectroscopy was exploited to perform compounds quantification; additionally, for curcumin analogues **2-6** and **8**, curcumin **1a** was used as standard.

At the outset, an assay validation was made comparing the experimental data with the permeability (*Pe*) values of ten commercial drugs of known *Pe* (Fig. 64). Two different experiments were carried out: analogues **137** and **140** were evaluated in the first test, whereas **135**, **139**, **2-6** and **8**, together with **1a** were tested later.

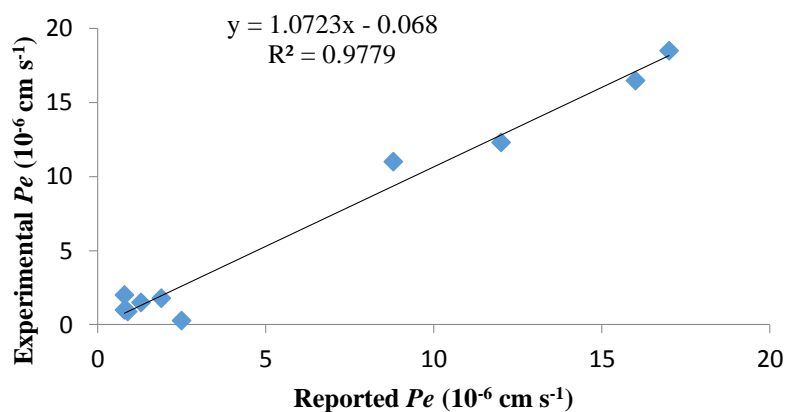


Figure 64. Linear correlation between experimental data and reported Pe of 10 commercial drugs.

From the obtained linear equation and following the pattern established in the literature for BBB permeation prediction,¹⁶⁴ the compounds were classified as permeable (CNS +) when their Pe was $> 4.22 \times 10^{-6} \text{ cm s}^{-1}$. Therefore, indole derivatives **135**, **137**, and **140**, as well as curcumin-based analogues **2**, **3**, **4** and **6** may pass the BBB, while **5** and **8** showed a borderline behavior (Table 27).

Table 27. Permeability (Pe $10^{-6} \text{ cm s}^{-1}$) in the PAMPA-BBB assay for 10 commercial drugs (used in the experiment validation) and for some synthesized compounds with their predictive penetration in the CNS^a.

comp	Bibl ^b	Pe ($10^{-6} \text{ cm s}^{-1}$) ^c	Prediction
Atenolol	0.8	2.0 ± 0.1	-
Caffeine	1.3	1.5 ± 0.3	-
Desipramine	12	12.3 ± 0.5	-
Enoxacin	0.9	0.9 ± 0.3	-
Hydrocortisone	1.9	1.8 ± 0.7	-
Ofloxacin	0.8	1.0 ± 0.4	-
Piroxicam	2.5	0.3 ± 0.1	-
Promazine	8.8	11.0 ± 0.1	-

Testosterone	17	18.5 ± 1.1	-
Verapamil	16	16.5 ± 1.9	-
135	-	13.0 ± 0.1	CNS +
137	-	14.2 ± 0.1	CNS +
139	-	2.0 ± 0.1	CNS -
140	-	11.4 ± 1.2	CNS +
2	-	7.7 ± 1.8	CNS +
3	-	8.2 ± 1.3	CNS +
4	-	7.8 ± 0.2	CNS +
5	-	2.8 ± 0.3	CNS +/CNS -
6	-	7.0 ± 0.7	CNS +
8	-	3.6 ± 0.1	CNS +/CNS -
1a	-	2.5 ± 0.1	CNS +/CNS -

^aPBS:EtOH (70:30) was used as solvent. ^bReference ¹⁶³. ^cData are the mean ± SD of 2 independent experiments.

5. *Conclusions*

Main goal of my PhD thesis was the identification of naturally inspired privileged scaffolds as starting point for the development of novel small molecules as multifunctional lead candidates for AD treatment or valuable probes to explore the chemical space of AD validated targets.

In view of the complex pathological mechanisms of AD, the multitarget approach has gained increasing acceptance as a useful tool to discover drug candidates that could promise improved efficacy compared to single-target drugs. In this scenario, BACE-1 and GSK-3 β emerged as AD validated targets and their concurrent inhibition has been identified as a promising therapeutic strategy.

From a medicinal chemistry standpoint, the curcumin pharmacophore, in its β -keto-enol form, incorporating some structural elements suitable for the modulation of both enzymes, was rationally envisaged as potential dualistic BACE-1/GSK-3 β inhibitor and was selected as lead compound for the design and synthesis of well-balanced dual modulators with good pharmacokinetic properties, mainly referred to the BBB crossing ability. Therefore, several synthetic efforts were dedicated at obtaining different series of novel curcumin-based derivatives, among which compounds of series Ia (β -keto-enol forms) and Ib (diketo tautomers) were mainly investigated for their capability to inhibit both structurally unrelated enzymes.

Generally, the biological *in vitro* results confirmed the enol tautomeric form as an important feature for achieving good inhibitory potency and chemical stability, and highlighted the intense effect of the nature of the substituents on the side aryl rings on BACE-1 and GSK-3 β inhibition. Remarkably, a number of derivatives proved to modulate BACE-1 and GSK-3 β enzymes with quite comparable potencies in the micromolar range. In particular, while a mild dualistic profile was shown for analogues **4** and **5**, a crucial achievement in the multitarget drug discovery context was represented by the subset of analogues **2**, **6**, and **7**, that proved to be well-balanced low-micromolar inhibitors of both enzymes. Among them, derivative **2**, thanks to the absence of evident neurotoxic effects and the

potential BBB permeability, clearly emerged as the most promising AD-modifying drug candidate to be further developed.

On the other hand compound **8**, showing a remarkable gap of potency (2 orders of magnitude) between its inhibition of BACE-1 and GSK-3 β , proved to be a single-target inhibitor of BACE-1, and it could be considered as a starting point for the development of optimized dual modulators. Furthermore, compounds **3**, **9**, and **10**, also characterized by higher potencies on BACE-1 with respect to GSK-3 β (submicromolar and low-micromolar IC₅₀ values, respectively), showed reduced deviation from the dualistic profile.

Beside A β and τ cascades, neuroinflammation has been recognized to play a crucial role in AD pathogenesis. In particular, an increase in expression of pro-inflammatory cytokines by activated microglia is a characteristic AD feature. Therefore, the capability to reduce microglial inflammatory responses without eliciting toxic effects could be considered an added value to realize a successful AD treatment. In this context, among the curcumin-based analogues that proved to decrease the pro-inflammatory cytokines release at non-toxic concentrations, **4**, **15** and **68** deserve particular attention due to their additional inhibitory activity on BACE-1 and GSK-3 β . In particular, **4** and **15**, displaying micromolar dualistic potencies on both enzymes accompanied by lack of cytotoxic effects and intrinsic antiinflammatory activity, could represent valuable lead compounds for the development of novel well-balanced dual BACE-1/GSK-3 β modulators, able to slow down the progression of neuroinflammatory diseases. Furthermore, compound **68**, due to a comparable aptitude to decrease the release of pro-inflammatory mediators by activated microglial cells, without affecting neither cell viability nor morphology, and a promising low-micromolar potency on GSK-3 β , could be considered an interesting hit for the design of GSK-3 β inhibitors endowed with good antiinflammatory activity.

In AD, a decrease in the levels of many antioxidant defense enzymes such as GSH cause oxidative stress, as a result of an imbalance between ROS generation and antioxidant processes. Therefore, compounds able to induce GSH could offer

substantial therapeutic efficacy as neuroprotective agents to delay the progression of the malady. In this respect, the curcumin-DF hybrids **74** and **75** showed a significant enhancement of GSH total levels, that could be correlated to the Michael acceptor reactivity of their additional α,β -unsaturated carbonyl function. Among them **75**, thanks to its low micromolar inhibitory activity on GSK-3 β and the lack of neurotoxic effects, could offer promises for the discovery of optimized GSK-3 β inhibitors with a neuroprotective potential.

Additional investigations are still in progress to further assess the great potential of the most interesting curcumin analogues as promising multifunctional lead compounds or drug candidates for an effective AD treatment.

Finally, concerning the indole-based derivatives designed and synthesized as a part of a drug discovery project aimed at discovering PKs inhibitors as BBB permeable promising pharmacological agents, the full satisfaction of the planned goals occurred with analogues **140** and **135**. In particular, **140** proved to be a low-micromolar ATP competitive CK1 δ inhibitor, able also to inhibit CK1 ϵ ; likewise, **135** showed a comparable low-micromolar activity on LRRK2 and its mutant form G2019S-LRRK2. Although the results are only preliminary and further investigations are required, both indole analogues could be considered as valuable lead compounds to be further developed.

6. *Experimental section*

General Chemical Methods

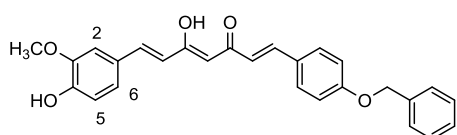
Starting materials, unless otherwise specified in the Experimental Section, were used as high-grade commercial products. Solvents were of analytical grade. Melting points were determined in open glass capillaries, using a Büchi apparatus and are uncorrected. $^1\text{H-NMR}$ and $^{13}\text{C-NMR}$ spectra were recorded on Varian Gemini 400 MHz, unless diversely indicated, and chemical shifts are reported as parts per million (ppm δ value) relative to the peak for tetramethylsilane (TMS) as internal standard. Standard abbreviations indicating spin multiplicities are given as follows: s (singlet), d (doublet), t (triplet), br (broad), q (quartet), dd (doublet of doublet) or m (multiplet). Mass spectra were recorded on a Waters ZQ 4000 apparatus operating in electrospray mode (ES). Chromatographic separations were performed on silica gel columns using the flash method (Kieselgel 40, 0.040-0.063 mm, Merck). Reactions were followed by thin layer chromatography (TLC) on precoated silica gel plates (Merck Silica Gel 60 F254) and then visualized with a UV lamp. Compounds were named following IUPAC rules as applied by Beilstein-Institute AutoNom (version 2.1), a PC-integrated software package for systematic names in organic chemistry.

Pabon reaction: general procedure A (synthesis of compounds 2-8, 11-17 and intermediates 22 and 23).

To a stirred solution of pentane-2,4-dione or intermediates **22** and **23** (1.00 mmol) in EtOAc (1.0 mL), B_2O_3 (1.0 molar equiv) was added, and the suspension was stirred for 30 min at 80 °C before addition of a solution of the appropriate aldehyde/s, (0.9 molar equiv for monoaryl or 1.8 molar equiv for bi-aryl curcumin derivatives), and tri-*n*-butyl borate [$\text{B}(\textit{n}\text{-BuO})_3$] (2.0 molar equiv for monoaryl or 4.0 molar equiv for bi-aryl curcumin derivatives) in EtOAc (0.5 mL). The reaction mixture was stirred at 80 °C for 30 min, then a solution of *n*-BuNH₂ (0.2 molar equiv for monoaryl or 0.4 molar equiv for bi-aryl curcumin derivatives) in EtOAc (1.0 mL) was added over a period of 15 min. The mixture was heated to 80 °C for 6-8 h and, after cooling to room temperature, it was acidified with HCl (0.5 N, 30

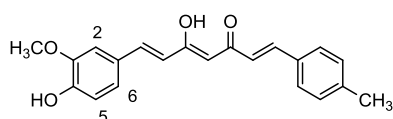
mL) and stirred at 80 °C for 30 min. The organic phase was separated and the aqueous layer was extracted with EtOAc (3 x 10.0 mL). The combined organic layers were sequentially washed with saturated aqueous NaHCO₃ and brine, dried over Na₂SO₄, filtered and concentrated under reduced pressure. The crude residue was purified by flash column chromatography followed by crystallization from suitable solvent or mixture of solvents.

(1E,4Z,6E)-1-(4-(benzyloxy)phenyl)-5-hydroxy-7-(4-hydroxy-3-methoxyphenyl)hepta-1,4,6-trien-3-one (2).



Reaction of intermediate **22** (1.17 g, 5.00 mmol) and 4-benzyloxybenzaldehyde (0.95 g, 4.50 mmol), following the general procedure A of the Pabon reaction, gave the crude product that was purified by flash chromatography (PE/EtOAc, 9:1) and further crystallization from EtOH. Orange-yellow powder, 44 % yield, mp 169-170 °C. ¹H-NMR (CDCl₃): δ 3.96 (s, 3H, OCH₃), 5.19 (s, 2H, OCH₂), 5.76 (s, 1H, keto-enol-CH), 6.45 (d, 2H, *J* = 16.0 Hz, CH=CH), 6.94 (d, 1H, *J* = 8.4 Hz, H-5), 6.98 (d, 2H, *J* = 8.4 Hz, Ar), 7.07 (d, 1H, *J* = 1.8 Hz, H-2), 7.12 (dd, 1H, *J* = 1.8 and 8.4 Hz, H-6), 7.40-7.45 (m, 5H, Bn), 7.53 (d, 2H, *J* = 8.4 Hz, Ar), 7.60 (d, 2H, *J* = 16.0 Hz, CH=CH). ¹³C-NMR (CDCl₃): δ 55.7, 70.4, 103.6, 111.9, 115.8, 116.4 (2C), 123.1, 123.2, 127.6, 128.2 (3C), 128.3 (2C), 128.5 (2C), 129.0, 129.3, 137.4, 140.4 (2C), 148.5, 149.5, 160.8, 186.7 (2C). ESI-MS (*m/z*): 451 (M + Na).

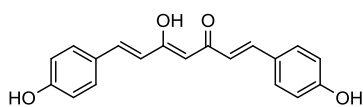
(1E,4Z,6E)-5-hydroxy-7-(4-hydroxy-3-methoxyphenyl)-1-(*p*-tolyl)hepta-1,4,6-trien-3-one (3).



Reaction of intermediate **22** (1.17 g, 5.00 mmol) and 4-methylbenzaldehyde (0.53 mL, 4.50 mmol), following the general procedure A of the Pabon reaction, gave the crude product that was purified by flash chromatography (PE/EtOAc, 9:1) and further crystallization from EtOH. Orange-yellow powder, 36 % yield, mp 136-138 °C. ¹H-NMR (CDCl₃): δ 2.38 (s, 3H, CH₃), 3.95 (s, 3H,

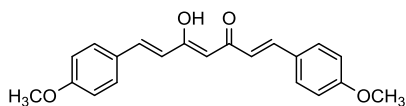
OCH₃), 5.81 (s, 1H, keto-enol-CH), 6.49 (d, 1H $J = 15.8$ Hz, CH=CH), 6.60 (d, 1H, $J = 15.8$ Hz, CH=CH), 6.94 (d, 1H, $J = 8.2$ Hz, H-5), 7.06 (d, 1H, $J = 1.8$ Hz, H-2), 7.13 (dd, 1H, $J = 1.8$ and 8.2 Hz, H-6), 7.20 (d, 2H, $J = 8.0$ Hz, Ar), 7.46 (d, 2H, $J = 8.0$ Hz, Ar), 7.59 (d, 1H, $J = 15.8$ Hz, CH=CH), 7.63 (d, 1H, $J = 15.8$ Hz, CH=CH). ¹³C-NMR (CDCl₃): δ 21.0, 55.7, 107.6, 112.9, 116.0, 121.5, 121.9, 126.7, 127.4 (2C), 129.3 (2C), 130.9, 134.1, 141.2 (2C), 137.9, 148.5, 150.2, 183.7 (2C). ESI-MS (m/z): 359 (M + Na).

(1E,4Z,6E)-5-hydroxy-1,7-bis(4-hydroxyphenyl)hepta-1,4,6-trien-3-one (4).



Reaction of pentane-2,4-dione (1.03 mL, 10.00 mmol) and 4-hydroxybenzaldehyde (2.24 g, 18.00 mmol), following the general procedure A of the Pabon reaction, gave the crude product that was purified by flash chromatography (PE/EtOAc, 7:3) and further crystallization from EtOH. Red-orange powder, 88 % yield, mp 228-230 °C. ¹H-NMR (acetone-*d*₆): δ 5.99 (s, 1H, keto-enol-CH), 6.67 (d, 2H, $J = 15.8$ Hz, CH=CH), 6.91 (d, 4H, $J = 8.6$ Hz, Ar), 7.57 (d, 4H, $J = 8.6$ Hz, Ar), 7.61 (d, 2H, $J = 15.8$ Hz, CH=CH). ¹H-NMR (DMSO-*d*₆): δ 6.22 (s, 1H, keto-enol-CH), 6.82 (d, 2H, $J = 16.4$ Hz, CH=CH), 6.98 (d, 4H, $J = 8.4$ Hz, Ar), 7.25 (d, 4H, $J = 8.4$ Hz, Ar), 7.35 (br s, 1H, OH), 7.62 (d, 2H, $J = 16.4$ Hz, CH=CH), 9.70 (br s, 2H, OH). ¹³C-NMR (acetone-*d*₆): δ 114.0, 116.5 (4C), 122.9, 127.9 (2C), 129.7, 130.0 (4C), 141.1 (2C), 161.1 (2C), 183.5 (2C). ESI-MS (m/z): 331 (M + Na).

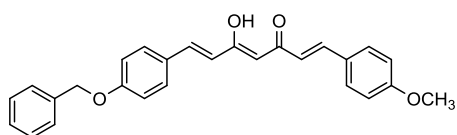
(1E,4Z,6E)-5-hydroxy-1,7-bis(4-methoxyphenyl)hepta-1,4,6-trien-3-one (5).



Reaction of pentane-2,4-dione (1.03 mL, 10.00 mmol) and 4-methoxybenzaldehyde (2.19 mL, 18.00 mmol), following the general procedure A of the Pabon reaction, gave the crude product purified by flash chromatography (PE/EtOAc, 9:1) and further crystallization from CH₂Cl₂/PE. Yellow powder, 87 % yield, mp 110-112 °C. ¹H-NMR (CDCl₃): δ 3.86 (s, 6H, OCH₃), 5.79 (s, 1H, keto-

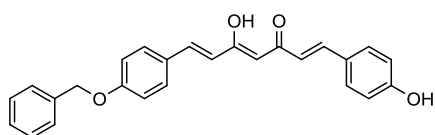
enol-CH), 6.51 (d, 2H, $J = 15.6$ Hz, CH=CH), 6.93 (d, 4H, $J = 7.2$ Hz, Ar), 7.52 (d, 4H, $J = 7.2$ Hz, Ar), 7.63 (d, 2H, $J = 15.6$ Hz, CH=CH). $^1\text{H-NMR}$ (DMSO- d_6): δ 3.80 (s, 6H, OCH₃), 6.09 (s, 1H, keto-enol-CH), 6.79 (d, 2H, $J = 15.6$ Hz, CH=CH), 7.00 (d, 4H, $J = 8.4$ Hz, Ar), 7.59 (d, 2H, $J = 15.6$ Hz, CH=CH), 7.68 (d, 4H, $J = 8.4$ Hz, Ar) (See Appendix for the $^1\text{H-NMR}$ spectra, Fig. A1a). $^{13}\text{C-NMR}$ (CDCl₃): δ 55.4 (2C), 113.8, 114.4 (4C), 121.8, 127.8 (2C), 129.5, 129.8 (4C), 140.1 (2C), 161.3 (2C), 183.3 (2C). $^{13}\text{C-NMR}$ (DMSO- d_6): δ 55.4 (2C), 101.4, 114.5 (4C), 121.8 (2C), 127.3 (2C), 130.2 (4C), 140.1 (2C), 161.1 (2C), 183.1 (2C). ESI-MS (m/z): 359 (M + Na).

(1E,4Z,6E)-7-(4-(benzyloxy)phenyl)-5-hydroxy-1-(4-methoxyphenyl)hepta-1,4,6-trien-3-one (6).



Reaction of intermediate **23** (1.47 g, 5.00 mmol) and 4-methoxybenzaldehyde (0.53 mL, 4.50 mmol), following the general procedure A of the Pabon reaction, gave the crude product that was purified by flash chromatography (PE/EtOAc, 8:2) and further crystallization from CH₂Cl₂/PE. Light orange-yellow powder, 48 % yield, mp 135-137 °C. $^1\text{H-NMR}$ (CDCl₃): δ 3.86 (s, 3H, OCH₃), 5.12 (s, 2H, OCH₂), 5.80 (s, 1H, keto-enol-CH), 6.51 (d, 2H, $J = 15.6$ Hz, CH=CH), 6.93 (d, 2H, $J = 8.0$ Hz, Ar), 7.00 (d, 2H, $J = 8.0$ Hz, Ar), 7.40-7.45 (m, 5H, Bn), 7.52 (d, 4H, $J = 8.0$ Hz, Ar), 7.63 (d, 2H, $J = 15.6$ Hz, CH=CH). $^{13}\text{C-NMR}$ (CDCl₃): δ 55.4, 70.5, 114.7, 114.5 (2C), 115.3 (2C), 122.0, 127.8 (2C), 128.1 (2C), 128.5, 128.9 (2C), 129.8, 129.9 (4C), 137.0, 140.3 (2C), 160.7, 161.0, 183.5 (2C). ESI-MS (m/z): 435 (M + Na).

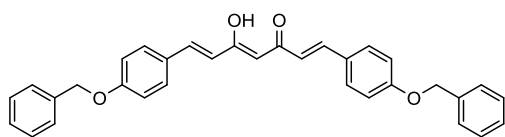
(1E,4Z,6E)-7-(4-(benzyloxy)phenyl)-5-hydroxy-1-(4-hydroxyphenyl)hepta-1,4,6-trien-3-one (7).



Reaction of intermediate **23** (1.47 g, 5.00 mmol) and 4-hydroxybenzaldehyde (0.56 g, 4.50 mmol), following the general procedure A of the Pabon reaction, gave the crude that was purified by flash chromatography

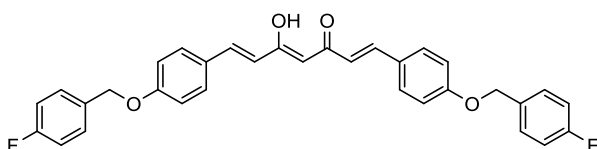
(PE/EtOAc, 9:1) and further crystallization from EtOH. Yellow powder, 42 % yield, mp 189-191 °C. ¹H-NMR (CDCl₃): δ 5.11 (s, 2H, OCH₂), 5.78 (s, 1H, keto-enol-CH), 6.49 (d, 1H, *J* = 16.0 Hz, CH=CH), 6.50 (d, 1H, *J* = 15.6 Hz, CH=CH), 6.85 (d, 2H, *J* = 8.0 Hz, Ar), 7.00 (d, 2H, *J* = 8.8 Hz, Ar), 7.40-7.45 (m, 5H, Bn), 7.47 (d, 2H, *J* = 8.0 Hz, Ar), 7.51 (d, 2H, *J* = 8.8 Hz, Ar), 7.61 (d, 1H, *J* = 15.6 Hz, CH=CH), 7.62 (d, 1H, *J* = 15.6 Hz, CH=CH). ¹³C-NMR (CDCl₃): δ 70.7, 114.8, 115.7 (2C), 116.5 (2C), 122.6, 127.9 (2C), 128.2 (2C), 128.3, 129.0 (2C), 129.9, 130.1 (4C), 136.9, 140.7 (2C), 160.8, 161.0, 183.6 (2C). ESI-MS (*m/z*): 421 (M + Na).

(1*E*,4*Z*,6*E*)-1,7-bis(4-(benzyloxy)phenyl)-5-hydroxyhepta-1,4,6-trien-3-one (8).



Reaction of pentane-2,4-dione (1.03 mL, 10.00 mmol) and 4-benzyloxybenzaldehyde (3.80 g, 18.00 mmol), following the general procedure A of the Pabon reaction, gave the crude product that was purified by flash chromatography (PE/EtOAc, 9:1) and further crystallization from CH₂Cl₂/PE. Yellow powder, 87 % yield, mp 161-162 °C. ¹H-NMR (CDCl₃): δ 5.11 (s, 4H, OCH₂), 5.78 (s, 1H, keto-enol-CH), 6.50 (d, 2H, *J* = 16.0 Hz, CH=CH), 6.99 (d, 4H, *J* = 8.4 Hz, Ar), 7.40-7.44 (m, 10H, Bn), 7.51 (d, 4H, *J* = 8.4 Hz, Ar), 7.62 (d, 2H, *J* = 16.0 Hz, CH=CH). ¹H-NMR (DMSO-*d*₆): δ 5.17 (s, 4H, OCH₂), 6.09 (s, 1H, keto-enol-CH), 6.79 (d, 2H, *J* = 16.4 Hz, CH=CH), 7.08 (d, 4H, *J* = 8.4 Hz, Ar), 7.40-7.43 (m, 10H, Bn), 7.59 (d, 4H, *J* = 8.4 Hz, Ar), 7.68 (d, 2H, *J* = 15.6 Hz, CH=CH). ¹³C-NMR (CDCl₃): δ 70.4 (2C), 115.6 (5C), 122.3, 127.7 (2C), 127.8 (2C), 128.4 (2C), 128.5 (2C), 128.9 (2C), 129.0 (2C), 130.1, 130.1 (4C), 136.8 (2C), 140.4 (2C), 160.8 (2C), 183.7 (2C). ESI-MS (*m/z*): 511 (M + Na).

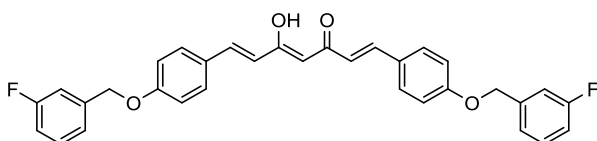
(1E,4Z,6E)-1,7-bis(4-((4-fluorobenzyl)oxy)phenyl)-5-hydroxyhepta-1,4,6-trien-3-one (11).



Reaction of pentane-2,4-dione (0.51 mL, 5.00 mmol) and benzaldehyde **24** (2.07 g, 9.00 mmol), following the general

procedure A of the Pabon reaction, gave the crude product that was purified by flash chromatography (PE/EtOAc, 9:1). Yellow powder, 31 % yield, mp 210-212 °C. ¹H-NMR (CDCl₃): δ 5.06 (s, 4H, OCH₂), 5.78 (s, 1H, keto-enol-CH), 6.50 (d, 2H, *J* = 15.6 Hz, CH=CH), 6.98 (d, 4H, *J* = 8.8 Hz, Ar), 7.09-7.13 (m, 4H, Ar, 4-FBn), 7.41-7.44 (m, 4H, Ar, 4-FBn), 7.51 (d, 4H, *J* = 8.8 Hz, Ar), 7.62 (d, 2H, *J* = 15.6 Hz, CH=CH). ¹³C-NMR (CDCl₃): δ 70.9 (2C), 114.5, 115.0 (d, 4C, *J* = 27.3 Hz), 115.7 (4C), 122.9, 128.9, 129.4 (4C), 129.5 (2C), 129.7 (d, 4C, *J* = 8.1 Hz), 131.9 (d, 2C, *J* = 4.0 Hz), 140.8 (2C), 159.7 (2C), 162.5 (d, 2C, *J* = 265.6 Hz), 183.8 (2C). ESI-MS (*m/z*): 547 (M + Na).

(1E,4Z,6E)-1,7-bis(4-((3-fluorobenzyl)oxy)phenyl)-5-hydroxyhepta-1,4,6-trien-3-one (12).

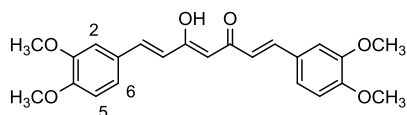


Reaction of pentane-2,4-dione (0.51 mL, 5.00 mmol) and benzaldehyde **25** (2.07 g, 9.00

mmol), following the general procedure A of the Pabon reaction, gave the crude product that was purified by flash chromatography (PE/EtOAc, 9:1). Yellow powder, 35 % yield, mp 160-162 °C. ¹H-NMR (CDCl₃): δ 5.10 (s, 4H, OCH₂), 5.78 (s, 1H, keto-enol-CH), 6.51 (d, 2H, *J* = 15.6 Hz, CH=CH), 6.98 (d, 4H, *J* = 8.8 Hz, Ar), 7.01-7.05 (m, 2H, Ar, 3-FBn), 7.16-7.18 (m, 2H, Ar, 3-FBn), 7.20-7.22 (m, 2H, Ar, 3-FBn), 7.35-7.37 (m, 2H, Ar, 3-FBn), 7.51 (d, 4H, *J* = 8.8 Hz, Ar), 7.62 (d, 2H, *J* = 15.6 Hz, CH=CH). ¹³C-NMR (CDCl₃): δ 72.6 (2C), 114.2 (d, 2C, *J* = 28.3 Hz), 115.1 (d, 2C, *J* = 26.3 Hz), 115.3 (5C), 123.3, 123.6 (d, 2C, *J* = 4.0 Hz), 127.8 (4C), 128.9 (3C), 129.3 (d, 2C, *J* = 8.1 Hz), 140.8 (d, 2C, *J* = 6.9 Hz), 143.8

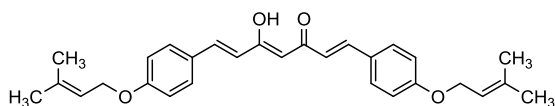
(2C), 160.6 (2C), 163.1 (d, 2C, $J = 264.6$ Hz), 183.7 (2C). ESI-MS (m/z): 547 (M + Na).

(1E,4Z,6E)-1,7-bis(3,4-dimethoxyphenyl)-5-hydroxyhepta-1,4,6-trien-3-one (13).



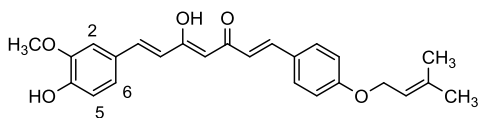
Reaction of pentane-2,4-dione (0.17 mL, 1.67 mmol) and 3,4-dimethoxybenzaldehyde (0.50 g, 3.01 mmol), following the general procedure A of the Pabon reaction, gave the crude product that was purified by crystallization from EtOH. Red-orange powder, 50 % yield, mp 108-110 °C. 15 H-NMR (CDCl₃): δ 3.94 (s, 6H, OCH₃), 3.95 (s, 6H, OCH₃), 5.84 (s, 1H, keto-enol-CH), 6.51 (d, 2H, $J = 16.0$ Hz, CH=CH), 6.89 (d, 2H, $J = 8.4$ Hz, H-5), 7.09 (s, 2H, H-2), 7.15 (d, 2H, $J = 8.0$ Hz, H-6), 7.62 (d, 2H, $J = 15.6$ Hz, CH=CH). 13 C-NMR (CDCl₃): δ 56.0 (4C), 100.9, 109.7 (2C), 111.1 (2C), 121.8 (2C), 122.4 (2C), 127.8 (2C), 140.0 (2C), 149.1 (2C), 150.9 (2C), 183.0 (2C). ESI-MS (m/z): 419 (M + Na).

(1E,4Z,6E)-5-hydroxy-1,7-bis(4-((3-methylbut-2-en-1-yl)oxy)phenyl)hepta-1,4,6-trien-3-one (14).



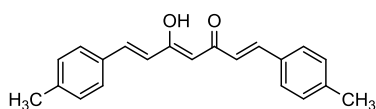
Reaction of pentane-2,4-dione (0.15 mL, 1.46 mmol) and benzaldehyde **26** (0.5 g, 2.63 mmol), following the general procedure A of the Pabon reaction, gave the crude product that was purified by flash chromatography (PE/EtOAc, 9.75:0.25) and further crystallization from EtOH. Yellow powder, 45 % yield, mp 165-167 °C. 1 H-NMR (CDCl₃): δ 1.76 (s, 6H, CH₃), 1.81 (s, 6H, CH₃), 4.56 (d, 4H, $J = 6.8$ Hz, OCH₂CH=), 5.50 (t, 2H, $J = 6.8$ Hz, OCH₂CH=), 5.78 (s, 1H, keto-enol-CH), 6.51 (d, 2H, $J = 15.6$ Hz, CH=CH), 6.93 (d, 4H, $J = 8.4$ Hz, Ar), 7.51 (d, 4H, $J = 8.4$ Hz, Ar), 7.63 (d, 2H, $J = 15.6$ Hz, CH=CH). 13 C-NMR (CDCl₃): δ 18.0 (2C), 24.9 (2C), 67.3 (2C), 102.0, 115.7 (4C), 121.6 (2C), 123.3 (2C), 128.5 (2C), 129.9 (4C), 137.9 (2C), 140.1 (2), 160.0 (2C), 183.6 (2C). ESI-MS (m/z): 467 (M + Na).

(1E,4Z,6E)-5-hydroxy-7-(4-hydroxy-3-methoxyphenyl)-1-(4-((3-methylbut-2-en-1-yl)oxy)phenyl)hepta-1,4,6-trien-3-one (15).



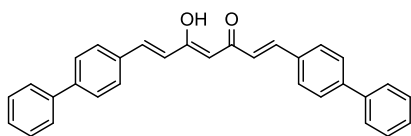
Reaction of intermediate **22** (1.17 g, 5.00 mmol) and benzaldehyde **26** (0.86 g, 4.50 mmol), following the general procedure A of the Pabon reaction, gave the crude product that was purified by flash chromatography (PE/EtOAc, 8.5:1.5) and further crystallization from EtOH. Orange powder, 41 % yield, mp 144-146 °C. ¹H-NMR (CDCl₃): δ 1.77 (s, 3H, CH₃), 1.82 (s, 3H, CH₃), 3.96 (s, 3H, OCH₃), 4.56 (d, 2H, *J* = 6.8 Hz, OCH₂CH=), 5.50 (t, 1H, *J* = 6.8 Hz, OCH₂CH=), 5.80 (s, 1H, keto-enol-CH), 5.85 (br s, 1H, OH), 6.49 (d, 1H, *J* = 15.6 Hz, CH=CH), 6.50 (d, 1H, *J* = 15.6 Hz, CH=CH), 6.94 (d, 2H, *J* = 8.0 Hz, Ar), 6.95 (d, 1H, *J* = 8.0 Hz, H-5), 7.07 (s, 1H, H-2), 7.13 (d, 1H, *J* = 8.0 Hz, H-6), 7.51 (d, 2H, *J* = 8.8 Hz, Ar), 7.60 (d, 1H, *J* = 15.6 Hz, CH=CH), 7.63 (d, 1H, *J* = 15.6 Hz, CH=CH). ¹³C-NMR (CDCl₃): 17.9, 25.0, 56.0, 67.0, 101.5, 109.7, 115.0, 115.6 (2C), 121.5, 123.0, 123.1, 123.3, 127.8, 128.6, 129.8 (2C), 138.0, 140.0 (2C), 147.0, 148.0, 159.9, 183.6 (2C). ESI-MS (*m/z*): 429 (M + Na).

(1E,4Z,6E)-5-hydroxy-1,7-di-p-tolylhepta-1,4,6-trien-3-one (16).



Reaction of pentane-2,4-dione (0.51 mL, 5.00 mmol) and 4-methylbenzaldehyde (1.06 mL, 9.00 mmol), following the general procedure A of the Pabon reaction, gave the crude product that was purified by flash chromatography (PE/EtOAc, 9.75:0.25) and further crystallization from CH₂Cl₂/PE. Mustard yellow powder, 50 % yield, mp 210-212 °C.^{146,147} ¹H-NMR (CDCl₃): δ 2.39 (s, 6H, CH₃), 5.83 (s, 1H, keto-enol-CH), 6.60 (d, 2H *J* = 15.8 Hz, CH=CH), 7.21 (d, 4H, *J* = 8.0 Hz, Ar), 7.47 (d, 4H, *J* = 8.0 Hz, Ar), 7.65 (d, 2H, *J* = 15.8 Hz, CH=CH). ¹³C-NMR (CDCl₃): δ 21.0 (2C), 108.0, 123.3 (2C), 127.4 (4C), 129.3 (4C), 134.0 (2C), 137.9 (2C), 143.8 (2C), 183.7 (2C). ESI-MS (*m/z*): 327 (M + Na).

(1E,4Z,6E)-1,7-di([1,1'-biphenyl]-4-yl)-5-hydroxyhepta-1,4,6-trien-3-one (17).



Reaction of pentane-2,4-dione (0.26 mL, 2.50 mmol), and biphenyl-4-carboxaldehyde (0.82 g, 4.50 mmol), following the general procedure A of the Pabon reaction, gave the crude product that was purified by flash chromatography (PE/EtOAc, 9.95:0.05) and further crystallization from CH₂Cl₂/PE. Yellow powder, 41 % yield, mp 249-251 °C. ¹H-NMR (CDCl₃): δ 5.90 (s, 1H, keto-enol-CH), 6.70 (d, 2H *J* = 15.6 Hz, CH=CH), 7.37-7.50 (m, 6H, Ar), 7.63-7.66 (m, 12H, Ar), 7.73 (d, 2H, *J* = 16.0 Hz, CH=CH). ¹³C-NMR (CDCl₃): δ 102.1, 124.1 (2C), 127.2 (4C), 127.7 (4C), 128.0 (2C), 128.8 (4C), 129.1 (4C), 134.2 (2C), 140.3 (4C), 143.0 (2C), 183.4 (2C). ESI-MS (*m/z*): 451 (M + Na).

Williamson reaction: general procedure for the synthesis of compounds 8-10, 18, 19-21, 108, 117-121, 127, 128 and benzaldehydes 24-26.

To a solution of phenol-derivative (1.00 mmol) in acetone (10.0 mL), anhydrous K₂CO₃ (1.2 or 2.0-2.2 molar equiv) and the appropriate alkyl or aryl halide (1.2 or 2.0-2.2 molar equiv) were added and the resulting mixture was heated to 80 °C for 6-48 h (the reaction was monitored by TLC). Upon reaction completion, the mixture was hot filtered and the solvent was evaporated under reduced pressure.

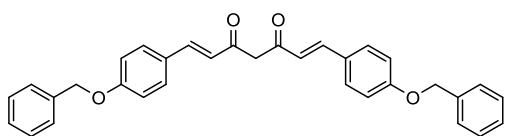
The two obtained tautomers were effectively isolated from the crude mixture by column chromatography over silica gel using a mixture of PE/EtOAc as eluent; in particular, the diketo tautomer proved to elute first. The final compounds were further purified by fractionated crystallization from CH₂Cl₂/PE.

(1E,4Z,6E)-1,7-bis(4-(benzyloxy)phenyl)-5-hydroxyhepta-1,4,6-trien-3-one (8);

(1E,6E)-1,7-bis(4-(benzyloxy)phenyl)hepta-1,6-diene-3,5-dione (19).

Reaction of **4** (0.50 g, 1.62 mmol) and benzyl bromide (0.47 mL, 3.56 mmol) for 8 h, according to the general Williamson reaction procedure, gave a

tautomeric mixture that was purified by flash chromatography (PE/EtOAc, 9:1). **8** (Rf: 0.12), previously obtained by the general procedure A of Pabon reaction (see above for characterization's details).

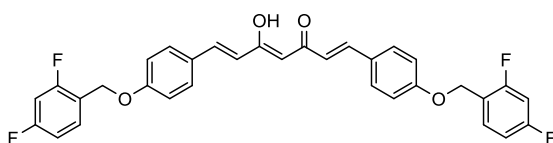


19 (Rf: 0.15), dark-yellow powder, 32 % yield, mp 145-147 °C. ¹H-NMR (CDCl₃): δ 3.96 (s, 2H, diketo-CH₂), 5.08 (s, 4H, OCH₂), 6.87 (d, 2H, *J* = 16.0 Hz, CH=CH), 6.94 (d, 4H, *J* = 8.4 Hz, Ar), 7.35-7.39 (m, 10H, Bn), 7.52 (d, 4H, *J* = 8.4 Hz, Ar), 7.73 (d, 2H, *J* = 16.0 Hz, CH=CH). ¹³C-NMR (CDCl₃): δ 55.7, 70.4 (2C), 115.6 (4C), 122.3 (2C), 127.9 (4C), 128.4 (2C), 128.5 (2C), 129.2 (4C), 130.0 (4C), 136.9 (2C), 140.5 (2C), 160.8 (2C), 196.4 (2C). ESI-MS (*m/z*): 511 (M + Na).

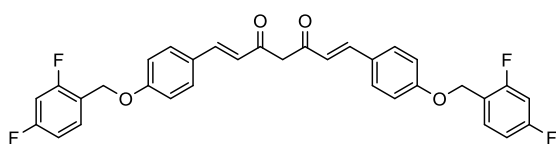
(1E,4Z,6E)-1,7-bis(4-((2,4-difluorobenzyl)oxy)phenyl)-5-hydroxyhepta-1,4,6-trien-3-one (9);

(1E,6E)-1,7-bis(4-((2,4-difluorobenzyl)oxy)phenyl)hepta-1,6-diene-3,5-dione (20).

Reaction of **4** (0.50 g, 1.60 mmol) and 2,4-difluorobenzyl bromide (0.48 mL, 3.52 mmol) for 20 h, according to the general Williamson reaction procedure, gave a tautomeric mixture that was purified by flash chromatography (PE/EtOAc, 9.5:0.5).



9 (Rf: 0.13), yellow powder, 32 % yield, mp 174-176 °C. ¹H-NMR (CDCl₃): δ 5.12 (s, 4H, OCH₂), 5.79 (s, 1H, keto-enol-CH), 6.51 (d, 2H, *J* = 16.0 Hz, CH=CH), 6.84-6.95 (m, 4H, Ar, 2,4-diFBn), 6.99 (d, 4H, *J* = 8.4 Hz, Ar), 7.46-7.48 (m, 2H, Ar, 2,4-diFBn), 7.52 (d, 4H, *J* = 8.4 Hz, Ar), 7.61 (d, 2H, *J* = 16.0 Hz, CH=CH). ¹³C-NMR (CDCl₃): δ 63.5 (2C), 104.0 (t, 2C, *J* = 25.6 Hz), 111.6 (dd, 2C, *J* = 3.8 and 21.4 Hz), 114.9 (4C), 115.2, 119.1 (dd, 2C, *J* = 4.0 and 14.6 Hz), 123.3, 128.4 (4C), 128.5 (2C), 130.5, 130.9 (dd, 2C, *J* = 5.3 and 9.8 Hz), 140.8 (2C), 160.7 (dd, 2C, *J* = 12.0 and 238.4 Hz), 163.2 (dd, 2C, *J* = 12.0 and 237.9 Hz), 163.4 (2C), 183.7 (2C). ESI-MS (*m/z*): 583 (M + Na).



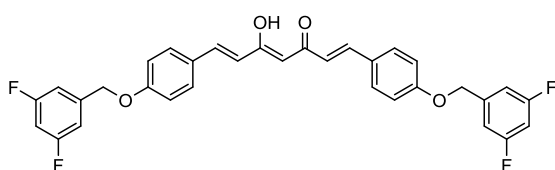
20 (Rf: 0.16), yellow powder, 28 % yield, 153-155 °C. ¹H-NMR

(CDCl₃): δ 3.98 (s, 2H, diketo-CH₂), 5.11 (s, 4H, OCH₂), 6.82 (d, 2H, *J* = 15.6 Hz, CH=CH), 6.88-6.92 (m, 4H, Ar, 2,4-diFBn), 6.96 (d, 4H, *J* = 8.4 Hz, Ar), 7.10-7.12 (m, 2H, Ar, 2,4-diFBn), 7.46 (d, 4H, *J* = 8.8 Hz, Ar), 7.75 (d, 2H, *J* = 15.6 Hz, CH=CH). ¹³C-NMR (CDCl₃): δ 55.4, 63.5 (2C), 104.0 (t, 2C, *J* = 25.7 Hz), 111.6 (dd, 2C, *J* = 4.0 and 21.9 Hz), 116.4 (4C), 119.2 (dd, 2C, *J* = 4.5 and 15.1 Hz), 126.4 (2C), 128.6 (4C), 129.0 (2C), 130.9 (dd, 2C, *J* = 5.4 and 10.6 Hz), 143.1 (2C), 160.6 (dd, 2C, *J* = 12.2 and 238.7 Hz), 160.8 (2C), 163.0 (dd, 2C, *J* = 12.2 and 238.6 Hz), 196.3 (2C). ESI-MS (*m/z*): 583 (M + Na).

(1E,4Z,6E)-1,7-bis(4-((3,5-difluorobenzyl)oxy)phenyl)-5-hydroxyhepta-1,4,6-trien-3-one (10);

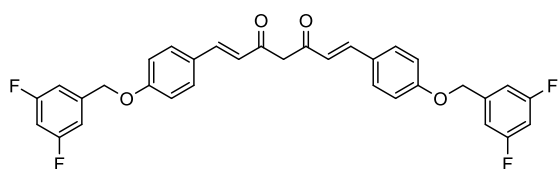
(1E,6E)-1,7-bis(4-((3,5-difluorobenzyl)oxy)phenyl)hepta-1,6-diene-3,5-dione (21).

Reaction of **4** (0.50 g, 1.60 mmol) and 3,5-difluorobenzyl bromide (0.48 mL, 3.52 mmol) for 20 h, according to the general Williamson reaction procedure, gave a tautomeric mixture that was purified by flash chromatography (PE/EtOAc, 9.5:0.5).



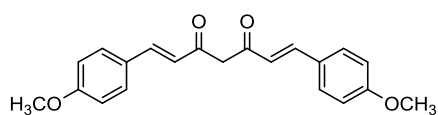
10 (Rf: 0.11), yellow powder, 60 % yield, mp 174-176 °C. ¹H-NMR

(CDCl₃): δ 5.09 (s, 4H, OCH₂), 5.80 (s, 1H, keto-enol-CH), 6.52 (d, 2H, *J* = 15.6 Hz, CH=CH), 6.56-6.67 (m, 2H, Ar, 3,5-diFBn), 6.73-6.81 (m, 2H, Ar, 3,5-diFBn), 6.93-6.99 (m, 2H, Ar, 3,5-diFBn), 6.97 (d, 4H, *J* = 8.8 Hz, Ar), 7.52 (d, 4H, *J* = 8.8 Hz, Ar), 7.63 (d, 2H, *J* = 15.6 Hz, CH=CH). ¹³C-NMR (CDCl₃): δ 71.6 (2C), 102.8 (t, 2C, *J* = 27.7 Hz), 112.2 (dd, 4C, *J* = 4.0 and 27.3 Hz), 114.9, 115.1 (4C), 122.9, 128.9 (4C), 129.1, 130.1 (2C), 141.6 (t, 2C, *J* = 7.2 Hz), 143.8 (2C), 159.9 (2C), 164.3 (dd, 4C, *J* = 6.9 and 261.8 Hz), 183.5 (2C). ESI-MS (*m/z*): 583 (M + Na).



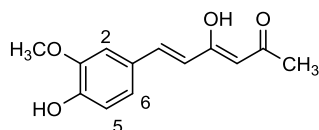
21 (Rf: 0.13), yellow powder, 28 % yield, mp 152-154 °C. ¹H-NMR (CDCl₃): δ 3.94 (s, 2H, diketo-CH₂), 5.07 (s, 4H, OCH₂), 6.60-6.72 (m, 2H, Ar, 3,5-diFBn), 6.75 (d, 2H, *J* = 15.2 Hz, CH=CH), 6.79-6.84 (m, 2H, Ar, 3,5-diFBn), 6.93 (d, 4H, *J* = 8.4 Hz, Ar), 6.93-6.98 (m, 2H, Ar, 3,5-diFBn), 7.43 (d, 4H, *J* = 8.8 Hz, Ar), 7.75 (d, 2H, *J* = 15.2 Hz, CH=CH). ¹³C-NMR (CDCl₃): δ 55.8, 71.7 (2C), 102.9 (t, 2C, *J* = 27.7 Hz), 112.2 (dd, 4C, *J* = 4.0 and 27.0 Hz), 115.3 (4C), 127.1 (2C), 129.5 (4C), 129.5 (2C), 140.6 (t, 2C, *J* = 6.8 Hz), 142.4 (2C), 160.6 (2C), 164.2 (dd, 4C, *J* = 6.4 and 261.3 Hz), 195.1 (2C). ESI-MS (*m/z*): 583 (M + Na).

(1E,6E)-1,7-bis(4-methoxyphenyl)hepta-1,6-diene-3,5-dione (18).



Reaction of **4** (0.15 g, 0.49 mmol) and iodomethane (0.07 mL, 1.08 mmol) for 24 h, according to the general Williamson reaction procedure, gave the crude product that was purified by flash chromatography (PE/EtOAc, 9.5:0.5) from which **18** was obtained as predominant component. Orange-yellow powder, 44 % yield, mp 103-105 °C. ¹H-NMR (CDCl₃): δ 3.48 (s, 2H, diketo-CH₂), 3.86 (s, 6H, OCH₃), 6.93 (d, 4H, *J* = 8.8 Hz, Ar), 7.01 (d, 2H, *J* = 14.8 Hz, CH=CH), 7.55 (d, 4H, *J* = 6.8 Hz, Ar), 7.72 (d, 2H, *J* = 14.8 Hz, CH=CH). ¹³C-NMR (CDCl₃): δ 55.3 (2C), 55.4, 114.4 (4C), 121.8 (2C), 128.2 (2C), 129.8 (4C), 141.2 (2C), 161.4 (2C), 196.6 (2C). ESI-MS (*m/z*): 359 (M + Na).

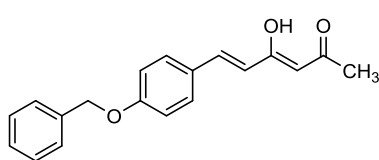
(3Z,5E)-4-hydroxy-6-(4-hydroxy-3-methoxyphenyl)hexa-3,5-dien-2-one (22).



Pentane-2,4-dione (2.05 mL, 20.00 mmol) and vanillin (1.00 g, 6.59 mmol), were allowed to react according to the general procedure A of the Pabon reaction. Nevertheless, in this particular case, 0.33 molar equiv of vanillin, B(*n*-BuO)₃ and *n*-BuNH₂ were employed to obtained the crude product,

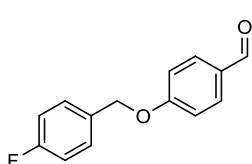
purified by flash chromatography (PE/acetone, 9:1) and further crystallization from EtOH. Yellow powder, 55 % yield, mp 144-146 °C.¹⁶⁵ ¹H-NMR (CDCl₃): δ 2.16 (s, 3H, CH₃), 3.94 (s, 3H, OCH₃), 5.40 (br s, 1H, OH), 5.63 (s, 1H, keto-enol-CH), 6.33 (d, 1H, *J* = 16.0 Hz, CH=CH), 6.92 (d, 1H, *J* = 8.0 Hz, H-5), 7.02 (d, 1H, *J* = 1.8 Hz, H-2), 7.09 (dd, 1H, *J* = 1.8 and 8.0 Hz, H-6), 7.53 (d, 1H, *J* = 16.0 Hz, CH=CH).

(3*Z*,5*E*)-6-(4-(benzyloxy)phenyl)-4-hydroxyhexa-3,5-dien-2-one (23).



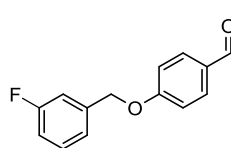
Pentane-2,4-dione (1.03 mL, 10.00 mmol) and 4-benzyloxybenzaldehyde (2.04 g, 9.00 mmol) were allowed to react according to the general procedure A of the Pabon reaction giving the crude product that was purified by flash chromatography (PE/EtOAc, 9.95:0.05) and further crystallization from CH₂Cl₂/PE. Yellow powder, 65 % yield, mp 121-122 °C. ¹H-NMR (CDCl₃): δ 2.18 (s, 3H, CH₃), 5.20 (s, 2H, OCH₂), 5.61 (s, 1H, keto-enol-CH), 6.33 (d, 1H, *J* = 16.0 Hz, CH=CH), 6.94 (d, 2H, *J* = 8.2 Hz, Ar), 7.40-7.45 (m, 5H, Bn), 7.53 (d, 2H, *J* = 8.2 Hz, Ar), 7.53 (d, 1H, *J* = 16.0 Hz, CH=CH).

4-(4-fluorobenzoyloxy)benzaldehyde (24).



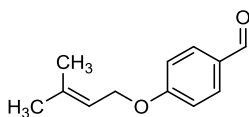
4-hydroxybenzaldehyde (1.24 g, 10.00 mmol) and 4-fluorobenzyl bromide (1.49 mL, 12.00 mmol) were allowed to react according to the general procedure of the Williamson reaction for 6 h to give the crude product that was purified by flash chromatography (PE/EtOAc, 9.5:0.5). White powder, 88 % yield, mp 190-192 °C. ¹H-NMR (CDCl₃): δ 5.08 (s, 2H, OCH₂), 6.99-7.00 (m, 2H, Ar, 4-FBn), 7.02 (d, 2H, *J* = 8.8 Hz, Ar), 7.10-7.14 (m, 2H, Ar, 4-FBn), 7.82 (d, 2H, *J* = 8.8 Hz, Ar), 9.80 (s, 1H, CHO).

4-(3-fluorobenzoyloxy)benzaldehyde (25).



4-hydroxybenzaldehyde (1.24 g, 10.00 mmol) and 3-fluorobenzyl bromide (1.49 mL, 12.00 mmol) were allowed to react according to the general procedure of the Williamson reaction for 6 h to give the crude product that was purified by flash chromatography (PE/EtOAc, 9.5:0.5). White powder, 85 % yield, mp 183-185 °C. ¹H-NMR (CDCl₃): δ 5.10 (s, 2H, OCH₂), 6.95 (d, 2H, *J* = 8.8 Hz, Ar), 6.93-6.99 (m, 1H, Ar, 3-FBn), 7.00-7.07 (m, 2H, Ar, 3-FBn), 7.23-7.31 (m, 1H, Ar, 3-FBn), 7.84 (d, 2H, *J* = 8.8 Hz, Ar), 9.80 (s, 1H, CHO).

4-((3-methylbut-2-en-1-yl)oxy)benzaldehyde (26).



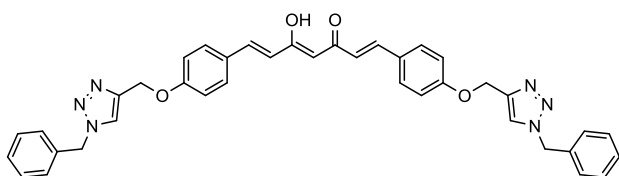
4-hydroxybenzaldehyde (1.00 g, 8.19 mmol) and 3,3-dimethylallyl bromide (1.14 mL, 9.83 mmol) were allowed to react according to the general procedure of the Williamson reaction for 8 h to give the crude product that was purified by crystallization from PE; yellow oil, 83 % yield. ¹H-NMR (CDCl₃): δ 1.76 (s, 3H, CH₃), 1.81 (s, 3H, CH₃), 4.60 (d, 2H, *J* = 6.8 Hz, OCH₂CH=), 5.45 (t, 1H, *J* = 6.8 Hz, OCH₂CH=), 7.00 (d, 2H, *J* = 8.8 Hz, Ar), 7.83 (d, 2H, *J* = 8.8 Hz, Ar), 9.88 (s, 1H, CHO).

Pabon reaction: general procedure B (synthesis of curcumin 1a and compounds 27-38, 66-69 and 72).

To a suspension of pentane-2,4-dione or intermediate **22** (1.00 mmol) and B₂O₃ (1.0 molar equiv) in DMF (1.5 mL), stirred for 30 min at 80 °C, B(*n*-BuO)₃ (2.0 molar equiv for monoaryl or 4.0 molar equiv for bi-aryl curcumin derivatives) was added. The resulting mixture was heated for additional 30 min and a sequential addition of the suitable functionalized or commercial aldehyde/s, (0.9-1.2 molar equiv for monoaryl or 1.8 molar equiv for bi-aryl curcumin derivatives) and *n*-BuNH₂ solution (0.2 molar equiv for monoaryl or 0.4 molar equiv for bi-aryl curcumin derivatives) in DMF (1.0 mL) was carried out. After stirring at 80 °C for 6-8 h, the resulting mixture was cooled to room temperature, acidified with HCl

(0.5 N, 8.0 mL) and stirred for 30 min. The crude product was obtained as precipitate, which was suspended in water, filtered off and purified by flash column chromatography and/or crystallization from suitable solvent or mixture of solvents, unless otherwise stated.

(1E,4Z,6E)-1,7-bis(4-((1-benzyl-1H-1,2,3-triazol-4-yl)methoxy)phenyl)-5-hydroxyhepta-1,4,6-trien-3-one (27).



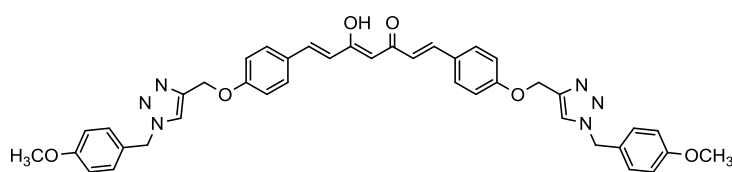
Reaction of pentane-2,4-dione (0.10 mL, 1.00 mmol) and the functionalized aldehyde **39** (0.53 g, 1.80 mmol), in line with

the general procedure B of the Pabon reaction, gave the crude product purified by flash chromatography (PE/EtOAc, 1:1) and further crystallization from acetone/PE. Yellow powder, 55 % yield, mp 122-124 °C. ¹H-NMR (CDCl₃): δ 5.23 (s, 4H, OCH₂), 5.55 (s, 4H, NCH₂), 5.79 (s, 1H, keto-enol-CH), 6.50 (d, 2H, *J* = 15.6 Hz, CH=CH), 7.00 (d, 4H, *J* = 8.0 Hz, Ar), 7.27-7.30 (m, 4H, Bn), 7.37-7.40 (m, 6H, Bn), 7.50 (d, 4H, *J* = 8.0 Hz, Ar), 7.54 (s, 2H), 7.61 (d, 2H, *J* = 15.6 Hz, CH=CH). ¹³C-NMR (CDCl₃): δ 55.0 (2C), 62.2 (2C), 101.5, 115.4 (4C), 121.9, 122.2 (2C), 122.8, 128.4 (4C), 128.5 (2C), 129.0 (2C), 129.5 (4C), 130.0 (4C), 136.2 (2C), 140.0, 140.8, 144.2 (2), 160.0 (2C), 186.6 (2C). ESI-MS (*m/z*): 673 (M + Na).

(1E,4Z,6E)-5-hydroxy-1,7-bis(4-((1-(4-methoxybenzyl)-1H-1,2,3-triazol-4-yl)methoxy)phenyl)hepta-1,4,6-trien-3-one (28a);

(1E,6E)-1,7-bis(4-((1-(4-methoxybenzyl)-1H-1,2,3-triazol-4-yl)methoxy)phenyl)hepta-1,6-diene-3,5-dione (28b).

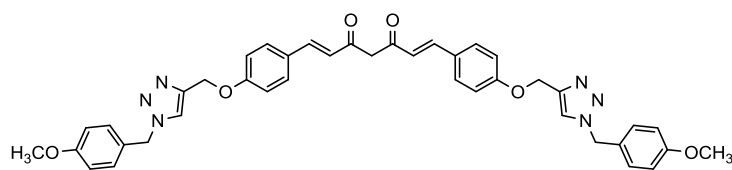
Reaction of pentane-2,4-dione (0.09 mL, 0.86 mmol) and the functionalized aldehyde **40** (0.50 g, 1.55 mmol), in line with the general procedure B of the Pabon reaction, gave the crude product purified by flash chromatography (PE/EtOAc, 1:1). In this case, the desired final compound was isolated as **28a** pure and as 2.4:1.0 mixture of **28a:28b**.



28a (pure), orange-brown powder, 30 % yield, mp 173-175 °C.

$^1\text{H-NMR}$ (CDCl_3): δ

3.82 (s, 6H, OCH_3), 5.22 (s, 4H, OCH_2), 5.48 (s, 4H, NCH_2), 5.79 (s, 1H, keto-enol-CH), 6.48 (d, 2H, $J = 15.6$ Hz, $\text{CH}=\text{CH}$), 6.88 (d, 4H, $J = 8.0$ Hz, Ar, 4- OCH_3Bn), 6.97 (d, 4H, $J = 8.0$ Hz, Ar), 7.25 (d, 4H, $J = 8.0$ Hz, Ar), 7.48 (d, 4H, $J = 8.0$ Hz, Ar, 4- OCH_3Bn), 7.48 (s, 2H), 7.59 (d, 2H, $J = 15.6$ Hz, $\text{CH}=\text{CH}$). $^{13}\text{C-NMR}$ (CDCl_3): δ 54.0 (2C), 55.5 (2C), 62.3 (2C), 101.6, 114.7 (4C), 115.4 (4C), 122.3 (2C), 122.6 (2C), 126.5 (2C), 128.5 (2C), 129.9 (8C), 134.7, 140.1, 144.2 (2C), 160.2 (2C), 167.3 (2C), 183.4 (2C). ESI-MS (m/z): 733 ($\text{M} + \text{Na}$).



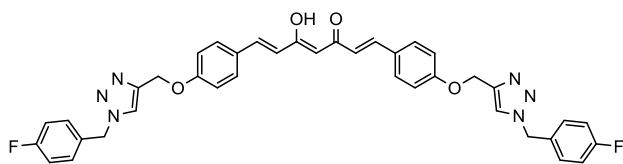
28b (29 % of the tautomeric mixture), orange-brown powder.

$^1\text{H-NMR}$ (CDCl_3): δ

3.82 (s, 6H, OCH_3), 3.94 (s, 2H, diketo- CH_2), 5.22 (s, 4H, OCH_2), 5.48 (s, 4H, NCH_2), 6.48 (d, 2H, $J = 15.6$ Hz, $\text{CH}=\text{CH}$), 6.88 (d, 4H, $J = 8.0$ Hz, Ar, 4- OCH_3Bn), 6.97 (d, 4H, $J = 8.0$ Hz, Ar), 7.25 (d, 4H, $J = 8.0$ Hz, Ar), 7.48 (d, 4H, $J = 8.0$ Hz, Ar, 4- OCH_3Bn), 7.48 (s, 2H), 7.59 (d, 2H, $J = 15.6$ Hz, $\text{CH}=\text{CH}$).

28a,b. $^{13}\text{C-NMR}$ (CDCl_3): 54.1 (4C), 55.9, 56.0 (4C), 62.0 (4C), 101.6, 115.0 (8C), 115.5 (8C), 122.3 (2C), 122.5 (4C), 126.4 (4C), 127.1 (2C), 129.0 (4C), 129.8 (8C), 130.1 (8C), 134.7, 140.1, 144.5 (4C), 147.1 (2C), 160.0 (4C), 167.0 (4C), 183.4 (2C), 196.0 (2C). ESI-MS (m/z): 733 ($\text{M} + \text{Na}$).

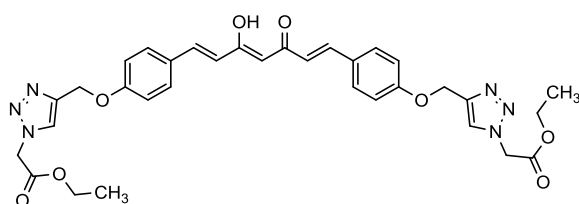
(1E,4Z,6E)-1,7-bis(4-((1-(4-fluorobenzyl)-1H-1,2,3-triazol-4-yl)methoxy)phenyl)-5-hydroxyhepta-1,4,6-trien-3-one (29).



Reaction of pentane-2,4-dione (0.03 mL, 0.29 mmol) and the functionalized aldehyde **41** (0.16 g, 0.52 mmol), in line

with the general procedure B of the Pabon reaction, gave the crude product purified by flash chromatography (PE/EtOAc, 1:1) and further crystallization from CH₂Cl₂/PE. Yellow powder, 35 % yield, mp 134-136 °C. ¹H-NMR (CDCl₃): δ 5.22 (s, 4H, OCH₂), 5.52 (s, 4H, NCH₂), 5.79 (s, 1H, keto-enol-CH), 6.51 (d, 2H, *J* = 15.6 Hz, CH=CH), 7.00 (d, 4H, *J* = 8.8 Hz, Ar), 7.06-7.10 (m, 4H, Ar, 4-FBn), 7.27-7.30 (m, 4H, Ar, 4-FBn), 7.51 (d, 4H, *J* = 8.4 Hz, Ar), 7.54 (s, 2H), 7.62 (d, 2H, *J* = 15.6 Hz, CH=CH). ¹³C-NMR (CDCl₃): δ 53.7 (2C), 62.2 (2C), 101.5, 115.3 (4C), 116.35 (d, 4C, *J* = 21.4 Hz), 121.9, 122.3, 122.7 (2C), 128.5 (2C), 129.9 (4C), 130.0 (2C), 130.2 (d, 4C, *J* = 8.1 Hz), 140.0, 140.8, 144.4 (2C), 160.0 (2C), 160.7 (d, 2C, *J* = 249.4 Hz), 183.2, 183.6. ESI-MS (*m/z*): 687 (M + H).

diethyl 2,2'-((((((1E,3Z,6E)-3-hydroxy-5-oxohepta-1,3,6-triene-1,7-diyl)bis(4,1-phenylene))bis(oxy))bis(methylene))bis(1H-1,2,3-triazole-4,1-diyl)) diacetate (30).

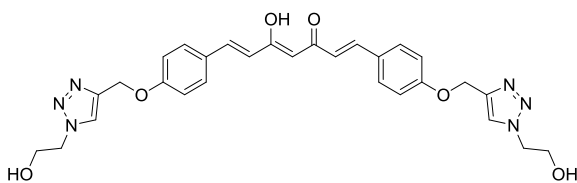


Reaction of pentane-2,4-dione (0.21 mL, 2.00 mmol) and the functionalized aldehyde **42** (1.04 g, 3.60 mmol), in line with the

general procedure B of the Pabon reaction, gave the crude product purified by two sequential crystallizations from: CH₂Cl₂/PE and acetone. Yellow powder, 80 % yield, mp 209-211 °C. ¹H-NMR (CDCl₃): δ 1.31 (t, 6H, *J* = 6.8 Hz, OCH₂CH₃), 4.29 (q, 4H, *J* = 6.8 Hz, OCH₂CH₃), 5.18 (s, 4H, NCH₂), 5.30 (s, 4H, OCH₂), 5.80 (s, 1H, keto-enol-CH), 6.51 (d, 2H, *J* = 15.6 Hz, CH=CH), 7.03 (d, 4H, *J* = 8.0 Hz, Ar), 7.52 (d, 4H, *J* = 8.4 Hz, Ar), 7.62 (d, 2H, *J* = 16.0 Hz, CH=CH), 7.78 (s, 2H). ¹³C-NMR (CDCl₃): δ 14.0 (2C), 50.9 (2C), 62.2, 62.7, 101.4, 115.4 (4C), 122.3

(2C), 124.3, 125.2, 127.7 (2C), 128.4 (2C), 129.9 (4C), 140.1 (2C), 144.4 (2C), 159.9, 166.2 (2C), 183.1, 183.4 (2C). ESI-MS (m/z): 665 (M + Na).

(1E,4Z,6E)-5-hydroxy-1,7-bis(4-((1-(2-hydroxyethyl)-1H-1,2,3-triazol-4-yl)methoxy)phenyl)hepta-1,4,6-trien-3-one (31).

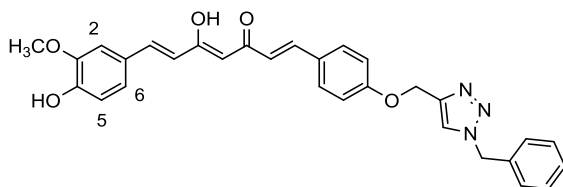


Reaction of pentane-2,4-dione (0.08 g, 0.80 mmol) and the functionalized aldehyde **43** (0.36 g, 1.44 mmol), in line with the

general procedure B of the Pabon reaction, gave the crude product purified by two sequential crystallizations from CH₂Cl₂/PE and acetone/PE. A further semipreparative TLC (CHCl₃/CH₃OH, 9.75:0.25) followed by crystallization from acetone/PE allowed obtaining **31** as yellow powder; 44 % yield, mp 238-240 °C.

¹H-NMR (acetone-*d*₆): δ 3.97 (t, 4H, *J* = 5.2 Hz, CH₂OH), 4.52 (t, 4H, *J* = 5.2 Hz, NCH₂), 5.25 (s, 4H, OCH₂), 6.03 (s, 1H, keto-enol-CH), 6.74 (d, 2H, *J* = 16.0 Hz, CH=CH), 7.13 (d, 4H, *J* = 8.8 Hz, Ar), 7.64 (d, 2H, *J* = 15.2 Hz, CH=CH), 7.67 (d, 4H, *J* = 8.8 Hz, Ar), 8.09 (s, 2H). ¹³C-NMR (acetone-*d*₆): δ 53.6 (2C), 61.7 (2C), 62.8 (2C), 102.1, 116.3 (4C), 123.2 (2C), 124.1, 125.6, 129.2 (2), 130.9 (4C), 140.7, 141.8, 143.8 (2C), 161.5 (2C), 184.2 (2C). ESI-MS (m/z): 581 (M + Na).

(1E,4Z,6E)-1-(4-((1-benzyl-1H-1,2,3-triazol-4-yl)methoxy)phenyl)-5-hydroxy-7-(4-hydroxy-3-methoxyphenyl)hepta-1,4,6-trien-3-one (32).

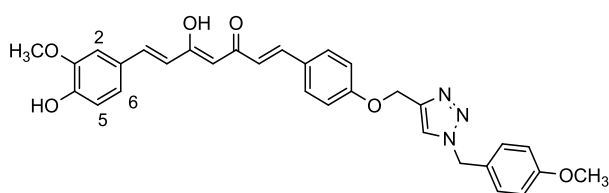


Reaction of intermediate **22** (0.20 g, 0.85 mmol) and the functionalized aldehyde **39** (0.30 g, 1.02 mmol), in line with the general procedure B of

the Pabon reaction, gave the crude product purified by flash chromatography (PE/EtOAc, 7:3) and further crystallization from EtOH. Yellow-brown powder, 69 % yield, mp 100-102 °C. ¹H-NMR (CDCl₃): δ 3.96 (s, 3H, OCH₃), 5.24 (s, 2H, OCH₂), 5.55 (s, 2H, NCH₂), 5.80 (s, 1H, keto-enol-CH), 5.88 (br s, 1H, OH), 6.49 (d, 1H, *J* = 15.6 Hz, CH=CH), 6.50 (d, 1H, *J* = 15.6 Hz, CH=CH), 6.94 (d, 1H, *J* =

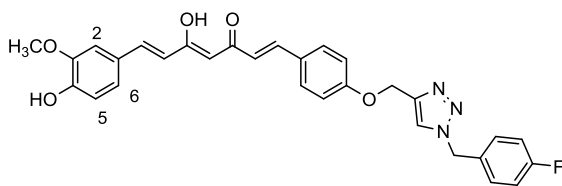
8.0 Hz, H-5), 7.00 (d, 2H, $J = 8.4$ Hz, Ar), 7.06 (s, 1H, H-2), 7.13 (d, 1H, $J = 8.4$ Hz, H-6), 7.27-7.30 (m, 2H, Bn), 7.37-7.40 (m, 3H, Bn), 7.50 (d, 2H, $J = 8.4$ Hz, Ar), 7.54 (s, 1H), 7.60 (d, 1H, $J = 15.6$ Hz, CH=CH), 7.61 (d, 1H, $J = 15.6$ Hz, CH=CH). $^{13}\text{C-NMR}$ (CDCl_3): δ 54.5, 56.1, 62.3, 101.5, 109.7, 115.0, 115.3 (2C), 121.9, 122.3, 122.8, 123.1, 127.8, 128.3 (2C), 128.5, 129.0, 129.3 (2C), 129.9 (2C), 134.5, 140.0, 140.8, 144.3, 146.9, 148.0, 159.9, 183.2, 186.6. ESI-MS (m/z): 532 (M + Na).

(1E,4Z,6E)-5-hydroxy-7-(4-hydroxy-3-methoxyphenyl)-1-(4-((1-(4-methoxybenzyl)-1H-1,2,3-triazol-4-yl)methoxy)phenyl)hepta-1,4,6-trien-3-one (33).



Reaction of intermediate **22** (0.20 g, 0.86 mmol) and the functionalized aldehyde **40** (0.25 g, 0.77 mmol), in line with the general procedure B of the Pabon reaction, gave the crude product purified by flash chromatography (PE/EtOAc, 6:4) and further crystallization from EtOH. Orange-brown powder, 45 % yield, mp 149-151 °C. $^1\text{H-NMR}$ (CDCl_3): δ 3.82 (s, 3H, OCH_3), 3.96 (s, 3H, OCH_3), 5.22 (s, 2H, OCH_2), 5.48 (s, 2H, NCH_2), 5.80 (s, 1H, keto-enol-CH), 5.88 (br s, 1H, OH), 6.49 (d, 1H, $J = 15.6$ Hz, CH=CH), 6.50 (d, 1H, $J = 16.0$ Hz, CH=CH), 6.91 (d, 2H, $J = 8.4$ Hz, Ar, 4- OCH_3Bn), 6.94 (d, 1H, $J = 8.0$ Hz, H-5), 6.99 (d, 2H, $J = 8.8$ Hz, Ar), 7.06 (d, 1H, $J = 1.6$ Hz, H-2), 7.13 (dd, 1H, $J = 1.6$ and 8.4 Hz, H-6), 7.25 (d, 2H, $J = 8.8$ Hz, Ar, 4- OCH_3Bn), 7.50 (d, 2H, $J = 8.8$ Hz, Ar), 7.51 (s, 1H), 7.60 (d, 1H, $J = 16.0$ Hz, CH=CH), 7.61 (d, 1H, $J = 16.0$ Hz, CH=CH). $^{13}\text{C-NMR}$ (CDCl_3): δ 53.9, 55.5, 56.1, 62.2, 101.5, 109.7, 114.6 (2C), 115.0, 115.3 (2C), 121.7, 122.2, 122.6, 123.1, 126.4, 127.8, 128.4, 129.9 (4C), 140.0, 140.7, 144.1, 147.0, 148.0, 159.9, 160.1, 183.2, 183.6. ESI-MS (m/z): 538 (M - H).

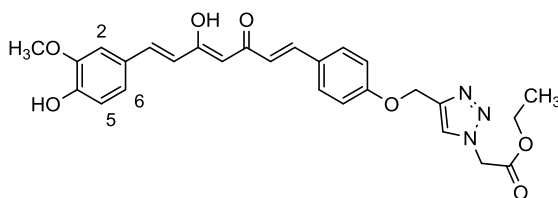
(1E,4Z,6E)-1-(4-((1-(4-fluorobenzyl)-1H-1,2,3-triazol-4-yl)methoxy)phenyl)-5-hydroxy-7-(4-hydroxy-3-methoxyphenyl)hepta-1,4,6-trien-3-one (34).



Reaction of intermediate **22** (0.07 g, 0.29 mmol) and the functionalized aldehyde **41** (0.08 g, 0.26 mmol), in line with the general procedure B of

the Pabon reaction, gave the crude product purified by flash chromatography (PE/EtOAc, 6:4) and further crystallization from EtOH. Orange powder, 40 % yield, mp 113-115 °C. ¹H-NMR (CDCl₃): δ 3.95 (s, 3H, OCH₃), 5.23 (s, 2H, NCH₂), 5.52 (s, 2H, OCH₂), 5.80 (s, 1H, keto-enol-CH), 6.49 (d, 1H, *J* = 15.6 Hz, CH=CH), 6.50 (d, 1H, *J* = 15.6 Hz, CH=CH), 6.94 (d, 1H, *J* = 8.4 Hz, H-5), 6.99 (d, 2H, *J* = 7.6 Hz, Ar), 7.06 (s, 1H, H-2), 7.07 (d, 1H, *J* = 7.6 Hz, H-6), 7.08-7.14 (m, 2H, Ar, 4-FBn), 7.24-7.27 (m, 2H, Ar, 4-FBn), 7.50 (d, 2H, *J* = 8.0 Hz, Ar), 7.55 (s, 1H), 7.60 (d, 1H, *J* = 15.6 Hz, CH=CH), 7.61 (d, 1H, *J* = 16.0 Hz, CH=CH). ¹³C-NMR (CDCl₃): δ 53.7, 56.1, 62.2, 101.5, 109.7, 114.9, 115.3 (2C), 116.4 (d, 2C, *J* = 21.4 Hz), 121.9, 122.3, 122.7, 123.1, 127.8, 128.5, 129.9 (2C), 130.0, 130.2 (d, 2C, *J* = 8.1 Hz), 140.0, 140.8, 144.4, 146.9, 148.0, 159.9, 160.7 (d, *J* = 249.4 Hz), 183.2, 183.6. ESI-MS (*m/z*): 550 (M + Na).

ethyl 2-(4-((4-((1E,4Z,6E)-5-hydroxy-7-(4-hydroxy-3-methoxyphenyl)-3-oxohepta-1,4,6-trien-1-yl)phenoxy)methyl)-1H-1,2,3-triazol-1-yl)acetate (35).

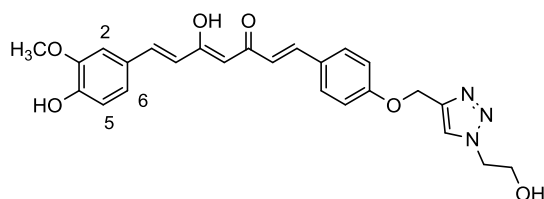


Reaction of intermediate **22** (0.44 g, 1.88 mmol) and the functionalized aldehyde **42** (0.54 g, 1.88 mmol), in line with the general procedure B of the Pabon reaction, gave the crude

product purified by flash chromatography (PE/acetone, 8:2) and two sequential crystallizations from EtOH and acetone. Mustard yellow powder, 79 % yield, mp 108-110 °C. ¹H-NMR (CDCl₃): δ 1.31 (t, 3H, *J* = 7.1 Hz, OCH₂CH₃), 3.96 (s, 3H, OCH₃), 4.29 (q, 2H, *J* = 6.8 Hz, OCH₂CH₃), 5.18 (s, 2H, NCH₂), 5.30 (s, 2H,

OCH₂), 5.80 (s, 1H, keto-enol-CH), 5.88 (br s, 1H, OH), 6.50 (d, 1H, *J* = 16.0 Hz, CH=CH), 6.51 (d, 1H, *J* = 16.0 Hz, CH=CH), 6.94 (d, 1H, *J* = 8.0 Hz, H-5), 7.02 (d, 2H, *J* = 8.4 Hz, Ar), 7.07 (s, 1H, H-2), 7.13 (d, 1H, *J* = 8.0 Hz, H-6), 7.52 (d, 2H, *J* = 8.4 Hz, Ar), 7.60 (d, 1H, *J* = 16.0 Hz, CH=CH), 7.62 (d, 1H, *J* = 15.6 Hz, CH=CH), 7.84 (s, 1H). ¹³C-NMR (CDCl₃): δ 14.2, 51.1, 56.1, 62.1, 62.7, 101.5, 109.8, 115.0, 115.4 (2C), 121.9, 122.3, 123.1, 124.3, 127.8, 128.5, 129.9 (2C), 140.0, 140.8, 144.4, 147.0, 148.0, 159.9, 166.3, 183.2, 183.6. ESI-MS (*m/z*): 528 (M + Na).

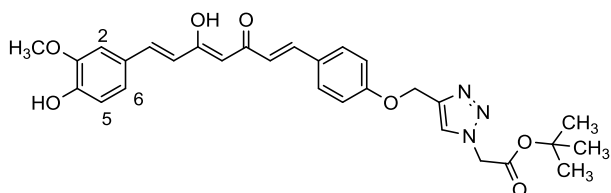
(1*E*,4*Z*,6*E*)-5-hydroxy-7-(4-hydroxy-3-methoxyphenyl)-1-(4-((1-(2-hydroxyethyl)-1*H*-1,2,3-triazol-4-yl)methoxy)phenyl)hepta-1,4,6-trien-3-one (36).



Reaction of intermediate **22** (0.17 g, 0.73 mmol) and the functionalized aldehyde **43** (0.18 g, 0.73 mmol), in line with the general procedure B of

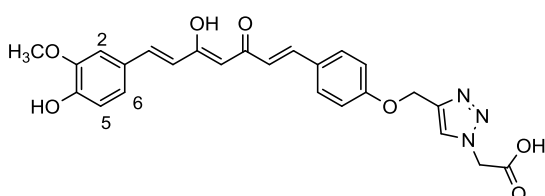
the Pabon reaction, gave the crude product purified by two sequential crystallizations from CH₂Cl₂ and acetone/PE. Orange-brown powder, 57 % yield, mp 164-166 °C. ¹H-NMR (acetone-*d*₆): δ 3.92 (s, 3H, OCH₃), 3.97 (t, 2H, *J* = 5.2 Hz, CH₂OH), 4.52 (t, 2H, *J* = 5.2 Hz, NCH₂), 5.25 (s, 2H, OCH₂), 6.00 (s, 1H, keto-enol-CH), 6.73 (d, 2H, *J* = 16.0 Hz, CH=CH), 6.89 (d, 1H, *J* = 8.4 Hz, H-5), 7.13 (d, 2H, *J* = 8.8 Hz, Ar), 7.19 (dd, 1H, *J* = 1.6 and 8.0 Hz, H-6), 7.35 (d, 1H, *J* = 1.6 Hz, H-2), 7.61 (d, 1H, *J* = 15.6 Hz, CH=CH), 7.63 (d, 1H, *J* = 16.0 Hz, CH=CH), 7.66 (d, 2H, *J* = 8.4 Hz, Ar), 8.10 (s, 1H), 8.26 (br s, 1H, OH). ¹³C-NMR (acetone-*d*₆): δ 53.4, 56.3, 61.5, 62.6, 101.9, 111.5, 116.1 (2C), 116.2, 122.3, 123.0, 123.9, 125.4, 128.1, 129.0, 130.7 (2C), 140.5, 141.6, 143.6, 148.8, 158.3, 161.3, 184.0 (2C). ESI-MS (*m/z*): 486 (M + Na).

***tert*-butyl 2-(4-((4-((1*E*,4*Z*,6*E*)-5-hydroxy-7-(4-hydroxy-3-methoxyphenyl)-3-oxohepta-1,4,6-trien-1-yl)phenoxy)methyl)-1*H*-1,2,3-triazol-1-yl)acetate (37).**



Reaction of intermediate **22** (0.12 g, 0.51 mmol) and the functionalized aldehyde **44** (0.19 g, 0.61 mmol), in line with the general procedure B of the Pabon reaction, gave the crude product purified by flash chromatography (PE/EtOAc, 8:2) and further crystallization from EtOH. Yellow powder, 80 % yield, mp 174-175 °C. ¹H-NMR (CDCl₃): δ 1.49 [s, 9H, C(CH₃)₃], 3.95 (s, 3H, OCH₃), 5.08 (s, 2H, NCH₂), 5.28 (s, 2H, OCH₂), 5.80 (s, 1H, keto-enol-CH), 5.93 (br s, 1H, OH), 6.49 (d, 1H, *J* = 15.6 Hz, CH=CH), 6.50 (d, 1H, *J* = 15.6 Hz, CH=CH), 6.94 (d, 1H, *J* = 8.1 Hz, H-5), 7.02 (d, 2H, *J* = 8.4 Hz, Ar), 7.06 (s, 1H, H-2), 7.13 (d, 1H, *J* = 8.1 Hz, H-6), 7.51 (d, 2H, *J* = 8.4 Hz, Ar), 7.60 (d, 1H, *J* = 15.6 Hz, CH=CH), 7.61 (d, 1H, *J* = 15.6 Hz, CH=CH), 7.77 (s, 1H). ¹³C-NMR (CDCl₃): δ 28.1 (3C), 51.8, 56.1, 62.2, 84.2, 101.5, 109.7, 115.0, 115.4 (2C), 121.9, 122.3, 123.1, 124.3, 127.8, 128.5, 129.9 (2C), 140.0, 140.7, 144.2, 147.0, 148.0, 160.0, 165.3, 183.3, 183.6. ESI-MS (*m/z*): 556 (M + Na).

2-(4-((4-((1*E*,4*Z*,6*E*)-5-hydroxy-7-(4-hydroxy-3-methoxyphenyl)-3-oxohepta-1,4,6-trien-1-yl)phenoxy)methyl)-1*H*-1,2,3-triazol-1-yl)acetic acid (38).



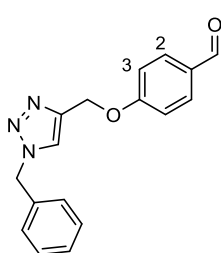
Reaction of intermediate **22** (0.18 g, 0.77 mmol) and the functionalized aldehyde **45** (0.24 g, 0.92 mmol), in line with the general procedure B of the Pabon reaction, gave the crude product purified by flash chromatography (PE/acetone, 3:7) and further crystallization from acetone/PE. Mustard yellow powder, 63 % yield, mp 204-206 °C. ¹H-NMR (1 % CD₃COOD in acetone-*d*₆): δ 3.91 (s, 3H, OCH₃), 5.29 (s, 2H, NCH₂), 5.32 (s, 2H, OCH₂), 5.35 (br s, 1H, OH), 6.71 (d, 2H, *J* = 16.0 Hz, CH=CH), 6.88 (d, 1H, *J* = 8.0 Hz, H-5), 7.01 (s, 1H, keto-enol-CH), 7.11 (d, 2H, *J* = 8.8 Hz, Ar), 7.17 (dd, 1H, *J* = 1.6 and 6.8 Hz, H-6), 7.33 (d, 1H, *J* = 2.0 Hz, H-2), 7.59 (d, 1H, *J* = 16.0 Hz, CH=CH), 7.61 (d, 1H, *J* = 15.6

Hz, CH=CH), 7.65 (d, 2H, $J = 8.8$ Hz, Ar), 8.15 (s, 1H). $^{13}\text{C-NMR}$ (1 % CD_3COOD in acetone- d_6): δ 50.0, 55.5, 62.2, 101.6, 109.8, 114.9, 115.3 (2C), 121.9, 122.3, 123.1, 124.3, 127.8, 128.5, 130.0 (2C), 140.1, 140.4, 144.0, 146.8, 148.0, 159.9, 165.2, 183.2, 183.7. ESI-MS (m/z): 500 (M + Na).

CCR: general procedure for the synthesis of functionalized aldehydes 39-44.

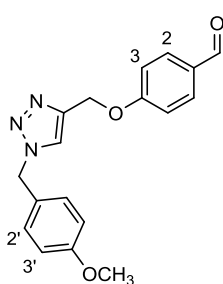
To a stirred solution of 4-(prop-2-ynyloxy)benzaldehyde (1.00 mmol) and the appropriate azido derivative (1.3 molar equiv) in DMSO or DMF (4.35 mL), trimethylamine (TEA) (0.1 molar equiv) was added dropwise, followed by slowly addition of a solution of CuSO_4 (0.1 molar equiv) and (+)-sodium L-ascorbate (0.5 molar equiv) in water (0.5 mL). The resulting mixture was diluted with DMSO or DMF (2.82 mL) and stirred for 2-3 h at room temperature. Upon reaction completion, the solution was poured into water and each desired aldehyde was obtained as precipitate, which was filtered off and used in the next synthetic step without further purification.

4-((1-benzyl-1H-1,2,3-triazol-4-yl)methoxy)benzaldehyde (39).



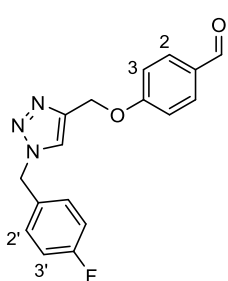
4-(prop-2-ynyloxy)benzaldehyde (0.26 g, 1.62 mmol) and benzyl azide (0.27 mL, 2.11 mmol) were allowed to react following the general procedure for the synthesis of functionalized aldehydes in DMSO. Light green powder, 60 % yield, 96-98 °C. $^1\text{H-NMR}$ (CDCl_3): δ 5.28 (s, 2H, OCH_2), 5.55 (s, 2H, NCH_2), 7.10 (d, 2H, $J = 8.4$ Hz, Ar, H-3), 7.27-7.30 (m, 3H, Bn), 7.39 (d, 2H, $J = 8.0$ Hz, Bn), 7.55 (s, 1H), 7.84 (d, 2H, $J = 8.4$ Hz, Ar, H-2), 9.90 (s, 1H, CHO).

4-((1-(4-methoxybenzyl)-1*H*-1,2,3-triazol-4-yl)methoxy)benzaldehyde (40).



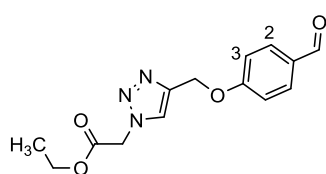
4-(prop-2-ynyloxy)benzaldehyde (0.21 g, 1.28 mmol) and **46** (0.27 g, 1.67 mmol) were allowed to react following the general procedure for the synthesis of functionalized aldehydes in DMF. Pink powder, 60 % yield, mp 83-85 °C. ¹H-NMR (CDCl₃): δ 3.81 (s, 3H, OCH₃), 5.25 (s, 2H, OCH₂), 5.48 (s, 2H, NCH₂), 6.90 (d, 2H, *J* = 8.4 Hz, Ar, H-3'), 7.08 (d, 2H, *J* = 8.4 Hz, Ar, H-3), 7.24 (d, 2H, *J* = 8.4 Hz, Ar, H-2'), 7.51 (s, 1H), 7.83 (d, 2H, *J* = 8.4 Hz, Ar, H-2), 9.89 (s, 1H, CHO).

4-((1-(4-fluorobenzyl)-1*H*-1,2,3-triazol-4-yl)methoxy)benzaldehyde (41).



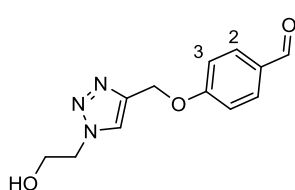
4-(prop-2-ynyloxy)benzaldehyde (0.19 g, 1.20 mmol) and **47** (0.24 g, 1.55 mmol) were allowed to react following the general procedure for the synthesis of functionalized aldehydes in DMF. Salmon pink powder, 43 % yield, mp 88-100 °C. ¹H-NMR (CDCl₃): δ 5.25 (s, 2H, OCH₂), 5.51 (s, 2H, NCH₂), 7.04-7.09 (m, 4H, Ar, H-3 and H-3'), 7.27 (d, 2H, *J* = 8.4 Hz, Ar, H-2'), 7.51 (s, 1H), 7.82 (d, 2H, *J* = 8.4 Hz, Ar, H-2), 9.88 (s, 1H, CHO).

ethyl 2-(4-((4-formylphenoxy)methyl)-1*H*-1,2,3-triazol-1-yl)acetate (42).



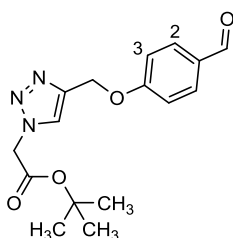
4-(prop-2-ynyloxy)benzaldehyde (0.26 g, 1.62 mmol) and **48** (0.27 g, 2.10 mmol) were allowed to react following the general procedure for the synthesis of functionalized aldehydes in DMSO. Pearl-grey powder, 77 % yield, mp 117-119 °C. ¹H-NMR (CDCl₃): δ 1.31 (t, 3H, *J* = 7.2 Hz, OCH₂CH₃), 4.29 (q, 2H, *J* = 6.8 Hz, OCH₂CH₃), 5.19 (s, 2H, NCH₂), 5.34 (s, 2H, OCH₂), 7.12 (d, 2H, *J* = 8.8 Hz, Ar, H-3), 7.81 (s, 1H), 7.85 (d, 2H, *J* = 8.0 Hz, Ar, H-2), 9.90 (s, 1H, CHO).

4-((1-(2-hydroxyethyl)-1H-1,2,3-triazol-4-yl)methoxy)benzaldehyde (43).



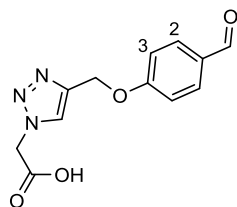
4-(prop-2-ynyloxy)benzaldehyde (0.29 g, 1.81 mmol) and **49** (0.20 g, 2.35 mmol) were allowed to react following the general procedure for the synthesis of functionalized aldehydes in DMSO. In this case, the crude product did not precipitate from the aqueous phase, that was extracted with CH₂Cl₂ (3 x 15.0 mL). The combined organic layers were washed with brine, dried over Na₂SO₄ and evaporated to dryness giving **43** as pale yellow oil, 50 % yield. ¹H-NMR (CDCl₃): δ 4.08 (t, 2H, *J* = 5.6 Hz, CH₂OH), 4.52 (t, 2H, *J* = 5.2 Hz, NCH₂), 5.30 (s, 2H, OCH₂), 7.12 (d, 2H, *J* = 8.8 Hz, Ar, H-3), 7.80 (s, 1H), 7.85 (d, 2H, *J* = 8.8 Hz, Ar, H-2), 9.90 (s, 1H, CHO).

tert-butyl 2-(4-((4-formylphenoxy)methyl)-1H-1,2,3-triazol-1-yl)acetate (44).



4-(prop-2-ynyloxy)benzaldehyde (0.53 g, 3.33 mmol) and **50** (0.68 g, 4.33 mmol) were allowed to react following the general procedure for the synthesis of functionalized aldehydes in DMSO. Beige powder, 71 % yield, mp 78-81 °C. ¹H-NMR (CDCl₃): δ 1.49 [s, 9H, C(CH₃)₃], 5.09 (s, 2H, NCH₂), 5.33 (s, 2H, OCH₂), 7.12 (d, 2H, *J* = 8.4 Hz, Ar, H-3), 7.79 (s, 1H), 7.85 (d, 2H, *J* = 8.8 Hz, Ar, H-2), 9.90 (s, 1H, CHO).

2-(4-((4-formylphenoxy)methyl)-1H-1,2,3-triazol-1-yl)acetic acid (45).



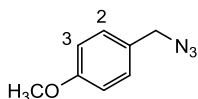
To a solution of **44** (0.30 g, 0.95 mmol) in CH₂Cl₂ (8.0 mL) TFA (0.74 mL, 9.92 mmol) was added dropwise upon a period of 15 min. The resulting solution was stirred at room temperature for 72 h and was then quenched by addition of a saturated aqueous NaHCO₃ solution (20.0 mL). The organic phase was separated, the aqueous layer was acidified with HCl (12.0 N) and extracted with EtOAc (3 x 20.0 mL). The combined EtOAc phases were washed

with brine, dried over Na₂SO₄ and concentrated to dryness affording **45** as pale green-grey solid; 98 % yield, 155-157 °C. ¹H-NMR (acetone-*d*₆): δ 5.35 (s, 2H, NCH₂), 5.38 (s, 2H, OCH₂), 7.25 (d, 2H, *J* = 8.4 Hz, Ar, H-3), 7.89 (d, 2H, *J* = 8.4 Hz, Ar, H-2), 8.20 (s, 1H), 9.92 (s, 1H, CHO).

General procedure for the synthesis of *p*-substituted benzyl azides **46 and **47**.**

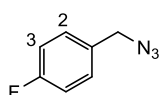
To a solution of the appropriate benzyl halide (1.00 mmol) in DMF (10.0 mL), sodium azide (NaN₃, 10.0 molar equiv) was added and the obtained mixture was heated to 60 °C for 10 h. Upon reaction completion, the solution was cooled to room temperature and was poured into water. The aqueous phase was extracted with diethyl ether (Et₂O) (3 x 20.0 mL) and the combined organic layers were washed with brine, dried over Na₂SO₄ and concentrated to dryness. The desired azide was employed in the following synthetic step without any further purification.

1-(azidomethyl)-4-methoxybenzene (46**).**



46 was obtained according to the general procedure for *p*-substituted benzyl azides starting from 4-methoxybenzyl chloride (0.86 mL, 6.38 mmol) and NaN₃ (4.15 g, 63.80 mmol); yellow oil, 67 % yield. ¹H-NMR (200 MHz, CDCl₃): δ 3.82 (s, 3H, OCH₃), 4.28 (s, 2H, N₃CH₂), 6.92 (d, 2H, *J* = 8.4 Hz, Ar, H-3), 7.26 (d, 2H, *J* = 8.4 Hz, Ar, H-2).

1-(azidomethyl)-4-fluorobenzene (47**).**

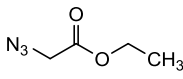


47 was obtained according to the general procedure for *p*-substituted benzyl azides starting from 4-fluorobenzyl bromide (0.66 mL, 5.29 mmol) and NaN₃ (3.44 g, 52.90 mmol); yellow oil, 50 % yield. ¹H-NMR (200 MHz, CDCl₃): δ 4.29 (s, 2H, N₃CH₂), 7.03-7.07 (m, 2H, Ar, H-3), 7.24-7.29 (m, 2H, Ar, H-2).

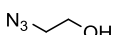
General procedure for the synthesis of azidoacetate intermediates **48** and **50**.

The appropriate alkyl halide (1.00 mmol) was slowly added to a solution of NaN₃ (5.0 molar equiv) in acetone/H₂O (4:1, 10.0 mL) and the resulting mixture was allowed to stir overnight at room temperature. The reaction mixture was diluted with water (10.0 mL), the aqueous phase was extracted with EtOAc (3 x 20.0 mL) and the combined organic layers were washed with brine, dried over Na₂SO₄, filtered and concentrated under reduced pressure. The resulting azide was employed in the next synthetic step without any further purification.

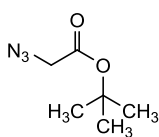
Ethyl azidoacetate (**48**).

 Ethyl bromoacetate (1.10 mL, 10.00 mmol) and NaN₃ (3.25 g, 50.00 mmol) were allowed to react according to the general synthetic procedure for azidoacetate derivatives to give **48** as pale yellow oil; 43 % yield. ¹H-NMR (CDCl₃): δ 1.32 (t, 3H, *J* = 7.2 Hz, OCH₂CH₃), 3.87 (s, 2H, N₃CH₂), 4.27 (q, 2H, *J* = 7.2 Hz, OCH₂CH₃).

2-azidoethan-1-ol (**49**).

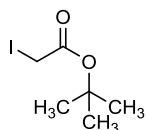
 A solution of 2-bromoethanol (0.57 mL, 8.00 mmol) and NaN₃ (1.04 g, 16.00 mmol) in water (50.0 mL) was heated at 50 °C for 22 h. Upon reaction completion, the reaction mixture was cooled to room temperature and was diluted with additional water (50.0 mL). The aqueous phase was extracted with EtOAc (3 x 30.0 mL) and the combined organic layers were washed with brine, dried over Na₂SO₄, filtered and concentrated affording **49** as pale yellow oil; 50 % yield. ¹H-NMR (CDCl₃): δ 2.39 (br s, 1H, OH), 3.42 (t, 2H, *J* = 5.2 Hz, CH₂OH), 3.78 (t, 2H, *J* = 5.6 Hz, N₃CH₂).

***tert*-butyl azidoacetate (50).**



tert-butyl iodoacetate (1.27 g, 5.25 mmol) and NaN₃ (1.71 g, 26.25 mmol) were allowed to react according to the general synthetic procedure for azidoacetate derivatives to give **50** as pale yellow oil; 82 % yield. ¹H-NMR (CDCl₃): δ 1.50 [s, 9H, C(CH₃)₃], 3.74 (s, 2H, N₃CH₂).

***tert*-butyl 2-iodoacetate (51).**



To a vigorously stirred suspension of anhydrous MgSO₄ (4.81 g, 40.00 mmol) in CH₂Cl₂ (40.0 mL), H₂SO₄ conc. (0.55 mL, 10.00 mmol) was added dropwise. The mixture was stirred for 15 min, after which the iodoacetic acid (1.86 g, 10.00 mmol) was added, following by addition of *tert*-butanol (4.78 mL, 50.00 mmol). The mixture was stirred for 72 h at room temperature. The reaction mixture was then quenched with saturated aqueous NaHCO₃ solution (40.0 mL) and stirred until all MgSO₄ dissolved. The organic phase was separated, washed with brine, dried over Na₂SO₄, and concentrated to afford **51** as yellow oil; 60 % yield. ¹H-NMR (CDCl₃): δ 1.47 [s, 9H, C(CH₃)₃], 3.61 (s, 2H, CH₂).

CCR in 4-position of the curcumin scaffold: general procedure for the synthesis of compounds 52a,b-54a,b, 83a,b, 84a,b, and 90a,b.

To a stirred solution of **55a,b** or **56** (1.00 mmol) and the appropriate azido derivative (1.3 molar equiv) in DMF or DMSO (4.35 mL), TEA (0.1 molar equiv) was added dropwise followed by slowly addition of a solution of CuSO₄ (0.1 molar equiv) and (+)-sodium L-ascorbate (0.5 molar equiv) in water (0.5 mL). The resulting mixture was diluted with DMF or DMSO (2.82 mL) and was stirred at room temperature overnight. Upon reaction completion, the mixture was poured into water and was worked up applying one of the following methods:

- a) The organic layer was diluted with CH₂Cl₂ or EtOAc and the water phase was extracted with the same organic solvent (3 x 25.0 mL). The combined

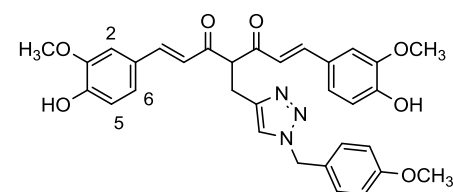
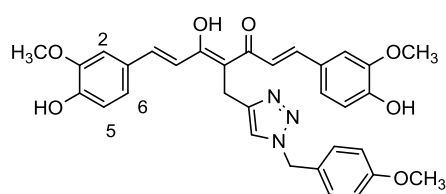
organic layers were dried over Na₂SO₄ and evaporated under reduced pressure.

b) The obtained precipitate was filtered under *vacuum* to dryness.

In both cases, purification of the crude product by flash chromatography and further crystallization from suitable solvent or mixture of solvents, afforded the desired final compound as tautomeric mixture.

(1E,4Z,6E)-5-hydroxy-1,7-bis(4-hydroxy-3-methoxyphenyl)-4-((1-(4-methoxybenzyl)-1H-1,2,3-triazol-4-yl)methyl)hepta-1,4,6-trien-3-one (52a);
(1E,6E)-1,7-bis(4-hydroxy-3-methoxyphenyl)-4-((1-(4-methoxybenzyl)-1H-1,2,3-triazol-4-yl)methyl)hepta-1,6-diene-3,5-dione (52b).

55a,b (0.36 g, 0.89 mmol) and azido **46** (0.19 g, 1.15 mmol) were allowed to react according to the general procedure of the CCR in 4-position of the curcumin scaffold in DMF (method **b**). The crude product was purified by flash chromatography (EP/EtOAc, 7:3) and further crystallization from CH₂Cl₂/PE. Red powder, 43 % yield (isolated as 1.0:1.2 mixture of **52a:52b**), mp 98-100°C.



52a (45 % of the tautomeric mixture). ¹H-NMR (CDCl₃): δ 3.68 (s, 3H, OCH₃), 3.92 (s, 6H, OCH₃), 4.06 (s, 2H, CH₂), 5.37 (s, 2H, NCH₂), 5.92 (br s, 2H, OH), 6.67 (d, 2H, *J* = 6.8 Hz, H-5), 6.70 (s, 2H, H-2), 6.81 (d, 2H, *J* = 8.8 Hz, H-6), 6.91 (d, 2H, *J* = 8.0 Hz, Ar), 6.98 (s, 1H), 7.07 (d, 2H, *J* = 8.4 Hz, Ar), 7.10 (d, 1H, *J* = 15.2 Hz, CH=CH), 7.12 (d, 1H, *J* = 15.6 Hz, CH=CH), 7.67 (d, 2H, *J* = 15.6 Hz, CH=CH).

52b (55 % of the tautomeric mixture). ¹H-NMR (CDCl₃): δ 3.27 (d, 2H, *J* = 7.2 Hz, CH₂), 3.72 (s, 3H, OCH₃), 3.92 (s, 6H, OCH₃), 4.77 (t, 1H, *J* = 7.2 Hz, diketo-CH), 5.37 (s, 2H, NCH₂), 5.88 (br s, 2H, OH), 6.67 (d, 2H, *J* = 6.8 Hz, H-5), 6.70 (s, 2H, H-2), 6.81 (d, 2H, *J* = 8.8 Hz, H-6), 6.83 (d, 2H, *J* = 15.2 Hz, CH=CH), 6.91 (d, 2H, *J* = 8.0 Hz, Ar), 7.02 (s, 1H), 7.07 (d, 2H, *J* = 8.4 Hz, Ar), 7.59 (d, 2H, *J* = 15.6 Hz, CH=CH). **52a,b.** ¹³C-NMR (CDCl₃): δ 24.9, 29.8, 53.7, 53.9, 55.3, 55.4, 56.1

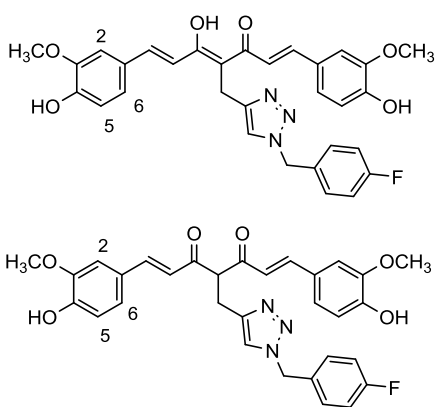
(2C), 56.2 (2C), 62.9, 107.8, 109.8 (2C), 109.9 (2C), 114.4 (2C), 114.5 (2C), 114.9 (2C), 115.0 (2C), 117.9, 121.9, 122.1 (2C), 123.5 (2C), 124.3 (2C), 127.6 (2C), 127.9 (4C), 129.3 (2C), 129.6 (2C), 129.7, 142.5, 145.1 (2C), 145.3 (2C), 147.0 (2C), 148.3 (4C), 149.0 (2C), 149.2 (2C), 159.9 (2C), 183.2 (2C), 194.6 (2C).

ESI-MS (m/z): 592 (M + Na).

(1E,4Z,6E)-4-((1-(4-fluorobenzyl)-1H-1,2,3-triazol-4-yl)methyl)-5-hydroxy-1,7-bis(4-hydroxy-3-methoxyphenyl)hepta-1,4,6-trien-3-one (53a);

(1E,6E)-4-((1-(4-fluorobenzyl)-1H-1,2,3-triazol-4-yl)methyl)-1,7-bis(4-hydroxy-3-methoxyphenyl)hepta-1,6-diene-3,5-dione (53b).

55a,b (0.24 g, 0.60 mmol) and azido **47** (0.12 g, 0.78 mmol) were allowed to react according to the general procedure of the CCR in 4-position of the curcumin scaffold in DMF (method **a**). The crude product was purified by flash chromatography (EP/EtOAc, 1:1) and further crystallization from CH₂Cl₂/PE. Dark red powder, 41 % yield (isolated as 1.3:1.0 mixture of **53a:53b**), mp 95-97 °C.



53a (57 % of the tautomeric mixture). ¹H-NMR (acetone-*d*₆): δ 3.89 (s, 6H, OCH₃), 4.05 (s, 2H, CH₂), 5.54 (s, 2H, NCH₂), 5.58 (br s, 2H, OH), 6.87 (d, 2H, *J* = 8.4 Hz, H-5), 6.88 (s, 2H, H-2), 6.93-6.98 (m, 2H, Ar), 7.18 (d, 2H, *J* = 8.0 Hz, H-6), 7.27 (d, 2H, *J* = 16.0 Hz, CH=CH), 7.27-7.34 (m, 2H, Ar), 7.62 (d, 2H, *J* = 15.6 Hz, CH=CH), 7.66 (s, 1H).

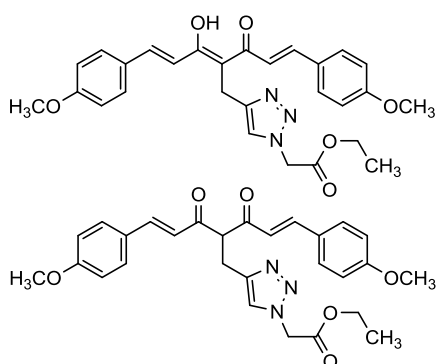
53b (43 % of the tautomeric mixture). ¹H-NMR (acetone-*d*₆): δ 3.27 (d, 2H, *J* = 6.8 Hz, CH₂), 3.89 (s, 6H, OCH₃), 4.93 (t, 1H, *J* = 6.8 Hz, diketo-CH), 5.54 (s, 2H, NCH₂), 5.58 (br s, 2H, OH), 6.87 (d, 2H, *J* = 8.4 Hz, H-5), 6.93 (s, 2H, H-2), 7.01-7.05 (m, 2H, Ar), 7.18 (d, 2H, *J* = 8.0 Hz, H-6), 7.27-7.34 (m, 2H, Ar), 7.29 (d, 2H, *J* = 15.6 Hz, CH=CH), 7.64 (d, 2H, *J* = 15.6 Hz, CH=CH), 7.75 (s, 1H).

53a,b. ¹³C-NMR (CDCl₃): δ 24.8, 29.8, 53.5, 53.6, 56.1 (4C), 62.9, 109.9 (4C), 115.0 (4C), 116.1 (d, 4C, *J* = 22.2 Hz), 117.8, 122.1, 122.3, 123.4 (4C), 124.3 (2C), 126.7 (2C), 127.9 (4C), 129.7 (2C), 129.9 (d, 4C, *J* = 8.4 Hz), 130.6, 142.6, 145.4

(2C), 147.0 (2C), 148.3 (4C), 149.0 (4C), 162.8 (d, 2C, $J = 255.6$ Hz), 183.2 (2C), 194.6 (2C). ESI-MS (m/z): 580 (M + Na).

ethyl 2-(4-((2Z,4E)-3-hydroxy-5-(4-methoxyphenyl)-2-((E)-3-(4-methoxyphenyl)acryloyl)penta-2,4-dien-1-yl)-1H-1,2,3-triazol-1-yl)acetate (54a);
ethyl 2-(4-((E)-5-(4-methoxyphenyl)-2-((E)-3-(4-methoxyphenyl)acryloyl)-3-oxopent-4-en-1-yl)-1H-1,2,3-triazol-1-yl)acetate (54b).

Intermediate **56** (0.30 g, 0.80 mmol) and azido **48** (0.13 g, 1.04 mmol) were allowed to react according to the general procedure of the CCR in 4-position of the curcumin scaffold in DMSO (method **a**). The crude product was purified by flash chromatography (PE/EtOAc, 8.5:1.5) and further crystallization from CH₂Cl₂/PE. Orange powder, 50 % yield (isolated as 1.5:1.0 mixture of **54a**:**54b**), mp 150-152 °C.



54a (60 % of the tautomeric mixture). ¹H-NMR (CDCl₃): δ 1.26 (t, 3H, $J = 7.2$ Hz, OCH₂CH₃), 3.84 (s, 6H, OCH₃), 4.09 (s, 2H, CH₂), 4.22 (q, 2H, $J = 7.2$ Hz, OCH₂CH₃), 5.08 (s, 2H, NCH₂), 6.90 (d, 4H, $J = 8.4$ Hz, Ar), 6.95 (d, 2H, $J = 15.6$ Hz, CH=CH), 7.38 (s, 1H), 7.50 (d, 4H, $J = 8.4$ Hz, Ar), 7.75 (d,

2H, $J = 15.2$ Hz, CH=CH).

54b (40 % of the tautomeric mixture). ¹H-NMR (CDCl₃): δ 1.18 (t, 3H, $J = 7.2$ Hz, OCH₂CH₃), 3.44 (d, 2H, $J = 7.2$ Hz, CH₂), 3.84 (s, 6H, OCH₃), 4.16 (q, 2H, $J = 7.2$ Hz, OCH₂CH₃), 4.77 (t, 1H, $J = 7.2$ Hz, diketo-CH), 5.08 (s, 2H, NCH₂), 6.74 (d, 2H, $J = 16.0$ Hz, CH=CH), 6.90 (d, 4H, $J = 8.4$ Hz, Ar), 7.51 (d, 4H, $J = 8.0$ Hz, Ar), 7.55 (s, 1H), 7.66 (d, 2H, $J = 16.0$ Hz, CH=CH). **54a,b**. ¹³C-NMR (CDCl₃): δ 14.1, 14.2, 23.3, 24.8, 51.0, 51.1, 55.5 (4C), 62.5 (2C), 63.3, 114.5 (8C), 116.6, 118.0, 122.2, 123.4, 123.7, 124.3, 127.0, 128.1, 130.2 (4C), 130.7 (4C), 131.1 (4C), 142.3 (2C), 144.9, 146.4, 149.1, 161.6 (4C), 162.1 (2C), 183.4 (2C), 194.5 (2C). ESI-MS (m/z): 526 (M + Na).

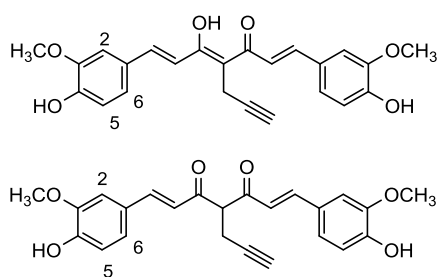
Pabon reaction: general procedure C (synthesis of compounds 58-60, 79-82, 85a,b-89a,b and intermediates 55a,b and 56).

To a suspension of alkylated pentane-2,4-dione (1.00 mmol) and B₂O₃ (1.0 molar equiv) in DMF (1.5 mL), stirred for 30 min at 80 °C, B(*n*-BuO)₃ (4.0 molar equiv) was added. The resulting mixture was heated for additional 30 min and a sequential addition of the suitable aldehyde (1.8 or 2.0 molar equiv) and of a solution of *n*-BuNH₂ (0.4 molar equiv) in DMF (1.0 mL) was carried out. After stirring at 80 °C for 8-10 h, the resulting solution was cooled to room temperature, acidified with HCl (0.5 N, 8.0 mL) and stirred for 30 min. The crude product was obtained as precipitate, which was suspended in water, filtered off and purified by flash column chromatography and/or crystallization from suitable solvent or mixture of solvents, unless otherwise stated.

(1*E*,4*Z*,6*E*)-5-hydroxy-1,7-bis(4-hydroxy-3-methoxyphenyl)-4-(prop-2-yn-1-yl)hepta-1,4,6-trien-3-one (55a);

(1*E*,6*E*)-1,7-bis(4-hydroxy-3-methoxyphenyl)-4-(prop-2-yn-1-yl)hepta-1,6-diene-3,5-dione (55b).

Reaction of **57a,b** (0.36 g, 2.61 mmol) and vanillin (0.71 g, 4.70 mmol), following the general procedure C of the Pabon reaction, gave the crude product that was purified by flash chromatography (PE/EtOAc, 7:3) and further crystallization from EtOH. Dark red powder, 58 % yield (isolated as 1.0:1.7 mixture of **55a:55b**), mp 144-147 °C.

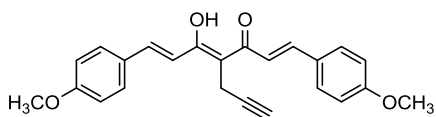


55a (37 % of the tautomeric mixture). ¹H-NMR (acetone-*d*₆): δ 2.53 (t, 1H, *J* = 2.4 Hz, ≡CH), 3.61 (d, 2H, *J* = 2.8 Hz, CH₂C≡), 3.92 (s, 6H, OCH₃), 6.90 (d, 2H, *J* = 8.4 Hz, H-5), 7.27 (dd, 2H, *J* = 2.0 and 8.0 Hz, H-6), 7.28 (d, 2H, *J* = 15.2 Hz, CH=CH), 7.40 (d, 2H, *J* = 2.0 Hz, H-2), 7.72 (d, 2H, *J* = 15.2 Hz, CH=CH).

55b (63 % of the tautomeric mixture). ¹H-NMR (acetone-*d*₆): δ 2.38 (t, 1H, *J* = 2.4 Hz, ≡CH), 2.79 (dd, 2H, *J* = 2.8 and 7.2 Hz, CH₂C≡), 3.88 (s, 6H, OCH₃), 4.69 (t,

1H, $J = 7.2$ Hz, diketo-CH), 6.88 (d, 2H, $J = 8.0$ Hz, H-5), 6.96 (d, 2H, $J = 15.6$ Hz, CH=CH), 7.22 (dd, 2H, $J = 2.0$ and 8.4 Hz, H-6), 7.37 (d, 2H, $J = 2.0$ Hz, H-2), 7.70 (d, 2H, $J = 15.6$ Hz, CH=CH).

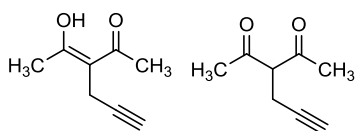
(1E,4Z,6E)-5-hydroxy-1,7-bis(4-methoxyphenyl)-4-(prop-2-yn-1-yl)hepta-1,4,6-trien-3-one (56).



Reaction of **57a,b** (1.41 g, 10.20 mmol) and 4-methoxybenzaldehyde (2.23 mL, 18.36 mmol), following the general procedure C of the Pabon reaction, gave **56** as precipitate that was filtered, washed with water and dried at high *vacuum*. Dark red powder, 52 % yield, mp 135-137 °C. ¹H-NMR (CDCl₃): δ 2.15 (t, 1H, $J = 2.4$ Hz, \equiv CH), 3.44 (d, 2H, $J = 2.4$ Hz, CH₂C \equiv), 3.87 (s, 6H, OCH₃), 6.94 (d, 4H, $J = 8.4$ Hz, Ar), 7.04 (d, 2H, $J = 15.2$ Hz, CH=CH), 7.58 (d, 4H, $J = 8.8$ Hz, Ar), 7.77 (d, 2H, $J = 15.2$ Hz, CH=CH).

(Z)-3-(1-hydroxyethylidene)hex-5-yn-2-one (57a);
3-(prop-2-yn-1-yl)pentane-2,4-dione (57b).

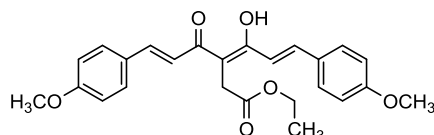
To a stirred suspension of pentane-2,4-dione (2.59 mL, 25.17 mmol) and anhydrous K₂CO₃ (2.32 g, 16.86 mmol) in acetone (150 mL), propargyl bromide solution (80 wt. % in toluene) (1.87 mL of 80 %, 1.50 mL, 16.86 mmol) was added dropwise. The reaction mixture was heated at 80 °C for 6 h and reaction progress was monitored by TLC. The mixture was hot filtered and the solvent was evaporated under reduced pressure. The resulting crude product was purified by column chromatography over silica gel using a mixture of PE/CH₂Cl₂ (8:1) as eluent. Off-white-pale yellow oil, 60 % yield (isolated as 1.7:1.0 mixture of **57a:57b**).



57a (63 % of the mixture). ¹H-NMR (CDCl₃): δ 2.03 (t, 1H, $J = 2.4$ Hz, \equiv CH), 2.18 (s, 6H, CH₃), 2.99 (d, 2H, $J = 2.4$ Hz, CH₂C \equiv).

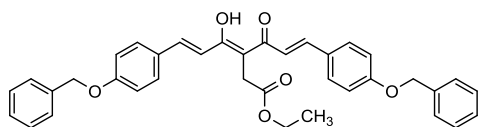
57b (37 % of the mixture). ¹H-NMR (CDCl₃): δ 2.03 (t, 1H, *J* = 2.4 Hz, ≡CH), 2.26 (s, 6H, CH₃), 2.70 (dd, 2H, *J* = 2.8 and 7.2 Hz, CH₂C≡), 3.86 (t, 1H, *J* = 7.2 Hz, diketo-CH).

ethyl (3*Z*,5*E*)-4-hydroxy-6-(4-methoxyphenyl)-3-((*E*)-3-(4-methoxyphenyl)acryloyl)hexa-3,5-dienoate (58).



Reaction of **64a,b** (1.00 g, 5.37 mmol) and 4-methoxybenzaldehyde (1.17 mL, 9.67 mmol), according to the general procedure C of the Pabon reaction, gave the crude product purified by flash chromatography (PE/EtOAc, 8:2) and further crystallization from CH₂Cl₂/PE. Red powder, 60 % yield, mp 125-127 °C. ¹H-NMR (CDCl₃): δ 1.26 (t, 3H, *J* = 7.0 Hz, OCH₂CH₃), 3.56 (s, 2H, CH₂), 3.86 (s, 6H, OCH₃), 4.20 (q, 2H, *J* = 6.8 Hz, OCH₂CH₃), 6.93 (d, 4H, *J* = 8.8 Hz, Ar), 7.05 (d, 2H, *J* = 15.2 Hz, CH=CH), 7.55 (d, 4H, *J* = 8.8 Hz, Ar), 7.75 (d, 2H, *J* = 15.4 Hz, CH=CH). ¹³C-NMR (CDCl₃): δ 14.4, 32.4, 55.5 (2C), 61.3, 104.7, 114.5 (4C), 118.4 (2C), 128.3 (2C), 130.1 (4C), 142.1 (2C), 161.5 (2C), 171.9, 183.7 (2C). ESI-MS (*m/z*): 445 (M + Na).

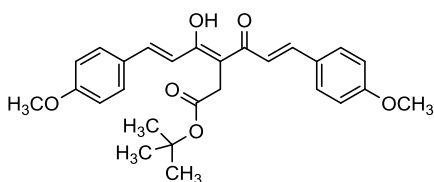
ethyl (3*Z*,5*E*)-6-(4-(benzyloxy)phenyl)-3-((*E*)-3-(4-(benzyloxy)phenyl)acryloyl)-4-hydroxyhexa-3,5-dienoate (59).



Reaction of **64a,b** (0.20 g, 1.07 mmol), and 4-benzyloxybenzaldehyde (0.41 g, 1.93 mmol), according to the general procedure C of the Pabon reaction, gave the crude product purified by flash chromatography (PE/EtOAc, 9:1) and further crystallization from CH₂Cl₂/PE. Yellow powder, 55 % yield, mp 148-150 °C. ¹H-NMR (CDCl₃): δ 1.26 (t, 3H, *J* = 7.2 Hz, OCH₂CH₃), 3.56 (s, 2H, CH₂), 4.16 (q, 2H, *J* = 7.2 Hz, OCH₂CH₃), 5.12 (s, 4H, OCH₂, Bn), 7.00 (d, 4H, *J* = 8.8 Hz, Ar), 7.05 (d, 2H, *J* = 15.4 Hz, CH=CH), 7.34-7.47 (m, 10H, Bn), 7.55 (d, 4H, *J* = 8.7 Hz, Ar), 7.75 (d, 2H, *J* = 15.4 Hz, CH=CH). ¹³C-NMR (CDCl₃): δ 14.4, 32.4, 61.3, 70.3 (2C), 115.4 (4C), 118.5 (2C), 127.6 (4C), 128.3

(2C), 128.5 (2C), 128.8 (4C), 130.1 (4C), 130.2, 136.6 (2C), 142.0 (2C), 160.7 (2C), 171.9, 183.7 (2C). ESI-MS (m/z): 597 (M + Na).

***tert*-butyl (3*Z*,5*E*)-4-hydroxy-6-(4-methoxyphenyl)-3-((*E*)-3-(4-methoxyphenyl)acryloyl)hexa-3,5-dienoate (60).**

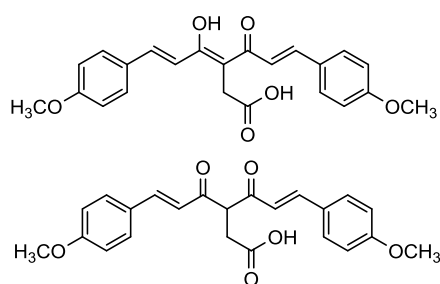


Reaction of **65a,b** (0.27 g, 1.26 mmol) and 4-methoxybenzaldehyde (0.28 mL, 2.27 mmol), according to the general procedure C of the Pabon reaction, gave the crude product purified by flash chromatography (PE/EtOAc, 8.5:1.5) and further crystallization from CH₂Cl₂/PE. Orange-yellow powder, 73 % yield, mp 154-156 °C. ¹H-NMR (CDCl₃): δ 1.45 [s, 9H, C(CH₃)₃], 3.47 (s, 2H, CH₂), 3.86 (s, 6H, OCH₃), 6.93 (d, 4H, *J* = 8.8 Hz, Ar), 7.08 (d, 2H, *J* = 15.4 Hz, CH=CH), 7.56 (d, 4H, *J* = 8.7 Hz, Ar), 7.74 (d, 2H, *J* = 15.4 Hz, CH=CH). ¹³C-NMR (CDCl₃): δ 28.2 (3C), 33.7, 55.5 (2C), 81.5, 105.3, 114.5 (4C), 118.7 (2C), 128.4 (2C), 130.1 (4C), 141.7 (2C), 161.5 (2C), 171.2, 183.7 (2). ESI-MS (m/z): 473 (M + Na).

(3*Z*,5*E*)-4-hydroxy-6-(4-methoxyphenyl)-3-((*E*)-3-(4-methoxyphenyl)acryloyl)hexa-3,5-dienoic acid (61a);

(*E*)-6-(4-methoxyphenyl)-3-((*E*)-3-(4-methoxyphenyl)acryloyl)-4-oxohex-5-enoic acid (61b).

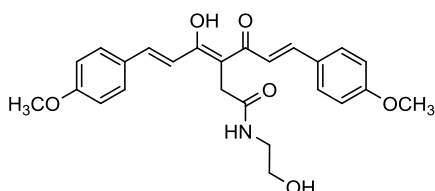
To a solution of compound **58** (0.80 g, 1.89 mmol) in CH₂Cl₂/CH₃OH (9:1, 3.67 mL), a sodium hydroxide (NaOH) solution in methanol (0.2 N, 18.9 mL) was added upon 30 min and the resulting mixture was stirred for 1 h at room temperature. The solvent was evaporated under reduced pressure obtaining a residue that was diluted with Et₂O and washed twice with fresh water (2 x 15.0 mL). The organic phase was separated and the aqueous layer was acidified with HCl (12.0 N) affording the crude product as precipitate, which was crystallized from CH₂Cl₂/PE giving **61a,b** as pale brown powder; 75 % yield (isolated as 2.2:1.0 mixture **61a:61b**), mp 147-149 °C.



61a (69 % of the tautomeric mixture). $^1\text{H-NMR}$ (CDCl_3): δ 3.77 (s, 2H, CH_2), 3.86 (s, 6H, OCH_3), 6.32 (d, 2H, $J = 16.4$ Hz, $\text{CH}=\text{CH}$), 6.93 (d, 4H, $J = 8.4$ Hz, Ar), 7.51 (d, 4H, $J = 7.6$ Hz, Ar), 7.73 (d, 2H, $J = 16.4$ Hz, $\text{CH}=\text{CH}$), 8.03 (br s, 1H, OH).

61b (31 % of the tautomeric mixture). $^1\text{H-NMR}$ (CDCl_3): δ 2.77 (d, 2H, $J = 6.8$ Hz, CH_2), 3.03 (t, 1H, $J = 6.4$ Hz, diketo-CH), 3.86 (s, 6H, OCH_3), 6.67 (d, 2H, $J = 16.4$ Hz, $\text{CH}=\text{CH}$), 6.93 (d, 4H, $J = 8.4$ Hz, Ar), 7.52 (d, 4H, $J = 7.6$ Hz, Ar), 7.59 (d, 2H, $J = 16.4$ Hz, $\text{CH}=\text{CH}$), 8.03 (br s, 1H, OH). **61a,b**. $^{13}\text{C-NMR}$ (CDCl_3) δ 28.2, 35.0, 55.5 (5C), 114.5 (4C), 114.6 (4C), 114.7, 123.6 (2C), 126.9, 127.1 (4C), 130.2 (8C), 130.8, 143.2 (2C), 146.9 (2C), 161.8 (2C), 161.9 (2C), 172.6 (2C), 178.7 (2C), 198.0 (2C). ESI-MS (m/z): 417 (M + Na).

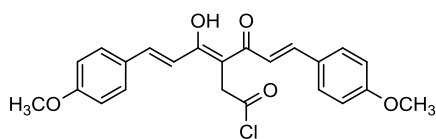
(3Z,5E)-4-hydroxy-N-(2-hydroxyethyl)-6-(4-methoxyphenyl)-3-((E)-3-(4-methoxyphenyl)acryloyl)hexa-3,5-dienamide (62).



A solution of **63** (0.12 g, 0.3 mmol) and ethanolamine (0.012 mL, 0.2 mmol) in CH_3CN (5.0 mL) was heated at 60 °C for 24 h. The solvent was removed under reduced pressure

and the crude product was purified by flash chromatography on silica gel using a mixture of $\text{CH}_2\text{Cl}_2/\text{CH}_3\text{OH}$ (9.75:0.25) as eluent to give **62** as pale yellow powder; 40 % yield, mp 214-216 °C. $^1\text{H-NMR}$ (CDCl_3): δ 1.89 (br s, 1H, OH), 3.55-3.58 (m, 2H, CH_2OH), 3.75 (s, 2H, CH_2), 3.80-3.86 (m, 2H, NHCH_2), 3.84 (s, 6H, OCH_3), 6.00 (br s, 1H, CONH), 6.30 (d, 2H, $J = 15.6$ Hz, $\text{CH}=\text{CH}$), 6.90 (d, 4H, $J = 8.4$ Hz, Ar), 7.46 (d, 4H, $J = 8.4$ Hz, Ar), 7.11 (d, 2H, $J = 15.6$ Hz, $\text{CH}=\text{CH}$). $^{13}\text{C-NMR}$ (CDCl_3): δ 31.2, 41.6, 55.3 (2C), 55.4, 114.3, 114.5 (4C), 123.4 (4C), 130.1 (4C), 143.0 (2C), 161.7 (2C), 172.4, 179.0 (2C). ESI-MS (m/z): 460 (M + Na).

(3Z,5E)-4-hydroxy-6-(4-methoxyphenyl)-3-((E)-3-(4-methoxyphenyl)acryloyl)hexa-3,5-dienoyl chloride (63).



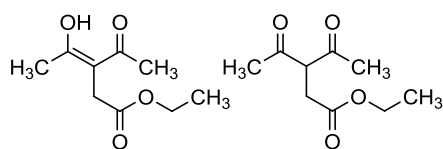
A mixture of acid derivatives **61a,b** (0.12 g, 0.3 mmol) and SOCl_2 (2.15 mL) was refluxed for 5 h. The solvent was removed under reduced pressure giving **63** as dark brown oil, which was used in the next reaction without any further purification; 96 % yield. $^1\text{H-NMR}$ (CDCl_3): δ 3.79 (s, 2H, CH_2), 3.86 (s, 6H, OCH_3), 6.33 (d, 2H, $J = 16.0$ Hz, $\text{CH}=\text{CH}$), 6.93 (d, 4H, $J = 8.0$ Hz, Ar), 7.52 (d, 4H, $J = 7.6$ Hz, Ar), 7.75 (d, 2H, $J = 15.6$ Hz, $\text{CH}=\text{CH}$).

Alkylation reaction of pentane-2,4-dione: general procedure A (synthesis of intermediates 64a,b and 65a,b).

A solution of pentane-2,4-dione (1.00 mmol) in THF (1.0 mL) was added to a stirred suspension of NaH (60 % dispersion in mineral oil, 1.2 molar equiv) in THF (5.0 mL) at 0 °C and under nitrogen atmosphere. The mixture was stirred at room temperature for 30 min before the addition dropwise of the appropriate alkyl bromide (1.2 molar equiv) solution in THF (5.0 mL) at 0 °C and was allowed to stand overnight at r.t. The solution was diluted with water, extracted with Et_2O (3 x 50.0 mL) and the combined organic layers were washed with brine, dried over Na_2SO_4 , filtered and concentrated under reduced pressure. The crude residue was purified by flash column chromatography on silica gel.

**ethyl (Z)-3-acetyl-4-hydroxypent-3-enoate (64a);
ethyl 3-acetyl-4-oxopentanoate (64b).**

Pentane-2,4-dione (2.57 mL, 25.00 mmol) and ethyl 2-bromoacetate (3.33 mL, 30.00 mmol) were allowed to react in agreement with the general procedure A of alkylation reaction to give the crude product that was purified by flash chromatography (PE/EtOAc, 9.5:0.5). Colourless oil, 90 % yield (isolated as 1:2 mixture of **64a:64b**).¹⁶⁶

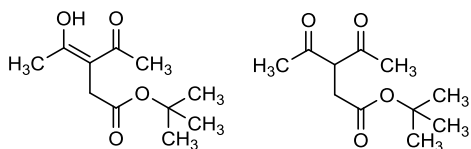


64a (33 % of the tautomeric mixture). $^1\text{H-NMR}$ (CDCl_3): δ 1.20-1.28 (m, 3H, OCH_2CH_3), 2.13 (s, 6H, CH_3), 3.22 (s, 2H, CH_2), 4.07-4.15 (m, 2H, OCH_2CH_3).

64b (67 % of the tautomeric mixture). $^1\text{H-NMR}$ (CDCl_3): δ 1.20-1.28 (m, 3H, OCH_2CH_3), 2.24 (s, 6H, CH_3), 2.85 (d, 2H, $J = 7.2$ Hz, CH_2), 4.07-4.15 (m, 3H, OCH_2CH_3 and diketo-CH).

***tert*-butyl (*Z*)-3-acetyl-4-hydroxypent-3-enoate (65a);
tert-butyl 3-acetyl-4-oxopentanoate (65b).**

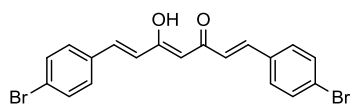
Pentane-2,4-dione (0.12 mL, 1.17 mmol) and **51** (0.40 g, 1.40 mmol) were allowed to react in agreement with the general procedure A of alkylation to give the crude product that was purified by flash chromatography (PE/EtOAc, 9.5:0.5). Pale yellow oil, 92 % yield (isolated as 1.1:1.0 mixture of **65a:65b**).



65a (52 % of the tautomeric mixture). $^1\text{H-NMR}$ (CDCl_3): δ 1.43 [s, 9H, $\text{C}(\text{CH}_3)_3$], 2.16 (s, 6H, CH_3), 3.14 (s, 2H, CH_2).

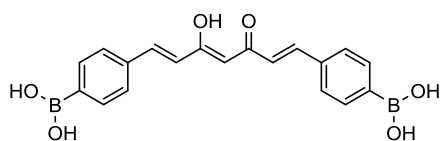
65b (48 % of the tautomeric mixture). $^1\text{H-NMR}$ (CDCl_3): δ 1.43 [s, 9H, $\text{C}(\text{CH}_3)_3$], 2.25 (s, 6H, CH_3), 2.81 (d, 2H, $J = 7.6$ Hz, CH_2), 4.07 (t, 1H, $J = 7.6$ Hz, diketo-CH).

(1*E*,4*Z*,6*E*)-1,7-bis(4-bromophenyl)-5-hydroxyhepta-1,4,6-trien-3-one (66).



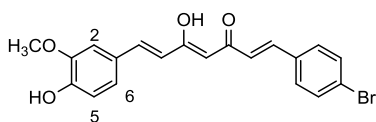
Reaction of pentane-2,4-dione (0.5 g, 4.95 mmol), and 4-bromobenzaldehyde (1.64 g, 8.91 mmol), according to the general procedure B of the Pabon reaction, gave the crude product purified by flash chromatography (PE/EtOAc, 9:1). Light brown powder, 62 % yield, mp 189-191 °C.¹⁴⁸ $^1\text{H-NMR}$ (CDCl_3): δ 5.84 (s, 1H, keto-enol-CH), 6.62 (d, 2H, $J = 15.6$ Hz, $\text{CH}=\text{CH}$), 7.43 (d, 4H, $J = 8.0$ Hz, Ar), 7.54 (d, 4H, $J = 8.0$ Hz, Ar), 7.61 (d, 2H, $J = 15.6$ Hz, $\text{CH}=\text{CH}$). $^{13}\text{C-NMR}$ (CDCl_3): δ 102.2, 124.5 (2C), 124.7 (2C), 129.6 (4C), 132.3 (4C), 134.0 (2C), 139.5 (2C), 183.2 (2C). ESI-MS (m/z): 455 (M + Na) and 459 (M + 4 + Na).

(4-((1E,3Z,6E)-7-(4-boronophenyl)-3-hydroxy-5-oxohepta-1,3,6-trien-1-yl)phenyl)boronic acid (67).



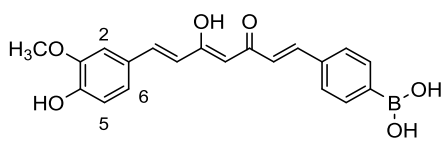
Reaction of pentane-2,4-dione (0.11 g, 1.10 mmol) and (4-formylphenyl)boronic acid (0.30 g, 2.00 mmol), according to the general procedure B of the Pabon reaction, gave the crude product as precipitate that was washed with water and filtered under *vacuum* to dryness. Sandy powder, 87 % yield, mp 290-292 °C (dec). ¹H-NMR (DMSO-*d*₆): δ 6.18 (s, 1H, keto-enol-CH), 6.97 (d, 2H, *J* = 16.0 Hz, CH=CH), 7.62 (d, 2H, *J* = 16.0 Hz, CH=CH), 7.66 (d, 4H, *J* = 8.0 Hz, Ar), 7.81 (d, 4H, *J* = 8.0 Hz, Ar), 8.16 (br s, 4H, OH). (See Appendix for the ¹H-NMR spectra, Fig. A2a). ¹³C-NMR (DMSO-*d*₆): δ 102.0, 124.0, 125.1, 127.8 (4C), 132.7 (2C), 135.2 (4C), 136.8 (2C), 140.1, 142.0, 181.9, 185.7. ESI-MS (*m/z*): 387 (M + Na).

(1E,4Z,6E)-1-(4-bromophenyl)-5-hydroxy-7-(4-hydroxy-3-methoxyphenyl)hepta-1,4,6-trien-3-one (68).



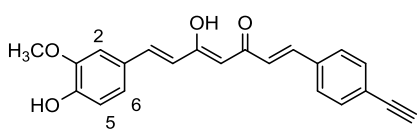
Reaction of intermediate **22** (0.43 g, 1.84 mmol) and 4-bromobenzaldehyde (0.30 g, 1.66 mmol), according to the general procedure B of the Pabon reaction, gave the crude product purified by flash chromatography (PE/EtOAc, 7:3) and further crystallization from EtOH. Orange powder, 73 % yield, mp 109-111 °C. ¹⁴⁹ ¹H-NMR (CDCl₃): δ 3.96 (s, 3H, OCH₃), 5.82 (s, 1H, keto-enol-CH), 5.85 (br s, 1H, OH), 6.50 (d, 1H, *J* = 16.0 Hz, CH=CH), 6.59 (d, 1H, *J* = 15.6 Hz, CH=CH), 6.94 (d, 1H, *J* = 8.0 Hz, H-5), 7.06 (d, 1H, *J* = 2.0 Hz, H-2), 7.13 (dd, 1H, *J* = 1.6 and 8.4 Hz, H-6), 7.41 (d, 2H, *J* = 8.0 Hz, Ar), 7.53 (d, 2H, *J* = 8.0 Hz, Ar), 7.54 (d, 1H, *J* = 16.0 Hz, CH=CH), 7.62 (d, 1H, *J* = 15.6 Hz, CH=CH). ¹³C-NMR (CDCl₃): δ 56.1, 102.5, 109.8, 115.0, 121.9, 124.3, 124.7, 127.8, 128.1, 129.8 (2C), 132.3 (2C), 134.0, 139.5, 140.0, 147.0, 148.0, 183.2 (2C). ESI-MS (*m/z*): 423 (M + Na) and 425 (M + 2 + Na).

4-((1E,4Z,6E)-5-hydroxy-7-(4-hydroxy-3-methoxyphenyl)-3-oxohepta-1,4,6-trien-1-yl)phenyl)boronic acid (69).



Reaction of intermediate **22** (0.43 g, 1.84 mmol) and (4-formylphenyl)boronic acid (0.30 g, 2.02 mmol), according with the general procedure B of the Pabon reaction, gave the crude product as precipitate that was washed with water and filtered under *vacuum* to dryness. Red brick powder, 91 % yield, mp 270-272 °C (dec). ¹H-NMR (DMSO-*d*₆): δ 3.84 (s, 3H, OCH₃), 6.14 (s, 1H, keto-enol-CH), 6.80 (d, 1H, *J* = 16.0 Hz, CH=CH), 6.83 (d, 1H, *J* = 8.0 Hz, H-5), 6.96 (d, 1H, *J* = 16.0 Hz, CH=CH), 7.16 (d, 1H, *J* = 7.4 Hz, H-6), 7.34 (s, 1H, H-2), 7.59 (d, 1H, *J* = 15.6 Hz, CH=CH), 7.60 (d, 1H, *J* = 15.6 Hz, CH=CH), 7.67 (d, 2H, *J* = 8.0 Hz, Ar), 7.84 (d, 2H, *J* = 8.0 Hz, Ar), 8.15 (br s, 2H, OH), 9.71 (br s, 1H, OH). (See Appendix for the ¹H-NMR spectra, Fig. A3a). ¹³C-NMR (DMSO-*d*₆): δ 56.1, 101.9, 111.6, 116.1, 121.5, 123.8, 125.0, 126.6, 127.6 (2C), 132.5, 135.0 (2C), 136.5, 140.0, 141.9, 148.4, 149.8, 181.7, 185.4. ESI-MS (*m/z*): 389 (M + Na).

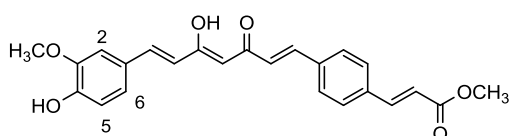
(1E,4Z,6E)-1-(4-ethynylphenyl)-5-hydroxy-7-(4-hydroxy-3-methoxyphenyl)hepta-1,4,6-trien-3-one (70).



To a mixture of **68** (0.13 g, 0.32 mmol), CuI (0.003 g, 0.016 mmol), PdCl₂(PPh₃)₂ (0.011 g, 0.016 mmol) and TEA (0.17 mL, 1.22 mmol) in THF (2.3 mL) under nitrogen atmosphere, trimethylsilylacetylene (TMSA) (0.09 mL, 0.64 mmol) in THF (1.0 mL) was added dropwise. The reaction mixture was stirred at room temperature for 24 h. The solvent was evaporated and the residue treatment with *n*-hexane allowed precipitating some impurities that were removed by filtration on celite. The filtrate was concentrated under reduced pressure and was purified by flash chromatography (PE/ EtOAc, 7:3) affording **70** as whitish oil, 52 % yield. ¹H-NMR (CDCl₃): δ 3.13 (s, 1H, ≡CH), 3.95 (s, 3H, OCH₃), 5.82 (s, 1H, keto-enol-CH), 5.85 (br s, 1H, OH), 6.49 (d, 1H, *J* = 16.0 Hz, CH=CH), 6.59 (d, 1H, *J* = 15.6 Hz, CH=CH), 6.94 (d, 1H, *J* = 7.6 Hz, H-5), 7.05 (s, 1H, H-2), 7.13

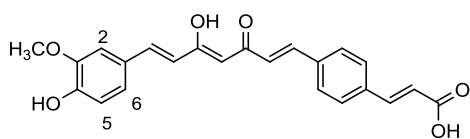
(d, 1H, $J = 8.0$ Hz, H-6), 7.41 (d, 2H, $J = 8.8$ Hz, Ar), 7.52 (d, 2H, $J = 8.0$ Hz, Ar), 7.53(d, 1H, $J = 15.6$ Hz, CH=CH), 7.61(d, 1H, $J = 16.4$ Hz, CH=CH). ^{13}C -NMR (CDCl_3): δ 56.1, 77.0, 83.6, 102.5, 109.8, 115.0, 119.0, 121.9, 124.7, 127.8, 128.1, 129.8 (2C), 132.3 (2C), 134.0, 139.5, 140.0, 147.0, 148.0, 183.2 (2C). ESI-MS (m/z): 369 (M + Na).

methyl (*E*)-3-(4-((1*E*,4*Z*,6*E*)-5-hydroxy-7-(4-hydroxy-3-methoxyphenyl)-3-oxohepta-1,4,6-trien-1-yl)phenyl)acrylate (71).



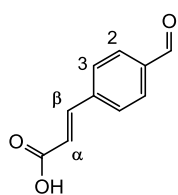
To a solution of compound **68** (0.09 g, 0.22 mmol) in DMF (2.0 mL), previously deoxygenated with a stream of N_2 for 10 min, methyl propiolate (0.02 mL, 0.26 mmol) was added dropwise, followed by addition of CuI (0.002 g, 0.01 mmol), $\text{Pd}(\text{PPh}_3)_4$ (0.013 g, 0.01 mmol) and TEA (0.09 mL, 0.65 mmol) under inert atmosphere (N_2 gas). The resulting mixture was heated to 70°C for 24 h and, after cooling to room temperature, was poured into water. The aqueous layer was then extracted with EtOAc (3 x 25.0 mL), the combined organic phases were dried over Na_2SO_4 and were concentrated under reduced pressure allowing to obtain the crude product that was purified by flash chromatography (PE/EtOAc, 8:2). Pale yellow solid, 50 % yield, mp $188\text{--}190^\circ\text{C}$. ^1H -NMR (CDCl_3): δ 3.74 (s, 3H COOCH_3), 3.93 (s, 3H, OCH_3), 5.53 (d, 1H, $J = 12.4$ Hz, CH=CH), 5.86 (s, 1H, keto-enol-CH), 6.58 (d, 1H, $J = 15.6$ Hz, CH=CH), 6.62 (d, 1H, $J = 16.0$, CH=CH), 7.08 (d, 1H, $J = 7.6$ Hz, H-5), 7.15 (s, 1H, H-2), 7.17 (d, 1H, $J = 8.0$ Hz, H-6), 7.43 (d, 2H, $J = 8.8$ Hz, Ar), 7.54 (d, 2H, $J = 8.0$ Hz, Ar), 7.61 (d, 1H, $J = 16.0$ Hz, CH=CH), 7.63 (d, 1H, $J = 16.0$ Hz, CH=CH), 7.74 (d, 1H, $J = 12.0$ Hz, CH=CH). ^{13}C -NMR (CDCl_3): δ 51.3, 56.1, 101.5, 102.0, 111.8, 120.2, 121.5, 124.2, 124.4, 124.5, 129.4 (2C), 132.2 (2C), 133.1, 133.9, 139.3, 139.7, 145.9, 150.6, 159.9, 167.5, 182.7, 183.3. ESI-MS (m/z): 429 (M + Na).

(E)-3-(4-((1E,4Z,6E)-5-hydroxy-7-(4-hydroxy-3-methoxyphenyl)-3-oxohepta-1,4,6-trien-1-yl)phenyl)acrylic acid (72).



Reaction of intermediate **22** (0.30 g, 1.28 mmol) and **73** (0.23 g, 1.28 mmol), according to the general procedure B of Pabon reaction, gave the crude product purified by flash chromatography (PE/acetone, 8:2) and further crystallization from acetone/PE. Orange powder, 51 % yield, mp 200-202 °C (dec). ¹H-NMR (acetone-*d*₆): δ 3.93 (s, 3H, OCH₃), 6.08 (s, 1H, keto-enol-CH), 6.60 (d, 2H, *J* = 16.0 Hz, CH=CH), 6.76 (d, 1H, *J* = 16.0 Hz, CH=CH), 6.90 (d, 1H, *J* = 8.0 Hz, H-5), 6.94 (d, 1H, *J* = 16.0 Hz, CH=CH), 7.21 (d, 1H, *J* = 8.4 Hz, H-6), 7.36 (s, 1H, H-2), 6.70 (d, 1H, *J* = 16.0 Hz, CH=CH), 7.64 (d, 2H, *J* = 8.0 Hz, Ar), 7.66 (d, 1H, *J* = 15.6 Hz, CH=CH), 7.75 (d, 2H, *J* = 8.0 Hz, Ar), 7.76 (br s, 1H, COOH). ¹³C-NMR (acetone-*d*₆): δ 56.5, 101.9, 102.4, 112.2, 120.6, 121.9, 124.6, 124.8, 124.9, 129.8 (2C), 132.6 (2C), 133.5, 134.3, 139.7, 140.1, 146.3, 150.9, 160.3, 167.9, 183.1, 183.7. ESI-MS (*m/z*): 415 (M + Na).

(E)-3-(4-formylphenyl)acrylic acid (73).

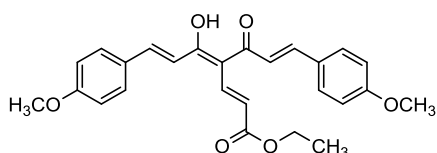


Terephthalaldehyde (0.50 g, 3.72 mmol), malonic acid (0.39 g, 3.72 mmol) and piperidine (0.05 mL, 0.44 mmol) were heated in pyridine (30.0 mL) to 80-90 °C for 18 h. Upon reaction completion, the mixture reaction acidification with HCl (12 N) afforded **67** as light yellow precipitate that was filtered to dryness; 62 % yield, mp 237-239 °C (dec). ¹H-NMR (acetone-*d*₆): δ 6.71 (d, 1H, *J* = 16.4 Hz, H-*α*), 7.75 (d, 1H, *J* = 16.0 Hz, H-*β*), 7.93 (d, 2H, *J* = 8.0 Hz, H-3), 7.99 (d, 2H, *J* = 8.4 Hz, H-2), 9.90 (s, 1H, CHO).

General procedure for the synthesis of curcumin-DF hybrids (74-76).

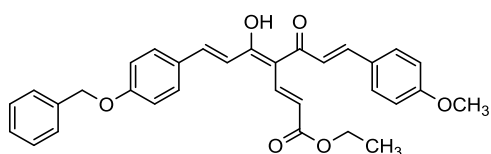
A solution of **5**, **6**, or **8** (1.00 mmol) in THF (25.0 mL) was slowly added to a suspension of NaH (60 % dispersion in mineral oil, 1.5 or 2.0 molar equiv) in THF (20.0 mL) at 0 °C and under nitrogen atmosphere. The reaction mixture was stirred at 0 °C for 30 min and at room temperature for 1-2 hours. Then, a solution of ethyl propiolate (2.0 or 3.0 molar equiv) in THF (1.0 mL) was added dropwise at 0 °C and the reaction mixture was stirred overnight at room temperature. Upon reaction completion, ice-cold water was added to the mixture and the aqueous layer was extracted with EtOAc (3 x 50.0 mL). The combined organic layers were washed with brine, dried over Na₂SO₄, filtered and concentrated under reduced pressure. The crude residue was purified by flash column chromatography and/or crystallization from the suitable solvent or mixture of solvents.

ethyl (2*E*,4*Z*,6*E*)-5-hydroxy-7-(4-methoxyphenyl)-4-((*E*)-3-(4-methoxyphenyl)acryloyl)hepta-2,4,6-trienoate (**74**).



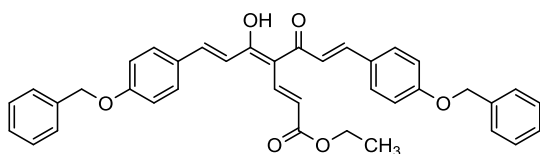
Reaction of **5** (0.50 g, 1.49 mmol) and ethyl propiolate (0.30 mL, 2.98 mmol), according to the general procedure for the synthesis of curcumin-DF hybrids, gave the crude product that was purified by flash chromatography (PE/EtOAc, 9.5:0.5) and further crystallization from EtOH. Red-orange powder, 71 % yield, mp 122-124 °C. ¹H-NMR (CDCl₃): δ 1.37 (t, 3H, *J* = 7.2 Hz, OCH₂CH₃), 3.87 (s, 6H, OCH₃), 4.31 (q, 2H, *J* = 6.8 Hz, OCH₂CH₃), 5.96 (d, 1H, *J* = 15.6 Hz, CH=CH), 6.94 (d, 4H, *J* = 8.4 Hz, Ar), 7.00 (d, 2H, *J* = 15.6 Hz, CH=CH), 7.55 (d, 4H, *J* = 8.4 Hz, Ar), 7.79 (d, 2H, *J* = 15.2 Hz, CH=CH), 7.89 (d, 1H, *J* = 15.6 Hz, CH=CH). ¹³C-NMR (CDCl₃): δ 14.5, 55.6 (2C), 60.7, 110.1, 114.6 (4C), 118.7 (2C), 122.7, 128.0 (2C), 130.4 (4C), 139.1, 142.7 (2C), 161.8 (2C), 167.0, 183.9 (2C). ESI-MS (*m/z*): 457 (M + Na).

ethyl (2E,4Z,6E)-7-(4-(benzyloxy)phenyl)-5-hydroxy-4-((E)-3-(4-methoxyphenyl)acryloyl)hepta-2,4,6-trienoate (75).



Reaction of **6** (0.20 g, 0.48 mmol) and ethyl propiolate (0.17 mL, 0.96 mmol), according to the general procedure for the synthesis of curcumin-DF hybrids, gave the crude product that was purified by two sequential crystallizations from EtOAc/PE and EtOH. Dark red powder, 41 % yield, mp 63-65 °C. ¹H-NMR (CDCl₃): δ 1.35 (t, 3H, *J* = 7.2 Hz, OCH₂CH₃), 3.87 (s, 3H, OCH₃), 4.31 (q, 2H, *J* = 6.8 Hz, OCH₂CH₃), 5.13 (s, 2H, OCH₂, Bn), 5.96 (d, 1H, *J* = 15.6 Hz, CH=CH), 6.94 (d, 2H, *J* = 8.7 Hz, Ar), 7.00 (d, 2H, *J* = 15.2 Hz, CH=CH), 7.01 (d, 2H, *J* = 8.0 Hz, Ar), 7.32-7.47 (m, 5H, Bn), 7.55 (d, 4H, *J* = 7.6 Hz, Ar), 7.78 (d, 2H, *J* = 15.6 Hz, CH=CH), 7.89 (d, 1H, *J* = 15.6 Hz, CH=CH). ¹³C-NMR (CDCl₃): δ 14.5, 55.6, 60.7, 70.3, 110.1, 114.6 (2C), 115.5 (2C), 118.8 (2C), 122.7, 127.6 (2C), 128.0, 128.2, 128.3, 128.8 (2C), 130.4 (4C), 136.5, 139.1, 142.6 (2C), 161.0, 161.8, 167.0, 183.7 (2C). ESI-MS (*m/z*): 533 (M + Na).

ethyl (2E,4Z,6E)-7-(4-(benzyloxy)phenyl)-4-((E)-3-(4-(benzyloxy)phenyl)acryloyl)-5-hydroxyhepta-2,4,6-trienoate (76).



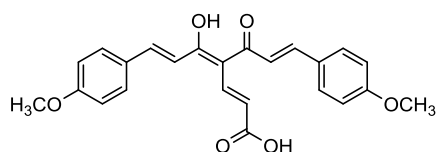
Reaction of **8** (0.25 g, 0.51 mmol) and ethyl propiolate (0.17 mL, 1.53 mmol), according to the general procedure for the synthesis of curcumin-DF hybrids, gave the crude product that was purified by flash chromatography (EP/acetone, 9.75:0.25) and two sequential crystallizations from EtOH and CH₂Cl₂/PE. Dark yellow-brown powder, 84 % yield, mp 153-155 °C. ¹H-NMR (CDCl₃): δ 1.38 (t, 3H, *J* = 7.2 Hz, OCH₂CH₃), 4.31 (q, 2H, *J* = 6.8 Hz, OCH₂CH₃), 5.13 (s, 4H, OCH₂, Bn), 5.95 (d, 1H, *J* = 15.6 Hz, CH=CH), 7.00 (d, 2H, *J* = 15.6 Hz, CH=CH), 7.01 (d, 4H, *J* = 8.8 Hz, Ar), 7.27-7.46 (m, 10H, Bn), 7.55 (d, 4H, *J* = 8.8 Hz, Ar), 7.78 (d, 2H, *J* = 15.2 Hz, CH=CH), 7.88 (d, 1H, *J* = 15.6 Hz, CH=CH). ¹³C-NMR (CDCl₃): δ 14.5, 60.7, 70.3 (2C), 110.1, 115.5 (4C), 118.9 (2C), 122.7, 127.6 (4C), 128.2 (2C), 128.3 (2C),

128.8 (4C), 130.4 (4C), 136.5 (2C), 139.1, 142.6 (2C), 161.0 (2C), 167.0, 183.8 (2C). ESI-MS (m/z): 609 (M + Na).

General procedure of saponification (synthesis of compounds **77** and **78**).

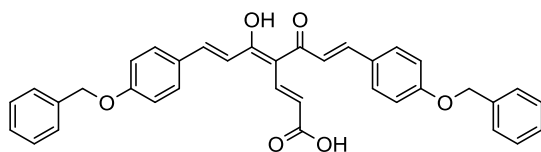
To a stirred solution of **74** or **76** (1.00 mmol) in CH₃OH (22.0 mL), a potassium hydroxide (KOH) solution in methanol (2.0 N, 1.82 mL) was added dropwise upon 30 min and the reaction mixture was stirred at 60 °C for 6-10 h. To complete the saponification, an additional amount of KOH solution in methanol (1.82 or 0.91 mL) was slowly added and the resulting mixture was stirred at 60 °C for additional 8 h. After cooling to room temperature, the solvent was evaporated giving a residue that was taken up in Et₂O and washed twice with a saturated aqueous NaHCO₃ solution (2 x 15.0 mL). The organic phase was separated and the aqueous layer was acidified with HCl (12.0 N) and extracted with CH₂Cl₂ (3 x 30.0 mL). The combined organic layers were washed with brine, dried over Na₂SO₄, filtered, and concentrated to dryness. A final crystallization from CH₂Cl₂/PE afforded the desired acid derivative.

(*2E,4Z,6E*)-5-hydroxy-7-(4-methoxyphenyl)-4-((*E*)-3-(4-methoxyphenyl)acryloyl)hepta-2,4,6-trienoic acid (**77**).



Acid derivative **77** was prepared following the general procedure of saponification starting for the corresponding ethyl ester **74** (0.10 g, 0.17 mmol) and a total amount of 0.50 mL of methanol KOH solution. Pale brown powder, 63 % yield, mp 188-190 °C. ¹H-NMR (CDCl₃): δ 3.86 (s, 6H, OCH₃), 6.31 (d, 2H, J = 16.0 Hz, CH=CH), 6.93 (d, 4H, J = 8.4 Hz, Ar), 6.96 (d, 2H, J = 16.4 Hz, CH=CH), 7.51 (d, 4H, J = 8.8 Hz, Ar), 7.73 (d, 2H, J = 16.0 Hz, CH=CH). ¹³C-NMR (CDCl₃): δ 56.0 (2C), 110.0, 115.0 (4C), 118.4 (2C), 123.0, 128.0 (2C), 130.0 (4C), 138.5, 142.7 (2C), 160.8 (2C), 168.7, 184.0 (2C). ESI-MS (m/z): 405 (M - H).

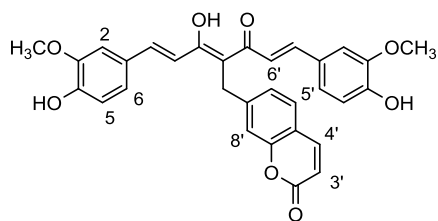
(2E,4Z,6E)-7-(4-(benzyloxy)phenyl)-4-((E)-3-(4-(benzyloxy)phenyl)acryloyl)-5-hydroxyhepta-2,4,6-trienoic acid (78).



The acid derivative **78** was prepared following the general procedure of saponification starting for the corresponding ethyl ester **76** (0.10 g,

0.17 mmol) and a total amount of 0.62 mL of methanol KOH solution. Pale brown powder, 75 % yield, mp 182-184 °C. ¹H-NMR (acetone-*d*₆): δ 5.19 (s, 4H, OCH₂, Bn), 6.39 (d, 2H, *J* = 15.6 Hz, CH=CH), 7.08 (d, 4H, *J* = 8.8 Hz, Ar), 7.34-7.42 (m, 10H, Bn), 7.49 (d, 4H, *J* = 7.6 Hz, Ar), 7.63 (d, 4H, *J* = 16.4 Hz, CH=CH). ¹³C-NMR (acetone-*d*₆): δ 70.0 (2C), 110.1, 116.0 (4C), 119.0 (2C), 122.7, 127.6 (4C), 128.1 (2C), 128.3 (2C), 128.8 (4C), 130.5 (4C), 136.5 (2C), 139.0, 142.6 (2C), 160.9 (2C), 168.0, 183.9 (2C). ESI-MS (*m/z*): 581 (M + Na).

7-((2Z,4E)-3-hydroxy-5-(4-hydroxy-3-methoxyphenyl)-2-((E)-3-(4-hydroxy-3-methoxyphenyl)acryloyl)penta-2,4-dien-1-yl)-2H-chromen-2-one (79).

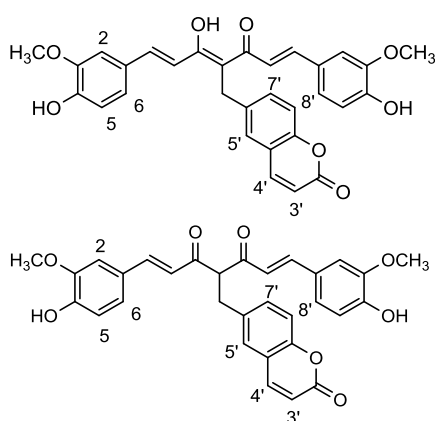


Intermediate **92** (0.10 g, 0.39 mmol) and vanillin (0.12 g, 0.77 mmol) were allowed to reach according to the general procedure C of the Pabon reaction giving the crude product that was purified by flash chromatography

(PE/EtOAc, 8:2) and further crystallization from *n*-hexane. Red powder, 57 % yield, mp 159-161 °C. ¹H-NMR (CDCl₃): δ 3.90 (s, 6H, OCH₃), 4.06 (s, 2H, CH₂), 5.87 (br s, 2H, OH), 6.38 (d, 1H, *J* = 9.6 Hz, H-3'), 6.78 (d, 2H, *J* = 15.2 Hz, CH=CH), 6.89 (dd, 2H, *J* = 1.2 and 8.4 Hz, H-6), 6.93 (s, 2H, H-2), 7.06 (d, 2H, *J* = 8.0 Hz, H-5), 7.13 (s, 1H, H-8'), 7.21 (d, 1H, *J* = 7.6 Hz, H-6'), 7.44 (d, 1H, *J* = 8.0 Hz, H-5'), 7.67 (d, 1H, *J* = 9.6 Hz, H-4'), 7.73 (d, 2H, *J* = 14.8 Hz, CH=CH). ¹³C-NMR (CDCl₃): δ 31.0, 56.2 (2C), 106.1, 110.0 (2C), 114.9 (2C), 116.5, 117.4 (2C), 119.6, 121.1, 123.6 (2C), 126.3, 126.9, 127.8 (2C), 138.7, 142.3 (2C), 143.1, 147.0 (2C), 148.4 (2C), 152.9, 160.9, 183.8 (2C). ESI-MS (*m/z*): 549 (M + Na).

6-((2*Z*,4*E*)-3-hydroxy-5-(4-hydroxy-3-methoxyphenyl)-2-((*E*)-3-(4-hydroxy-3-methoxyphenyl)acryloyl)penta-2,4-dien-1-yl)-2*H*-chromen-2-one (80a);
(1*E*,6*E*)-1,7-bis(4-hydroxy-3-methoxyphenyl)-4-((2-oxo-2*H*-chromen-6-yl)methyl)hepta-1,6-diene-3,5-dione (80b).

The mixture of intermediates **93a,b** (0.27 g, 1.04 mmol) and vanillin (0.32 g, 2.08 mmol) was allowed to react according to the general procedure C of the Pabon reaction giving the crude product that was purified by flash chromatography (PE/EtOAc, 7:3) and further crystallization from *n*-hexane. Red-orange powder, 47 % yield (isolated as 1:1 mixture of **80a:80b**), mp 183-185 °C.



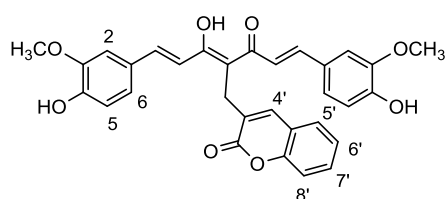
80a (50 % of the tautomeric mixture). ¹H-NMR (CDCl₃): 3.71 (s, 2H, CH₂), 3.97 (s, 6H, OCH₃), 6.42 (d, 1H, *J* = 9.6 Hz, H-3'), 6.69 (d, 2H, *J* = 15.6 Hz, CH=CH), 6.84 (dd, 2H, *J* = 1.6 and 8.0 Hz, H-6), 6.90 (s, 2H, H-2), 7.15 (d, 2H, *J* = 8.4 Hz, H-5), 7.32 (d, 1H, *J* = 2.0 Hz, H-5'), 7.35 (d, 1H, *J* = 7.2 Hz, H-8'), 7.41-7.43 (m, 1H, H-7'), 7.60 (d, 2H, *J* = 15.6 Hz,

CH=CH), 7.65 (d, 1H, *J* = 9.2 Hz, H-4').

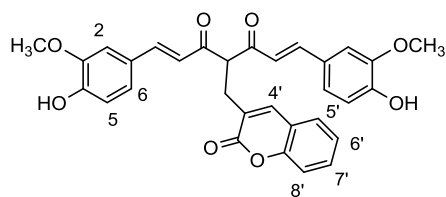
80b (50 % of the tautomeric mixture). ¹H-NMR (CDCl₃): δ 3.40 (d, 2H, *J* = 7.4 Hz, CH₂), 3.97 (s, 6H, OCH₃), 4.00 (t, 1H, *J* = 7.4 Hz, diketo-CH), 6.43 (d, 1H, *J* = 9.6 Hz, H-3'), 6.74 (d, 2H, *J* = 15.6 Hz, CH=CH), 6.84 (dd, 2H, *J* = 1.6 and 8.0 Hz, H-6), 6.90 (s, 2H, H-2), 7.15 (d, 2H, *J* = 8.4 Hz, H-5), 7.34 (d, 1H, *J* = 2.0 Hz, H-5'), 7.37 (d, 1H, *J* = 7.2 Hz, H-8'), 7.41-7.43 (m, 1H, H-7'), 7.66 (d, 1H, *J* = 9.2 Hz, H-4'), 7.73 (d, 2H, *J* = 15.6 Hz, CH=CH). **80a,b**. ¹³C-NMR (CDCl₃): δ 31.1, 42.0, 56.0 (4C), 67.2, 106.8, 109.9 (4C), 115.0 (4C), 117.1 (2), 117.6, 118.0 (2C), 118.1, 119.3, 121.1, 123.4 (4C), 124.0 (2C), 126.6, 126.7, 127.9 (4C), 131.3, 131.6, 137.3, 139.0, 142.0 (2C), 143.5 (2C), 146.8 (4C), 147.0 (2C), 148.3 (4C), 152.9, 153.3, 160.9 (2C), 183.9 (2C), 199.6 (2C). ESI-MS (*m/z*): 549 (M + Na).

3-((2*Z*,4*E*)-3-hydroxy-5-(4-hydroxy-3-methoxyphenyl)-2-((*E*)-3-(4-hydroxy-3-methoxyphenyl)acryloyl)penta-2,4-dien-1-yl)-2*H*-chromen-2-one (81a);
(1*E*,6*E*)-1,7-bis(4-hydroxy-3-methoxyphenyl)-4-((2-oxo-2*H*-chromen-3-yl)methyl)hepta-1,6-diene-3,5-dione (81b).

The mixture of intermediates **94a,b** (0.15 g, 0.58 mmol) and vanillin (0.16 g, 1.04 mmol) was allowed to react according to the general procedure C of the Pabon reaction giving the crude product that was purified by crystallization from CH₂Cl₂/PE. A 3:1 mixture of **81a:81b** was obtained and a further crystallization with the same solvents system allowed isolating pure **81a** as red-brown powder.



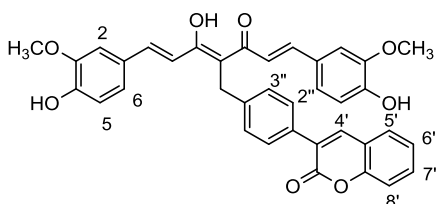
81a (pure), 35 % yield, mp 160-162 °C. ¹H-NMR (CDCl₃): δ 3.90 (s, 2H, CH₂), 3.93 (s, 6H, OCH₃), 5.88 (br s, 2H, OH), 6.76 (d, 2H, *J* = 15.6 Hz, CH=CH), 6.90 (d, 2H, *J* = 8.0 Hz, H-5), 7.01 (s, 2H, H-2), 7.10 (d, 2H, *J* = 8.4 Hz, H-6), 7.22-7.27 (m, 1H, H-6'), 7.35 (d, 1H, *J* = 8.4 Hz, H-8'), 7.41 (d, 1H, *J* = 7.2 Hz, H-5'), 7.46 (s, 1H, H-4'), 7.46-7.51 (m, 1H, H-7'), 7.77 (d, 2H, *J* = 15.6 Hz, CH=CH). ¹³C-NMR (CDCl₃): δ 26.2, 56.2 (2C), 106.1, 109.9 (2C), 115.0 (2C), 116.5, 117.4 (2C), 119.6, 123.6 (2C), 124.7, 127.8, 127.9, 128.8, 131.3, 139.9, 143.2 (2C), 146.9 (2C), 148.4 (2C), 153.0, 162.3, 152.9, 183.9 (2C).



81b (25 % of the tautomeric mixture). ¹H-NMR (CDCl₃): δ 3.26 (d, 2H, *J* = 6.7 Hz, CH₂), 3.93 (s, 6H, OCH₃), 4.92 (t, 1H, *J* = 8.0 Hz, diketo-CH), 5.88 (br s, 2H, OH), 6.71 (d, 2H, *J* = 16.0 Hz, CH=CH), 6.92 (d, 2H, *J* = 8.1 Hz, H-5), 7.06 (s, 2H, H-2), 7.14 (d, 2H, *J* = 8.1 Hz, H-6), 7.22-7.27 (m, 1H, H-6'), 7.31 (d, 1H, *J* = 8.0 Hz, H-8'), 7.41 (d, 1H, *J* = 7.6 Hz, H-5'), 7.46 (s, 1H, H-4'), 7.46-7.51 (m, 1H, H-7'), 7.73 (d, 2H, *J* = 16.0 Hz, CH=CH). **81a,b.** ¹³C-NMR (CDCl₃): δ 26.2, 30.8, 56.2 (4C), 60.0, 106.1, 109.8 (2C), 109.9 (2C), 114.9 (2C), 116.5 (2C), 117.3 (2C), 119.5, 122.5 (2C), 123.6 (2C), 124.4, 124.6, 124.7 (2C), 126.8 (2C), 127.7 (2C), 127.8 (2C), 127.9 (2C), 128.7 (2C), 131.3 (2C), 139.9 (2C), 142.4, 143.3 (2C), 145.5 (2C),

146.9 (2C), 147.0 (2C), 148.3 (2C), 148.8 (2C), 153.0 (2C), 162.3 (2C), 183.9 (2C), 194.8 (2). ESI-MS (m/z): 549 (M + Na).

3-(4-((2Z,4E)-3-hydroxy-5-(4-hydroxy-3-methoxyphenyl)-2-((E)-3-(4-hydroxy-3-methoxyphenyl)acryloyl)penta-2,4-dien-1-yl)phenyl)-2H-chromen-2-one (82).

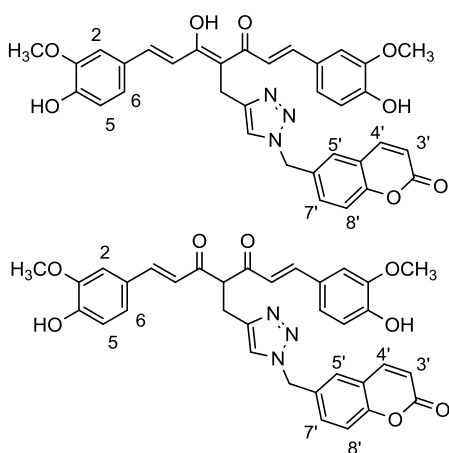


The mixture of intermediate **96a,b** (0.14 g, 0.42 mmol) and vanillin (0.12 g, 0.76 mmol) was allowed to react according to the general procedure C of the Pabon reaction giving the crude product, which was purified by crystallization from EtOH. Red powder, 40 % yield, mp 102-104 °C. ¹H-NMR (CDCl₃): δ 3.92 (s, 6H, OCH₃), 4.03 (s, 2H, CH₂), 5.83 (br s, 2H, OH), 6.84 (d, 2H, $J = 15.3$ Hz, CH=CH), 6.91 (d, 2H, $J = 8.2$ Hz, H-5), 6.95 (s, 2H, H-2), 7.08 (d, 2H, $J = 8.2$ Hz, H-6), 7.31 (d, 1H, $J = 7.5$ Hz, H-8'), 7.34-7.40 (m, 1H, H-6'), 7.40 (d, 2H, $J = 8.4$ Hz, H-3''), 7.51-7.56 (m, 2H, H-5' and H-7'), 7.70 (d, 2H, $J = 8.8$ Hz, H-2''), 7.73 (d, 2H, $J = 16.0$ Hz, CH=CH), 7.80 (s, 1H, H-4'). ¹³C-NMR (CDCl₃): δ 29.8, 56.1 (2C), 108.5, 110.0 (2C), 114.9 (2C), 116.6, 118.4, 119.8, 123.1 (2C), 124.7, 127.1, 128.0 (2C), 128.1 (2C), 128.2 (2C), 129.1, 131.6, 133.1, 133.2, 139.8, 142.1, 142.3 (2C), 146.9 (2C), 148.1 (2C), 153.6, 162.8, 183.8 (2C). ESI-MS (m/z): 625 (M + Na).

6-((4-((2Z,4E)-3-hydroxy-5-(4-hydroxy-3-methoxyphenyl)-2-((E)-3-(4-hydroxy-3-methoxyphenyl)acryloyl)penta-2,4-dien-1-yl)-1H-1,2,3-triazol-1-yl)methyl)-2H-chromen-2-one (83a);

(1E,6E)-1,7-bis(4-hydroxy-3-methoxyphenyl)-4-((1-((2-oxo-2H-chromen-6-yl)methyl)-1H-1,2,3-triazol-4-yl)methyl)hepta-1,6-diene-3,5-dione (83b).

Reaction of **55a,b** (0.08 g, 0.20 mmol) and **104** (0.05 g, 0.25 mmol), according to the general procedure of the CCR in 4-position of the curcumin scaffold in DMF (method **a**), afforded the crude product, which was purified by flash chromatography (PE/EtOAc, 1:1). Red brick powder, 33 % yield (isolated as 1.6:1.0 mixture of **83a:84b**), mp 188-190 °C.



83a (62 % of the tautomeric mixture). $^1\text{H-NMR}$ (acetone- d_6): δ 3.75 (s, 6H, OCH₃), 4.07 (s, 2H, CH₂), 5.39 (br s, 2H, OH), 5.64 (s, 2H, NCH₂), 6.31 (d, 1H, $J = 10.0$ Hz, H-3'), 6.86 (d, 2H, $J = 8.0$ Hz, H-5), 7.17 (d, 2H, $J = 8.4$ Hz, H-6), 7.25 (d, 2H, $J = 15.6$ Hz, CH=CH), 7.29 (s, 2H, H-2), 7.32 (d, 1H, $J = 1.6$ Hz, H-5'), 7.51 (d, 1H, $J = 8.4$ Hz, H-8'), 7.62 (d, 2H, $J = 15.2$ Hz, CH=CH), 7.63 (d, 1H, $J = 10.0$ Hz, H-4'), 7.64 (d, 1H, $J = 8.8$ Hz, H-7'), 7.80 (s, 1H).

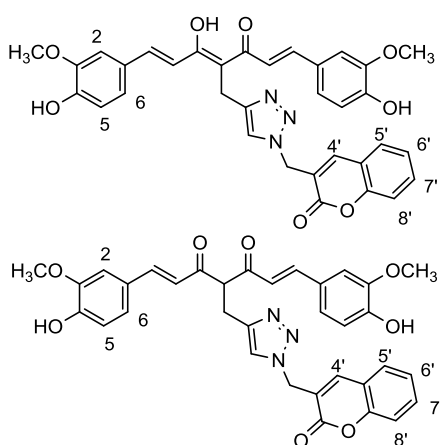
83b (38 % of the tautomeric mixture). $^1\text{H-NMR}$ (acetone- d_6): δ 3.28 (d, 2H, $J = 7.2$ Hz, CH₂), 3.87 (s, 6H, OCH₃), 4.92 (t, 1H, $J = 7.6$ Hz, diketo-CH), 5.39 (br s, 2H, OH), 5.64 (s, 2H, NCH₂), 6.37 (d, 1H, $J = 9.6$ Hz, H-3'), 6.86 (d, 2H, $J = 8.0$ Hz, H-5), 6.90 (d, 2H, $J = 16.0$ Hz, CH=CH), 7.15 (d, 2H, $J = 8.0$ Hz, H-6), 7.29 (s, 2H, H-2), 7.32 (d, 1H, $J = 1.6$ Hz, H-5'), 7.47 (d, 1H, $J = 8.4$ Hz, H-8'), 7.61 (d, 2H, $J = 15.2$ Hz, CH=CH), 7.64 (d, 1H, $J = 8.8$ Hz, H-7'), 7.72 (s, 1H), 7.84 (d, 1H, $J = 10.0$ Hz, H-4'). **83a,b**. $^{13}\text{C-NMR}$ (acetone- d_6): δ 23.5, 27.2, 56.0 (4C), 50.5 (2C), 58.3, 108.0, 109.8 (4C), 115.0 (4C), 117.1 (2C), 117.4 (2C), 117.9 (2C), 119.3 (2C), 123.6 (4C), 124.8 (2C), 126.0 (2C), 126.7 (2C), 127.9 (4C), 131.6 (2C), 133.3 (2C), 142.8 (2C), 143.3 (2C), 143.5, 146.8 (2C), 147.0 (4C), 148.6, 148.4 (4C), 152.9 (2C), 161.8 (2C), 183.9 (2C), 195.4 (2C). ESI-MS (m/z): 630 (M + Na).

3-((4-((2Z,4E)-3-hydroxy-5-(4-hydroxy-3-methoxyphenyl)-2-((E)-3-(4-hydroxy-3-methoxyphenyl)acryloyl)penta-2,4-dien-1-yl)-1H-1,2,3-triazol-1-yl)methyl)-2H-chromen-2-one (84a);

(1E,6E)-1,7-bis(4-hydroxy-3-methoxyphenyl)-4-((1-((2-oxo-2H-chromen-3-yl)methyl)-1H-1,2,3-triazol-4-yl)methyl)hepta-1,6-diene-3,5-dione (84b).

Reaction of **55a,b** (0.08 g, 0.20 mmol) and **105** (0.05 g, 0.25 mmol), according to the general procedure of the CCR in 4-position of the curcumin scaffold in DMF (method **a**), afforded the crude product, which was purified by flash chromatography (PE/EtOAc, 1:1) and further crystallization from CH₂Cl₂/PE.

Light brown-yellow powder, 35 % yield (isolated as 1.0:1.3 mixture of **84a**:**84b**), mp 148-150 °C.

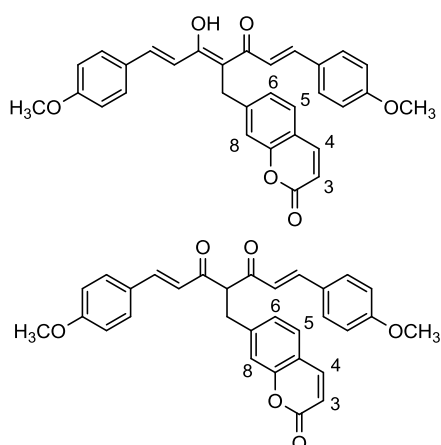


84a (43 % of the tautomeric mixture). $^1\text{H-NMR}$ (CDCl_3): δ 3.90 (s, 6H, OCH_3), 4.08 (s, 2H, CH_2), 5.39 (s, 2H, NCH_2), 6.60 (d, 2H, $J = 16.4$ Hz, $\text{CH}=\text{CH}$), 6.89 (d, 2H, $J = 7.6$ Hz, H-5), 6.95 (s, 2H, H-2), 7.01-7.04 (m, 2H, H-6), 7.07 (s, 1H), 7.27-7.33 (m, 1H, H-6'), 7.36 (d, 1H, $J = 8.8$ Hz, H-8'), 7.50-7.54 (m, 2H, H-5' and H-7'), 7.60 (s, 1H, H-4'), 7.60 (d, 2H, $J = 16.0$ Hz, $\text{CH}=\text{CH}$).

84b (57 % of the tautomeric mixture). $^1\text{H-NMR}$ (CDCl_3): δ 3.43 (d, 2H, $J = 7.1$ Hz, CH_2), 3.92 (s, 6H, OCH_3), 4.75 (t, 1H, $J = 6.8$ Hz, diketo-CH), 5.42 (s, 2H, NCH_2), 6.71 (d, 2H, $J = 15.6$ Hz, $\text{CH}=\text{CH}$), 6.89 (d, 2H, $J = 7.6$ Hz, H-5), 6.95 (s, 2H, H-2), 7.01-7.04 (m, 2H, H-6), 7.07 (s, 1H), 7.27-7.33 (m, 1H, H-6'), 7.36 (d, 1H, $J = 8.8$ Hz, H-8'), 7.50-7.54 (m, 2H, H-5' and H-7'), 7.60 (s, 1H, H-4'), 7.70 (d, 2H, $J = 16.0$ Hz, $\text{CH}=\text{CH}$). **84a,b**. $^{13}\text{C-NMR}$ (CDCl_3): δ 23.4, 27.0, 56.2 (4C), 50.9 (2C), 58.1, 107.7, 109.8 (2C), 109.9 (2C), 116.5 (4C), 117.3 (2C), 119.5 (2C), 122.5 (2C), 123.6 (4C), 124.3, 124.7, 124.8 (2C), 126.1 (2C), 127.9 (4C), 128.7 (2C), 131.3 (2C), 139.9 (2C), 142.4 (2C), 143.2 (2C), 145.5 (2C), 146.9 (4C), 148.3 (2C), 148.8 (4C), 153.0 (2C), 162.3 (2C), 183.9 (2C), 194.8 (2C). ESI-MS (m/z): 630 ($\text{M} + \text{Na}$).

7-((2Z,4E)-3-hydroxy-5-(4-methoxyphenyl)-2-((E)-3-(4-methoxyphenyl)acryloyl)penta-2,4-dien-1-yl)-2H-chromen-2-one (85a);
(1E,6E)-1,7-bis(4-methoxyphenyl)-4-((2-oxo-2H-chromen-7-yl)methyl)hepta-1,6-diene-3,5-dione (85b).

Intermediate **92** (0.18 g, 0.70 mmol) and 4-methoxybenzaldehyde (0.15 mL, 1.26 mmol) were allowed to reach according to the general procedure C of the Pabon reaction to give the crude product that was purified by flash chromatography (PE/EtOAc, 9:1) and two sequential crystallizations from: EtOH and $\text{CH}_2\text{Cl}_2/\text{PE}$. Yellow powder, 48 % yield (isolated as 4:1 mixture of **85a**:**85b**), mp 177-179 °C.

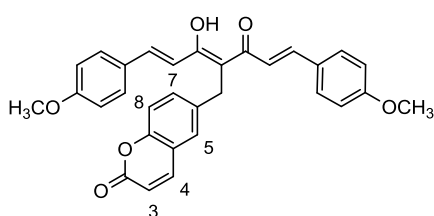


85a (80 % of the tautomeric mixture). $^1\text{H-NMR}$ (CDCl_3): δ 3.83 (s, 6H, OCH_3), 4.06 (s, 2H, CH_2), 6.38 (d, 1H, $J = 10.0$ Hz, H-3), 6.79 (d, 2H, $J = 15.2$ Hz, $\text{CH}=\text{CH}$), 6.88 (d, 4H, $J = 8.8$ Hz, Ar), 7.21 (d, 1H, $J = 7.6$ Hz, H-6), 7.31 (s, 1H, H-8), 7.43 (d, 4H, $J = 8.0$ Hz, Ar), 7.44 (d, 1H, $J = 8.0$ Hz, H-5), 7.68 (d, 1H, $J = 9.2$ Hz, H-4), 7.77 (d, 2H, $J = 15.2$ Hz, $\text{CH}=\text{CH}$).

85b (20 % of the tautomeric mixture). $^1\text{H-NMR}$ (CDCl_3): δ 3.43 (d, 2H, $J = 7.4$ Hz, CH_2), 3.85 (s, 6H, OCH_3), 4.42 (t, 1H, $J = 8.0$ Hz, diketo-CH), 6.36 (d, 1H, $J = 9.2$ Hz, H-3), 6.73 (d, 2H, $J = 15.6$ Hz, $\text{CH}=\text{CH}$), 6.88 (d, 4H, $J = 8.8$ Hz, Ar), 7.21 (d, 1H, $J = 7.6$ Hz, H-6), 7.31 (s, 1H, H-8), 7.44 (d, 1H, $J = 8.0$ Hz, H-5), 7.50 (d, 4H, $J = 8.0$ Hz, Ar), 7.64 (d, 2H, $J = 16.4$ Hz, $\text{CH}=\text{CH}$), 7.68 (d, 1H, $J = 9.2$ Hz, H-4).

85a,b. $^{13}\text{C-NMR}$ (CDCl_3): δ 42.0, 50.5, 55.3 (2C), 55.6 (2C), 67.2, 107.6, 113.8 (2C), 114.4 (4C), 114.5 (4C), 116.0, 116.1, 116.7, 124.1 (2C), 127.1, 128.1 (4C), 128.4, 128.8 (4C), 129.9 (4C), 130.1 (4C), 130.8, 131.3, 141.4, 143.2 (2C), 145.5 (2C), 146.7 (2C), 154.5 (2C), 158.6 (2C), 161.4 (2C), 161.6 (2C), 182.6 (2C), 199.6 (2). ESI-MS (m/z): 517 (M + Na).

6-((2Z,4E)-3-hydroxy-5-(4-methoxyphenyl)-2-((E)-3-(4-methoxyphenyl)acryloyl)penta-2,4-dien-1-yl)-2H-chromen-2-one (86).

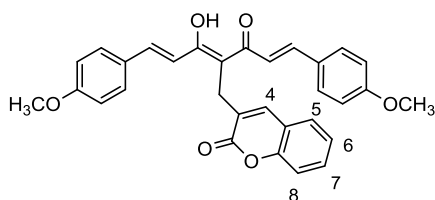


The mixture of intermediates **93a,b** (0.16 g, 0.62 mmol) and 4-methoxybenzaldehyde (0.14 mL, 1.12 mmol) was allowed to react according to the general procedure C of the Pabon reaction to give the crude product that

was purified by flash chromatography (PE/EtOAc, 9:1) and further crystallization from $\text{CH}_2\text{Cl}_2/\text{PE}$. Red powder, 60 % yield, mp 201-203 °C. $^1\text{H-NMR}$ (CDCl_3): δ 3.83 (s, 6H, OCH_3), 4.03 (s, 2H, CH_2), 6.41 (d, 1H, $J = 9.2$ Hz, H-3), 6.77 (d, 2H, $J = 15.2$ Hz, $\text{CH}=\text{CH}$), 6.88 (d, 4H, $J = 8.8$ Hz, Ar), 7.32 (d, 1H, $J = 1.6$ Hz, H-5),

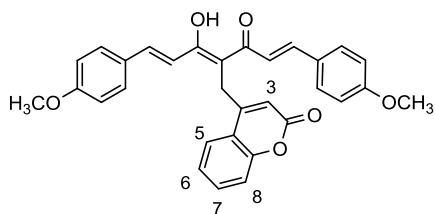
7.35 (d, 1H, $J = 8.8$ Hz, H-8), 7.42 (d, 4H, $J = 8.8$ Hz, Ar), 7.52 (dd, 1H, $J = 2.0$ and 7.2 Hz, H-7), 7.66 (d, 1H, $J = 9.6$ Hz, H-4), 7.77 (d, 2H, $J = 15.2$ Hz, CH=CH). ^{13}C -NMR (CDCl_3): δ 31.1, 55.5 (2C), 107.8, 114.6 (4C), 117.1, 117.4, 118.0 (2C), 119.3, 126.7, 128.0 (2C), 130.1 (4C), 131.6, 137.3, 142.3 (2C), 143.5, 153.0, 160.9, 161.6 (2C), 183.9 (2C). ESI-MS (m/z): 517 (M + Na).

3-((2Z,4E)-3-hydroxy-5-(4-methoxyphenyl)-2-((E)-3-(4-methoxyphenyl)acryloyl)penta-2,4-dien-1-yl)-2H-chromen-2-one (87).



The mixture of intermediates **94a,b** (0.21 g, 0.81 mmol) and 4-methoxybenzaldehyde (0.18 mL, 1.46 mmol) was allowed to react according to the general procedure C of the Pabon reaction to give the crude product that was purified by crystallization from $\text{CH}_2\text{Cl}_2/\text{PE}$. Orange-brown powder, 65 % yield, mp 160-162 °C. ^1H -NMR (CDCl_3): δ 3.83 (s, 6H, OCH_3), 3.88 (s, 2H, CH_2), 6.76 (d, 2H, $J = 15.2$ Hz, CH=CH), 6.88 (d, 4H, $J = 8.4$ Hz, Ar), 7.21-7.25 (m, 1H, H-6), 7.36 (d, 1H, $J = 8.0$ Hz, H-8), 7.40 (dd, 1H, $J = 1.2$ and 7.8 Hz, H-5), 7.45 (s, 1H, H-4), 7.48 (d, 4H, $J = 8.8$ Hz, Ar), 7.49-7.53 (m, 1H, H-7), 7.81 (d, 2H, $J = 15.6$ Hz, CH=CH). ^{13}C -NMR (CDCl_3): δ 26.5, 55.5 (2C), 105.6, 114.6 (4C), 116.5, 117.5 (2C), 119.6, 124.6, 127.9 (2C), 128.0, 128.6, 130.2 (4C), 131.2, 139.5, 142.7 (2C), 153.0, 161.7 (2C), 162.1, 184.0 (2C). ESI-MS (m/z): 517 (M + Na).

4-((2Z,4E)-3-hydroxy-5-(4-methoxyphenyl)-2-((E)-3-(4-methoxyphenyl)acryloyl)penta-2,4-dien-1-yl)-2H-chromen-2-one (88).

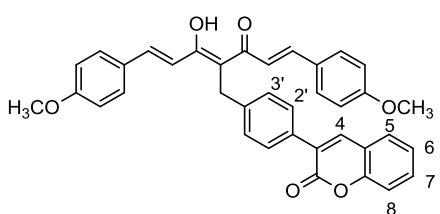


The mixture of intermediates **95a,b** (0.18 g, 0.70 mmol) and 4-methoxybenzaldehyde (0.15 mL, 1.26 mmol) was allowed to react according to the general procedure C of the Pabon reaction to give the crude product that was purified by flash chromatography (PE/EtOAc , 9:1) and two sequential crystallizations from EtOH and $\text{CH}_2\text{Cl}_2/\text{PE}$. Red-orange powder, 68 % yield, mp 204-206 °C. ^1H -NMR (CDCl_3): δ 3.82 (s, 6H, OCH_3), 4.06 (s, 2H, CH_2), 6.33 (s,

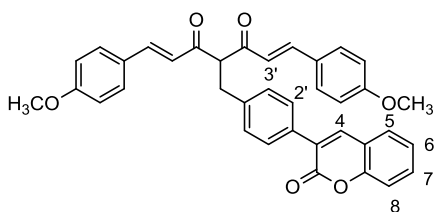
1H, H-3), 6.58 (d, 2H, $J = 15.2$ Hz, CH=CH), 6.85 (d, 4H, $J = 7.2$ Hz, Ar), 7.40 (d, 4H, $J = 7.2$ Hz, Ar), 7.43-7.47 (m, 2H, H-6 and H-8), 7.66 (t, 1H, $J = 7.2$ Hz, H-7), 7.80 (d, 2H, $J = 15.2$ Hz, CH=CH), 7.89 (d, 1H, $J = 8.0$ Hz, H-5). ^{13}C -NMR (CDCl_3): δ 28.2, 55.5 (2C), 103.7, 114.5 (4C), 115.3, 117.0 (2C), 117.7, 119.3, 123.7, 124.7, 127.8 (2C), 130.2 (4C), 133.3, 143.1 (2C), 153.8, 154.1, 160.8, 161.7 (2C), 183.9 (2C). ESI-MS (m/z): 517 (M + Na).

3-(4-((2Z,4E)-3-hydroxy-5-(4-methoxyphenyl)-2-((E)-3-(4-methoxyphenyl)acryloyl)penta-2,4-dien-1-yl)phenyl)-2H-chromen-2-one (89a);
(1E,6E)-1,7-bis(4-methoxyphenyl)-4-(4-(2-oxo-2H-chromen-3-yl)benzyl)hepta-1,6-diene-3,5-dione (89b).

The mixture of intermediates **96a,b** (0.20 g, 0.60 mmol) and 4-methoxybenzaldehyde (0.13 mL, 1.08 mmol), was allowed to reach according to the general procedure C of the Pabon reaction to give the crude product that was purified by crystallization from $\text{CH}_2\text{Cl}_2/\text{PE}$. Orange powder, 55 % yield (isolated as 1.7:1.0 mixture of **89a:89b**), mp 173-175 °C.



89a (63 % of the tautomeric mixture). ^1H -NMR (CDCl_3): δ 3.83 (s, 6H, OCH_3), 4.03 (s, 2H, CH_2), 6.74 (d, 2H, $J = 15.6$ Hz, CH=CH), 6.88 (d, 4H, $J = 8.4$ Hz, Ar), 7.34-7.41 (m, 4H, H-6, H-8 and H-3'), 7.45 (d, 4H, $J = 8.8$ Hz, Ar), 7.49-7.55 (m, 3H, H-7 and H-2'), 7.60 (dd, 1H, $J = 4.4$ and 8.0 Hz, H-5), 7.76 (d, 2H, $J = 15.2$ Hz, CH=CH), 7.81 (s, 1H, H-4).



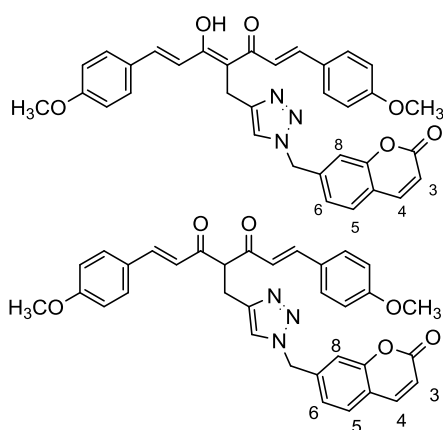
89b (37 % of the tautomeric mixture). ^1H -NMR (CDCl_3): δ 3.40 (d, 2H, $J = 6.2$ Hz, CH_2), 3.83 (s, 6H, OCH_3), 4.46 (t, 1H, $J = 8.0$ Hz, diketo-CH), 6.84 (d, 2H, $J = 15.6$ Hz, CH=CH), 6.87 (d, 4H, $J = 8.0$ Hz, Ar), 7.30 (d, 2H, $J = 8.0$ Hz, Ar), 7.34-7.41 (m, 4H, H-6, H-8 and H-3'), 7.49-7.55 (m, 3H, H-7 and H-2'), 7.60 (dd, 1H, $J = 4.4$ and 8.0 Hz, H-5), 7.62 (d, 2H, $J = 16.4$ Hz, CH=CH), 7.70 (d, 2H, $J = 8.4$ Hz, Ar), 7.83 (s, 1H, H-4). **89a,b.** ^{13}C -NMR (CDCl_3): δ 31.6, 34.4, 55.5 (4C), 66.7, 108.4, 114.5 (4C), 114.6 (4C), 116.6 (2C), 118.4,

119.8 (2C), 121.9, 124.6, 124.7, 127.0 (2C), 127.9 (2C), 128.0 (4C), 128.1 (2C), 128.2 (2C), 128.9, 129.1, 129.3 (2C), 130.1 (8C), 130.7, 130.9, 131.3, 131.5, 133.0 (2C), 139.7 (2C), 141.8 (2C), 141.9 (2C), 144.8, 146.0, 153.6 (2C), 160.8, 161.4 (4C), 162.2, 183.9 (2C), 194.5 (2C). ESI-MS (m/z): 569 (M - H).

7-((4-((2Z,4E)-3-hydroxy-5-(4-methoxyphenyl)-2-((E)-3-(4-methoxyphenyl)acryloyl)penta-2,4-dien-1-yl)-1H-1,2,3-triazol-1-yl)methyl)-2H-chromen-2-one (90a);

(1E,6E)-1,7-bis(4-methoxyphenyl)-4-((1-((2-oxo-2H-chromen-7-yl)methyl)-1H-1,2,3-triazol-4-yl)methyl)hepta-1,6-diene-3,5-dione (90b).

Reaction of **56** (0.14 g, 0.37 mmol) and **103** (0.48 g, 1.04 mmol), according to the general procedure of the CCR in 4-position of the curcumin scaffold in DMSO (method **b**), afforded the crude product, which was purified by flash chromatography (PE/EtOAc, 7:3) and further crystallization from CH₂Cl₂/PE. Orange powder, 49 % yield (isolated as 1.8:1.0 mixture of **90a**:**90b**), 163-165 °C.



90a (65 % of the tautomeric mixture). ¹H-NMR (CDCl₃): δ 3.85 (s, 6H, OCH₃), 4.08 (s, 2H, CH₂), 5.53 (s, 2H, NCH₂), 6.43 (d, 1H, $J = 10.0$ Hz, H-3), 6.90 (d, 4H, $J = 8.8$ Hz, Ar), 6.98 (d, 1H, $J = 8.0$ Hz, H-6), 7.15 (s, 1H), 7.30 (d, 2H, $J = 15.2$ Hz, CH=CH), 7.48 (d, 1H, $J = 7.6$ Hz, H-5), 7.46 (d, 4H, $J = 8.8$ Hz, Ar), 7.57 (d, 1H, $J = 9.2$ Hz, H-4), 7.70 (d, 2H, $J = 15.2$ Hz, CH=CH), 7.77 (s, 1H, H-8).

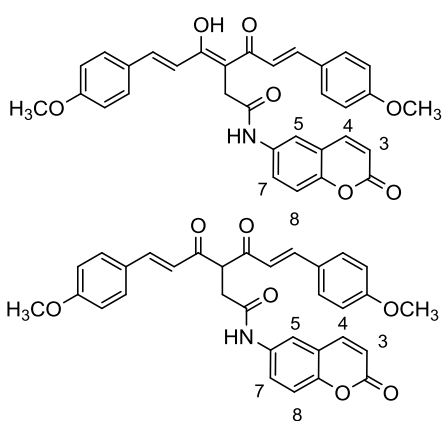
90b (35 % of the tautomeric mixture). ¹H-NMR (CDCl₃): δ 3.41 (d, 2H, $J = 7.2$ Hz, CH₂), 3.85 (s, 6H, OCH₃), 4.78 (t, 1H, $J = 7.2$ Hz, diketo-CH), 5.53 (s, 2H, NCH₂), 6.40 (d, 1H, $J = 9.6$ Hz, H-3), 6.71 (d, 2H, $J = 15.6$ Hz, CH=CH), 6.90 (d, 4H, $J = 8.8$ Hz, Ar), 7.02 (d, 1H, $J = 7.2$ Hz, H-6), 7.15 (s, 1H), 7.49 (d, 4H, $J = 8.4$ Hz, Ar), 7.54 (d, 1H, $J = 8.0$ Hz, H-5), 7.58 (d, 1H, $J = 9.2$ Hz, H-4), 7.66 (d, 2H, $J = 16.4$ Hz, CH=CH), 7.68 (d, 1H, $J = 1.6$ Hz, H-8). **90a,b.** ¹³C-NMR (CDCl₃): δ 23.3, 24.9, 53.6 (2C), 55.5 (4C), 63.1, 107.7, 114.6 (10C), 116.1, 117.4 (2C), 117.9 (4C), 122.2 (2C), 123.5 (2C), 126.9, 128.0 (2C), 128.7 (2C), 130.1 (8C), 130.7 (4C),

139.0 (2C), 142.2 (2C), 142.7 (2C), 144.9 (2C), 149.5 (2C), 160.2 (2C), 161.6 (2C), 162.2 (2C), 183.3 (2C), 195.6 (2C). ESI-MS (m/z): 598 (M + Na).

(3Z,5E)-4-hydroxy-6-(4-methoxyphenyl)-3-((E)-3-(4-methoxyphenyl)acryloyl)-N-(2-oxo-2H-chromen-6-yl)hexa-3,5-dienamide (91a);

(E)-6-(4-methoxyphenyl)-3-((E)-3-(4-methoxyphenyl)acryloyl)-4-oxo-N-(2-oxo-2H-chromen-6-yl)hex-5-enamide (91b).

To a solution of **61a,b** (0.29 g, 0.34 mmol) in CH₂Cl₂ (15.0 mL) cooled to 0 °C, under nitrogen atmosphere, addition of EDC (0.07 g, 0.34 mmol) and DMAP (0.008 g, 0.068 mmol) was carried out. After 15 min, a solution of the amine **106** (0.07 g, 0.41 mmol) in CH₂Cl₂ (2.0 mL) was added dropwise and the resulting mixture was stirred at 0 °C for 2 h and overnight at room temperature. Upon reaction completion, the mixture was diluted with additional CH₂Cl₂ and sequentially washed with water and brine. The organic phase was dried over Na₂SO₄, filtered and evaporated under *vacuum* affording the crude product that was purified by flash chromatography (PE/EtOAc, 8:2), semipreparative TLC (CHCl₃) and further crystallization from CH₂Cl₂/PE. Pale yellow powder, 41 % yield (isolated as 1.0:3.3 mixture of **91a**:**91b**), mp 228-230 °C.



91a (23 % of the tautomeric mixture). ¹H-NMR (CDCl₃): δ 3.87 (s, 6H, OCH₃), 3.95 (s, 2H, CH₂), 6.42 (d, 2H, $J = 15.6$ Hz, CH=CH), 6.46 (d, 1H, $J = 9.2$ Hz, H-3), 6.94 (d, 4H, $J = 8.8$ Hz, Ar), 7.32 (d, 1H, $J = 8.8$ Hz, H-8), 7.36 (br s, 1H, CONH), 7.47 (dd, 1H, $J = 2.4$ and 8.8 Hz, H-7), 7.52 (d, 4H, $J = 8.8$ Hz, Ar), 7.72 (d, 1H, $J = 9.2$ Hz, H-4), 7.75 (d, 2H, $J = 14.4$ Hz, CH=CH), 8.15 (s, 1H, H-5).

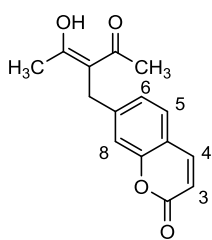
91b (77 % of the tautomeric mixture). ¹H-NMR (CDCl₃): δ 3.46-3.53 (m, 2H, CH₂), 3.87 (s, 6H, OCH₃), 4.01 (t, 1H, $J = 6.4$ Hz, diketo-CH), 6.42 (d, 2H, $J = 15.6$ Hz,

CH=CH), 6.46 (d, 1H, $J = 9.2$ Hz, H-3), 6.94 (d, 4H, $J = 8.8$ Hz, Ar), 7.32 (d, 1H, $J = 8.8$ Hz, H-8), 7.36 (br s, 1H, CONH), 7.47 (dd, 1H, $J = 2.4$ and 8.8 Hz, H-7), 7.52 (d, 4H, $J = 8.8$ Hz, Ar), 7.72 (d, 1H, $J = 9.2$ Hz, H-4), 7.75 (d, 2H, $J = 14.4$ Hz, CH=CH), 8.15 (s, 1H, H-5). **91a,b**. ^{13}C -NMR (CDCl_3): δ 28.0, 34.9, 55.3 (4C), 55.5, 114.3 (4C), 114.4 (4C), 114.5, 117.0 (2C), 118.0 (2C), 119.3 (2C), 123.4 (2C), 126.7 (2C), 126.9 (2C), 128.7 (2C), 128.9 (2C), 129.9 (4C), 130.0 (4C), 133.6 (2C), 137.0 (2C), 143.0 (2C), 143.8 (2C), 146.8 (2C), 154.0 (2C), 160.9 (2C), 161.6 (2C), 161.7 (2C), 173.2, 174.3, 178.5 (2C), 197.9 (2C). ESI-MS (m/z): 560 (M + Na).

Alkylation reaction of pentane-2,4-dione: general procedure B (synthesis of intermediates 92-96a,b).

- 1) A solution of pentane-2,4-dione (1.00 mmol) in THF (1.0 mL) was added to a stirred suspension of NaH (60 % dispersion in mineral oil, 1.2 molar equiv) in THF (5.0 mL) at 0 °C and under nitrogen atmosphere. The suspension was stirred at room temperature for 30 min before the addition dropwise of the appropriate bromomethyl-coumarin/bromotolyl-coumarin solution (1.2 molar equiv) in THF (5.0 mL) at 0 °C. The resulting mixture was stirred overnight at room temperature and the reaction was quenched with water. The aqueous phase was extracted with Et_2O (3 x 50.0 mL) and the combined organic layers were washed with brine, dried over Na_2SO_4 , filtered and concentrated in *vacuo*. The crude residue was purified by flash column chromatography on silica gel.
- 2) To a solution of pentane-2,4-dione (1.00 mmol) in acetone (10.0 mL), anhydrous K_2CO_3 (0.5 molar equiv) and the appropriate bromomethyl-coumarin (0.5 molar equiv) were added. The reaction mixture was heated to 80 °C for 6 h and TLC monitored the reaction progress. Upon reaction completion, the mixture was hot filtered, the solvent was evaporated and the crude product was purified by column chromatography over silica gel.

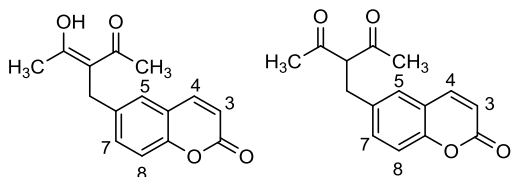
(Z)-7-(2-acetyl-3-hydroxybut-2-en-1-yl)-2H-chromen-2-one (92).



Reaction of pentane-2,4-dione (0.40 mL, 3.90 mmol) and bromo derivative **97** (0.47 g, 1.95 mmol), according to the general procedure B of pentane-2,4-dione alkylation (method **2**), gave the crude product that was purified by flash chromatography (PE/EtOAc, 9.5:0.5). Pale yellow powder, 80 % yield, mp 69-71 °C. ¹H-NMR (CDCl₃): δ 2.01 (s, 6H, CH₃), 3.76 (s, 2H, CH₂), 6.40 (d, 1H, *J* = 10.0 Hz, H-3), 7.10 (d, 1H, *J* = 8.0 Hz, H-6), 7.15 (s, 1H, H-8), 7.44 (d, 1H, *J* = 8.0 Hz, H-5), 7.70 (d, 1H, *J* = 9.2 Hz, H-4).

(Z)-6-(2-acetyl-3-hydroxybut-2-en-1-yl)-2H-chromen-2-one (93a);
3-((2-oxomp-2H-chromen-6-yl)methyl)pentane-2,4-dione (93b).

Reaction of pentane-2,4-dione (0.11 mL, 1.05 mmol) and bromo derivative **98** (0.30 g, 1.25 mmol), according to the general procedure B of pentane-2,4-dione alkylation (method **1**), gave the crude product that was purified by flash chromatography (PE/EtOAc, 9.75:0.25). White powder, 60 % yield (isolated as 1:1 mixture of **93a:93b**), 168-170 °C.



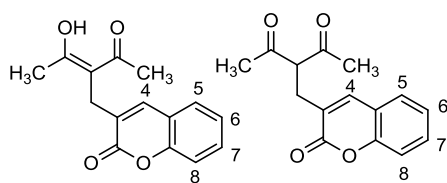
93a (50 % of the tautomeric mixture).

¹H-NMR (CDCl₃): δ 2.09 (s, 6H, CH₃), 3.72 (s, 2H, CH₂), 6.43 (d, 1H, *J* = 9.6 Hz, H-3), 7.27 (d, 1H, *J* = 2.4 Hz, H-5), 7.30 (d, 1H, *J* = 7.6 Hz, H-8), 7.33-7.37 (m, 1H, H-7), 7.68 (d, 1H, *J* = 9.6 Hz, H-4).

93b (50 % of the tautomeric mixture). ¹H-NMR (CDCl₃): δ 2.17 (s, 6H, CH₃), 3.20 (d, 2H, *J* = 7.6 Hz, CH₂), 4.02 (t, 1H, *J* = 7.6 Hz, diketo-CH), 6.42 (d, 1H, *J* = 9.6 Hz, H-3), 7.29 (d, 1H, *J* = 2.0 Hz, H-5), 7.28 (d, 1H, *J* = 7.6 Hz, H-8), 7.33-7.37 (m, 1H, H-7), 7.66 (d, 1H, *J* = 9.2 Hz, H-4).

(Z)-3-(2-acetyl-3-hydroxybut-2-en-1-yl)-2H-chromen-2-one (94a);
3-((2-oxo-2H-chromen-3-yl)methyl)pentane-2,4-dione (94b).

Reaction of pentane-2,4-dione (0.18 mL, 1.74 mmol) and bromo derivative **99** (0.50 g, 2.09 mmol) according to the general procedure B of pentane-2,4-dione alkylation (method **1**), gave the crude product that was purified by flash chromatography (PE/EtOAc, 9.75:0.25). White powder, 58 % yield (isolated as 1:0.1 mixture of **94a:94b**), 114-116 °C.

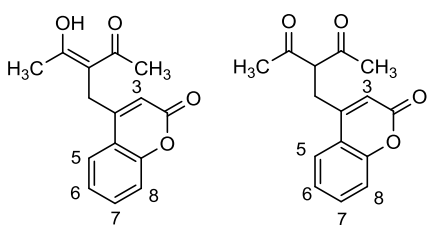


94a (91 % of the tautomeric mixture). ¹H-NMR (CDCl₃): δ 2.11 (s, 6H, CH₃), 3.56 (s, 2H, CH₂), 7.27-7.30 (m, 1H, H-6), 7.34 (s, 1H, H-4), 7.37 (d, 1H, *J* = 8.4 Hz, H-8), 7.46 (d, 1H, *J* = 7.2 Hz, H-5), 7.52 (t, 1H, *J* = 7.2 Hz, H-7).

94b (9 % of the tautomeric mixture). ¹H-NMR (CDCl₃): δ 2.28 (s, 6H, CH₃), 3.06 (d, 2H, *J* = 7.2 Hz, CH₂), 4.29 (t, 1H, *J* = 7.2 Hz, diketo-CH), 7.27-7.30 (m, 1H, H-6), 7.34 (s, 1H, H-4), 7.37 (d, 1H, *J* = 8.4 Hz, H-8), 7.46 (d, 1H, *J* = 7.2 Hz, H-5), 7.52 (t, 1H, *J* = 7.2 Hz, H-7).

(Z)-4-(2-acetyl-3-hydroxybut-2-en-1-yl)-2H-chromen-2-one (95a);
3-((2-oxo-2H-chromen-4-yl)methyl)pentane-2,4-dione (95b).

Reaction of pentane-2,4-dione (0.19 mL, 1.88 mmol) and bromo derivative **100** (0.54 g, 2.26 mmol), according to the general procedure B of pentane-2,4-dione alkylation (method **1**), gave the crude product that was purified by flash chromatography (PE/EtOAc, 8:2). White powder, 53 % yield (isolated as 4.3:1.0 mixture of **95a:95b**), mp 114-116 °C.



95a (81 % of the tautomeric mixture). ¹H-NMR (CDCl₃): δ 2.07 (s, 6H, CH₃), 3.77 (s, 2H, CH₂), 6.22 (s, 1H, H-3), 7.36-7.42 (m, 2H, H-6 and H-8), 7.61 (t, 1H, *J* = 7.6 Hz, H-7), 7.75 (d, 1H, *J* = 8.0 Hz, H-5).

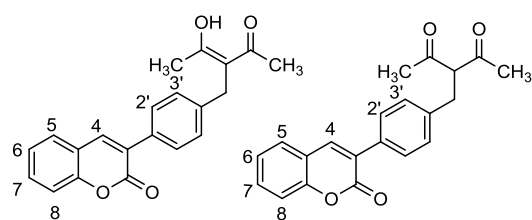
95b (19 % of the tautomeric mixture). ¹H-NMR (CDCl₃): δ 2.27 (s, 6H, CH₃), 3.35 (d, 2H, *J* = 6.8 Hz, CH₂), 4.20 (t, 1H, *J* = 7.2 Hz, diketo-CH), 6.22 (s, 1H, H-3),

7.36-7.42 (m, 2H, H-6 and H-8), 7.61 (t, 1H, $J = 7.6$ Hz, H-7), 7.75 (d, 1H, $J = 8.0$ Hz, H-5).

(Z)-3-(4-(2-acetyl-3-hydroxybut-2-en-1-yl)phenyl)-2H-chromen-2-one (96a);

3-(4-(2-oxo-2H-chromen-3-yl)benzyl)pentane-2,4-dione (96b).

Reaction of pentane-2,4-dione (0.16 mL, 1.60 mmol) and bromo derivative **101** (0.61 g, 1.92 mmol), according to the general procedure B of pentane-2,4-dione alkylation (method **1**), gave the crude product that was purified by flash chromatography (PE/EtOAc, 9.5:0.5). Beige powder, 45 % yield (isolated as 2:1 mixture of **96a:96b**), mp 115-117 °C.



96a (67 % of the tautomeric mixture).

$^1\text{H-NMR}$ (CDCl_3): δ 2.08 (s, 6H, CH_3), 3.72 (s, 2H, CH_2), 7.30-7.33 (m, 2H, H-6 and H-8), 7.39 (d, 2H, $J = 8.0$ Hz, H-3'), 7.55-7.58 (m, 2H, H-5 and H-7),

7.68 (d, 2H, $J = 8.0$ Hz, H-2'), 7.80 (s, 1H, H-4).

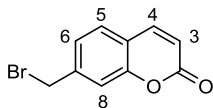
96b (33 % of the tautomeric mixture). $^1\text{H-NMR}$ (CDCl_3): δ 2.18 (s, 6H, CH_3), 3.21 (d, 2H, $J = 7.2$ Hz, CH_2), 4.02 (t, 1H, $J = 7.6$ Hz, diketo-CH), 7.30-7.33 (m, 2H, H-6 and H-8), 7.39 (d, 2H, $J = 8.0$ Hz, H-3'), 7.55-7.58 (m, 2H, H-5 and H-7), 7.68 (d, 2H, $J = 8.0$ Hz, H-2'), 7.80 (s, 1H, H-4).

General procedure of bromination (synthesis of intermediates 97-101).

To a solution of the appropriate methyl-coumarin or tolyl-coumarin (1.00 mmol) in CCl_4 (10.0 mL), NBS (1.1 molar equiv) and a catalytic amount of $(\text{PhCO})_2\text{O}_2$ were added. The resulting mixture was heated to 50 °C for 6-18 h by employing the light of a lamp to trigger the reaction via radical mechanism. Upon reaction completion, the mixture was hot filtered to remove the succinimide as a side-product of reaction. The desired bromo derivative crystallized from CCl_4 or was obtained through evaporation of the reaction solvent and further purification of

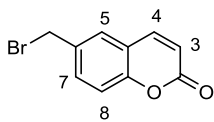
the crude residue by flash column chromatography or crystallization from the suitable mixture of solvents.

7-(bromomethyl)-2*H*-chromen-2-one (97).



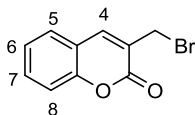
7-methylcoumarin (0.50 g, 3.12 mmol) and NBS (0.61 g, 3.43 mmol) reaction, following the general procedure of bromination, allowed obtaining the crude product that was purified by flash chromatography (PE/EtOAc, 8:2). Yellow powder, 68 % yield, mp 151-153 °C. ¹H-NMR (CDCl₃): δ 4.74 (s, 2H, CH₂Br), 6.41 (d, 1H, *J* = 10.0 Hz, H-3), 7.30 (d, 1H, *J* = 8.0 Hz, H-6), 7.33 (s, 1H, H-8), 7.44 (d, 1H, *J* = 8.0 Hz, H-5), 7.67 (d, 1H, *J* = 9.2 Hz, H-4).

6-(bromomethyl)-2*H*-chromen-2-one (98).



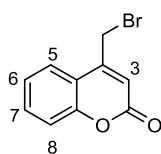
6-methylcoumarin (1.50 g, 9.37 mmol) and NBS (1.83 g, 10.31 mmol) reaction, following the general procedure of bromination, allowed obtaining **98** as yellow powder by crystallization from the solvent of reaction; 80 % yield, mp 114-116 °C. ¹H-NMR (CDCl₃): δ 4.28 (s, 2H, CH₂Br), 6.20 (d, 1H, *J* = 9.6 Hz, H-3), 7.06 (d, 1H, *J* = 8.0 Hz, H-8), 7.27-7.32 (m, 2H, H-5 and H-7), 7.44 (d, 1H, *J* = 9.6 Hz, H-4).

3-(bromomethyl)-2*H*-chromen-2-one (99).



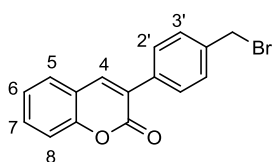
3-methylcoumarin (1.50 g, 9.37 mmol) and NBS (1.83 g, 10.31 mmol) reaction, following the general procedure of bromination, allowed obtaining the crude product that was crystallized from CH₂Cl₂/PE. Orange powder, 85 % yield, mp 113-115 °C. ¹H-NMR (CDCl₃): δ 4.42 (s, 2H, CH₂Br), 7.29-7.34 (m, 2H, H-6 and H-8), 7.48-7.53 (m, 2H, H-5 and H-7), 7.84 (s, 1H, H-4).

4-(bromomethyl)-2H-chromen-2-one (100).



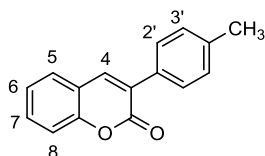
4-methylcoumarin (1.06 g, 6.62 mmol) and NBS (1.30 g, 7.28 mmol) reaction, following the general procedure of bromination, allowed obtaining **100** as pale yellow powder by crystallization from the solvent of reaction; 73 % yield, mp 161-163 °C. ¹H-NMR (CDCl₃): δ 4.50 (s, 2H, CH₂Br), 6.54 (s, 1H, H-3), 7.34-7.39 (m, 2H, H-6 and H-8), 7.58 (td, 1H, *J* = 1.6 and 7.2 Hz, H-7), 7.74 (dd, 1H, *J* = 1.2 and 6.8 Hz, H-5).

3-(4-(bromomethyl)phenyl)-2H-chromen-2-one (101)



102 (1.5 g, 6.35 mmol) and NBS (1.30 g, 6.99 mmol) reaction, following the general procedure of bromination, allowed obtaining the crude product that was purified by crystallization from CH₂Cl₂/PE. Pale yellow powder, 73 % yield, mp 170-172 °C. ¹H-NMR (CDCl₃): δ 4.55 (s, 2H, CH₂Br), 7.32 (t, 1H, *J* = 6.8 Hz, H-6), 7.39 (d, 1H, *J* = 8.0 Hz, H-8), 7.49 (d, 2H, *J* = 8.4 Hz, H-3'), 7.56 (t, 1H, *J* = 7.2 Hz, H-7), 7.57 (d, 1H, *J* = 7.6 Hz, H-5), 7.72 (d, 2H, *J* = 8.0 Hz, H-2'), 7.84 (s, 1H, H-4).

3-(p-tolyl)-2H-chromen-2-one (102).



Salicylaldehyde (2.43 mL, 23.21 mmol), phenylacetic acid (3.49 g, 23.21 mmol), acetic anhydride (4.39 mL, 46.42 mmol) and TEA (3.23 mL, 23.21 mmol) were heated to 150 °C for 12 h. After cooling to room temperature, the reaction mixture was taken up in CH₂Cl₂ and was washed with a 10 % K₂CO₃ solution. The aqueous phase was extracted twice with CH₂Cl₂ (2 x 30.0 mL), the combined organic phases were washed with brine, dried over Na₂SO₄ and concentrated *in vacuo*. The residue was washed with PE and crystallized from CH₂Cl₂/PE to give **102** as beige powder; 73 % yield, mp 156-158 °C. ¹H-NMR (CDCl₃): δ 2.42 (s, 3H, CH₃), 7.27-7.32 (m, 3H, H-3' and H-6), 7.38 (d, 1H, *J* = 8.0 Hz, H-8), 7.54 (t, 1H,

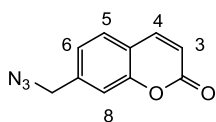
$J = 7.2$ Hz, H-7), 7.55 (d, 1H, $J = 8.0$ Hz, H-5), 7.62 (d, 2H, $J = 7.6$ Hz, H-2'), 7.81 (s, 1H, H-4).

General procedure for the synthesis of azidomethyl-coumarins 103-105.

To a solution of the appropriate halide (1.00 mmol) in acetone (10.0 mL), a solution of NaN₃ (1.2 molar equiv) in water (0.30 mL) was added dropwise; the mixture was stirred at 40 °C for 4 h and, after cooling to room temperature, was stirred overnight. Upon reaction completion, the solution was poured into water and two different work up procedures were performed:

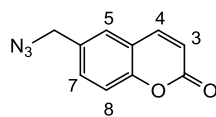
- 1) the crude product was obtained as precipitate that was filtered off;
- 2) the aqueous phase was extracted with CH₂Cl₂ (3 x 25.0 mL), the combined organic layers were dried over Na₂SO₄ and the solvent was removed under reduced pressure.

7-(azidomethyl)-2H-chromen-2-one (103).



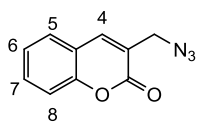
103 was obtained as off-white powder according to the general procedure for azidomethyl-coumarins (method **1**) starting from **97** (0.25 g, 1.05 mmol) and NaN₃ (0.08 g, 1.26 mmol); 90 % yield, mp 68-70 °C. ¹H-NMR (CDCl₃): δ 4.47 (s, 2H, N₃CH₂), 6.45 (d, 1H, $J = 9.6$ Hz, H-3), 7.26 (d, 1H, $J = 8.8$ Hz, H-6), 7.31 (s, 1H, H-8), 7.52 (d, 1H, $J = 7.2$ Hz, H-5), 7.72 (d, 1H, $J = 9.2$ Hz, H-4).

6-(azidomethyl)-2H-chromen-2-one (104).



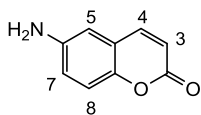
104 was obtained as off-white powder according to the general procedure for azidomethyl-coumarins (method **2**) starting from **98** (0.08 g, 0.33 mmol) and NaN₃ (0.03 g, 0.40 mmol); 75 % yield, mp 66-68 °C. ¹H-NMR (200 MHz, CDCl₃): δ 4.43 (s, 2H, N₃CH₂), 6.48 (d, 1H, $J = 9.6$ Hz, H-3), 7.35-7.52 (m, 2H, H-7 and H-8), 7.47 (s, 1H, H-5), 7.72 (d, 1H, $J = 9.4$ Hz, H-4).

3-(azidomethyl)-2*H*-chromen-2-one (105).



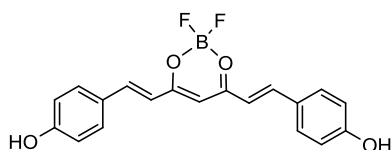
105 was obtained as pale yellow powder according to the general procedure for azidomethyl-coumarins (method **1**) starting from **99** (0.24 g, 1.00 mmol) and NaN₃ (0.08 g, 1.20 mmol); 98 % yield, mp 66-68 °C. ¹H-NMR (CDCl₃): δ 4.41 (s, 2H, N₃CH₂), 7.28-7.39 (m, 2H, H-6 and H-8), 7.55-7.61 (m, 2H, H-5 and H-7), 7.78 (s, 1H, H-4).

6-amino-2*H*-chromen-2-one (106).



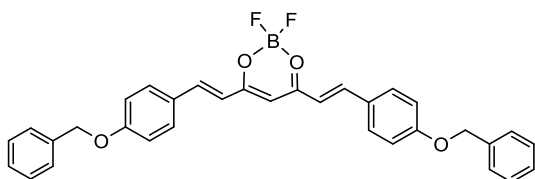
A solution of 6-nitro-2*H*-chromen-2-one (0.80 g, 4.19 mmol) in THF (50.0 mL) was hydrogenated (H₂, 308 mL, 13.75 mmol) over Pd/CaCO₃. The catalyst was removed by filtration on celite pad and the filtrate was evaporated under reduced pressure providing **106** as yellow powder; 90 % yield, mp 148-150 °C. ¹H-NMR (acetone-*d*₆): δ 6.30 (d, 1H, *J* = 9.6 Hz, H-3), 6.84 (d, 1H, *J* = 2.8 Hz, H-5), 6.95 (dd, 1H, *J* = 2.8 and 8.4 Hz, H-7), 7.06 (d, 1H, *J* = 8.4 Hz, H-8), 7.78 (d, 1H, *J* = 9.2 Hz, H-4).

4,4'-((1*E*,1'*E*)-(2,2-difluoro-2*H*-1λ³,3,2λ⁴-dioxaborinine-4,6-diyl)bis(ethene-2,1-diyl))diphenol (107).



To a solution of **4** (0.40 g in 1.30 mmol) in CHCl₃ (25.0 mL), BF₃·Et₂O (10.70 mL, 86.67 mmol) was added dropwise. The resulting mixture was stirred for 5 h at room temperature and was finally poured into water. The organic layer was separated, and the aqueous phase was extracted with CH₂Cl₂ (3 x 15 mL). The combined organic phases were washed with water, dried over Na₂SO₄ and evaporated to dryness affording **107** as purplish red powder; 80 % yield, mp 250-252 °C. ¹⁵⁰¹H-NMR (acetone-*d*₆) δ 6.39 (s, 1H, keto-enol-CH), 6.90 (d, 2H, *J* = 15.2 Hz, CH=CH), 6.96 (d, 4H, *J* = 8.4 Hz, Ar), 7.74 (d, 4H, *J* = 8.8 Hz, Ar), 7.97 (d, 2H, *J* = 15.6 Hz, CH=CH). ¹³C-NMR (acetone-*d*₆) δ 102.1, 117.1 (4C), 118.8 (2C) 127.1 (2C), 132.6 (4C), 147.2 (2C), 162.1 (2C), 180.7 (2C). ESI-MS (*m/z*): 379 (M + Na).

4,6-bis((*E*)-4-(benzyloxy)styryl)-2,2-difluoro-2*H*-1 λ^3 ,3,2 λ^4 -dioxaborinine (108).



Reaction of **107** (0.20 g, 0.56 mmol), and benzyl bromide (0.13 mL, 1.12 mmol) for 12 h, in agreement with the general procedure of the Williamson

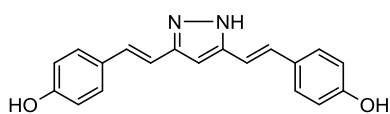
reaction, gave the crude product that was purified by flash chromatography (PE/EtOAc, 7:3) and further crystallization from CH₂Cl₂/PE. Red powder, 69 % yield, mp 172-174 °C. ¹H-NMR (acetone-*d*₆) δ 5.25 (s, 4H, OCH₂), 6.43 (s, 1H, keto-enol-CH), 6.97 (d, 2H, *J* = 15.6 Hz, CH=CH), 7.15 (d, 4H, *J* = 8.8 Hz, Ar), 7.42 (m, 10H, Bn), 7.83 (d, 4H, *J* = 8.8 Hz, Ar), 8.00 (d, 2H, *J* = 16.0 Hz, CH=CH). ¹³C-NMR (acetone-*d*₆) δ 70.2 (2C), 101.6, 115.4 (2C), 115.1 (2C), 122.1 (2C), 127.6 (4C), 128.3 (2C), 128.4 (2C), 128.8 (2C), 128.9 (4C), 129.9 (2C), 136.2 (2C), 140.3 (2C), 162.0 (2C), 179.6 (2C). ESI-MS (*m/z*): 559 (M + Na).

Cyclization reaction: general procedure for the synthesis of pyrazoles 109-113, 122 and 125, dihydropyrazole 115 and isoxazole 114.

To a stirred solution of compound **4** (1.00 mmol) in CH₃COOH (10.0 mL), heated to 60 °C for 30 min, NH₂NH₂·H₂O/CH₃NHNH₂/the appropriate arylhydrazine/NH₂OH·HCl (5.0 molar equiv) was added dropwise. The reaction mixture was refluxed for 5-20 h and then, after cooling to room temperature, was allowed to stir for 12 h. Upon reaction completion, one of the following work up was performed:

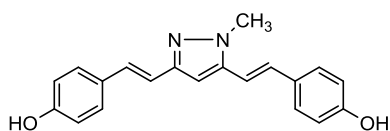
- a) the obtained precipitate was filtered off, washed with water and dried;
- b) the reaction was quenched with water and brought to pH 7 with NaHCO₃ obtaining a precipitate, that was filtered, dried and purified by crystallization from suitable solvent or mixture of solvents or by flash column chromatography and further crystallization.

4,4'-((1E,1'E)-(1H-pyrazole-3,5-diyl)bis(ethene-2,1-diyl)diphenol (109).



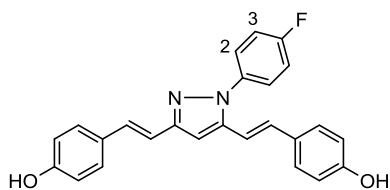
4 (0.60 g, 1.95 mmol) and $\text{NH}_2\text{NH}_2\cdot\text{H}_2\text{O}$ (0.47 mL, 9.75 mmol) were allowed to react in line with the general procedure of cyclization (method **a**, 20 h of reflux) to give **109** as beige powder, 76 % yield, mp 275-277 °C.¹⁵¹ $^1\text{H-NMR}$ (CDCl_3): δ 6.66 (s, 1H), 6.85 (d, 4H, $J = 8.4$ Hz, Ar), 6.96 (d, 2H, $J = 16.4$ Hz, CH=CH), 7.13 (d, 2H, $J = 16.4$ Hz, CH=CH), 7.41 (d, 4H, $J = 8.4$ Hz, Ar). $^{13}\text{C-NMR}$ (acetone- d_6): δ 99.9, 116.4 (2C), 116.5 (4C), 128.6 (4C), 129.6 (2C), 130.5 (2C), 148.0 (2C), 158.3 (2C). ESI-MS (m/z): 327 (M + Na).

4,4'-((1E,1'E)-(1-methyl-1H-pyrazole-3,5-diyl)bis(ethene-2,1-diyl)diphenol (110).



4 (0.20 g, 0.65 mmol) and CH_3NHNH_2 (0.17 mL, 3.25 mmol) were allowed to react in line with the general procedure of cyclization (method **b**, 20 h of reflux) to give the crude product that was purified by flash chromatography (PE/EtOAc, 1:1). Light brown powder, 59 % yield, mp 278-280 °C.¹⁵¹ $^1\text{H-NMR}$ (CDCl_3) δ 3.91 (s, 3H, NCH_3), 6.73 (s, 1H), 6.84 (d, 2H, $J = 8.0$ Hz, Ar), 6.86 (d, 2H, $J = 8.0$ Hz, Ar), 7.01 (d, 2H, $J = 16.0$ Hz, CH=CH), 7.11 (d, 2H, $J = 16.0$ Hz, CH=CH), 7.40 (d, 2H, $J = 8.4$ Hz, Ar), 7.49 (d, 2H, $J = 8.4$ Hz, Ar). $^{13}\text{C-NMR}$ (CDCl_3): δ 36.2, 100.0, 116.2 (2C), 116.9 (4C), 128.5 (4C), 130.0 (2C), 130.5 (2C), 148.0 (2C), 158.4 (2C). ESI-MS (m/z): 341 (M + Na).

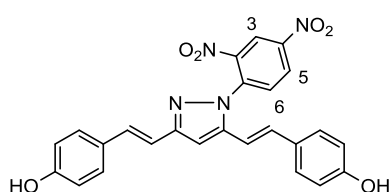
4,4'-((1E,1'E)-(1-(4-fluorophenyl)-1H-pyrazole-3,5-diyl)bis(ethene-2,1diyl)diphenol (111).



4 (0.20 g, 0.65 mmol) and 4-fluorophenylhydrazine hydrochloride (0.53 g, 3.25 mmol) were allowed to react in line with the general procedure of cyclization (method **a**, 20 h of reflux) to give the crude product as precipitate that was purified by flash chromatography (PE/EtOAc, 6:4) and further crystallization from EtOH. Beige

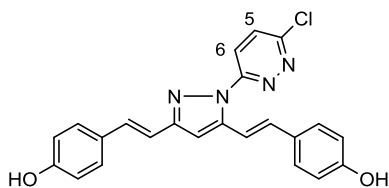
powder, 40 % yield, mp 230-232°C.¹⁵¹ ¹H-NMR (acetone-*d*₆): δ 6.79 (d, 1H, *J* = 16.4 Hz, CH=CH), 6.84 (d, 2H, *J* = 8.4 Hz, Ar), 6.88 (d, 2H, *J* = 8.8 Hz, Ar), 7.03 (d, 1H, *J* = 16.4 Hz, CH=CH), 7.06 (s, 1H), 7.27 (d, 1H, *J* = 16.4 Hz, CH=CH), 7.31 (d, 1H, *J* = 16.4 Hz, CH=CH), 7.33-7.37 (m, 2H, H-3), 7.40 (d, 2H, *J* = 8.4 Hz, Ar), 7.47 (d, 2H, *J* = 8.4 Hz, Ar), 7.63-7.67 (m, 2H, H-2). ¹³C-NMR (acetone-*d*₆): δ. 100.1, 116.2 (2C, *J* = 27.1 Hz), 116.5 (2C), 116.8 (4C), 125.5 (2C, *J* = 8.1 Hz), 128.9 (4C), 129.6 (2C), 130.6 (2C), 135.8 (d, *J* = 4.0 Hz), 149.5 (2C), 158.4 (2C), 162.81 (d, *J* = 265.0 Hz). ESI-MS (*m/z*): 421 (M + Na).

4,4'-((1*E*,1'*E*)-(1-(2,4-dinitrophenyl)-1*H*-pyrazole-3,5-diyl)bis(ethene-2,1-diyl))diphenol (112**).**



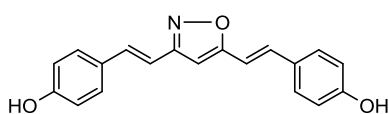
4 (0.10 g, 0.32 mmol) and 2,4-dinitrophenylhydrazine hydrochloric acid solution (0.38 mL, 1.62 mmol) were allowed to react in line with the general procedure of cyclization (method **a**, 20 h of reflux) to give **112** as precipitate after addition of water to the reaction mixture. Red-brown powder, 79 % yield, mp 174-176 °C.¹⁵¹ ¹H-NMR (acetone-*d*₆): δ 6.83 (d, 2H, *J* = 8.4 Hz, Ar), 6.87 (d, 2H, *J* = 8.4 Hz, Ar), 6.88 (d, 1H, *J* = 17.2 Hz, CH=CH), 6.92 (d, 1H, *J* = 16.8 Hz, CH=CH), 7.14 (s, 1H), 7.25 (d, 1H, *J* = 17.2 Hz, CH=CH), 7.29 (d, 1H, *J* = 16.8 Hz, CH=CH), 7.41 (d, 2H, *J* = 8.4 Hz, Ar), 7.47 (d, 2H, *J* = 8.4 Hz, Ar), 8.09 (d, 1H, *J* = 8.8 Hz, H-6), 8.75 (dd, 1H, *J* = 2.8 and 9.2 Hz, H-5), 8.91 (d, 1H, *J* = 2.4 Hz, H-3). ¹³C-NMR (acetone-*d*₆): δ 102.5, 111.0, 115.3 (2C), 115.4 (2C), 117.4 (2C), 128.8 (4C), 129.6, 129.7, 132.3, 134.7, 136.7, 136.9, 137.6, 143.9, 145.5, 146.3, 154.4, 158.4 (2C). ESI-MS (*m/z*): 493 (M + Na).

4,4'-((1*E*,1'*E*)-(1-(6-chloropyridazin-3-yl)-1*H*-pyrazole-3,5-diyl)bis(ethene-2,1-diyl)diphenol (113).



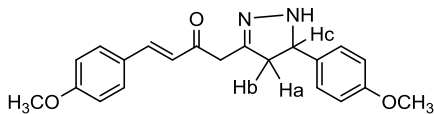
4 (0.20 g, 0.65 mmol) and 3-chloro-6-hydrazinopyridazine (0.47 g, 3.25 mmol) were allowed to react in line with the general procedure of cyclization (method **a**, 20 h of reflux) to give the crude product that, after washing with saturated aqueous NaHCO₃ solution, was purified by flash chromatography (PE/EtOAc, 1:1) and further crystallization from CH₂Cl₂/PE. Mustard yellow powder, 37 % yield, mp 236-238 °C (dec). ¹H-NMR (acetone-*d*₆): δ 6.86 (d, 2H, *J* = 8.4 Hz, Ar), 6.88 (d, 2H, *J* = 8.8 Hz, Ar), 6.98 (d, 1H, *J* = 16.4 Hz, CH=CH), 7.08 (s, 1H), 7.10 (d, 1H, *J* = 10.4 Hz, H-5), 7.22 (d, 1H, *J* = 16.0 Hz, CH=CH), 7.26 (d, 1H, *J* = 16.0 Hz, CH=CH), 7.44 (d, 2H, *J* = 8.4 Hz, Ar), 7.47 (d, 2H, *J* = 8.4 Hz, Ar), 7.51 (d, 1H, *J* = 16.4 Hz, CH=CH), 8.01 (d, 1H, *J* = 10.4 Hz, H-6), 8.60 (br s, 2H, OH). ¹³C-NMR (acetone-*d*₆): δ 101.0, 116.2 (2C), 116.4 (4C), 128.9 (4C), 125.0, 128.8, 129.6 (2C), 130.9 (2C), 148.0 (2C), 150.6, 156.0, 158.3 (2C). ESI-MS (*m/z*): 439 (M + Na) and 441 (M + 2 + Na).

4,4'-((1*E*,1'*E*)-isoxazole-3,5-diyl)bis(ethene-2,1-diyl)diphenol (114).



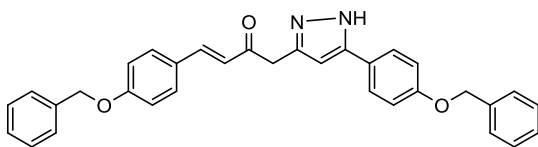
4 (0.20 g, 0.65 mmol) and NH₂OH·HCl (0.14 mL, 3.25 mmol) were allowed to react in line with the general procedure of cyclization (method **a**, 16 h of reflux) to give **114** as brown powder; 75 % yield, mp 273-275 °C.¹⁵² ¹H-NMR (acetone-*d*₆): δ 6.74 (s, 1H), 6.89 (d, 2H, *J* = 8.4 Hz, Ar), 6.90 (d, 2H, *J* = 8.0 Hz, Ar), 6.99 (d, 2H, *J* = 16.4 Hz, CH=CH), 7.30 (d, 1H, *J* = 16.4 Hz, CH=CH), 7.33 (d, 1H, *J* = 16.4 Hz, CH=CH), 7.51 (d, 2H, *J* = 7.6 Hz, Ar), 7.53 (d, 2H, *J* = 8.0 Hz, Ar), 8.71 (br s, 1H, OH), 8.77 (br s, 1H, OH). ¹³C-NMR (CDCl₃): δ 98.5, 111.2, 113.8, 116.6 (2C), 116.7 (2C), 128.3, 128.6, 129.5 (2C), 129.7 (2C), 135.2, 136.6, 159.2, 159.5, 163.2, 169.5. ESI-MS (*m/z*): 328 (M + Na).

(E)-4-(4-methoxyphenyl)-1-(5-(4-methoxyphenyl)-4,5-dihydro-1H-pyrazol-3-yl)but-3-en-2-one (115).



5 (0.07 g, 0.19 mmol) and $\text{NH}_2\text{NH}_2 \cdot \text{H}_2\text{O}$ (0.05 mL, 0.95 mmol) were allowed to react in line with the general procedure of cyclization (method **b**, 8 h of reflux). In this case, the aqueous phase neutralization with NaHCO_3 , did not give a precipitate, so it was extracted with Et_2O (3 x 25.0 mL), the combined organic phases were dried over Na_2SO_4 , concentrated under reduced pressure obtaining the crude product, which was purified by flash column chromatography on silica gel (PE/EtOAc, 6:4). Beige powder, 38 % yield, mp 160-162 °C. $^1\text{H-NMR}$ (acetone- d_6): δ 3.00 (dd, 1H, $J = 4.0$ and 17.2 Hz, Ha), 3.67 (dd, 1H, $J = 12.0$ and 17.6 Hz, Hb), 3.76 (s, 3H, OCH_3), 3.83 (s, 3H, OCH_3), 3.90 (s, 2H, CH_2), 5.46 (dd, 1H, $J = 4.4$ and 11.6 Hz, Hc), 6.86 (d, 2H, $J = 8.8$ Hz, Ar), 6.95 (d, 1H, $J = 16.4$ Hz, $\text{CH}=\text{CH}$), 6.96 (d, 2H, $J = 8.8$ Hz, Ar), 7.02 (d, 1H, $J = 16.4$ Hz, $\text{CH}=\text{CH}$), 7.13 (d, 2H, $J = 8.4$ Hz, Ar), 7.56 (d, 2H, $J = 8.8$ Hz, Ar). $^{13}\text{C-NMR}$ (acetone- d_6): δ 22.0, 41.8, 55.5, 55.7, 60.0, 114.7 (2C), 115.2 (2C), 119.4, 127.7 (2C), 129.4 (2C), 129.8, 135.9, 137.7, 155.9, 159.9, 161.4, 167.9. ESI-MS (m/z): 351 (M + H) and 373 (M + Na).

(E)-4-(4-(benzyloxy)phenyl)-1-(5-(4-(benzyloxy)phenyl)-1H-pyrazol-3-yl)but-3-en-2-one (116).

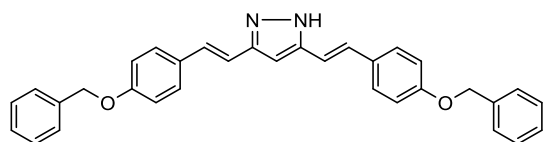


To a solution of **8** (0.20 g, 0.41 mmol) in EtOH (3.0 mL), $\text{NH}_2\text{NH}_2 \cdot 2\text{HCl}$ (0.04 g, 0.38 mmol) and a catalytic amount of CH_3COOH (0.5 mL) were added dropwise. The reaction mixture was refluxed for 40 h and, upon reaction completion, the solvent was evaporated under reduced pressure affording a residue that was diluted with EtOAc (15.0 mL) and poured into water. The organic phase was separated, the water layer was extracted twice with EtOAc (2 x 15.0 mL) and the combined organic phases were washed with brine, dried over Na_2SO_4 and concentrated. The crude product was crystallized from EtOH affording **116** as off-white powder; 32 % yield, mp 213-215 °C. $^1\text{H-NMR}$

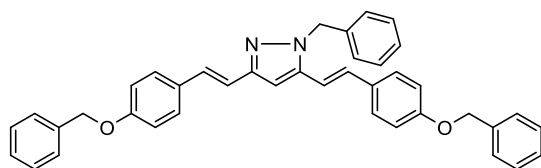
NMR (acetone- d_6): δ 4.10 (s, 2H, CH₂), 5.08 (s, 2H, OCH₂), 5.11 (s, 2H, OCH₂), 6.63 (s, 1H), 6.95 (d, 2H, $J = 6.8$ Hz, Ar), 6.99 (d, 2H, $J = 8.8$ Hz, Ar), 7.11 (d, 1H, $J = 16.4$ Hz, CH=CH), 7.12 (d, 1H, $J = 16.0$ Hz, CH=CH), 7.22-7.37 (m, 10H, Bn), 7.42 (d, 2H, $J = 8.4$ Hz, Ar), 7.46 (d, 2H, $J = 8.8$ Hz, Ar). ¹³C-NMR (acetone- d_6): δ 42.2, 70.0 (2C), 101.9, 115.6 (4C), 123.9, 125.9 (2C), 127.8, 128.2 (6C), 128.3 (4C), 128.5 (2C), 129.1, 137.0 (2C), 140.4, 145.9, 147.0, 160.6 (2C), 197.0. ESI-MS (m/z): 523 (M + Na).

**3,5-bis((*E*)-4-(benzyloxy)styryl)-1*H*-pyrazole (117);
1-benzyl-3,5-bis((*E*)-4-(benzyloxy)styryl)-1*H*-pyrazole (118).**

Reaction of **109** (0.25 g, 0.82 mmol) and benzyl bromide (0.20 mL, 1.64 mmol), following the general procedure of the Williamson reaction (16 h of reflux), gave a precipitate (**117**) after partial acetone removal, which was filtered off and sequentially washed with acetone and EtOH. Complete solvent concentration under *vacuum* afforded then **118** as crude product that was purified by flash chromatography (PE/EtOAc, 7:3).



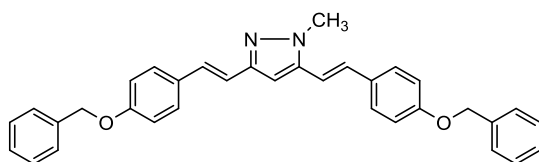
117. White powder, 30 % yield, mp 217-219 °C. ¹H-NMR (CDCl₃): δ 5.09 (s, 4H, OCH₂), 6.62 (s, 1H), 6.91 (d, 2H, $J = 16.4$ Hz, CH=CH), 6.95 (d, 4H, $J = 8.4$ Hz, Ar), 7.14 (d, 2H, $J = 16.4$ Hz, CH=CH), 7.35-7.43 (m, 10H, Bn), 7.43 (d, 4H, $J = 8.8$ Hz, Ar). ¹H-NMR (DMSO- d_6): δ 5.13 (s, 4H, OCH₂), 6.70 (s, 1H), 6.95 (d, 2H, $J = 16.4$ Hz, CH=CH), 7.03 (d, 4H, $J = 8.0$ Hz, Ar), 7.12 (d, 2H, $J = 16.4$ Hz, CH=CH), 7.39 (d, 4H, $J = 6.8$ Hz, Ar), 7.33-7.51 (m, 10H, Bn). ¹³C-NMR (DMSO- d_6): δ 69.3 (2C), 99.7, 115.1 (4C), 116.1 (2C), 127.7 (8C), 127.9 (2C), 128.4 (6C), 129.3 (2C), 129.5 (2C), 137.0 (2C), 158.2 (2C). ESI-MS (m/z): 485 (M + H).



118. White powder, 45 % yield, mp 152-154 °C. ¹H-NMR (CDCl₃): δ 5.08 (s, 4H, OCH₂), 5.42 (s, 2H, NCH₂, Bn), 6.70 (s, 1H), 6.71 (d, 1H, $J = 15.6$ Hz, CH=CH), 6.94 (d, 4H, $J = 8.8$ Hz, Ar), 6.97 (d, 4H, $J = 8.4$ Hz, Ar), 7.00 (d,

2H, $J = 16.4$ Hz, CH=CH), 7.10 (d, 1H, $J = 16.4$ Hz, CH=CH), 7.31-7.36 (m, 5H, Bn), 7.35-7.43 (m, 10H, Bn). $^{13}\text{C-NMR}$ (DMSO- d_6): δ 52.9, 69.4 (2C), 99.9, 115.4 (4C), 116.2 (2C), 127.8 (8C), 127.9, 128.0 (2C), 128.5 (6C), 128.6 (2C), 128.9 (2C), 129.3 (2C), 129.4 (2C), 136.0, 137.2 (2C), 158.3 (2C). ESI-MS (m/z): 597 (M + Na).

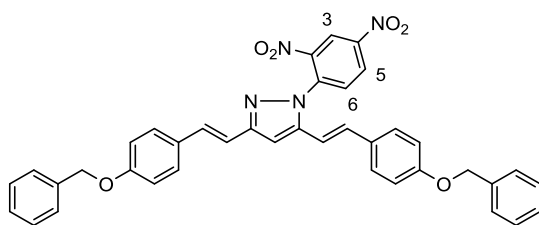
3,5-bis((*E*)-4-(benzyloxy)styryl)-1-methyl-1*H*-pyrazole (119).



Reaction of **110** (0.05 g, 0.18 mmol) and benzyl bromide (0.04 mL, 0.36 mmol), according to the general procedure of the Williamson reaction

(36 h of reflux), gave the crude product that was purified by flash chromatography (PE/EtOAc, 8:2). Beige powder, 61 % yield, mp 165-167 °C. $^1\text{H-NMR}$ (CDCl_3): δ 3.89 (s, 3H, NCH₃), 5.16 (s, 4H, OCH₂), 6.63 (s, 1H), 6.78 (d, 1H, $J = 16.0$ Hz, CH=CH), 6.95 (d, 1H, $J = 16.4$ Hz, CH=CH), 6.97 (d, 4H, $J = 8.8$ Hz, Ar), 7.00 (d, 4H, $J = 8.4$ Hz, Ar), 7.10 (d, 2H, $J = 16.4$ Hz, CH=CH), 7.35-7.43 (m, 10H, Bn). $^{13}\text{C-NMR}$ (CDCl_3): δ 36.5, 69.5 (2C), 100.6, 115.1 (4C), 116.0 (2C), 127.6 (8C), 127.7 (2C), 128.2 (4C), 128.3 (2C), 129.5 (2C), 130.0 (2C), 136.7 (2C), 159.0 (2C). ESI-MS (m/z): 521 (M + Na).

3,5-bis((*E*)-4-(benzyloxy)styryl)-1-(2,4-dinitrophenyl)-1*H*-pyrazole (120).

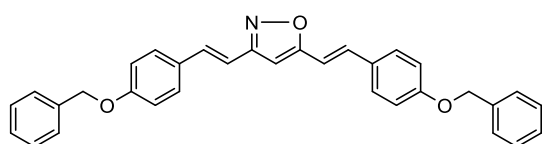


Reaction of **112** (0.10 g, 0.21 mmol) and benzyl bromide (0.08 mL, 0.63 mmol), according to the general procedure of the Williamson reaction (12 h of reflux), gave the crude product

that was purified by two sequential crystallizations from: $\text{CH}_2\text{Cl}_2/\text{PE}$ and acetone/PE. Dark brown powder, 80 % yield, mp 143-145 °C. $^1\text{H-NMR}$ (CDCl_3): δ 5.10 (s, 2H, OCH₂), 5.11 (s, 2H, OCH₂), 6.55 (d, 1H, $J = 16.0$ Hz, CH=CH), 6.88 (s, 1H), 6.94 (d, 1H, $J = 16.0$ Hz, CH=CH), 6.99 (d, 4H, $J = 8.4$ Hz, Ar), 7.12 (d,

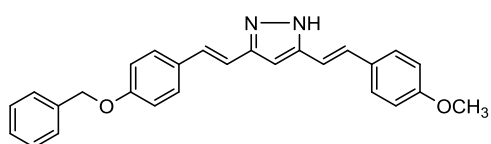
1H, $J = 15.2$ Hz, CH=CH), 7.16 (d, 1H, $J = 16.0$ Hz, CH=CH), 7.35 (d, 4H, $J = 8.0$ Hz, Ar), 7.39-7.47 (m, 10H, Bn), 7.82 (d, 1H, $J = 8.8$ Hz, H-6), 8.57 (dd, 1H, $J = 2.4$ and 9.2 Hz, H-5), 8.85 (d, 1H, $J = 2.0$ Hz, H-3). ^{13}C -NMR (CDCl_3): δ 70.2 (2C), 102.5, 111.0, 115.3 (2C), 115.4 (2C), 117.4, 121.4, 127.5 (2C), 127.6 (4C), 128.2 (2C), 128.3, 128.4, 128.7 (4C), 128.8 (2C), 129.6, 129.7, 132.3, 134.7, 136.7, 136.9, 137.6, 143.9, 145.5, 146.3, 154.4, 159.1, 159.7. ESI-MS (m/z): 673 (M + Na).

3,5-bis((*E*)-4-(benzyloxy)styryl)isoxazole (121).



Reaction of **114** (0.28 g, 0.92 mmol) and benzyl bromide (0.12 mL, 1.84 mmol), according to the general procedure of the Williamson reaction (48 h of reflux), gave the crude product that was purified by flash chromatography (PE/EtOAc, 7:3) and further crystallization from $\text{CH}_2\text{Cl}_2/\text{PE}$. Light brown powder, 69 % yield, mp 207-209 °C. ^1H -NMR (CDCl_3): δ 5.12 (s, 4H, OCH_2), 6.43 (s, 1H), 6.84 (d, 1H, $J = 16.0$ Hz, CH=CH), 7.00 (d, 4H, $J = 8.4$ Hz, Ar), 7.13 (d, 1H, $J = 16.4$ Hz, CH=CH), 7.31 (d, 1H, $J = 16.0$ Hz, CH=CH), 7.41 (d, 1H, $J = 16.4$ Hz, CH=CH), 7.41-7.49 (m, 10H, Bn), 7.48 (d, 4H, $J = 8.4$ Hz, Ar). ^{13}C -NMR (CDCl_3): δ 70.2 (2C), 101.5, 111.2, 114.0, 116.6 (2C), 116.8 (2C), 128.2 (6C), 128.3, 128.4 (4C), 128.7, 129.5 (2C), 129.7 (2C), 135.2, 136.7, 137.1 (2C), 160.7 (2C), 163.1, 169.5. ESI-MS (m/z): 508 (M + Na).

3-((*E*)-4-(benzyloxy)styryl)-5-((*E*)-4-methoxystyryl)-1*H*-pyrazole (122).



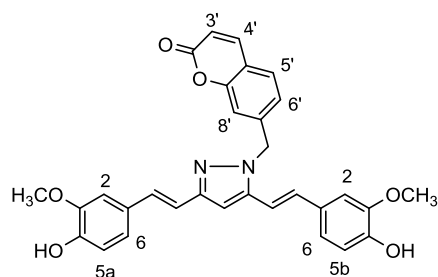
Reaction of **6** (0.10 g, 0.24 mmol) and $\text{NH}_2\text{NH}_2 \cdot \text{H}_2\text{O}$ (0.06 mL, 1.20 mmol), in line with the general procedure of cyclization (method **b**, 5 h of reflux), gave the crude product that was purified by crystallization from acetone/PE. Beige powder, 63 % yield, mp 75-77 °C. ^1H -NMR (CDCl_3): δ 3.82 (s, 3H, OCH_3), 5.16 (s, 2H, OCH_2), 6.69 (s, 1H), 6.94 (d, 2H, $J = 8.4$ Hz, Ar), 6.97 (d, 1H, $J = 15.2$ Hz, CH=CH), 7.00 (d, 1H, $J = 16.0$ Hz, CH=CH),

7.04 (d, 2H, $J = 8.4$ Hz, Ar), 7.16 (d, 2H, $J = 16.4$ Hz, CH=CH), 7.32 (d, 1H, $J = 7.2$ Hz, Ar), 7.34 (d, 1H, $J = 7.2$ Hz, Ar), 7.39 (d, 1H, $J = 7.2$ Hz, Ar), 7.41 (d, 1H, $J = 7.2$ Hz, Ar), 7.49-7.52 (m, 5H, Bn). ^{13}C -NMR (CDCl_3): δ 55.6, 70.3, 99.9, 114.5 (2C), 116.4 (2C), 116.5 (2C), 127.7 (3C), 128.4 (4C), 129.4 (2C), 129.5, 129.6, 130.3, 130.5, 137.1, 147.9, 148.0, 158.3, 161.3. ESI-MS (m/z): 431 (M + Na).

***N*-alkylation of the curcumin pyrazole **125**: general procedure for the synthesis of **123** and **124**.**

125 (1.00 mmol) and the appropriate bromomethyl-coumarin (1.0 molar equiv) were dissolved in THF (30.0 mL) following by a dropwise addition of TEA (1.0 molar equiv). The resulting mixture was refluxed for 8 h and, after cooling to room temperature, was stirred overnight. The solvent was evaporated and the crude residue was purified by flash chromatography on silica gel and further crystallization.

7-((3,5-bis(*E*)-4-hydroxy-3-methoxystyryl)-1*H*-pyrazol-1-yl)methyl)-2*H*-chromen-2-one (123**).**

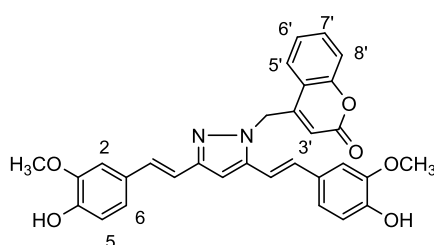


125 (0.10 g, 0.27 mmol) and **97** (0.06 g, 0.27 mmol) were allowed to react according to the general procedure of curcumin pyrazole *N*-alkylation. The crude product was purified by flash chromatography (toluene/acetone, 8.5:1.5) and further crystallization from $\text{CH}_2\text{Cl}_2/\text{PE}$ to afford **123** as pale grey-green powder; 50 % yield, mp 160-162 °C.

^1H -NMR (acetone- d_6): δ 3.85 (s, 3H, OCH_3), 3.92 (s, 3H, OCH_3), 5.64 (s, 2H, NCH_2), 6.37 (d, 1H, $J = 9.6$ Hz, H-3'), 6.80 (d, 1H, $J = 8.0$ Hz, H-5a), 6.82 (d, 1H, $J = 8.0$ Hz, H-5b), 6.88 (s, 1H), 6.98 (d, 1H, $J = 16.4$ Hz, CH=CH), 6.96-7.05 (m, 1H, H-6'), 7.10 (d, 1H, $J = 16.4$ Hz, CH=CH), 7.14 (d, 2H, $J = 6.8$ Hz, H-6), 7.13 (d, 1H, $J = 16.4$ Hz, CH=CH), 7.19 (d, 1H, $J = 15.6$ Hz, CH=CH), 7.20 (s, 2H, H-2), 7.23 (s, 1H, H-8'), 7.64 (d, 1H, $J = 8.4$ Hz, H-5'), 7.93 (d, 1H, $J = 9.6$ Hz, H-4').

^{13}C -NMR (acetone- d_6): δ 53.0, 56.4 (2), 100.1, 109.9, 110.6, 112.8, 115.8, 116.1, 116.2, 117.3, 119.2, 119.3, 121.3, 121.7, 124.0, 129.6, 129.8, 130.6, 130.8, 133.6, 143.7, 143.8, 144.3, 147.7, 148.4, 148.7 (2C), 151.6, 155.3, 160.6. ESI-MS (m/z): 545 (M + Na).

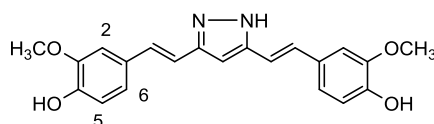
4-((3,5-bis(*E*)-4-hydroxy-3-methoxystyryl)-1*H*-pyrazol-1-yl)methyl)-2*H*-chromen-2-one (124**).**



125 (0.15 g, 0.41 mmol) and **100** (0.10 g, 0.41 mmol) were allowed to react according to the general procedure of curcumin pyrazole *N*-alkylation. The crude product was purified by flash chromatography (toluene/acetone

8.5:1.5) and further crystallization from $\text{CH}_2\text{Cl}_2/\text{PE}$ to afford **124** as beige powder; 35 % yield, mp 179-180 °C. ^1H -NMR (CDCl_3): δ 3.96 (s, 6H, OCH_3), 5.31 (s, 2H, NCH_2), 6.58 (d, 1H, $J = 15.6$ Hz, $\text{CH}=\text{CH}$), 6.74 (s, 1H), 6.85 (d, 2H, $J = 16.4$ Hz, $\text{CH}=\text{CH}$), 6.93 (d, 2H, $J = 8.0$ Hz, H-5), 6.92 (d, 1H, $J = 15.2$ Hz, $\text{CH}=\text{CH}$), 6.97 (s, 1H, H-3'), 7.01 (d, 1H, $J = 6.8$ Hz, H-8'), 7.06 (d, 2H, $J = 8.8$ Hz, H-6), 7.30 (s, 2H, H-2), 7.35-7.42 (m, 1H, H-6'), 7.62 (t, 1H, $J = 7.6$ Hz, H-7'), 7.69 (d, 1H, $J = 7.6$ Hz, H-5'). ^{13}C -NMR (CDCl_3): 53.0, 56.6 (2C), 100.3, 110.0, 110.6, 113.0, 115.9, 116.0, 116.5, 117.0, 119.2 (2C), 121.3, 121.7, 124.0, 129.7 (2C), 130.7, 131.0, 133.7, 143.7 (2C), 144.0, 147.5, 148.5, 148.8 (2C), 150.6, 155.0, 162.6. ESI-MS (m/z): 545 (M + Na).

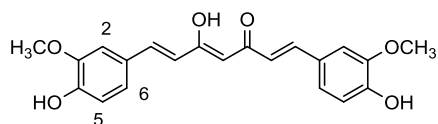
4,4'-((1*E*,1'*E*)-(1*H*-pyrazole-3,5-diyl)bis(ethene-2,1-diyl))bis(2-methoxyphenol) (125**).**



Curcumin **1a** (0.20 g, 0.54 mmol) and $\text{NH}_2\text{NH}_2 \cdot \text{H}_2\text{O}$ (0.13 mL, 2.70 mmol) reaction, according to the general procedure of cyclization (method **b**, 5 h of reflux), gave **125** as beige precipitate that was used in the next synthetic step without further purification; 50 % yield, mp 212-214 °C.¹⁵⁸ ^1H -NMR (acetone- d_6): δ 3.91 (s, 6H, OCH_3), 6.65 (s, 1H), 6.83 (d, 2H, $J = 8.0$ Hz,

H-5), 6.98 (dd, 2H, $J = 1.6$ and 7.2 Hz, H-6), 7.00 (d, 2H, $J = 16.4$ Hz, CH=CH), 7.12 (d, 2H, $J = 16.4$ Hz, CH=CH), 7.21 (d, 2H, $J = 2.0$ Hz, H-2).

(1E,4Z,6E)-5-hydroxy-1,7-bis(4-hydroxy-3-methoxyphenyl)hepta-1,4,6-trien-3-one (1a).

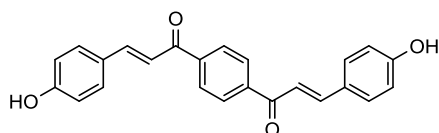


Reaction of pentane-2,4-dione (0.51 mL, 5.00 mmol) and vanillin (1.37 g, 9.00 mmol) according to the general procedure B of the Pabon reaction afforded the crude product that was purified by flash chromatography (PE/acetone, 7:3) and further crystallization from EtOH. Orange powder, 80 % yield, mp 181-183 °C. 155 1 H-NMR (CDCl₃): δ 3.93 (s, 6H, OCH₃), 5.78 (s, 1H, keto-enol-CH), 5.84 (br s, 2H, OH), 6.46 (d, 2H, $J = 16.0$ Hz, CH=CH), 6.92 (d, 2H, $J = 8.4$ Hz, H-5), 7.03 (d, 2H, $J = 1.4$ Hz, H-2), 7.10 (dd, 2H, $J = 1.4$ and 8.0 Hz, H-6), 7.57 (d, 2H, $J = 16.0$ Hz, CH=CH).

General procedure for the synthesis of 1,4- and 1,3-bis(chalcones) 126 and 129.

1,4- or 1,3-diacetylbenzene (1.00 mmol) and the 4-hydroxybenzaldehyde (1.5 molar equiv) were solubilized in EtOH (20.0 mL) and, after cooling to 0 °C, HCl_g was bubbled for 15 min. The resulting mixture was tightly stoppered and kept at 0 °C for 30 min and overnight at room temperature to promote the desired final compound crystallization.

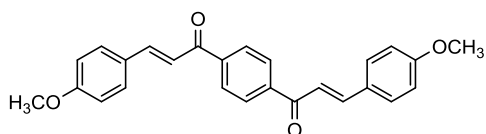
(2E,2'E)-1,1'-(1,4-phenylene)bis(3-(4-hydroxyphenyl)prop-2-en-1-one) (126).



1,4-diacetylbenzene (0.15 g, 0.92 mmol) and 4-hydroxybenzaldehyde (0.17g, 1.38 mmol) were allowed to react according to the general procedure for the synthesis of bischalcones to afford **126** as dark red-brown powder; 80 % yield, mp 314-316 °C. 153 1 H-NMR (DMSO-*d*₆): δ 6.86 (d, 4H, $J = 8.4$ Hz, Ar), 7.72 (d, 2H, $J = 15.6$ Hz, CH=CH), 7.77 (d, 4H, $J = 8.4$ Hz, Ar), 7.76 (d, 2H,

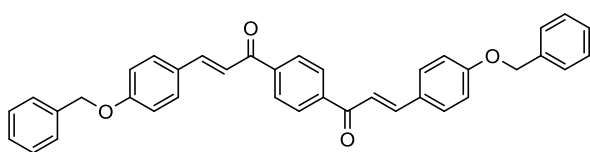
$J = 15.6$ Hz, CH=CH), 8.24 (s, 4H), 10.17 (br s, 2H, OH). ^{13}C -NMR (DMSO- d_6): δ 115.9 (4C), 118.5 (2C), 125.7 (2C), 128.6 (4C), 131.3 (4C), 140.9 (2C), 145.3 (2C), 160.4 (2C), 188.7 (2). ESI-MS (m/z): 393 (M + Na).

(2*E*,2'*E*)-1,1'-(1,4-phenylene)bis(3-(4-methoxyphenyl)prop-2-en-1-one)
(127).



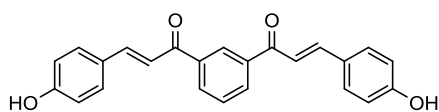
Reaction of **126** (0.15 g, 0.40 mmol) and iodomethane (0.08 mL, 0.88 mmol), in line with the general procedure of the Williamson reaction (8 h of reflux), gave the crude product that was crystallized from $\text{CH}_2\text{Cl}_2/\text{PE}$. Yellow powder, 45 % yield, mp 173-175 °C. 153 ^1H -NMR (CDCl_3): δ 3.88 (s, 6H, OCH_3), 6.97 (d, 4H, $J = 8.8$ Hz, Ar), 7.42 (d, 2H, $J = 15.6$ Hz, CH=CH), 7.64 (d, 4H, $J = 8.8$ Hz, Ar), 7.83 (d, 2H, $J = 15.6$ Hz, CH=CH), 8.11 (s, 4H). ^{13}C -NMR (CDCl_3): δ 55.5 (2C), 116.0 (4C), 118.4 (2C), 125.7 (2C), 128.4 (4C), 131.0 (4C), 141.4 (2C), 145.0 (2C), 160.8 (2C), 189.0 (2). ESI-MS (m/z): 421 (M + Na).

(2*E*,2'*E*)-1,1'-(1,4-phenylene)bis(3-(4-(benzyloxy)phenyl)prop-2-en-1-one)
(128).



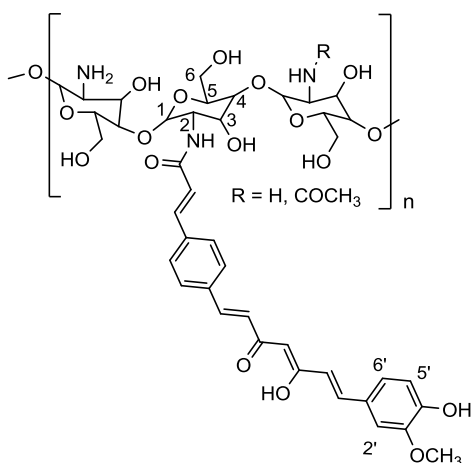
Reaction of **126** (0.15 g, 0.40 mmol) and benzyl bromide (0.11 mL, 0.88 mmol), in line with the general procedure of the Williamson reaction (12 h of reflux), gave the crude product that was crystallized from $\text{CH}_2\text{Cl}_2/\text{PE}$. Pale yellow powder, 40 % yield, mp 222-224 °C. ^1H -NMR (CDCl_3): δ 5.13 (s, 4H, OCH_2), 7.03 (d, 4H, $J = 8.8$ Hz, Ar), 7.26-7.45 (m, 12H, Bn and CH=CH), 7.63 (d, 4H, $J = 8.4$ Hz, Ar), 7.81 (d, 2H, $J = 15.6$ Hz, CH=CH), 8.09 (s, 4H). ^{13}C -NMR (CDCl_3): δ 70.4 (2C), 116.3 (4C), 119.0 (2C), 125.9 (2C), 127.8 (4C), 128.4 (2C), 128.5 (4C), 128.9 (4C), 131.3 (4C), 136.8 (2C), 140.9 (2C), 144.5 (2C), 160.7 (2C), 189.2 (2). ESI-MS (m/z): 573 (M + Na).

(2*E*,2'*E*)-1,1'-(1,3-phenylene)bis(3-(4-hydroxyphenyl)prop-2-en-1-one)
(129).



1,3-diacetylbenzene (0.15 g, 0.92 mmol) and 4-hydroxybenzaldehyde (0.17 g, 1.38 mmol) were allowed to react according to the general procedure for the synthesis of bischalcones to give **129** as dark red-brown powder; 62 % yield, mp 259-261 °C.¹⁵⁴ ¹H-NMR (DMSO-*d*₆): δ 6.76 (d, 2H, *J* = 8.0 Hz, Ar), 6.93 (d, 2H, *J* = 8.4 Hz, Ar), 7.13 (d, 2H, *J* = 8.0 Hz, Ar), 7.23 (d, 2H, *J* = 8.0 Hz, Ar), 7.67-7.72 (m, 1H), 7.72 (d, 2H, *J* = 15.6 Hz, CH=CH), 7.79 (d, 2H, *J* = 15.6 Hz, CH=CH), 8.24 (d, 1H, *J* = 7.6 Hz, Ar), 8.32 (d, 1H, *J* = 7.2 Hz, Ar), 8.65 (s, 1H). ¹³C-NMR (DMSO-*d*₆): δ 116.4 (4C), 123.0 (2C), 125.6 (2C), 129.9 (4C), 130.3, 131.4, 133.7 (2C), 139.9 (2C), 144.3 (2C), 159.9 (2C), 190.7 (2). ESI-MS (*m/z*): 393 (M + Na).

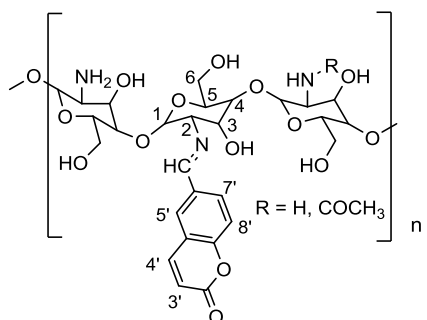
Curcumin/CS-based bioconjugate (130).



Chitosan % DD = 78 % (0.10 g) was dissolved in 15.0 mL of 1 % (v/v) CH₃COOH solution and was stirred at room temperature overnight. Then, the mixture was cooled to 0 °C, **72** (0.17 g, 0.44 mmol), EDC (0.08 g, 0.44 mmol) and DMAP (0.01g, 0.088 mmol) were added and the reaction mixture was stirred for 1 h. The obtained suspension was successively heated to 50 °C for 5 h and, after cooling to room temperature, was allowed to stir overnight. Excess of EDC and **72** precipitated from the mixture and was removed by *vacuum* filtration. The filtrate was alkalinized to pH 8 with NaHCO₃ and was centrifuged giving **130** as precipitate that was filtered off and washed with Et₂O. Beige powder (% DS = 14 %). ¹H-NMR (1 % CD₃COOD in D₂O): δ 2.01 (s, 3H, NHCOCH₃), 3.15 (br s, 1H, H-2 β-D-glucose), 3.57-3.97 (m, 8H, H-3,4,5,6 β-D-

glucose and OCH₃), 4.79 (s, 1H, H-1 β-D-glucose), 6.64 (d, 2H, *J* = 15.6 Hz, CH=CH), 6.83 (d, 2H, *J* = 6.8 Hz, Ar), 7.03 (d, 1H, *J* = 8.8 Hz, H-5'), 7.48 (d, 1H, *J* = 2.0 Hz, H-2'), 7.54 (d, 1H, *J* = 6.8 Hz, H-6'), 7.73 (d, 2H, *J* = 15.2 Hz, CH=CH), 7.80 (d, 2H, *J* = 7.6 Hz, Ar), 7.95 (d, 2H, *J* = 12.0 Hz, CH=CH), 9.76 (s, NHCO).

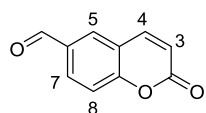
Coumarin/CS-based bioconjugate (**131**).



Chitosan % DD = 99 % (0.20 g) was dissolved in 20.0 mL of 1 % (v/v) CH₃COOH solution and the obtained mixture was stirred for 1 h at room temperature. Then, a solution of **132** (0.21 g, 1.20 mmol) in CH₃OH/acetone (5:1, 12.0 mL) was added dropwise and the resulting

mixture was stirred for 72 h. The aqueous phase was washed with EtOAc to remove the excess of **132** and was then alkalinized to pH 8 with NaHCO₃ to give the unreacted chitosan as precipitate that was removed by *vacuum* filtration. The filtrate was lyophilized and the resulting residue was washed with CH₃OH. The finally concentration of the washing methanol afforded **131** as white powder (% DS = 14 %). ¹H-NMR (1 % CD₃COOD in D₂O): δ 2.01 (s, 3H, NHCOCH₃), 2.65 (br s, 1H, H-2 β-D-glucose), 3.25-3.35 (m, 5H, H-3,4,5,6 β-D-glucose), 4.79 (br s, 1H, H-1 β-D-glucose), 6.49 (d, 1H, *J* = 9.6 Hz, H-3'), 7.39 (d, 1H, *J* = 8.4 Hz, H-8'), 7.69 (dd, 1H, *J* = 2.0 and 8.8 Hz, H-7'), 7.75 (d, 1H, *J* = 2.0 Hz, H-5'), 7.98 (d, 1H, *J* = 9.6 Hz, H-4'), 8.04 (s, 1H, HC=N).

2-oxo-2H-chromene-6-carbaldehyde (**132**)



A mixture of **98** (1.75 g, 7.30 mmol), HMTA (1.40 g, 10.00 mmol), formic acid 40 % (0.92 mL) in EtOH 60 % (40.0 mL) was refluxed for 48 h. Then, the solvent was removed under reduced pressure obtaining a residue that was diluted with CH₂Cl₂ (25.0 mL) and washed with water. The organic layer was separated and the aqueous phase was extracted twice with CH₂Cl₂ (2 x 30.0 mL). The combined organic phases were

washed with brine, dried over Na₂SO₄, filtered, and concentrated to dryness. The crude product was purified by flash column chromatography (EP/EtOAc, 7:3) to give **132** as white powder; 70 % yield, mp 168-170 °C. ¹H-NMR (CDCl₃): δ 6.53 (d, 1H, *J* = 9.6 Hz, 1H, H-3), 7.50 (d, 1H, *J* = 8.4 Hz, H-8), 7.80 (d, 1H, *J* = 9.6 Hz, H-4), 8.00-8.10 (m, 2H, H-5 and H-7), 9.99 (s, 1H, CHO).

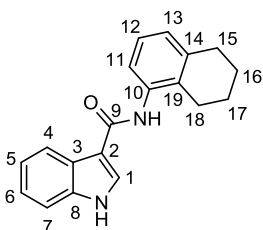
Acid and amine coupling reaction: general procedure for the synthesis of indole-based derivatives 133-143.

- a) Conventional heating: a suspension of EDC·HCl (1.3 molar equiv), DMAP (0.2 molar equiv) and TEA (1.3 molar equiv) in DMF (2.0 mL), stirred for 1 h at room temperature under N₂ atmosphere, was slowly added to the 1*H*-indole-3-carboxylic acid or 6-methoxy-1*H*-indole-3-carboxylic acid (1.00 mmol) solution in DMF (2.0 mL). The resulting solution was stirred for additional 2 h under inert atmosphere (N₂ gas) before the slowly addition of the appropriate amine solution (1.0 molar equiv) in DMF (1.0 mL). The reaction mixture was refluxed for 11-15 h and, after cooling to room temperature, was stirred overnight.
- b) Microwave irradiation: EDC·HCl (1.3 molar equiv), DMAP (0.2 molar equiv) and TEA (1.3 molar equiv) in DMF (2.0 mL) were stirred for 1 h at room temperature under N₂ atmosphere. The mixture was slowly added to the 1*H*-indole-3-carboxylic acid or 6-methoxy-1*H*-indole-3-carboxylic acid (1.00 mmol) solution in DMF (2.0 mL) and MW stirred the resulting solution for 15 min at 50 °C. Then, a solution of the appropriate amine (1.0 molar equiv) in DMF (1.0 mL) was slowly added and MW stirred the reaction mixture for 1-2 h at 200 °C.

In both cases, upon reaction completion, DMF was evaporated under reduced pressure to obtain a residue that was dissolved in EtOAc or CH₂Cl₂ and washed with water. The organic phase was separated, and the aqueous layer was extracted twice (2 x 25.0 mL) with EtOAc or CH₂Cl₂. The combined organic phases were

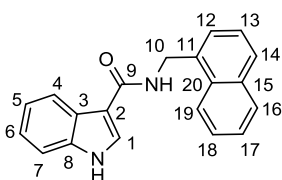
dried over anhydrous MgSO₄, filtered and concentrated affording a crude product that was purified by flash column chromatography.

***N*-(5,6,7,8-tetrahydronaphthalen-1-yl)-1*H*-indole-3-carboxamide (133).**



1*H*-indole-3-carboxylic acid (0.40 g, 2.48 mmol) and 5,6,7,8-tetrahydro-1-naphthalenamine (0.35 mL, 2.48 mmol) reaction, in agreement with the general procedure of coupling reaction (method **a**, 11 h of reflux), afforded the crude product that was purified by flash chromatography (*n*-hexane/EtOAc, 15:1). Off-white powder, 7 % yield, mp 222-224 °C. ¹H-NMR (DMSO-*d*₆): δ 1.69-1.75 (m, 4H, H-16 and H-17), 2.68-2.71 (m, 2H, H-18), 2.75-2.78 (m, 2H, H-15), 6.95 (dd, 1H, *J* = 1.3 and 7.6 Hz, H-13), 7.08-7.24 (m, 4H, H-5, H-6, H-11 and H-12), 7.47 (dd, 1H, *J* = 1.0 and 8.0 Hz, H-7), 8.13-8.17 (m, 1H, H-4), 8.23 (d, 1H, *J* = 2.7 Hz, H-1), 9.15 (s, 1H, CONH), 11.69 (d, 1H, *J* = 2.9 Hz, NH). ¹³C-NMR (DMSO-*d*₆): δ 22.5 (C-16), 22.6 (C-17), 24.5 (C-18), 29.3 (C-15), 110.5 (C-2), 111.9 (C-7), 120.6 (C-5), 121.1 (C-4), 122.0 (C-6), 123.9 (C-11), 125.0 (C-12), 126.2 (C-13), 126.4 (C-3), 128.4 (C-1), 132.4 (C-19), 136.2 (C-10), 136.5 (C-8), 137.4 (C-14), 163.3 (C-9). HPLC: purity 97 %; ES-MS (*m/z*): 291 (M + H).

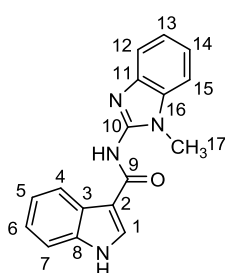
***N*-(naphthalen-1-ylmethyl)-1*H*-indole-3-carboxamide (134).**



1*H*-indole-3-carboxylic acid (0.25 g, 1.55 mmol) and 1-naphthylmethanamine (0.24 g, 1.55 mmol) reaction, in agreement with the general procedure of coupling reaction (method **b**, 1 h and 30 min of heating at 200 °C), afforded the crude product that was purified by flash chromatography (*n*-hexane/EtOAc, 9:1). Off-white powder, 6 % yield, mp 218-220 °C. ¹H-NMR (500 MHz, DMSO-*d*₆): δ 4.96 (d, 2H, *J* = 5.8 Hz, H-10), 7.08-7.17 (m, 2H, H-5 and H-6), 7.43 (d, 1H, *J* = 8.0 Hz, H-7), 7.48 (t, 1H, *J* = 7.5 Hz, H-13), 7.51-7.59 (m, 3H, H-12, H-17 and H-18), 7.85 (d, 1H, *J* = 8.1 Hz, H-14), 7.95 (dd, 1H, *J* = 1.6 and 7.9 Hz, H-16), 8.09 (d, 1H, *J* = 2.9 Hz, H-1), 8.19 (d, 1H, *J* = 7.7 Hz, H-4), 8.25-8.21 (m, 1H, H-19),

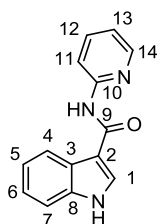
8.45 (t, 1H, $J = 5.8$ Hz, CONH), 11.56 (s, 1H, NH). ^{13}C -NMR (126 MHz, DMSO- d_6): δ 39.8 (C-10), 110.4 (C-2), 111.8 (C-7), 120.4 (C-5), 121.1 (C-4), 121.9 (C-6), 123.6 (C-19), 125.3 (C-12), 125.4 (C-17), 125.7 (C-13), 126.2 (C-18), 126.3 (C-3), 127.3 (C-14), 127.9 (C-1), 128.5 (C-16), 130.9 (C-20), 133.3 (C-15), 135.5 (C-11), 136.1 (C-8), 164.5 (C-9). HPLC: purity 97 %; ESI-MS (m/z): 301 (M + H).
See appendix for 2D spectra: ^1H , ^1H -COSY, ^1H , ^{13}C -HSQC and ^1H , ^{13}C -HMBC (Figs. A4a, A4b and A4c, respectively).

***N*-(1-methyl-1*H*-benzo[d]imidazol-2-yl)-1*H*-indole-3-carboxamide (135).**



1*H*-indole-3-carboxylic acid (0.25 g, 1.55 mmol) and 1-methyl-1*H*-benzimidazol-2-amine (0.23 g, 1.55 mmol) reaction, in agreement with the general procedure of coupling reaction (method **b**, 1 h of heating at 200 °C), afforded the crude product that was purified a first time through Isolera (automated flash chromatography system) using $\text{CH}_2\text{Cl}_2/\text{CH}_3\text{OH}$ in gradient and then by flash chromatography (*n*-hexane/EtOAc, 8:2). Off-white powder, 17 % yield, mp 223-225 °C. ^1H -NMR (DMSO- d_6): δ 3.71 (s, 3H, H-17), 7.13-7.23 (m, 4H, H-5, H-6, H-14 and H-15), 7.40 (d, 1H, $J = 7.4$ Hz, H-7), 7.42-7.46 (m, 1H, H-13), 7.46-7.51 (m, 1H, H-12), 8.10 (d, 1H, $J = 2.8$ Hz, H-1), 8.43 (dd, 1H, $J = 3.1$ and 6.3 Hz, H-4), 11.54-11.59 (m, 1H, NH), 12.57 (s, 1H, CONH). ^{13}C -NMR (DMSO- d_6): δ 28.1 (C-17), 108.9 (C-7), 111.4 (C-12), 111.9 (C-13), 116.0 (C-2), 120.3 (C-5), 121.5 (C-4), 121.6 (C-15), 122.1 (C-6), 122.2 (C-14), 126.4 (C-3), 129.1 (C-16), 130.1 (C-11), 131.2 (C-1), 136.7 (C-8), 152.3 (C-10), 173.4 (C-9). HPLC: purity > 99 %; ESI-MS (m/z): 291 (M + H).

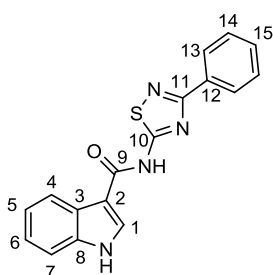
***N*-(pyridin-2-yl)-1*H*-indole-3-carboxamide (136).**



1*H*-indole-3-carboxylic acid (0.25 g, 1.55 mmol) and 2-pyridinamine (0.15 g, 1.55 mmol) reaction, in agreement with the general procedure of coupling reaction (method **b**, 1 h of heating at 200 °C), afforded the crude product that was purified by flash

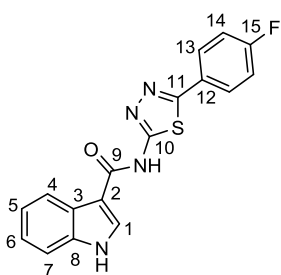
chromatography (*n*-hexane/EtOAc, 7:3). Off-white powder, 8 % yield, mp 233-235 °C. ¹H-NMR (DMSO-*d*₆): δ 7.08 (dd, 1H, *J* = 5.2 and 6.8 Hz, H-13), 7.14-7.22 (m, 2H, H-5 and H-6), 7.44-7.48 (m, 1H, H-7), 7.77-7.81 (m, 1H, H-12), 8.23-8.26 (m, 1H, H-11), 8.28 (d, 1H, *J* = 8.5 Hz, H-4), 8.32-8.36 (m, 1H, H-14), 8.55 (s, 1H, H-1), 10.30 (s, 1H, CONH), 11.80 (s, 1H, NH). ¹³C-NMR (DMSO-*d*₆): δ 109.8 (C-2), 112.0 (C-7), 114.1 (C-14), 118.8 (C-13), 120.9 (C-5), 121.1 (C-4), 122.3 (C-6), 126.6 (C-3), 129.8 (C-1), 136.3 (C-8), 137.9 (C-12), 147.7 (C-11), 152.8 (C-10), 163.6 (C-9). HPLC: purity > 99 %; ESI-MS (*m/z*): 238 (M + H).

***N*-(3-phenyl-1,2,4-thiadiazol-5-yl)-1*H*-indole-3-carboxamide (137).**



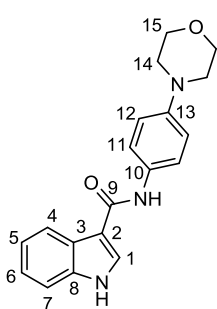
1*H*-indole-3-carboxylic acid (0.25 g, 1.55 mmol) and 3-phenyl-1,2,4-thiadiazol-5-ylamine (0.27 g, 1.55 mmol) reaction, in agreement with the general procedure of coupling reaction (method **b**, 1 h of heating at 200 °C), afforded the crude product that was purified by flash chromatography (*n*-hexane/EtOAc, 9:1) and further washing with Et₂O. White powder, 3 % yield, mp 303-305 °C. ¹H-NMR (500 MHz, DMSO-*d*₆): δ 7.21-7.29 (m, 2H, H-5 and H-6), 7.50-7.57 (m, 4H, H-7, H-14 and H-15), 8.20-8.23 (m, 2H, H-13), 8.23-8.26 (m, 1H, H-4), 8.68 (d, 1H, *J* = 3.0 Hz, H-1), 12.12 (d, 1H, *J* = 3.2 Hz, NH), 13.11 (s, 1H, CONH). ¹³C-NMR (126 MHz, DMSO-*d*₆): δ 107.1 (C-2), 112.4 (C-7), 120.8 (C-4), 121.8 (C-5), 123.0 (C-6), 126.2 (C-3), 127.4 (2C, C-13), 128.9 (2C, C-14), 130.1 (C-15), 131.6 (C-1), 133.0 (C-12), 136.4 (C-8), 163.5 (C-9), 176.1 (C-10), 166.6 (C-11). HPLC: purity 99 %; ESI-MS (*m/z*): 321 (M + H).

***N*-(5-(4-fluorophenyl)-1,3,4-thiadiazol-2-yl)-1*H*-indole-3-carboxamide (138).**



1*H*-indole-3-carboxylic acid (0.25 g, 1.55 mmol) and 5-(4-fluorophenyl)-1,3,4-thiadiazol-2-amine (0.30 g, 1.55 mmol) reaction, in agreement with the general procedure of coupling reaction (method **b**, 2 h of heating at 200 °C), afforded the crude product that was purified two times by flash chromatography (*n*-hexane/EtOAc, 7:3; CH₂Cl₂/CH₃OH, 9.9:0.1). White powder, 7 % yield, mp 285-287 °C. ¹H-NMR (DMSO-*d*₆): δ 7.13 (m, 2H, H-5 and H-6), 7.32-7.39 (m, 2H, H-14), 7.44-7.49 (m, 1H, H-7), 7.97-8.02 (m, 2H, H-13), 8.30 (dd, 1H, *J* = 2.3 and 6.7 Hz, H-4), 8.42 (s, 1H, H-1), 11.84 (s, 1H, NH), 12.60 (s, 1H, CONH). ¹³C-NMR (DMSO-*d*₆): δ 112.0 (C-7), 116.2 (d, 2C, *J* = 21.9 Hz, C-14), 120.7 (C-5), 121.5 (C-4), 122.0 (C-6), 126.6 (C-3), 128.5 (C-2), 128.5 (d, 2C, *J* = 8.2 Hz, C-13), 130.2 (C-1), 136.4 (C-8), 157.9 (C-10), 161.4 (C-12), 162.7 (d, *J* = 247.5, C-15), 163.9 (C-11), 165.5 (C-9). HPLC: purity 98 %; ESI-MS (*m/z*): 339 (M + H).

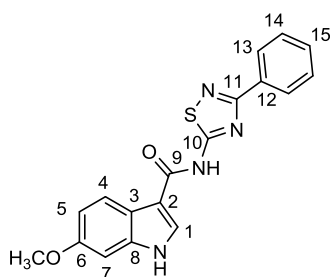
***N*-(4-morpholinophenyl)-1*H*-indole-3-carboxamide (139).**



1*H*-indole-3-carboxylic acid (0.25 g, 1.55 mmol) and 4-(4-morpholinyl)aniline (0.28 g, 1.55 mmol) reaction, in agreement with the general procedure of coupling reaction (method **b**, 1 h of heating at 200 °C), afforded the crude product that was purified by flash chromatography (CH₂Cl₂/CH₃OH, 9.9:0.1) and further washing with Et₂O. Off-white powder, 17 % yield, mp 281-283 °C. ¹H-NMR (DMSO-*d*₆): δ 3.03-3.09 (m, 4H, H-14), 3.70-3.77 (m, 4H, H-15), 6.89-6.95 (m, 2H, H-12), 7.10-7.20 (m, 2H, H-5 and H-6), 7.47-7.59 (m, 1H, H-7), 7.59-7.65 (m, 2H, H-11), 8.17-8.21 (m, 1H, H-4), 8.24 (d, 1H, *J* = 3.0 Hz, H-1), 9.55 (s, 1H, CONH), 11.67 (d, 1H, *J* = 3.0 Hz, NH). ¹³C-NMR (DMSO-*d*₆): δ 49.1 (2C, C-14), 66.2 (2C, C-15), 110.7 (C-2), 111.9 (C-7), 115.4 (2C, C-12), 120.5 (C-4), 121.0 (2C, C-11), 121.1 (C-5), 122.2 (C-6), 126.4 (C-3),

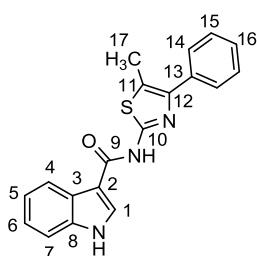
128.2 (C-1), 132.1 (C-10), 136.2 (C-8), 146.9 (C-13), 162.9 (C-9). HPLC: purity 97 %; ESI-MS (m/z): 322 (M + H). See appendix for 2D spectra: ^1H , ^1H -COSY, ^1H , ^{13}C -HSQC and ^1H , ^{13}C -HMBC (Figs. A5a, A5b and A5c, respectively).

6-methoxy-*N*-(3-phenyl-1,2,4-thiadiazol-5-yl)-1*H*-indole-3-carboxamide (140).



6-methoxy-1*H*-indole-3-carboxylic acid (0.25 g, 1.31 mmol) and 3-phenyl-1,2,4-thiadiazol-5-ylamine (0.23 g, 1.31 mmol) reaction, in agreement with the general procedure of coupling reaction (method **b**, 2 h and 20 min of heating at 200 °C), afforded the crude product that was purified by Isolera using *n*-hexane/EtOAc in gradient and further washing with Et₂O. White powder, 6 % yield, mp 272-274 °C. ^1H -NMR (300 MHz, acetone-*d*₆): δ 3.84 (s, 3H, OCH₃). 6.95 (dd, 1H, J = 2.3 and 8.8 Hz, H-5), 7.10 (d, 1H, J = 2.2 Hz, H-7), 7.42-7.54 (m, 3H, H-14 and H-15), 8.29-8.20 (m, 3H, H-4 and H-13), 8.54-8.59 (m, 1H, H-1), 11.09 (s, 1H, NH), 11.81 (s, 1H, CONH). ^{13}C -NMR (75 MHz, acetone-*d*₆): δ 55.7 (OCH₃), 96.0 (C-7), 109.0 (C-2), 112.9 (C-5), 121.5 (C-3), 122.8 (C-4), 128.5 (2C, C-13), 129.4 (2C, C-14), 130.3 (C-1), 130.7 (C-15), 134.4 (C-12), 138.6 (C-8), 158.3 (C-6), 164.3 (C-9), 167.9 (C-11), 176.9 (C-10). ESI-MS (m/z): 351 (M + H). See appendix for 2D spectra: ^1H , ^1H -COSY and ^1H , ^{13}C -HMBC (Figs. A6a and A6b, respectively).

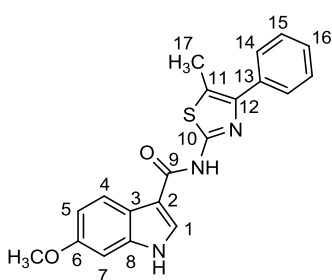
***N*-(5-methyl-4-phenylthiazol-2-yl)-1*H*-indole-3-carboxamide (141).**



1*H*-indole-3-carboxylic acid (0.25 g, 1.55 mmol) and 5-methyl-4-phenyl-1,3-thiazol-2-amine (0.30 g, 1.55 mmol) reaction, in agreement with the general procedure of coupling reaction (method **a**, 15 h of reflux), afforded the crude product that was purified by flash chromatography (*n*-hexane/EtOAc, 9.5:0.5) and further semipreparative TLC (CH₂Cl₂). White powder, 4 % yield, mp 299-301 °C. ^1H -NMR (300 MHz, DMSO-*d*₆): δ 2.50 (s, 3H, H-17), 7.15-7.26 (m, 2H, H-5 and H-6), 7.31-7.39 (m, 1H, H-16), 7.42-7.52 (m, 3H, H-7

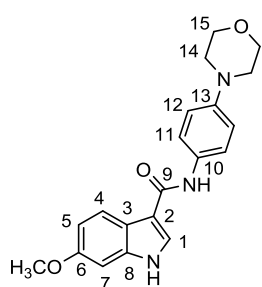
and H-15), 7.66-7.73 (m, 2H, H-14), 8.21-8.28 (m, 1H, H-4), 8.58 (d, 1H, $J = 3.0$ Hz, H-1), 11.92 (m, 1H, NH), 12.10 (s, 1H, CONH). $^{13}\text{C-NMR}$ (75 MHz, $\text{DMSO-}d_6$): δ 11.8 (C-17), 108.1 (C-2), 112.1 (C-7), 120.3 (C-11), 121.0 (C-4), 121.2 (C-5), 122.6 (C-6), 126.4 (C-3), 127.1 (C-16), 128.0 (2C, C-14), 128.3 (2C, C-15), 130.2 (C-1), 135.1 (C-13), 136.4 (C-8), 144.0 (C-12), 154.8 (C-10), 162.3 (C-9). ESI-MS (m/z): 334 (M + H).

6-methoxy-*N*-(5-methyl-4-phenylthiazol-2-yl)-1*H*-indole-3-carboxamide (142).



6-methoxy-1*H*-indole-3-carboxylic acid (0.25 g, 1.31 mmol) and 5-methyl-4-phenyl-1,3-thiazol-2-amine (0.25 g, 1.31 mmol) reaction, in agreement with the general procedure of coupling reaction (method **b**, 2 h and 20 min of heating at 200 °C), afforded the crude product that was purified by flash chromatography (*n*-hexane/EtOAc, 9:1). White powder, 16 % yield, mp 296-298 °C. $^1\text{H-NMR}$ (300 MHz, $\text{DMSO-}d_6$): δ 2.49 (s, 3H, H-17), 3.79 (s, 3H, OCH_3), 6.84 (dd, 1H, $J = 2.3$ and 8.8 Hz, H-5), 6.96 (d, 1H, $J = 2.3$ Hz, H-7), 7.30-7.37 (m, 1H, H-16), 7.46 (t, 2H, $J = 7.6$ Hz, H-15), 7.65-7.72 (m, 2H, H-14), 8.08 (d, 1H, $J = 8.7$ Hz, H-4), 8.45 (d, 1H, $J = 3.0$ Hz, H-1), 11.70 (s, 1H, NH), 12.04 (s, 1H, CONH). $^{13}\text{C-NMR}$ (75 MHz, $\text{DMSO-}d_6$): δ 11.8 (C-17), 55.2 (OCH_3), 95.0 (C-7), 108.1 (C-2), 111.3 (C-5), 120.3 (C-11), 120.4 (C-3), 121.6 (C-4), 127.1 (C-16), 128.0 (2C, C-14), 128.3 (2C, C-15), 129.1 (C-1), 135.1 (C-13), 137.1 (C-8), 144.0 (C-12), 154.8 (C-10), 156.2 (C-6), 162.3 (C-9). ESI-MS (m/z): 364 (M + H).

6-methoxy-*N*-(4-morpholinophenyl)-1*H*-indole-3-carboxamide (143).



6-methoxy-1*H*-indole-3-carboxylic acid (0.25 g, 1.31 mmol) and 4-(4-morpholinyl)aniline (0.23 g, 1.31 mmol) reaction, in agreement with the general procedure of coupling reaction (method **b**, 1 h and 40 min of heating at 200 °C), afforded the crude product that was purified by Isolera using CH₂Cl₂/CH₃OH in gradient and further washing with Et₂O.

White powder, 2 % yield, mp 288-290 °C. ¹H-NMR (500 MHz, acetone-*d*₆): δ 3.09 (t, 4H, *J* = 4.7 Hz, H-14), 3.74-3.79 (m, 4H, H-15), 3.81 (s, 3H, OCH₃), 6.83 (dd, 1H, *J* = 2.3 and 8.7 Hz, H-5), 6.93 (d, 2H, *J* = 8.7 Hz, H-12), 7.00 (d, 1H, *J* = 2.3 Hz, H-7), 7.69 (d, 2H, *J* = 8.7 Hz, H-11), 8.01 (d, 1H, *J* = 2.8 Hz, H-1), 8.18 (d, 1H, *J* = 8.8 Hz, H-4), 8.87 (s, 1H, CONH), 10.55 (s, 1H, NH). ¹³C-NMR (126 MHz, acetone-*d*₆): δ 50.7 (2C, C-14), 55.7 (OCH₃), 67.5 (2C, C-15), 95.5 (C-7), 111.8 (C-5), 113.0 (C-2), 116.7 (2C, C-12), 121.7 (2C, C-11), 121.8 (C-4), 123.0 (C-1), 126.8 (C-3), 133.6 (C-10), 138.4 (C-8), 148.4 (C-13), 157.8 (C-6), 163.9 (C-9). ESI-MS (*m/z*): 352 (M + H).

7. Appendix

7.1. 1D and 2D NMR SAMPLE COMPOUNDS

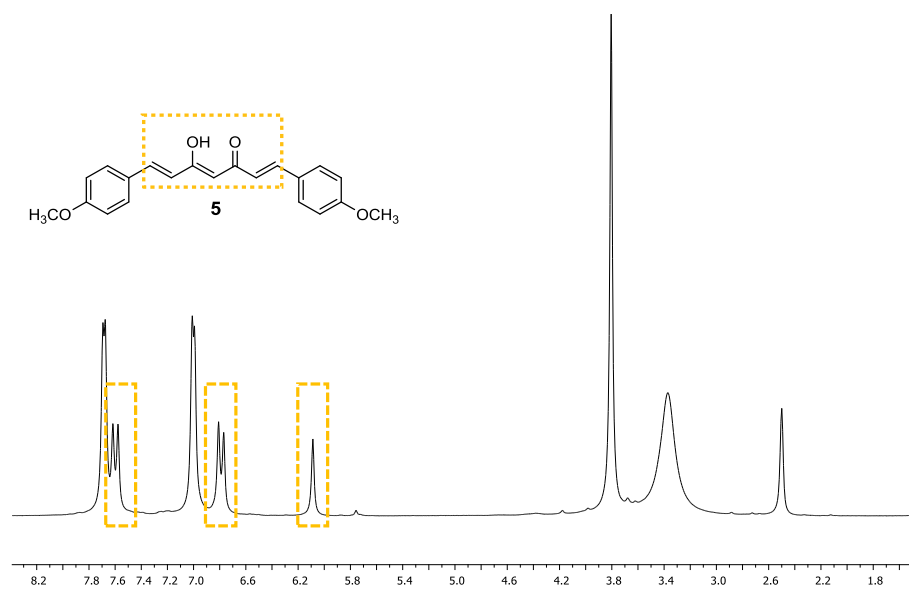


Figure A1a. 400 MHz, ^1H -NMR spectra of compound **5** in $\text{DMSO-}d_6$.

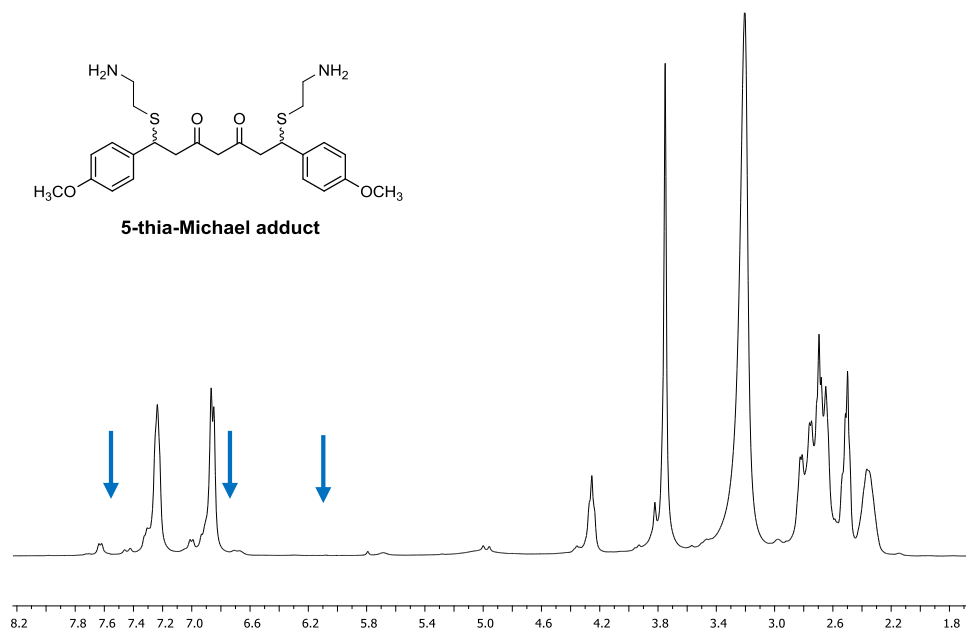


Figure A1b. 400 MHz, ^1H -NMR spectrum of the **5**-positive assay in $\text{DMSO-}d_6$ with a 1:2 stoichiometric ratio of **5**/cysteamine.

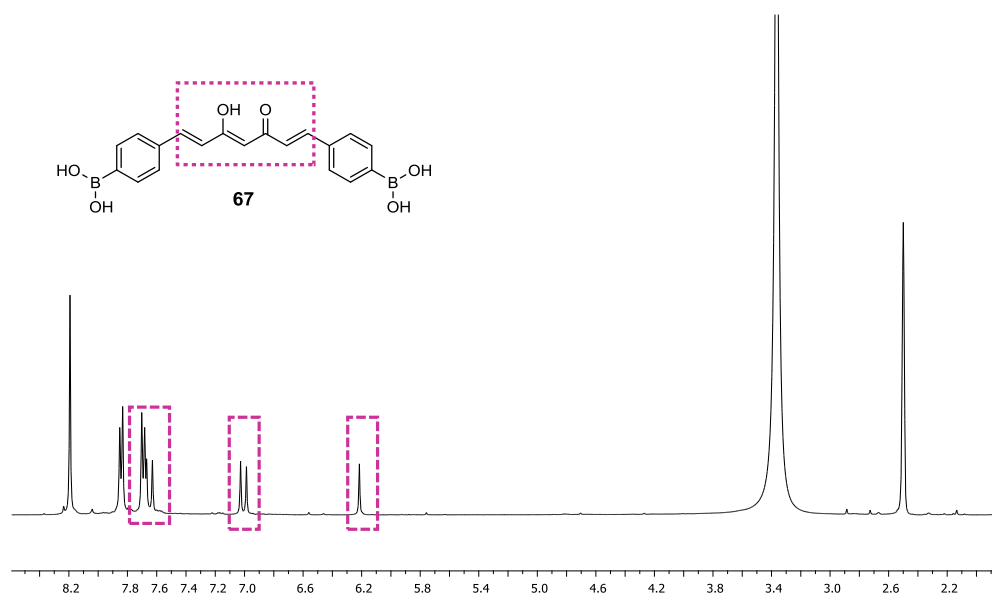


Figure A2a. 400 MHz, $^1\text{H-NMR}$ spectra of compound **67** in $\text{DMSO-}d_6$.

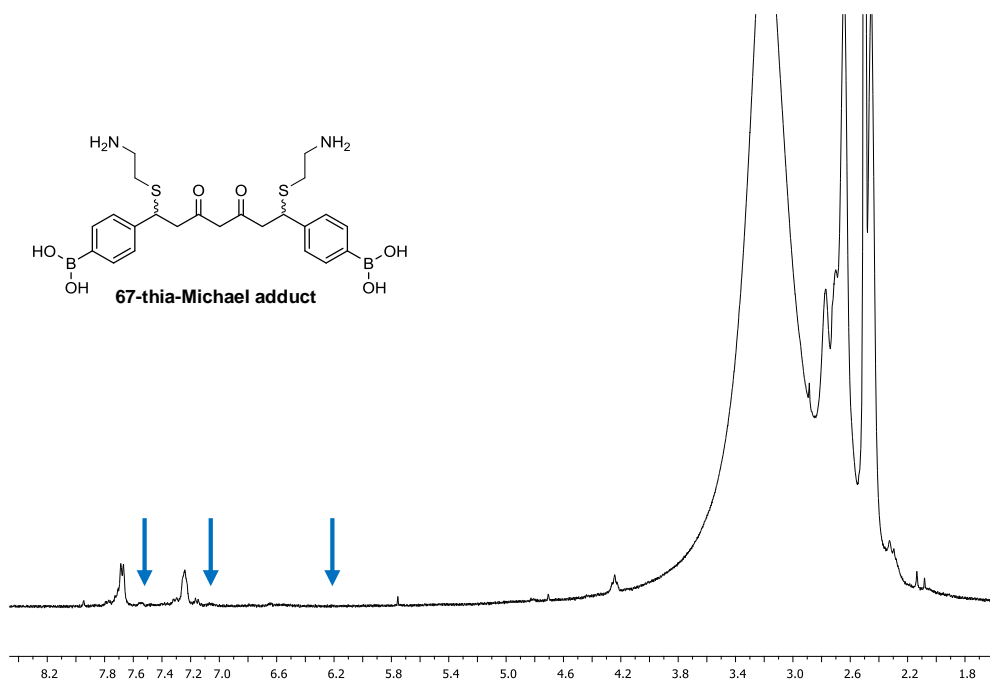


Figure A2b. 400 MHz, $^1\text{H-NMR}$ spectrum of the **67**-positive assay in $\text{DMSO-}d_6$ with a 1:2 stoichiometric ratio of **67**/cysteamine.

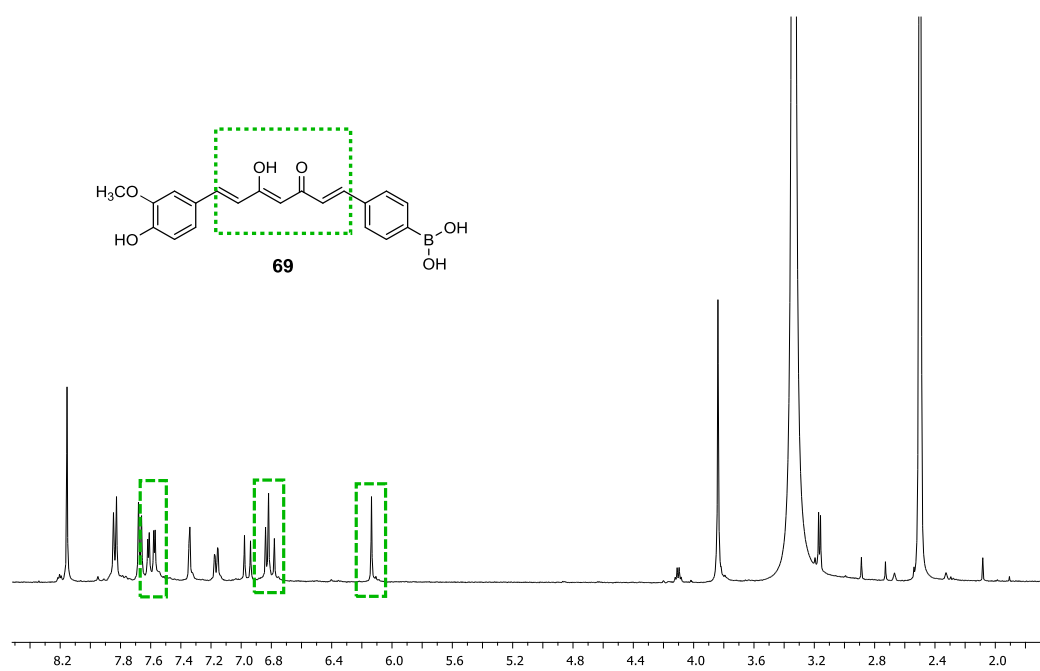


Figure A3a. 400 MHz, $^1\text{H-NMR}$ spectra of compound **69** in $\text{DMSO-}d_6$.

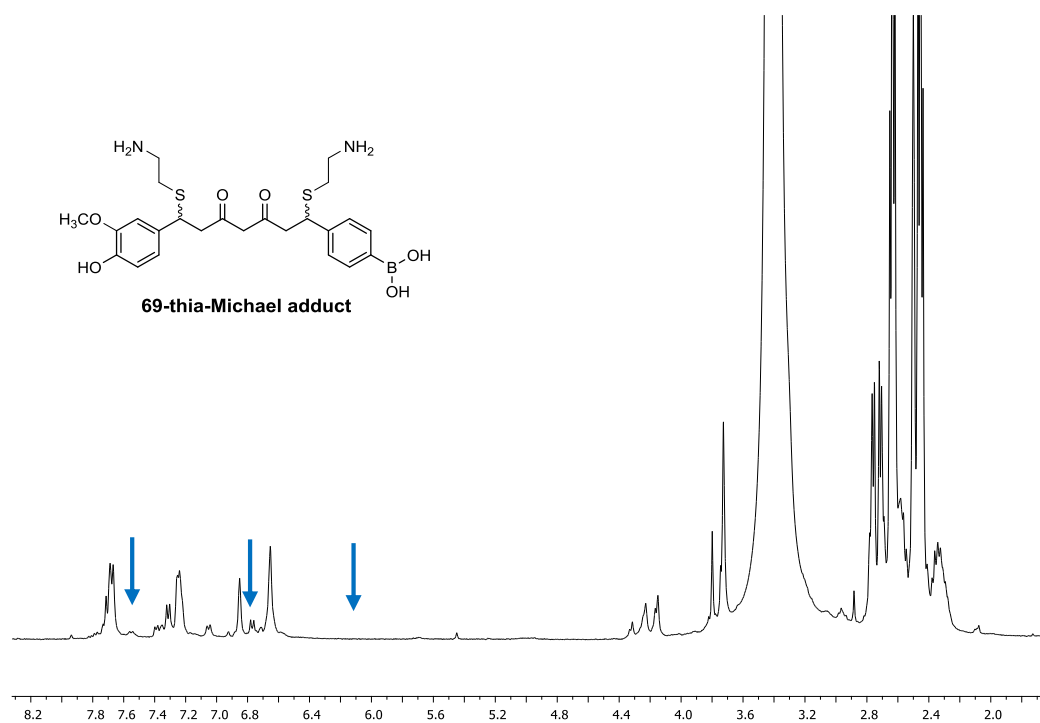
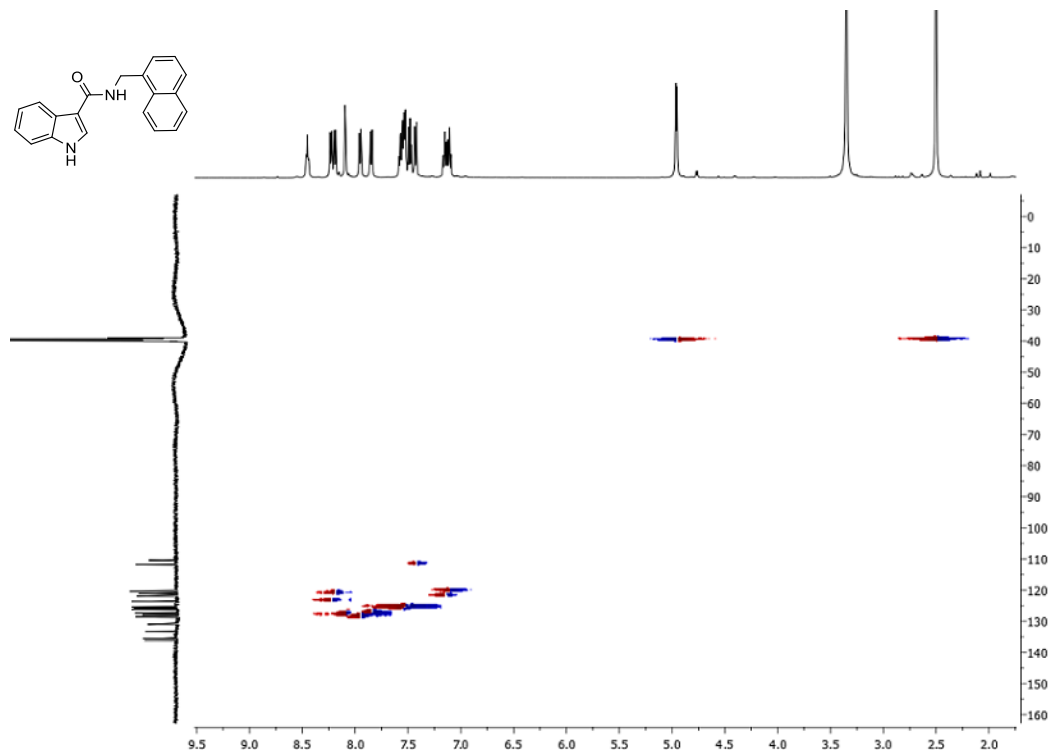
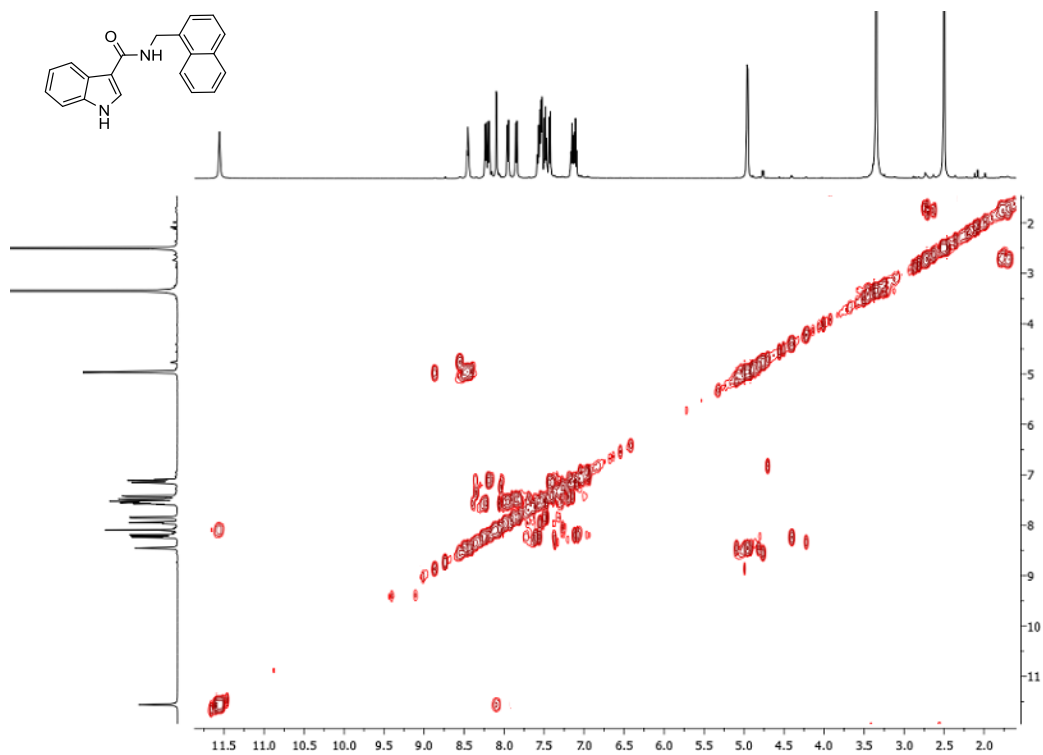


Figure A3b. 400 MHz, $^1\text{H-NMR}$ spectrum of the **69**-positive assay in $\text{DMSO-}d_6$ with a 1:2 stoichiometric ratio of **69**/cysteamine.



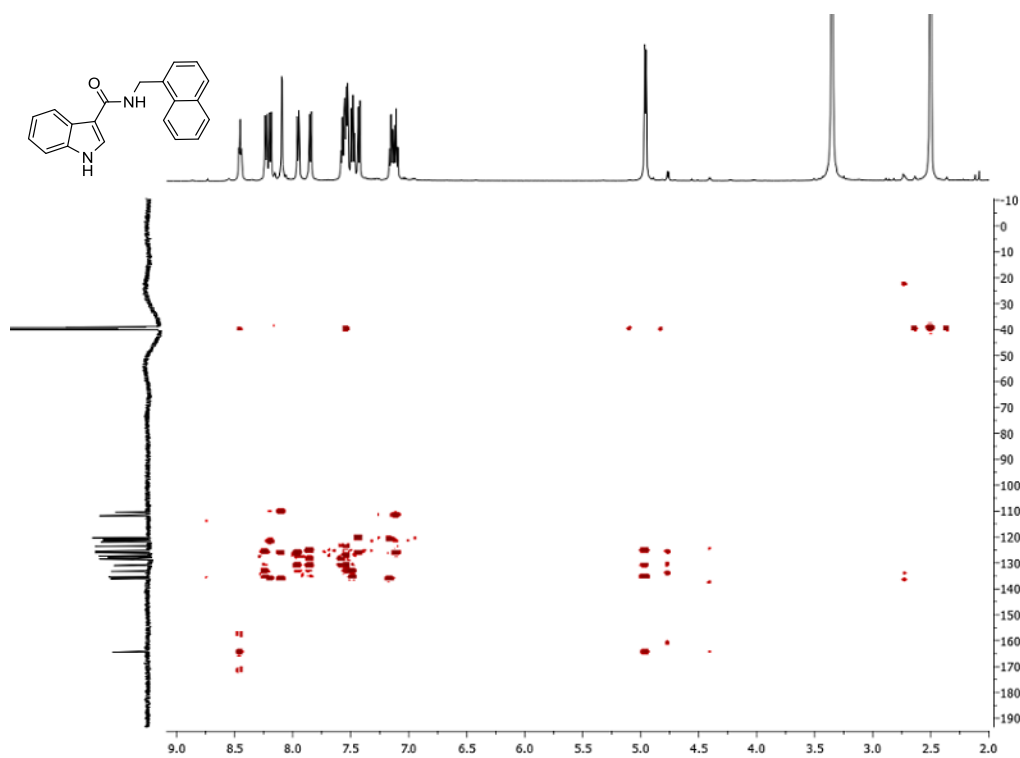


Figure A4c. 500 MHz, ^1H , ^{13}C -HMBC spectrum of compound **134** in $\text{DMSO-}d_6$

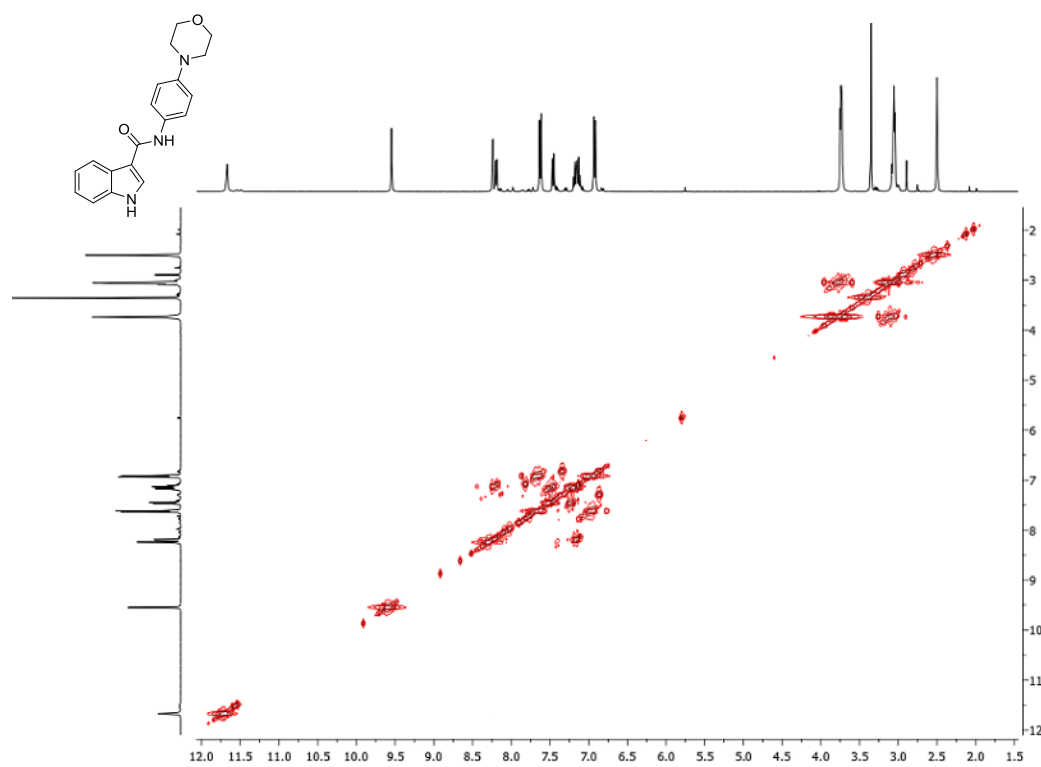


Figure A5a. 400 MHz, ^1H , ^1H -COSY spectrum of compound **139** in $\text{DMSO-}d_6$.

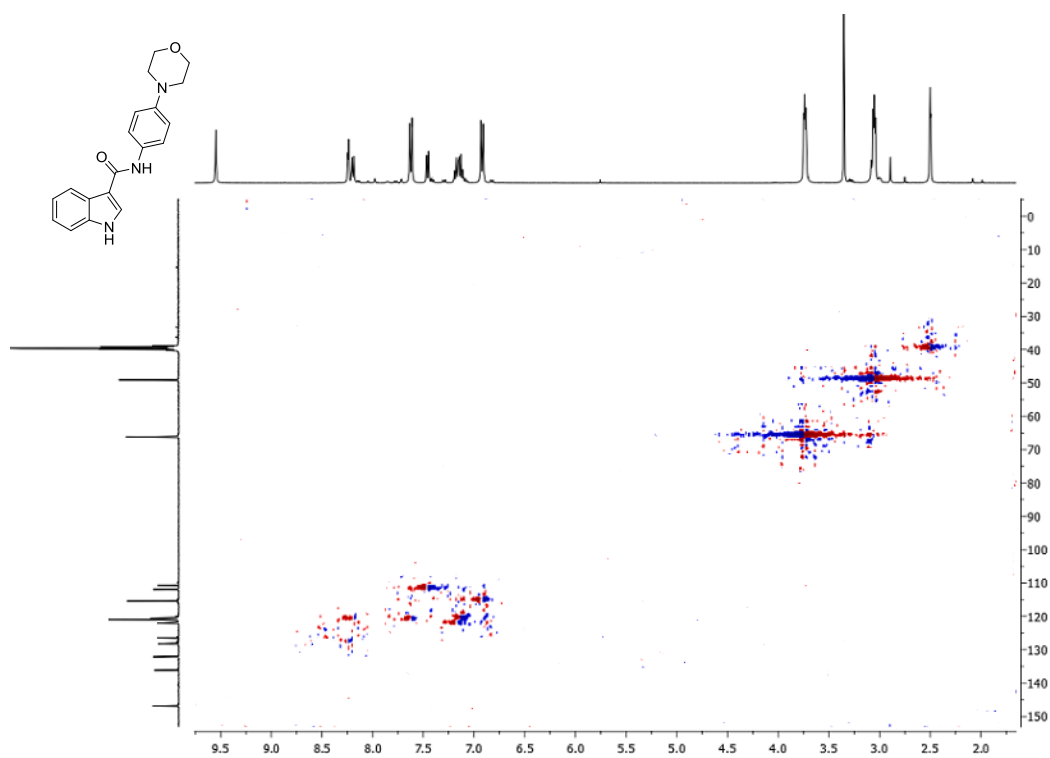


Figure A5b. 400 MHz, ^1H , ^{13}C -HSQC spectrum of compound **139** in $\text{DMSO-}d_6$.

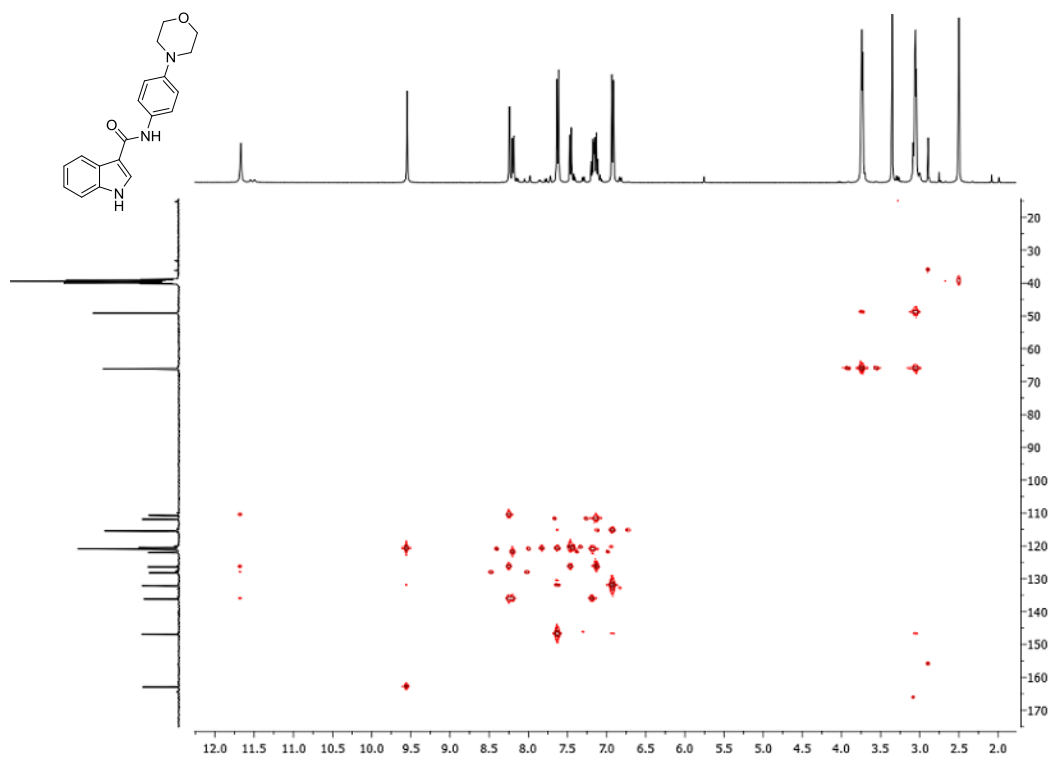
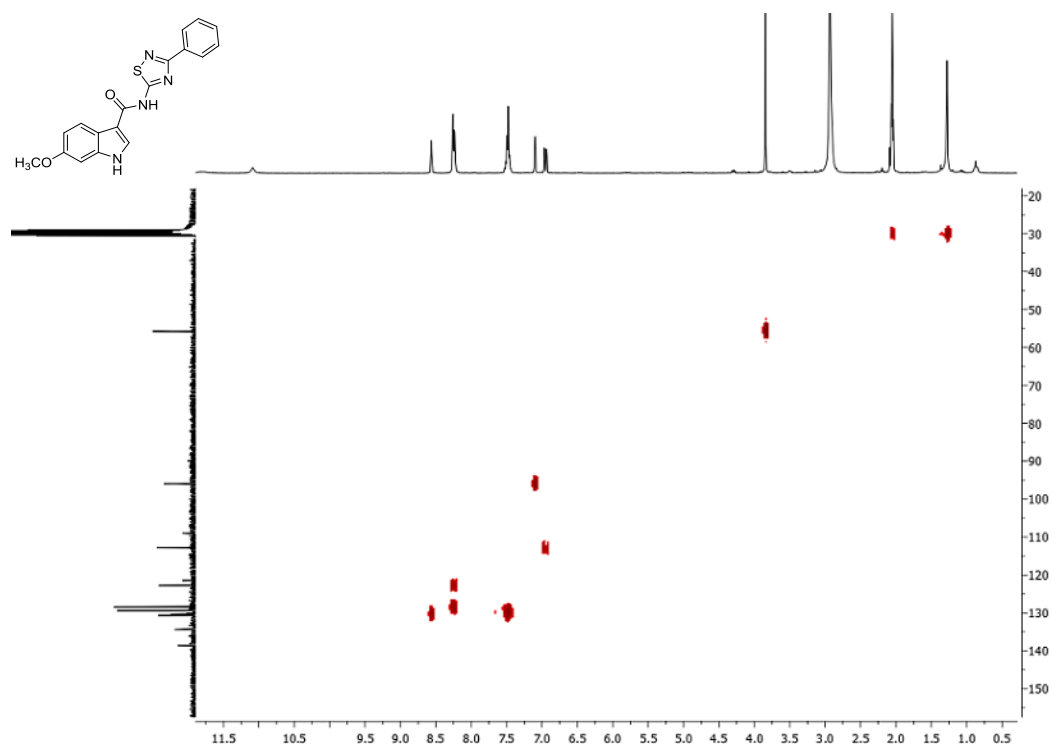
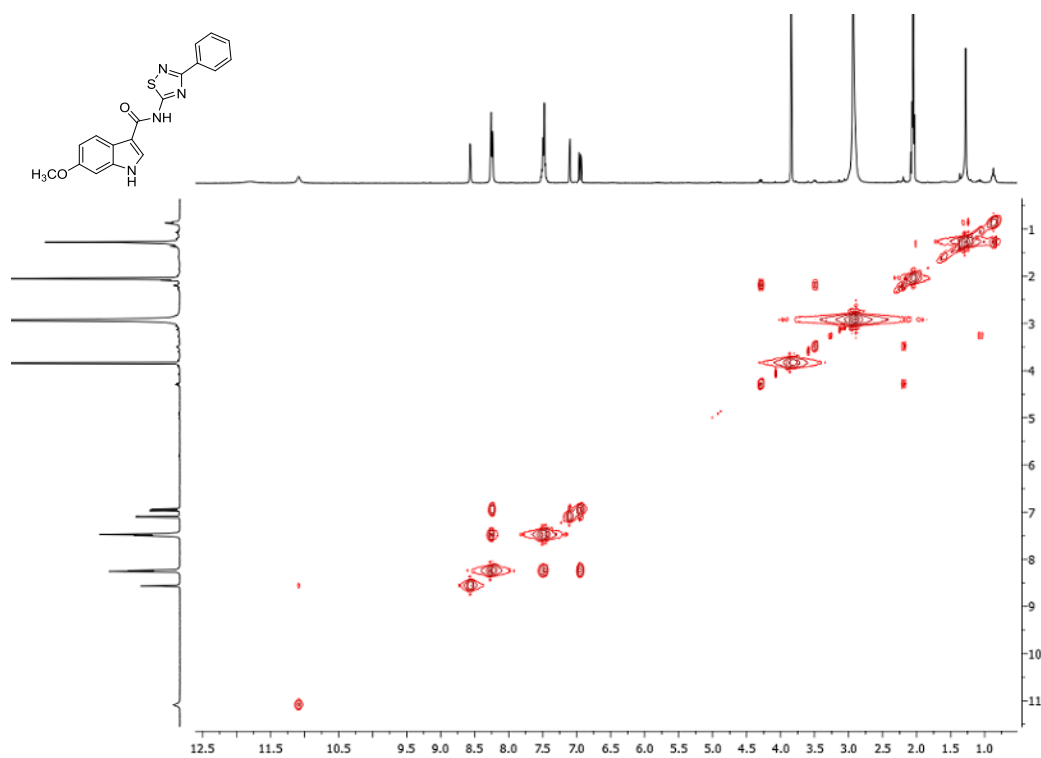


Figure A5c. 400 MHz, ^1H , ^{13}C -HMBC spectrum of compound **139** in $\text{DMSO-}d_6$.



8. *Bibliographic references*

1. Dulsat, C., A report from the 65th Annual Meeting of the American Academy of Neurology (March 16-23, 2013, San Diego, California, USA). *Drugs Today (Barc)* **2013**, *49* (5), 341-5.
2. Selkoe, D. J., Developing preventive therapies for chronic diseases: lessons learned from Alzheimer's disease. *Nutr. Rev.* **2007**, *65* (12 Pt 2), S239-43.
3. a) Gauthier, S.; Feldman, H.; Hecker, J.; Vellas, B.; Ames, D.; Subbiah, P.; Whalen, E.; Emir, B.; Group, D. M. S. I., Efficacy of donepezil on behavioral symptoms in patients with moderate to severe Alzheimer's disease. *Int. Psychogeriatr.* **2002**, *14* (4), 389-404; b) Silvestrelli, G.; Lanari, A.; Parnetti, L.; Tomassoni, D.; Amenta, F., Treatment of Alzheimer's disease: from pharmacology to a better understanding of disease pathophysiology. *Mech. Ageing Dev.* **2006**, *127* (2), 148-57.
4. Price, B. H.; Gurvit, H.; Weintraub, S.; Geula, C.; Leimkuhler, E.; Mesulam, M., Neuropsychological patterns and language deficits in 20 consecutive cases of autopsy-confirmed Alzheimer's disease. *Arch. Neurol.* **1993**, *50* (9), 931-7.
5. Esteban-Santillan, C.; Praditsuwan, R.; Ueda, H.; Geldmacher, D. S., Clock drawing test in very mild Alzheimer's disease. *J. Am. Geriatr. Soc.* **1998**, *46* (10), 1266-9.
6. Walsh, D. M.; Selkoe, D. J., Deciphering the molecular basis of memory failure in Alzheimer's disease. *Neuron* **2004**, *44* (1), 181-93.
7. a) Gómez-Isla, T.; Hollister, R.; West, H.; Mui, S.; Growdon, J. H.; Petersen, R. C.; Parisi, J. E.; Hyman, B. T., Neuronal loss correlates with but exceeds neurofibrillary tangles in Alzheimer's disease. *Ann. Neurol.* **1997**, *41* (1), 17-24; b) Khachaturian, Z. S., Diagnosis of Alzheimer's disease. *Arch. Neurol.* **1985**, *42* (11), 1097-105; c) Uylings, H. B.; de Brabander, J. M., Neuronal changes in normal human aging and Alzheimer's disease. *Brain Cogn.* **2002**, *49* (3), 268-76.
8. Di Martino, R. M.; De Simone, A.; Andrisano, V.; Bisignano, P.; Bisi, A.; Gobbi, S.; Rampa, A.; Fato, R.; Bergamini, C.; Perez, D. I.; Martinez, A.; Bottegoni, G.; Cavalli, A.; Belluti, F., Versatility of the Curcumin Scaffold:

- Discovery of Potent and Balanced Dual BACE-1 and GSK-3 β Inhibitors. *J. Med. Chem.* **2016**, *59* (2), 531-44.
9. Mattson, M. P., Pathways towards and away from Alzheimer's disease. *Nature* **2004**, *430* (7000), 631-9.
 10. Desai, A. K.; Grossberg, G. T., Diagnosis and treatment of Alzheimer's disease. *Neurology* **2005**, *64* (12 Suppl 3), S34-9.
 11. Mohamed, T.; Rao, P. P., Alzheimer's disease: emerging trends in small molecule therapies. *Curr. Med. Chem.* **2011**, *18* (28), 4299-320.
 12. Hershenson, F. M.; Moos, W. H., Drug development for senile cognitive decline. *J. Med. Chem.* **1986**, *29* (7), 1125-30.
 13. Rampa, A.; Belluti, F.; Gobbi, S.; Bisi, A., Hybrid-based multi-target ligands for the treatment of Alzheimer's disease. *Curr. Top. Med. Chem.* **2011**, *11* (22), 2716-30.
 14. Scarpini, E.; Scheltens, P.; Feldman, H., Treatment of Alzheimer's disease: current status and new perspectives. *Lancet Neurol.* **2003**, *2* (9), 539-47.
 15. Scott, L. J.; Goa, K. L., Galantamine: a review of its use in Alzheimer's disease. *Drugs* **2000**, *60* (5), 1095-122.
 16. Cummings, J. L., Treatment of Alzheimer's disease: current and future therapeutic approaches. *Rev. Neurol. Dis.* **2004**, *1* (2), 60-9.
 17. a) Golde, T. E., Disease modifying therapy for AD? *J. Neurochem.* **2006**, *99* (3), 689-707; b) Grill, J. D.; Cummings, J. L., Current therapeutic targets for the treatment of Alzheimer's disease. *Expert Rev. Neurother.* **2010**, *10* (5), 711-28.
 18. Pimplikar, S. W., Neuroinflammation in Alzheimer's disease: from pathogenesis to a therapeutic target. *J. Clin. Immunol.* **2014**, *34 Suppl 1*, S64-9.
 19. a) Hardy, J.; Allsop, D., Amyloid deposition as the central event in the aetiology of Alzheimer's disease. *Trends Pharmacol. Sci.* **1991**, *12* (10), 383-8; b) Hardy, J. A.; Higgins, G. A., Alzheimer's disease: the amyloid cascade hypothesis. *Science* **1992**, *256* (5054), 184-5.

20. Hardy, J.; Selkoe, D. J., The amyloid hypothesis of Alzheimer's disease: progress and problems on the road to therapeutics. *Science* **2002**, *297* (5580), 353-6.
21. Mattson, M. P., Cellular actions of beta-amyloid precursor protein and its soluble and fibrillogenic derivatives. *Physiol. Rev.* **1997**, *77* (4), 1081-132.
22. Silva, T.; Reis, J.; Teixeira, J.; Borges, F., Alzheimer's disease, enzyme targets and drug discovery struggles: from natural products to drug prototypes. *Ageing Res. Rev.* **2014**, *15*, 116-45.
23. a) Boddapati, S.; Levites, Y.; Sierks, M. R., Inhibiting β -secretase activity in Alzheimer's disease cell models with single-chain antibodies specifically targeting APP. *J. Mol. Biol.* **2011**, *405* (2), 436-47; b) Willem, M.; Lammich, S.; Haass, C., Function, regulation and therapeutic properties of beta-secretase (BACE1). *Semin. Cell Dev. Biol.* **2009**, *20* (2), 175-82.
24. a) Selkoe, D. J., Soluble oligomers of the amyloid beta-protein impair synaptic plasticity and behavior. *Behav. Brain Res.* **2008**, *192* (1), 106-13; b) Dineley, K. T.; Kaye, R.; Neugebauer, V.; Fu, Y.; Zhang, W.; Reese, L. C.; Tagliatela, G., Amyloid-beta oligomers impair fear conditioned memory in a calcineurin-dependent fashion in mice. *J. Neurosci. Res.* **2010**, *88* (13), 2923-32.
25. Lustbader, J. W.; Cirilli, M.; Lin, C.; Xu, H. W.; Takuma, K.; Wang, N.; Caspersen, C.; Chen, X.; Pollak, S.; Chaney, M.; Trinchese, F.; Liu, S.; Gunn-Moore, F.; Lue, L. F.; Walker, D. G.; Kuppasamy, P.; Zewier, Z. L.; Arancio, O.; Stern, D.; Yan, S. S.; Wu, H., ABAD directly links A β to mitochondrial toxicity in Alzheimer's disease. *Science* **2004**, *304* (5669), 448-52.
26. Tamagno, E.; Parola, M.; Guglielmotto, M.; Santoro, G.; Bardini, P.; Marra, L.; Tabaton, M.; Danni, O., Multiple signaling events in amyloid beta-induced, oxidative stress-dependent neuronal apoptosis. *Free Radic. Biol. Med.* **2003**, *35* (1), 45-58.
27. Evin, G.; Lessene, G.; Wilkins, S., BACE inhibitors as potential drugs for the treatment of Alzheimer's disease: focus on bioactivity. *Recent Pat. CNS Drug Discov.* **2011**, *6* (2), 91-106.

28. Bennett, B. D.; Babu-Khan, S.; Loeloff, R.; Louis, J. C.; Curran, E.; Citron, M.; Vassar, R., Expression analysis of BACE2 in brain and peripheral tissues. *J. Biol. Chem.* **2000**, *275* (27), 20647-51.
29. a) Fischer, F.; Molinari, M.; Bodendorf, U.; Paganetti, P., The disulphide bonds in the catalytic domain of BACE are critical but not essential for amyloid precursor protein processing activity. *J. Neurochem.* **2002**, *80* (6), 1079-88; b) Haniu, M.; Denis, P.; Young, Y.; Mendiaz, E. A.; Fuller, J.; Hui, J. O.; Bennett, B. D.; Kahn, S.; Ross, S.; Burgess, T.; Katta, V.; Rogers, G.; Vassar, R.; Citron, M., Characterization of Alzheimer's beta-secretase protein BACE. A pepsin family member with unusual properties. *J. Biol. Chem.* **2000**, *275* (28), 21099-106.
30. Kacker, P.; Bottegoni, G.; Cavalli, A., Computational methods in the discovery and design of BACE-1 inhibitors. *Curr. Med. Chem.* **2012**, *19* (36), 6095-111.
31. Mancini, F.; De Simone, A.; Andrisano, V., Beta-secretase as a target for Alzheimer's disease drug discovery: an overview of in vitro methods for characterization of inhibitors. *Anal. Bioanal. Chem.* **2011**, *400* (7), 1979-96.
32. Tamagno, E.; Bardini, P.; Obbili, A.; Vitali, A.; Borghi, R.; Zaccheo, D.; Pronzato, M. A.; Danni, O.; Smith, M. A.; Perry, G.; Tabaton, M., Oxidative stress increases expression and activity of BACE in NT2 neurons. *Neurobiol. Dis.* **2002**, *10* (3), 279-88.
33. Ghosh, A. K.; Devasamudram, T.; Hong, L.; DeZutter, C.; Xu, X.; Weerasena, V.; Koelsch, G.; Bilcer, G.; Tang, J., Structure-based design of cycloamide-urethane-derived novel inhibitors of human brain memapsin 2 (beta-secretase). *Bioorg. Med. Chem. Lett.* **2005**, *15* (1), 15-20.
34. Silvestri, R., Boom in the development of non-peptidic beta-secretase (BACE1) inhibitors for the treatment of Alzheimer's disease. *Med. Res. Rev.* **2009**, *29* (2), 295-338.
35. Belluti, F.; De Simone, A.; Tarozzi, A.; Bartolini, M.; Djemil, A.; Bisi, A.; Gobbi, S.; Montanari, S.; Cavalli, A.; Andrisano, V.; Bottegoni, G.; Rampa, A.,

Fluorinated benzophenone derivatives: balanced multipotent agents for Alzheimer's disease. *Eur. J. Med. Chem.* **2014**, *78*, 157-66.

36. Rampa, A.; Mancini, F.; De Simone, A.; Falchi, F.; Belluti, F.; Di Martino, R. M.; Gobbi, S.; Andrisano, V.; Tarozzi, A.; Bartolini, M.; Cavalli, A.; Bisi, A., From AChE to BACE1 inhibitors: The role of the amine on the indanone scaffold. *Bioorg. Med. Chem. Lett.* **2015**, *25* (14), 2804-8.

37. a) Nagy, Z.; Esiri, M. M.; Jobst, K. A.; Morris, J. H.; King, E. M.; McDonald, B.; Litchfield, S.; Smith, A.; Barnetson, L.; Smith, A. D., Relative roles of plaques and tangles in the dementia of Alzheimer's disease: correlations using three sets of neuropathological criteria. *Dementia* **1995**, *6* (1), 21-31; b) Arriagada, P. V.; Growdon, J. H.; Hedley-Whyte, E. T.; Hyman, B. T., Neurofibrillary tangles but not senile plaques parallel duration and severity of Alzheimer's disease. *Neurology* **1992**, *42* (3 Pt 1), 631-9.

38. Iqbal, K.; Liu, F.; Gong, C. X.; Alonso, A. e. C.; Grundke-Iqbal, I., Mechanisms of tau-induced neurodegeneration. *Acta Neuropathol.* **2009**, *118* (1), 53-69.

39. Mazanetz, M. P.; Fischer, P. M., Untangling tau hyperphosphorylation in drug design for neurodegenerative diseases. *Nat. Rev. Drug Discov.* **2007**, *6* (6), 464-79.

40. Reddy, P. H., Abnormal tau, mitochondrial dysfunction, impaired axonal transport of mitochondria, and synaptic deprivation in Alzheimer's disease. *Brain Res.* **2011**, *1415*, 136-48.

41. Cowan, C. M.; Quraishe, S.; Hands, S.; Sealey, M.; Mahajan, S.; Allan, D. W.; Mudher, A., Rescue from tau-induced neuronal dysfunction produces insoluble tau oligomers. *Sci. Rep.* **2015**, *5*, 17191.

42. Lee, H. G.; Perry, G.; Moreira, P. I.; Garrett, M. R.; Liu, Q.; Zhu, X.; Takeda, A.; Nunomura, A.; Smith, M. A., Tau phosphorylation in Alzheimer's disease: pathogen or protector? *Trends Mol. Med.* **2005**, *11* (4), 164-9.

43. a) Hanks, S. K.; Hunter, T., Protein kinases 6. The eukaryotic protein kinase superfamily: kinase (catalytic) domain structure and classification. *FASEB J.* **1995**,

- 9 (8), 576-96; b) Cohen, P.; Alessi, D. R., Kinase drug discovery--what's next in the field? *ACS Chem. Biol.* **2013**, *8* (1), 96-104.
44. Palomo, V.; Soteras, I.; Perez, D. I.; Perez, C.; Gil, C.; Campillo, N. E.; Martinez, A., Exploring the binding sites of glycogen synthase kinase 3. Identification and characterization of allosteric modulation cavities. *J. Med. Chem.* **2011**, *54* (24), 8461-70.
45. Rylatt, D. B.; Aitken, A.; Bilham, T.; Condon, G. D.; Embi, N.; Cohen, P., Glycogen synthase from rabbit skeletal muscle. Amino acid sequence at the sites phosphorylated by glycogen synthase kinase-3, and extension of the N-terminal sequence containing the site phosphorylated by phosphorylase kinase. *Eur. J. Biochem.* **1980**, *107* (2), 529-37.
46. Billingsley, M. L.; Kincaid, R. L., Regulated phosphorylation and dephosphorylation of tau protein: effects on microtubule interaction, intracellular trafficking and neurodegeneration. *Biochem. J.* **1997**, *323* (Pt 3), 577-91.
47. Lei, P.; Ayton, S.; Bush, A. I.; Adlard, P. A., GSK-3 in Neurodegenerative Diseases. *Int. J. Alzheimers Dis.* **2011**, *2011*, 189246.
48. ter Haar, E.; Coll, J. T.; Austen, D. A.; Hsiao, H. M.; Swenson, L.; Jain, J., Structure of GSK3beta reveals a primed phosphorylation mechanism. *Nat. Struct. Biol.* **2001**, *8* (7), 593-6.
49. Llorens-Martín, M.; Jurado, J.; Hernández, F.; Avila, J., GSK-3 β , a pivotal kinase in Alzheimer disease. *Front. Mol. Neurosci.* **2014**, *7*, 46.
50. Martinez, A.; Castro, A.; Dorronsoro, I.; Alonso, M., Glycogen synthase kinase 3 (GSK-3) inhibitors as new promising drugs for diabetes, neurodegeneration, cancer, and inflammation. *Med. Res. Rev.* **2002**, *22* (4), 373-84.
51. Martinez, A.; Gil, C.; Perez, D. I., Glycogen synthase kinase 3 inhibitors in the next horizon for Alzheimer's disease treatment. *Int. J. Alzheimers Dis.* **2011**, *2011*, 280502.
52. Bidon-Chanal, A.; Fuertes, A.; Alonso, D.; Pérez, D. I.; Martínez, A.; Luque, F. J.; Medina, M., Evidence for a new binding mode to GSK-3: allosteric

- regulation by the marine compound palinurin. *Eur. J. Med. Chem.* **2013**, *60*, 479-89.
53. Ittner, L. M.; Götz, J., Amyloid- β and tau--a toxic pas de deux in Alzheimer's disease. *Nat. Rev. Neurosci.* **2011**, *12* (2), 65-72.
54. Liu, Z.; Li, P.; Wu, J.; Wang, Y.; Li, P.; Hou, X.; Zhang, Q.; Wei, N.; Zhao, Z.; Liang, H.; Wei, J., The cascade of oxidative stress and tau protein autophagic dysfunction in Alzheimer's disease. In *Alzheimer's Disease-Challenges for the Future*, Zerr, I., Ed. 2015.
55. a) Marcus, D. L.; Thomas, C.; Rodriguez, C.; Simberkoff, K.; Tsai, J. S.; Strafaci, J. A.; Freedman, M. L., Increased peroxidation and reduced antioxidant enzyme activity in Alzheimer's disease. *Exp. Neurol.* **1998**, *150* (1), 40-4; b) Omar, R. A.; Chyan, Y. J.; Andorn, A. C.; Poeggeler, B.; Robakis, N. K.; Pappolla, M. A., Increased Expression but Reduced Activity of Antioxidant Enzymes in Alzheimer's Disease. *J. Alzheimers Dis.* **1999**, *1* (3), 139-145; c) Furuta, A.; Price, D. L.; Pardo, C. A.; Troncoso, J. C.; Xu, Z. S.; Taniguchi, N.; Martin, L. J., Localization of superoxide dismutases in Alzheimer's disease and Down's syndrome neocortex and hippocampus. *Am. J. Pathol.* **1995**, *146* (2), 357-67; d) Padurariu, M.; Ciobica, A.; Hritcu, L.; Stoica, B.; Bild, W.; Stefanescu, C., Changes of some oxidative stress markers in the serum of patients with mild cognitive impairment and Alzheimer's disease. *Neurosci. Lett.* **2010**, *469* (1), 6-10.
56. de Vries, H. E.; Witte, M.; Hondius, D.; Rozemuller, A. J.; Drukarch, B.; Hoozemans, J.; van Horssen, J., Nrf2-induced antioxidant protection: a promising target to counteract ROS-mediated damage in neurodegenerative disease? *Free Radic. Biol. Med.* **2008**, *45* (10), 1375-83.
57. Markesbery, W. R., Oxidative stress hypothesis in Alzheimer's disease. *Free Radic. Biol. Med.* **1997**, *23* (1), 134-47.
58. Sutherland, G. T.; Chami, B.; Youssef, P.; Witting, P. K., Oxidative stress in Alzheimer's disease: Primary villain or physiological by-product? *Redox Rep.* **2013**, *18* (4), 134-41.

59. Morales, I.; Guzmán-Martínez, L.; Cerda-Troncoso, C.; Farías, G. A.; Maccioni, R. B., Neuroinflammation in the pathogenesis of Alzheimer's disease. A rational framework for the search of novel therapeutic approaches. *Front. Cell Neurosci.* **2014**, *8*, 112.
60. Wang, W. Y.; Tan, M. S.; Yu, J. T.; Tan, L., Role of pro-inflammatory cytokines released from microglia in Alzheimer's disease. *Ann. Transl. Med.* **2015**, *3* (10), 136.
61. Pan, X. D.; Zhu, Y. G.; Lin, N.; Zhang, J.; Ye, Q. Y.; Huang, H. P.; Chen, X. C., Microglial phagocytosis induced by fibrillar β -amyloid is attenuated by oligomeric β -amyloid: implications for Alzheimer's disease. *Mol. Neurodegener.* **2011**, *6*, 45.
62. a) Tenhunen, R.; Marver, H. S.; Schmid, R., The enzymatic conversion of heme to bilirubin by microsomal heme oxygenase. *Proc. Natl. Acad. Sci. USA* **1968**, *61* (2), 748-55; b) Maines, M. D., Heme oxygenase: function, multiplicity, regulatory mechanisms, and clinical applications. *FASEB J.* **1988**, *2* (10), 2557-68.
63. Yamazaki, H.; Tanji, K.; Wakabayashi, K.; Matsuura, S.; Itoh, K., Role of the Keap1/Nrf2 pathway in neurodegenerative diseases. *Pathol. Int.* **2015**, *65* (5), 210-9.
64. Torres-Lista, V.; Parrado-Fernández, C.; Alvarez-Montón, I.; Frontiñán-Rubio, J.; Durán-Prado, M.; Peinado, J. R.; Johansson, B.; Alcaín, F. J.; Giménez-Llort, L., Neophobia, NQO1 and SIRT1 as premorbid and prodromal indicators of AD in 3xTg-AD mice. *Behav. Brain Res.* **2014**, *271*, 140-6.
65. Saharan, S.; Mandal, P. K., The emerging role of glutathione in Alzheimer's disease. *J. Alzheimers Dis.* **2014**, *40* (3), 519-29.
66. Kaspar, J. W.; Niture, S. K.; Jaiswal, A. K., Nrf2:INrf2 (Keap1) signaling in oxidative stress. *Free Radic. Biol. Med.* **2009**, *47* (9), 1304-9.
67. Jung, K. A.; Kwak, M. K., The Nrf2 system as a potential target for the development of indirect antioxidants. *Molecules* **2010**, *15* (10), 7266-91.
68. Ma, Q., Role of nrf2 in oxidative stress and toxicity. *Annu. Rev. Pharmacol. Toxicol.* **2013**, *53*, 401-26.

69. Choi, B. H.; Kang, K. S.; Kwak, M. K., Effect of redox modulating NRF2 activators on chronic kidney disease. *Molecules* **2014**, *19* (8), 12727-59.
70. Baird, L.; Dinkova-Kostova, A. T., The cytoprotective role of the Keap1-Nrf2 pathway. *Arch. Toxicol.* **2011**, *85* (4), 241-72.
71. Holland, R.; Fishbein, J. C., Chemistry of the cysteine sensors in Kelch-like ECH-associated protein 1. *Antioxid. Redox Signal.* **2010**, *13* (11), 1749-61.
72. Talalay, P.; De Long, M. J.; Prochaska, H. J., Identification of a common chemical signal regulating the induction of enzymes that protect against chemical carcinogenesis. *Proc. Natl. Acad. Sci. USA* **1988**, *85* (21), 8261-5.
73. Wilson, A. J.; Kerns, J. K.; Callahan, J. F.; Moody, C. J., Keap calm, and carry on covalently. *J. Med. Chem.* **2013**, *56* (19), 7463-76.
74. Jain, A. K.; Jaiswal, A. K., Phosphorylation of tyrosine 568 controls nuclear export of Nrf2. *J. Biol. Chem.* **2006**, *281* (17), 12132-42.
75. Kanninen, K.; White, A. R.; Koistinaho, J.; Malm, T., Targeting Glycogen Synthase Kinase-3 β for Therapeutic Benefit against Oxidative Stress in Alzheimer's Disease: Involvement of the Nrf2-ARE Pathway. *Int. J. Alzheimers Dis.* **2011**, *2011*, 985085.
76. Jain, A. K.; Jaiswal, A. K., GSK-3 β acts upstream of Fyn kinase in regulation of nuclear export and degradation of NF-E2 related factor 2. *J. Biol. Chem.* **2007**, *282* (22), 16502-10.
77. Longenecker, K. L.; Roach, P. J.; Hurley, T. D., Three-dimensional structure of mammalian casein kinase I: molecular basis for phosphate recognition. *J. Mol. Biol.* **1996**, *257* (3), 618-31.
78. a) Perez, D. I.; Gil, C.; Martinez, A., Protein kinases CK1 and CK2 as new targets for neurodegenerative diseases. *Med. Res. Rev.* **2011**, *31* (6), 924-54; b) Flotow, H.; Graves, P. R.; Wang, A. Q.; Fiol, C. J.; Roeske, R. W.; Roach, P. J., Phosphate groups as substrate determinants for casein kinase I action. *J. Biol. Chem.* **1990**, *265* (24), 14264-9.

79. Flajolet, M.; He, G.; Heiman, M.; Lin, A.; Nairn, A. C.; Greengard, P., Regulation of Alzheimer's disease amyloid-beta formation by casein kinase I. *Proc. Natl. Acad. Sci. USA* **2007**, *104* (10), 4159-64.
80. Lewis, P. A., The function of ROCO proteins in health and disease. *Biol. Cell* **2009**, *101* (3), 183-91.
81. Deng, J.; Lewis, P. A.; Greggio, E.; Sluch, E.; Beilina, A.; Cookson, M. R., Structure of the ROC domain from the Parkinson's disease-associated leucine-rich repeat kinase 2 reveals a dimeric GTPase. *Proc. Natl. Acad. Sci. USA* **2008**, *105* (5), 1499-504.
82. Kawakami, F.; Shimada, N.; Ohta, E.; Kagiya, G.; Kawashima, R.; Maekawa, T.; Maruyama, H.; Ichikawa, T., Leucine-rich repeat kinase 2 regulates tau phosphorylation through direct activation of glycogen synthase kinase-3 β . *FEBS J.* **2014**, *281* (1), 3-13.
83. Kim, B.; Yang, M. S.; Choi, D.; Kim, J. H.; Kim, H. S.; Seol, W.; Choi, S.; Jou, I.; Kim, E. Y.; Joe, E. H., Impaired inflammatory responses in murine Lrrk2-knockdown brain microglia. *PLoS One* **2012**, *7* (4), e34693.
84. Bolognesi, M. L., Polypharmacology in a single drug: multitarget drugs. *Curr. Med. Chem.* **2013**, *20* (13), 1639-45.
85. Cavalli, A.; Bolognesi, M. L.; Minarini, A.; Rosini, M.; Tumiatti, V.; Recanatini, M.; Melchiorre, C., Multi-target-directed ligands to combat neurodegenerative diseases. *J. Med. Chem.* **2008**, *51* (3), 347-72.
86. Zheng, H.; Fridkin, M.; Youdim, M., From single target to multitarget/network therapeutics in Alzheimer's therapy. *Pharmaceuticals (Basel)* **2014**, *7* (2), 113-35.
87. Morphy, R.; Rankovic, Z., Designed multiple ligands. An emerging drug discovery paradigm. *J. Med. Chem.* **2005**, *48* (21), 6523-43.
88. Bottegoni, G.; Favia, A. D.; Recanatini, M.; Cavalli, A., The role of fragment-based and computational methods in polypharmacology. *Drug Discov. Today* **2012**, *17* (1-2), 23-34.

89. Costantino, L.; Barlocco, D., Privileged structures as leads in medicinal chemistry. *Curr. Med. Chem.* **2006**, *13* (1), 65-85.
90. DeSimone, R. W.; Currie, K. S.; Mitchell, S. A.; Darrow, J. W.; Pippin, D. A., Privileged structures: applications in drug discovery. *Comb. Chem. High Throughput Screen.* **2004**, *7* (5), 473-94.
91. de Sá Alves, F. R.; Barreiro, E. J.; Fraga, C. A., From nature to drug discovery: the indole scaffold as a 'privileged structure'. *Mini Rev. Med. Chem.* **2009**, *9* (7), 782-93.
92. a) Borges, F.; Roleira, F.; Milhazes, N.; Santana, L.; Uriarte, E., Simple coumarins and analogues in medicinal chemistry: occurrence, synthesis and biological activity. *Curr. Med. Chem.* **2005**, *12* (8), 887-916; b) Matos, M. J.; Santana, L.; Uriarte, E.; Abreu, O. A.; E., Molina, E.; Yordi, E. G., Coumarins-an important class of phytochemicals. In *Phytochemicals-Isolation, Characterization and Role in Human Health* [Online] Rao, V., Ed. 2015.
93. Jameel, E.; Umar, T.; Kumar, J.; Hoda, N., Coumarin: A Privileged Scaffold for the Design and Development of Antineurodegenerative Agents. *Chem. Biol. Drug Des.* **2016**, *87* (1), 21-38.
94. Batovska, D. I.; Todorova, I. T., Trends in utilization of the pharmacological potential of chalcones. *Curr. Clin. Pharmacol.* **2010**, *5* (1), 1-29.
95. Welsch, M. E.; Snyder, S. A.; Stockwell, B. R., Privileged scaffolds for library design and drug discovery. *Curr. Opin. Chem. Biol.* **2010**, *14* (3), 347-61.
96. Vasilevich, N. I.; Kombarov, R. V.; Genis, D. V.; Kirpichenok, M. A., Lessons from natural products chemistry can offer novel approaches for synthetic chemistry in drug discovery. *J. Med. Chem.* **2012**, *55* (16), 7003-9.
97. Chen, J.; Li, W.; Yao, H.; Xu, J., Insights into drug discovery from natural products through structural modification. *Fitoterapia* **2015**, *103*, 231-41.
98. Hong, J., Role of natural product diversity in chemical biology. *Curr. Opin. Chem. Biol.* **2011**, *15* (3), 350-4.
99. Drahl, C.; Cravatt, B. F.; Sorensen, E. J., Protein-reactive natural products. *Angew. Chem. Int. Ed. Engl.* **2005**, *44* (36), 5788-809.

100. Gersch, M.; Kreuzer, J.; Sieber, S. A., Electrophilic natural products and their biological targets. *Nat. Prod. Rep.* **2012**, *29* (6), 659-82.
101. Amslinger, S., The tunable functionality of alpha,beta-unsaturated carbonyl compounds enables their differential application in biological systems. *ChemMedChem.* **2010**, *5* (3), 351-6.
102. Silvermam, R. B., Model studies for a molecular mechanism of action of oral anticoagulants. *J. Am. Chem. Soc.* **1981**, *103*, 3910-3915.
103. Avonto, C.; Tagliatela-Scafati, O.; Pollastro, F.; Minassi, A.; Di Marzo, V.; De Petrocellis, L.; Appendino, G., An NMR spectroscopic method to identify and classify thiol-trapping agents: revival of Michael acceptors for drug discovery? *Angew. Chem. Int. Ed. Engl.* **2011**, *50* (2), 467-71.
104. Minassi, A.; Sánchez-Duffhues, G.; Collado, J. A.; Muñoz, E.; Appendino, G., Dissecting the pharmacophore of curcumin. Which structural element is critical for which action? *J. Nat. Prod.* **2013**, *76* (6), 1105-12.
105. Ahmed T, G. A., Therapeutic potential of turmeric in Alzheimer's disease: curcumin or curcuminoids? *Phytother. Res.* **2014**, *28* (4), 517-525.
106. Shanmugam, M. K.; Rane, G.; Kanchi, M. M.; Arfuso, F.; Chinnathambi, A.; Zayed, M. E.; Alharbi, S. A.; Tan, B. K.; Kumar, A. P.; Sethi, G., The multifaceted role of curcumin in cancer prevention and treatment. *Molecules* **2015**, *20* (2), 2728-69.
107. Esatbeyoglu, T.; Huebbe, P.; Ernst, I. M.; Chin, D.; Wagner, A. E.; Rimbach, G., Curcumin--from molecule to biological function. *Angew. Chem. Int. Ed. Engl.* **2012**, *51* (22), 5308-32.
108. a) Oetari, S.; Sudibyo, M.; Commandeur, J. N.; Samhoedi, R.; Vermeulen, N. P., Effects of curcumin on cytochrome P450 and glutathione S-transferase activities in rat liver. *Biochem. Pharmacol.* **1996**, *51* (1), 39-45; b) Tønnesen, H. H.; Karlsen, J., Studies on curcumin and curcuminoids. VI. Kinetics of curcumin degradation in aqueous solution. *Z. Lebensm. Unters. Forsch.* **1985**, *180* (5), 402-

- 4; c) Price, L. C.; Buescher, R. W., Kinetics of alkaline degradation of the food pigments curcumin and curcuminoids. *J. Food Sci.* **1997**, *62* (2), 267-269.
109. Prasad, S.; Gupta, S. C.; Tyagi, A. K.; Aggarwal, B. B., Curcumin, a component of golden spice: from bedside to bench and back. *Biotechnol. Adv.* **2014**, *32* (6), 1053-64.
110. Anand, P.; Thomas, S. G.; Kunnnumakkara, A. B.; Sundaram, C.; Harikumar, K. B.; Sung, B.; Tharakan, S. T.; Misra, K.; Priyadarsini, I. K.; Rajasekharan, K. N.; Aggarwal, B. B., Biological activities of curcumin and its analogues (Congeners) made by man and Mother Nature. *Biochem. Pharmacol.* **2008**, *76* (11), 1590-611.
111. Yallapu, M. M.; Jaggi, M.; Chauhan, S. C., Curcumin nanomedicine: a road to cancer therapeutics. *Curr. Pharm. Des.* **2013**, *19* (11), 1994-2010.
112. Kurien, B. T.; Singh, A.; Matsumoto, H.; Scofield, R. H., Improving the solubility and pharmacological efficacy of curcumin by heat treatment. *Assay Drug Dev. Technol.* **2007**, *5*, 567-576.
113. Aggarwal, B. B.; Sundaram, C.; Malani, N.; Ichikawa, H., Curcumin: the Indian solid gold. *Adv. Exp. Med. Biol.* **2007**, *595*, 1-75.
114. Salem, M.; Rohanib, S.; Gillies, E. R., Curcumin, a promising anti-cancer therapeutic: a review of its chemical properties, bioactivity and approaches to cancer cell delivery. *RSC Adv.* **2014**, *4*, 10815-10829.
115. Chin, D.; Huebbe, P.; Pallauf, K.; Rimbach, G., Neuroprotective properties of curcumin in Alzheimer's disease--merits and limitations. *Curr. Med. Chem.* **2013**, *20* (32), 3955-85.
116. Huang, H.C.; Xu, K.; Jiang, ZF., Curcumin-mediated neuroprotection against amyloid- β -induced mitochondrial dysfunction involves the inhibition of GSK-3 β . *J. Alzheimers Dis.* **2012**, *32* (4), 981-996.
117. Jayasena, T.; Poljak, A.; Smythe, G.; Braidy, N.; Münch, G.; Sachdev, P., The role of polyphenols in the modulation of sirtuins and other pathways involved in Alzheimer's disease. *Ageing Res. Rev.* **2013**, *12* (4), 867-83.

118. Goel, A.; Kunnumakkara, A. B.; Aggarwal, B. B., Curcumin as "Curecumin": from kitchen to clinic. *Biochem. Pharmacol.* **2008**, *75* (4), 787-809.
119. Rojo, A. I.; Sagarra, M. R.; Cuadrado, A., GSK-3 β downregulates the transcription factor Nrf2 after oxidant damage: relevance to exposure of neuronal cells to oxidative stress. *J. Neurochem.* **2008**, *105* (1), 192-202.
120. Ferrari, E.; Benassi, R.; Sacchi, S.; Pignedoli, F.; Asti, M.; Saladini, M., Curcumin derivatives as metal-chelating agents with potential multifunctional activity for pharmaceutical applications. *J. Inorg. Biochem.* **2014**, *139*, 38-48.
121. Patra, D.; Barakat, C., Synchronous fluorescence spectroscopic study of solvatochromic curcumin dye. *Spectrochim. Acta A Mol. Biomol. Spectrosc.* **2011**, *79* (5), 1034-41.
122. Willmann, J. K.; van Bruggen, N.; Dinkelborg, L. M.; Gambhir, S. S., Molecular imaging in drug development. *Nat. Rev. Drug Discov.* **2008**, *7* (7), 591-607.
123. Nolting, D. D.; Nickels, M. L.; Guo, N.; Pham, W., Molecular imaging probe development: a chemistry perspective. *Am. J. Nucl. Med. Mol. Imaging* **2012**, *2* (3), 273-306.
124. a) Lavis, L. D.; Raines, R. T., Bright ideas for chemical biology. *ACS Chem. Biol.* **2008**, *3* (3), 142-55; b) Lavis, L. D.; Raines, R. T., Bright building blocks for chemical biology. *ACS Chem. Biol.* **2014**, *9* (4), 855-66.
125. Mutsuga, M.; Chambers, J. K.; Uchida, K.; Tei, M.; Makibuchi, T.; Mizorogi, T.; Takashima, A.; Nakayama, H., Binding of curcumin to senile plaques and cerebral amyloid angiopathy in the aged brain of various animals and to neurofibrillary tangles in Alzheimer's brain. *J. Vet. Med. Sci.* **2012**, *74* (1), 51-7.
126. Koronyo, Y.; Salumbides, B. C.; Black, K. L.; Koronyo-Hamaoui, M., Alzheimer's disease in the retina: imaging retinal $\text{A}\beta$ plaques for early diagnosis and therapy assessment. *Neurodegener. Dis.* **2012**, *10* (1-4), 285-93.
127. Chen, K.; Chen, X., Design and development of molecular imaging probes. *Curr. Top. Med. Chem.* **2010**, *10* (12), 1227-36.

128. Aulić, S.; Bolognesi, M. L.; Legname, G., Small-molecule theranostic probes: a promising future in neurodegenerative diseases. *Int. J. Cell. Biol.* **2013**, *2013*, 150952.
129. a) Peng, H.; Liu, X.; Wang, G.; Li, M.; Bratlie, K. M.; Cochran, E.; Wang, Q., Polymeric multifunctional nanomaterials for theranostics. *J. Mater. Chem. B* **2015**, *3*, 6856-6870; b) Amiri, H.; Saeidi, K.; Borhani, P.; Manafirad, A.; Ghavami, M.; Zerbi, V., Alzheimer's disease: pathophysiology and applications of magnetic nanoparticles as MRI theranostic agents. *ACS Chem. Neurosci.* **2013**, *4* (11), 1417-29.
130. Poduslo, J. F.; Wengenack, T. M.; Curran, G. L.; Wisniewski, T.; Sigurdsson, E. M.; Macura, S. I.; Borowski, B. J.; Jack, C. R., Molecular targeting of Alzheimer's amyloid plaques for contrast-enhanced magnetic resonance imaging. *Neurobiol. Dis.* **2002**, *11* (2), 315-29.
131. Rodrigues, S.; Dionísio, M.; López, C. R.; Grenha, A., Biocompatibility of chitosan carriers with application in drug delivery. *J. Funct. Biomater.* **2012**, *3* (3), 615-41.
132. Rinaudo, M., Chitin and chitosan: properties and applications. *Prog. Polym. Sci.* **2006**, *31* (7), 603-632.
133. Xia, W.; Liu, P.; Zhang, J.; Chen, J., Biological activities of chitosan and chitoooligosaccharides. *Food Hydrocoll.* **2011**, *25* (2), 170-179.
134. Agnihotri, S. A.; Mallikarjuna, N. N.; Aminabhavi, T. M., Recent advances on chitosan-based micro- and nanoparticles in drug delivery. *J. Control Release* **2004**, *100* (1), 5-28.
135. Dodane, V.; Vilivalam, V. D., Pharmaceutical applications of chitosan. *Pharmaceutical Science and Technology Today* **1998**, *1* (6), 246-253.
136. Kumar, M. N. V. R., A review of chitin and chitosan applications. *React. Funct. Polym.* **2000**, *46* (1), 1-27.
137. Riva, R.; Ragelle, H.; des Rieux, A.; Duhem, N.; Jérôme, C.; Préat, V., Chitosan and chitosan derivatives in drug delivery and tissue engineering. *Adv. Polym. Sci.* **2011**, *244*, 19-44.

138. Wilson, B.; Samanta, M. K.; Santhi, K.; Kumar, K. P.; Ramasamy, M.; Suresh, B., Chitosan nanoparticles as a new delivery system for the anti-Alzheimer drug tacrine. *Nanomedicine* **2010**, *6* (1), 144-52.
139. Fazil, M.; Md, S.; Haque, S.; Kumar, M.; Baboota, S.; Sahni, J. K.; Ali, J., Development and evaluation of rivastigmine loaded chitosan nanoparticles for brain targeting. *Eur. J. Pharm. Sci.* **2012**, *47* (1), 6-15.
140. Das, R. K.; Kasoju, N.; Bora, U., Encapsulation of curcumin in alginate-chitosan-pluronic composite nanoparticles for delivery to cancer cells. *Nanomedicine* **2010**, *6* (1), 153-60.
141. Kerch, G., The potential of chitosan and its derivatives in prevention and treatment of age-related diseases. *Mar. Drugs* **2015**, *13* (4), 2158-82.
142. Basu, A.; Kunduru, K. R.; Abtey, E.; Domb, A. J., Polysaccharide-Based Conjugates for Biomedical Applications. *Bioconjug. Chem.* **2015**, *26* (8), 1396-412.
143. Lee, C. M.; Jang, D.; Kim, J.; Cheong, S. J.; Kim, E. M.; Jeong, M. H.; Kim, S. H.; Kim, D. W.; Lim, S. T.; Sohn, M. H.; Jeong, Y. Y.; Jeong, H. J., Oleyl-chitosan nanoparticles based on a dual probe for optical/MR imaging in vivo. *Bioconjug. Chem.* **2011**, *22* (2), 186-92.
144. Galbiati, A.; Tabolacci, C.; Morozzo Della Rocca, B.; Mattioli, P.; Beninati, S.; Paradossi, G.; Desideri, A., Targeting tumor cells through chitosan-folate modified microcapsules loaded with camptothecin. *Bioconjug. Chem.* **2011**, *22* (6), 1066-72.
145. Qiu, X.; Liu, Z.; Shao, W. Y.; Liu, X.; Jing, D. P.; Yu, Y. J.; An, L. K.; Huang, S. L.; Bu, X. Z.; Huang, Z. S.; Gu, L. Q., Synthesis and evaluation of curcumin analogues as potential thioredoxin reductase inhibitors. *Bioorg. Med.Chem.* **2008**, *16* (17), 8035-41.
146. Kim, H. K.; Yang, C. H., Synthetic curcumin derivatives inhibit Jun-Fos-DNA complex formation. *Bull. Korean Chem. Soc.* **2004**, *25* (12), 1769-1774.
147. Khan, M. A.; El-Khatib, R.; Rainsford, K. D.; Whitehouse, M. W., Synthesis and anti-inflammatory properties of some aromatic and heterocyclic aromatic curcuminoids. *Bioorg. Chem.* **2012**, *40* (1), 30-8.

148. Gomes, Dde. C.; Alegrio, L. V.; Leon, L. L.; de Lima, M. E., Total synthesis and anti-leishmanial activity of some curcumin analogues. *Arzneimittelforschung* **2002**, *52* (9), 695-8.
149. Konno, H.; Endo, H.; Ise, S.; Miyazaki, K.; Aoki, H.; Sanjoh, A.; Kobayashi, K.; Hattori, Y.; Akaji, K., Synthesis and evaluation of curcumin derivatives toward an inhibitor of beta-site amyloid precursor protein cleaving enzyme 1. *Bioorg. Med. Chem. Lett.* **2014**, *24* (2), 685-90.
150. Tang, B.; Wang, Y.; Wang, C.; Sun, J.; Qi, W. Boron difluoride dye fluorescent probe, synthesizing method of boron difluoride dye fluorescent probe and application of boron difluoride dye fluorescent probe in detecting hydrogen ion in cell CN 102603782 A, 2012.
151. Luo, J.; Ding, W.; Zhang, Y.; Yang, Z.; Li, Y.; Ding, L., Semisynthesis and acaricidal activities of isoxazole and pyrazole derivatives of a natural product bisdemethoxycurcumin. *J. Pest. Sci.* **2013**, *38* (4), 214-219.
152. Changtam, C.; Hongmanee, P.; Suksamrarn, A., Isoxazole analogs of curcuminoids with highly potent multidrug-resistant antimycobacterial activity. *Eur. J. Med. Chem.* **2010**, *45* (10), 4446-57.
153. Luo, H.; Yang, W.; Li, Y.; Zeng, H.; Yin, S. Process for preparation of curcumin analogs bis[3-(substituted-phenyl)acryloyl]benzenes. CN 101475460 A, 2009.
154. Artico, M.; Di Santo, R.; Costi, R.; Novellino, E.; Greco, G.; Massa, S.; Tramontano, E.; Marongiu, M. E.; De Montis, A.; La Colla, P., Geometrically and conformationally restrained cinnamoyl compounds as inhibitors of HIV-1 integrase: synthesis, biological evaluation, and molecular modeling. *J. Med. Chem.* **1998**, *41* (21), 3948-60.
155. Pabon, H. J. J., A synthesis of curcumin and related compounds. *Recl. Trav. Chim. Pays-Bas.* **1964**, *38* (4), 379-386.
156. Kolb, K. E.; Field, K. W.; Schatz, P. F., A One-Step Synthesis of Cinnamic Acids Using Malonic Acid: The Verley-Doebner Modification of the Knoevenagel Condensation. *J. Chem. Educ.* **1990**, *67* (12), A304.

157. Cho, C. S., Palladium-catalyzed Sonogashira coupling reaction followed by isomerization and cyclization. *J. Organomet. Chem.* **2005**, 690 (17), 4094-4097.
158. Narlawar, R.; Pickhardt, M.; Leuchtenberger, S.; Baumann, K.; Krause, S.; Dyrks, T.; Weggen, S.; Mandelkow, E.; Schmidt, B., Curcumin-derived pyrazoles and isoxazoles: Swiss army knives or blunt tools for Alzheimer's disease? *ChemMedChem.* **2008**, 3 (1), 165-72.
159. Wang, X.; Kim, J. R.; Lee, S. B.; Kim, Y. J.; Jung, M. Y.; Kwon, H. W.; Ahn, Y. J., Effects of curcuminoids identified in rhizomes of *Curcuma longa* on BACE-1 inhibitory and behavioral activity and lifespan of Alzheimer's disease *Drosophila* models. *BMC Complement Altern. Med.* **2014**, 14, 88.
160. Baki, A.; Bielik, A.; Molnár, L.; Szendrei, G.; Keserü, G. M., A high throughput luminescent assay for glycogen synthase kinase-3 β inhibitors. *Assay Drug Dev. Technol.* **2007**, 5 (1), 75-83.
161. Mercanti, G.; Ragazzi, E.; Toffano, G.; Giusti, P.; Zusso, M., Phosphatidylserine and curcumin act synergistically to down-regulate release of interleukin-1 β from lipopolysaccharide-stimulated cortical primary microglial cells. *CNS Neurol. Disord. Drug Targets* **2014**, 13 (5), 792-800.
162. Ma, H.; Deacon, S.; Horiuchi, K., The challenge of selecting protein kinase assays for lead discovery optimization. *Expert Opin. Drug Discov.* **2008**, 3 (6), 607-621.
163. Di, L.; Kerns, E. H.; Fan, K.; McConnell, O. J.; Carter, G. T., High throughput artificial membrane permeability assay for blood-brain barrier. *Eur. J. Med. Chem.* **2003**, 38 (3), 223-32.
164. Crivori, P.; Cruciani, G.; Carrupt, P. A.; Testa, B., Predicting blood-brain barrier permeation from three-dimensional molecular structure. *J. Med. Chem.* **2000**, 43 (11), 2204-16.
165. Lin, L.; Shi, Q.; Nyarko, A. K.; Bastow, K. F.; Wu, C. C.; Su, C. Y.; Shih, C. C.; Lee, K. H., Antitumor agents. 250. Design and synthesis of new curcumin analogues as potential anti-prostate cancer agents. *J. Med. Chem.* **2006**, 49 (13), 3963-72.

166. Takahashi, M.; Tanaka, M.; Sakamoto, E.; Imai, M.; Funakoshi, K.; Sakai, K.; Suemune, H., Application of Rh-catalyzed cyclization to the formation of a chiral quaternary carbon. *Chem. Pharm. Bull. (Tokyo)* **2000**, *48* (11), 1822-5.